R87AEB432

NASA CR-179486

NASA

National Aeronautics and
Space Administration

Development of Gas-to-Gas Lift Pad Dynamic Seals

Final Report

Volumes I and II

by

A.N. Pope, Principal Investigator
D.W. Pugh

General Electric Company
Aircraft Engine Business Group
Cincinnati, Ohio 45215

Prepared for

National Aeronautics and Space Administration
Lewis Research Center
21000 Brookpark Road
Cleveland, Ohio 44135

(NASA-CR-179486) DEVELOPMENT OF GAS-TO-GAS LIFT PAD DYNAMIC SEALS, VOLUMES 1 AND 2 Final Report (General Electric Co.) 189 p Avail: NTIS HC A09/MF A01 CSCL 11A

N87-22245

Unclas

G3/37 0072742

NASA Lewis Research Center
Contract NAS3-20043

R87AEB432 NASA CR-179486

National Aeronautics and
Space Administration

Development of Gas-to-Gas Lift Pad Dynamic Seals

Final Report

Volumes I and II

by

A.N. Pope, Principal Investigator
D.W. Pugh

General Electric Company
Aircraft Engine Business Group
Cincinnati, Ohio 45215

Prepared for

National Aeronautics and Space Administration
Lewis Research Center
21000 Brookpark Road
Cleveland, Ohio 44135

NASA Lewis Research Center
Contract NAS3-20043

1. Report No.	2. Government Accession No.	3. Recipient's Catalog No.
NASACR-179486		
4. Title and Subtitle DEVELOPMENT OF GAS TO GAS LIFT PAD DYNAMIC SEALS		5. Report Date May 1987
		6. Performing Organization Code
7. Author(s) A. N. Pope (Vol. I) D. W. Pugh (Vol. II)		8. Performing Organization Report No. R87-AEB432
		10. Work Unit No.
9. Performing Organization Name and Address General Electric Company Cincinnati, Ohio 45215		11. Contract or Grant No. NAS3-20043
		13. Type of Report and Period Covered Contractor Report
12. Sponsoring Agency Name and Address NASA Lewis Research Center Cleveland, Ohio 44135		14. Sponsoring Agency Code

15. Supplementary Notes

Project Manager, H. J. Scibbe, Structures Division, NASA Lewis Research Center, Cleveland, Ohio 44135

16. Abstract

Dynamic tests were performed on self-acting (hydrodynamic) carbon face rotary shaft seals to assess their potential, relative to presently used labyrinth seals, for improving performance of aircraft gas turbine engines by reducing air leakage flow rate at compressor end seal locations.

Seals of 23.762 cm (9.355 inch) mean face diameter were tested through the speed range of 1100 radians per second (10,500 RPM), pressure range through 217.2 N/cm^2 (315 psia) and sealed air temperature range through 811K (1000^{o}F), with seal downstream air pressure at approximately one (1) atmosphere, absolute.

Three (3) self-acting bearing configurations, designed to supply load support at the interface of the stationary carbon seal and rotating seal race, were tested. Two configurations, the shrouded taper and shrouded flat step, were incorporated on the face of the stationary carbon seal element. The third configuration, inward pumping spiral grooves, was incorporated on the hard faced surface of the rotating seal race. Test results demonstrated seal leakage air flow rates from 75 to 95% lower than can be achieved with "best" state-of-the-art labyrinth designs and led to identification of the need for a more geometrically stable seal design configuration which is presently being manufactured for subsequent test evaluation.

17. Key Words (Suggested by Author(s))		18. Distribution Statement
Self-Acting	Labyrinth	
Hydrodynamic	Aircraft Gas Turbine	
Shrouded Taper	Performance	
Shrouded Step		
Spiral Groove		

19. Security Classif. (of this report)	20. Security Classif. (of this page)	21. No. of Pages	22. Price*
Unclassified	Unclassified	182	

* For sale by the National Technical Information Service, Springfield, Virginia 22161

NASA-C-168 (Rev. 10-75)

FOREWORD

This program was sponsored by the Lewis Research Center of the National Aeronautics and Space Administration under Contract NAS3-20043. The period of performance for this program was from June 4, 1976, through December, 1985. This report is Volume I of two volumes. It encompasses the period of performance from program initiation on June 4, 1976, through approximately April 18, 1981, which covers work up to, but not including, program modification number 6. Volume II covers performance initiated with program modification number 6 through program termination.

Technical direction was provided by the NASA Project Managers, Dr. John Zuk, the late Mr. L. P. Ludwig, and Messrs. H. J. Scibbe and Eliseo DiRusso of the Seals and Rotor Dynamics Section. Messrs. Leonard W. Shopen and Willie C. Fleming, NASA Lewis Research Center, were the Contracting Officers.

Mr. J. C. Clark, Manager, Bearings, Seals and Drives Design Technology, was the Technical Program Manager for General Electric. Mr. A. N. Pope was the Principal Investigator.

VOLUME I

TABLE OF CONTENTS

VOLUME I

TABLE OF CONTENTS (Concluded)

VOLUME II

TABLE OF CONTENTS

VOLUME II

TABLE OF CONTENTS (Concluded)

VOLUME I
LIST OF ILLUSTRATIONS

VOLUME I

LIST OF ILLUSTRATIONS (Concluded)

VOLUME II

LIST OF ILLUSTRATIONS

VOLUME I

LIST OF TABLES

VOLUME I

Background

The initial design and procurement of seal hardware used in this program was done during the development cycle for a large military transport engine in the 1967 time period. The purpose was to serve as a backup for a labyrinth type compressor discharge balance piston seal in the event additional performance margin was required. Maximum design condition was the following:

Seal delta-P	350 PSI (241 N/sq cm)
Temperature, Air In	1000 degrees F (811° K)
Shaft Speed	9900 RPM (1037 rad/sec)
Pitch Line Velocity	392 Ft/Sec (119 m/sec)

A cross-section view of the seal and race assembly is shown on Figure 1. The carbon seal face wafer, item 9, procured initially for the military program, contained shrouded composite slider gas bearings in the carbon face. This seal was rig tested for 4 hours 58 minutes with maximum conditions of 280 psid (193 N/sq cm) at 785F (691K) and 140 psid (96.5 N/sq cm) at 1003F (812K) with shaft speed at 9900 RPM. Seal performance was good with negligible wear. Subsequent planned testing was dropped at this point because engine testing did not demonstrate need for additional performance improvement. Some months later (late 1968) an additional short test was performed to determine if the seal could operate at higher shaft speed and lower pressure. Test duration was 5 hours 45 minutes, including 3 hours at 15,100 RPM (600 Ft/Sec or 182.9 m/sec pitch line velocity). Maximum pressures and temperatures at this speed were 90 psid at 635F (62 N/sq cm at 603K) and 50 psid at 820F (34.5 N/sq cm at 711K).

Although all the above testing demonstrated the potential of the seal for use as an energy conserving device in gas turbine engines, no additional development funding was obtained until 1976 at which time the NASA Lewis Research Center, recognizing the potential of this seal type and the need for energy conservation, initiated funding to proceed on the development program summarized in this report.

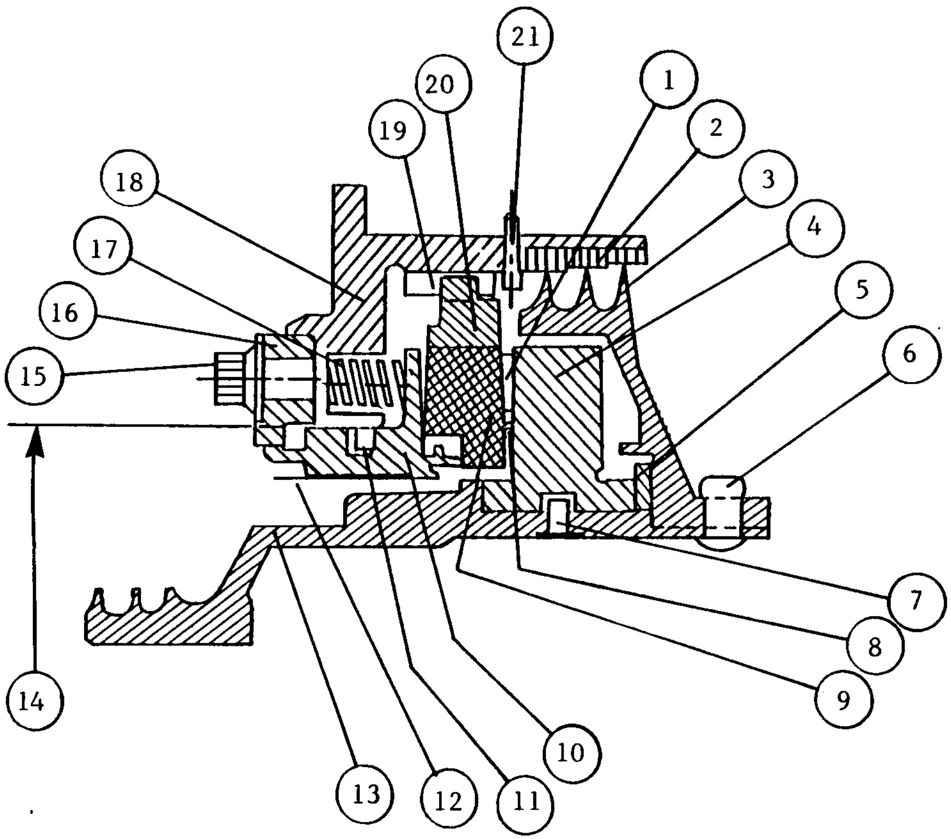

	Description
1	Hydrodynamic Air Bearing
2	Honeycomb Seal
3	Labyrinth Seal
4	Race
5	Wave Spring
6	Lock Rivet
7	Rotation Lock
8	Seal Dam
9	Carbon Wafer
10	Piston Ring Carrier
11	Piston Ring
12	Heat Shield
13	Race Holder (Adapter to Shaft)
14	Balance Diameter
15	Bolt
16	Rotation Lock
17	Coil Springs
18	Seal Housing
19	Splines
20	Shrink Ring
21	Assembly Lock

Figure 1. Assembly, Hydrodynamic Face Seal.

Seal Hardware Description

The following is a brief description of hardware comprising the seal and race assembly (reference Figure 1):

Item 3 - Piston Ring Secondary Seal

Three piston ring types were tested. The initial design was of Inconel 718 material with an open end gap, no wear pads and with aluminum oxide coating on the transverse sealing face. A narrow land on the piston ring outside diameter forms a gas seal at the seal pressure balance diameter which is located in the bore of the housing, Item 6. The balance diameter is also coated with aluminum oxide. The face of the piston ring seals against a narrow land projecting from the face of the ring gland located in the piston ring carrier, Item 4. The second design was the same as above except that it contained vented wear pads on its outside diameter. The third design was manufactured from a high temperature seal carbon material grade, with a single overlapping tongue and socket (sealed) end gap, and vented wear pads on both the outside diameter and transverse face of the ring. The narrow axially projecting land on the face of the gland was removed so that the ring contacted a flat transverse surface in the ring carrier gland.

Item 4 - Piston Ring Carrier

This part contains the gland to carry the piston ring secondary seal and transmits the axial seal closing force from the coil springs, Item 7, and balance piston pressure to the carbon face wafer assembly, Item 9. The thin Sheet in the bore is a welded in heat shield. Parent metal is Inconel 718. The face bearing against the left side transverse face of the carbon wafer is coated with aluminum oxide.

Item 6 - Seal Housing

Material of this part is Inconel 718. The seal balance diameter is at the bore of this part and is coated with aluminum oxide to provide a non-galling radial seat for the piston ring. The housing contains three

equally spaced female radial splines held in close true position location with respect to the balance diameter. Three male splines on the seal carbon wafer assembly, Item 9, engage the female splines in the seal housing. The wafer splines are held in close true position tolerance to the carbon face sealing dam. The purpose of this method of engagement is to maintain close concentricity between the seal face dam in the carbon wafer and the balance diameter of the seal housing.

A honeycomb stationary labyrinth seal seat is located on the inner diameter of the housing sleeve to the right of the assembly retention pins, Item 8.

Item 7 - Coil Springs

Coil spring material is Inconel X750. The springs provide force to seat the piston ring carrier, Item 4, against the carbon wafer and the carbon wafer against the face of the seal race, Item 10.

Item 9 - Seal Carbon Wafer Assembly

This assembly consists of a high temperature seal carbon material shrunk inside the bore of an Inconel 718 shrink ring. The female splines (refer to Item 6, above) on the original hardware were Inconel 718 material. For this program, inserts of a high temperature carbon material were fitted by rework on original hardware and were used in all subsequent hardware to provide a better wear surface.

The face of the carbon wafer contains the primary sealing dam and self-acting hydrodynamic gas bearing pads in the high pressure region outboard of the sealing dam. Wafers were tested with and without the vented wear pads located inboard of the face sealing dam. The radial width of the sealing dam was .045 inch (.1143 cm), and its radial location with respect to the balance diameter on the seal housing, Item 6, is selected to balance the axial pressure force acting to close the seal face against the face of the race to the required magnitude. The wafer is also pressure seated against the

transverse face of the piston ring carrier, Item 4, by the location of a sealing land of approximately .06 inch (.1524 cm) radial width projecting from the left side face of the carbon wafer.

Item 10 - Rotating Seal Race

Race material is Inconel 718. The face mating with the seal carbon wafer is coated with aluminum oxide. The race is seated axially against the shoulder of the shaft adapter, Item 15, by pressure and spring force. Three anti-rotation pins, Item 14, fixed in the shaft adapter and engaging slots in the bore of the race prevent the race from rotating with respect to the adapter.

Item 12 - Wave Spring

A wave spring of Inconel 718 material provides an axial force to seat the race, Item 10, axially against the shoulder of the shaft adapter, Item 15, while operating at very low pressure conditions.

Item 11 - Rotating Labyrinth Seal

Material of the rotating labyrinth seal is Inconel 718. The labyrinth is a safety feature added to restrict the loss of high pressure air in the event of a gross failure of the self-acting face seal. Pressure drop across the labyrinth seal is negligible at any normal flow rate experienced with the self-acting seal. Static radial clearance is large (approximately .02 inch or .0508 cm) to preclude generation of rub debris which might otherwise enter and damage the seal face.

Summary

Analytical and experimental evaluations were conducted on inward flow self-acting gas-to-gas face seals utilizing the following gas bearing configurations to generate load carrying capacity at the interface of the stationary seals and the rotating seal races:

	Gas Bearing Configuration	Gas Bearing Location
1	Shrouded Taper	Stationary Carbon Face
2	Shrouded Step	Stationary Carbon Face
3	Spiral Groove	Rotating Race Face

Seals utilizing the above three (3) gas bearing configurations were tested at the following concurrent maximum operating conditions:

Seal Upstream Air Pressure	315 psia (217.2 N/sq cm)
Seal Downstream Air Pressure	1 atmosphere (abs.)
Seal Upstream Air Temperature	1000 degrees F (811K)
Seal Face Pitch Line Velocity	429 ft/sec (131 m/s)
Seal Race Angular Velocity	1100 rad/sec (at 10,500 RPM)

All configurations demonstrated the capability of operating successfully throughout the operating test range while restricting air leakage flow rates to between one-twentieth and one-quarter of the rates expected for a "best configuration" labyrinth air seal. Design problems, involving primarily the capability for maintaining control of geometry, were identified. A design configuration having the potential for substantially improving geometric stability and further reducing air leakage flow rates was identified and is described in Volume II of this report.

Introduction

Performance of jet engines is affected by efficiency of the air seals used to restrict air leakage flow rates at gaps between stationary and rotating engine components, particularly in the area of the primary (high pressure) gas flow path. Historically, these inner air seals have been axial flow labyrinth configurations which throttle the gas through a series of annular constrictions formed by labyrinth "knives" operating with a

premachined radial clearance between the tips of the rotating knife edges and the bore of a stationary cylindrical sleeve. On a new installation, radial clearance will be in the range of .0005 to .001 times the diameter. During operation this clearance is affected by differential thermal expansion, centrifugal and pressure strains, rotor dynamics, hardware vibration, material wear and erosion, etc. Because of the extreme range of peripheral velocities, gas temperature, pressure, etc., and the variation of these parameters with time response and random duty cycles, it is very difficult to control operating clearances on new engine installations and even more difficult to prevent deterioration of sealing performance with engine service time.

Some percentage of the labyrinth seal leakage flow can be used to cool engine components. The practice of using compressor discharge labyrinth seal leakage flow for this purpose, however, is usually not energy efficient since the magnitude of the flow is generally in excess of that required. A more efficient solution would be to use bleed air from a lower stage of compression with cooler air and less loss of cycle energy. Other potential applications such as geared fans or turboprops may require large diameter high pressure balance piston seals to react the net system rotor thrust pressure forces. Labyrinth seals used for these applications are inherently inefficient.

Gas film technology seals have the potential to recoup 50 to 95% of this wasted leakage flow. Self-acting hydrodynamic face seals have repeatedly demonstrated successful operation with a controlled leakage flow clearance in the magnitude of .0003 to .001 inch (.0008 to .0025 cm) over a range of engine operating parameters with resulting leakage rates 75 to 90 percent lower than attainable with labyrinth seals. The purpose of this program was to add impetus to the continuing development of these types of energy conservative sealing devices with the view towards eventual introduction into engine installations.

The configuration of the self-acting seals tested is shown on Figure 1. Testing was conducted using three (3) types of self-acting gas bearings.

Shrouded composite slider bearings and shrouded (Rayleigh) stepped bearings, both of which were machined into the stationary seal carbon faces, were tested. The third configuration tested incorporated inward flow spiral groove gas bearings in the hard facing of the rotating seal race.

Test Equipment

Static Fixture

A bench fixture in which static air leakage rates can be determined for the test seal and race assembly is shown on Figures 2 and 3. The fixture is configured for rapid assembly/disassembly when compared to the dynamic test rig and is used to screen parasitic leakage flow rates prior to assembly in the dynamic rig, to isolate sources of air leakage through the seal assembly and as a vehicle in which to measure pressure induced strain in components of the seal assembly.

Air leakage and flow rate measurements are taken with the same instruments used on the dynamic test rig to minimize error between static and dynamic test set-ups.

Dynamic Test Facility

The rig in which dynamic seal testing is conducted is shown on Figures 4 and 5. It is a two bearing, stiff shaft machine driven by a 40 horsepower variable speed eddy-current motor coupling through a flat belt on crowned pulleys. Both rig shaft bearings are oil jet cooled and lubricated. The forward bearing (test end of shaft) is a ball thrust bearing which must support an axial thrust force of 18,000 pounds (8165 kg) when the seal is operating at maximum test pressure. The aft bearing (drive end of shaft) is also a ball bearing which is preloaded axially by a 200 pound (91 kg) spring force. Buffer pressure introduced between tandem sets of circumferentially

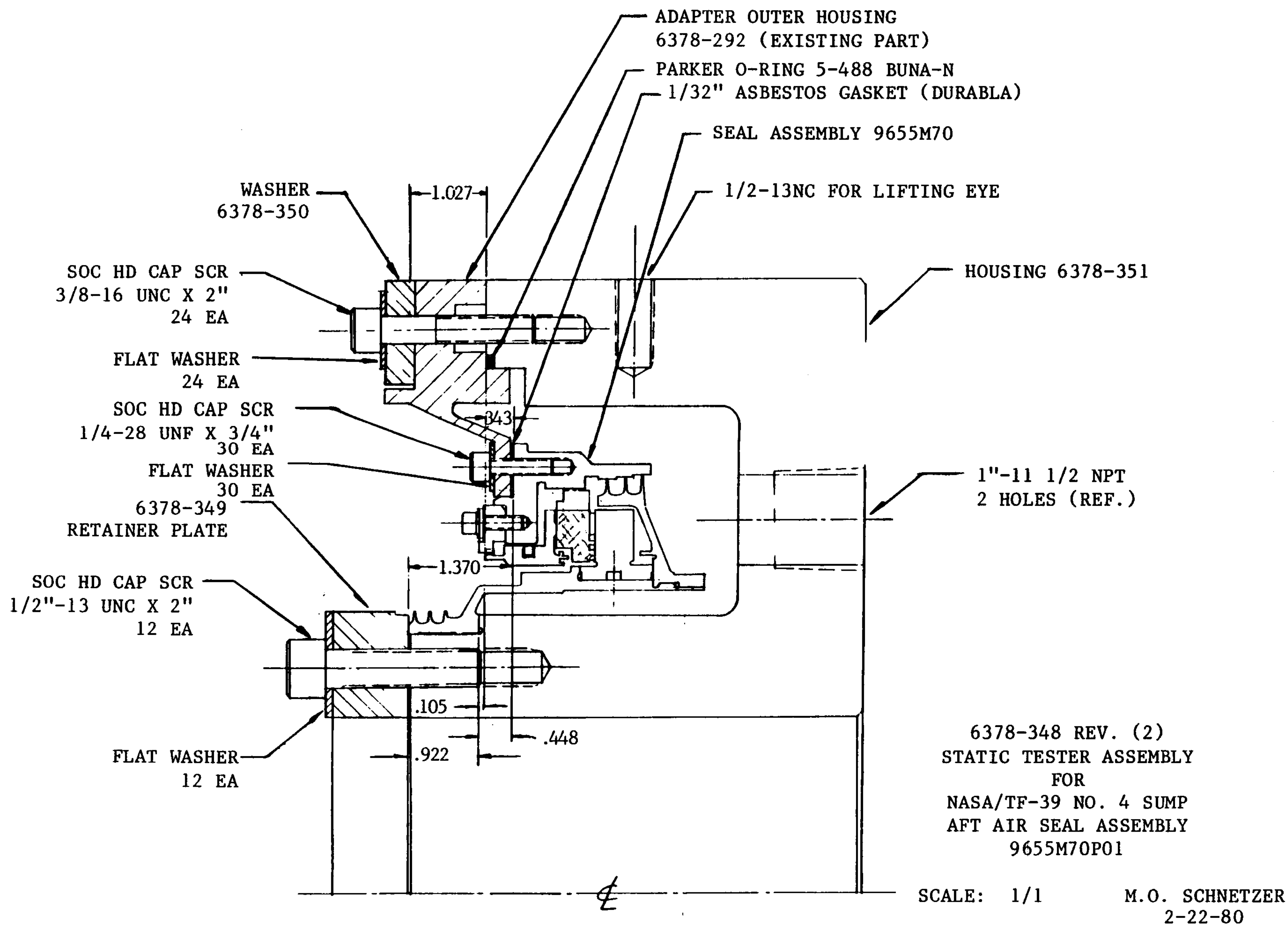

Figure 2. Cross-section View - Static Test Set-up.

ORIGINAL PAGE IS
OF POOR QUALITY

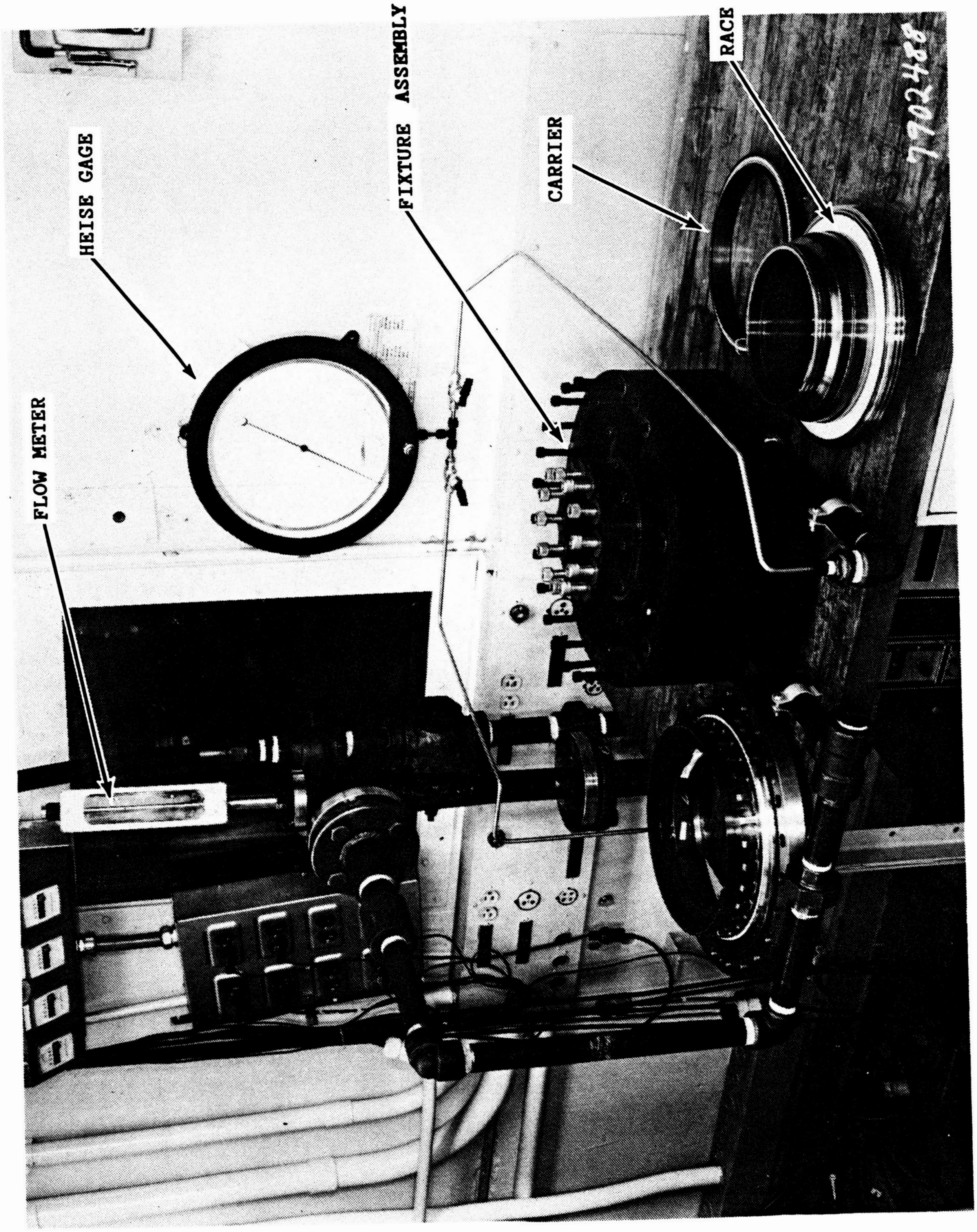

Figure 3. Static Test Fixture.

ORIGINAL PAGE IS
OF POOR QUALITY

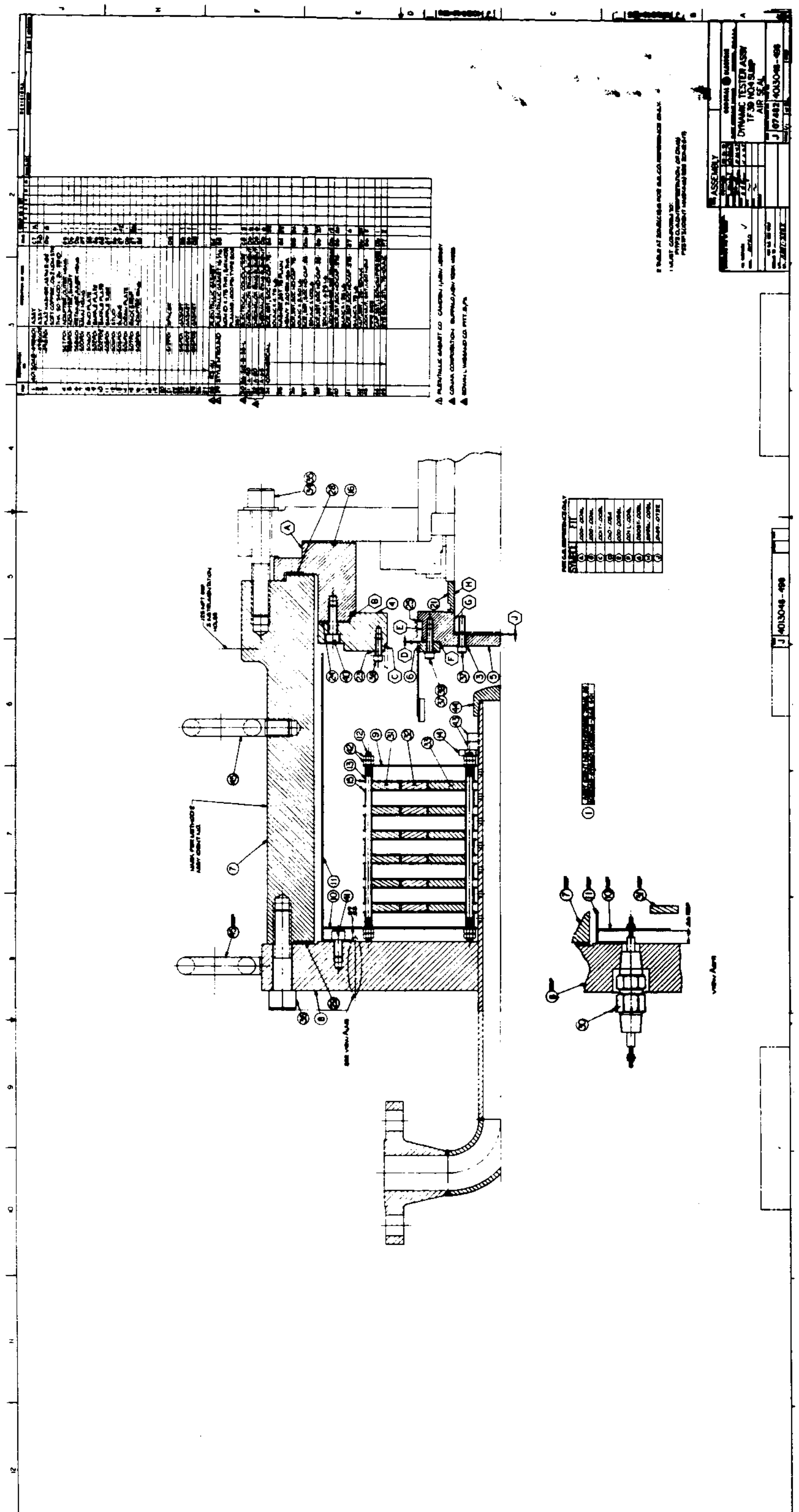

Figure 4. Dynamic Test Rig.

**ORIGINAL PAGE IS
OF POOR QUALITY**

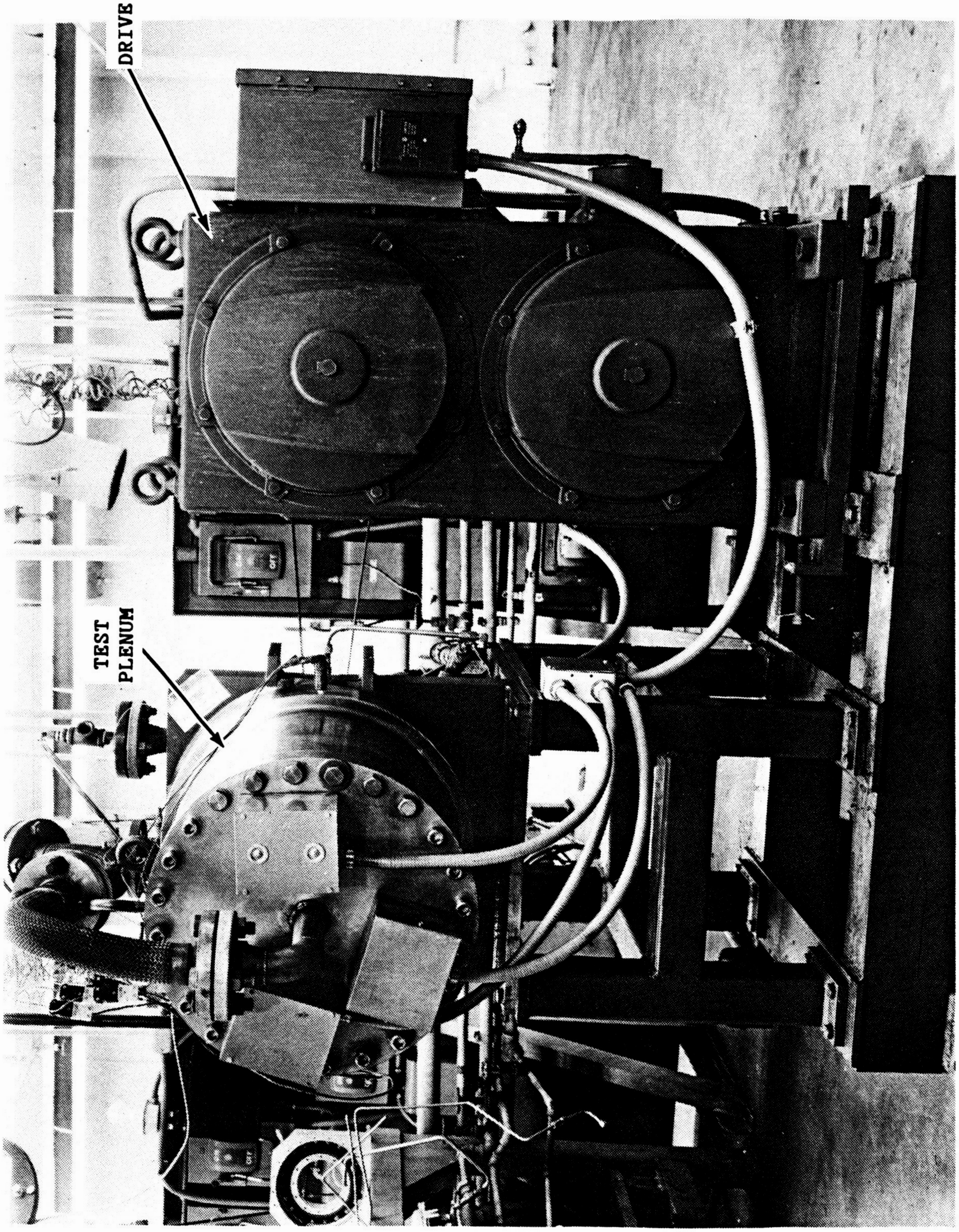

Figure 5. Dynamic Test Rig Assembly.

segmented carbon bore rubbing seal elements contain the bearing lubrication at both ends of the shaft. The forward tandem carbon seal also prevents hot test leakage air ingestion into the bearing lube compartment.

A thermally insulated hat-piece forms the high pressure plenum upstream of the test seal and contains six (6) banks of "pancake" shaped electrical resistance type air heaters to control seal air upstream temperature. Each bank is rated at 4050 watts for a total capacity of 24.3 kw.

High pressure air is delivered to the seal from a Gardner-Denver two-stage piston type air compressor rated for 500 psig (138 N/sq cm) maximum pressure and capable of delivering a maximum flow rate of approximately 56 SCFM (.038 kg/sec) of air at 200 psig (138 N/sq cm).

Seal air inlet flow rate is metered through a steel tube rotometer mounted in the high pressure piping in close proximity to the high pressure plenum hat-piece cover plate. The rotometer scale is 100 scfm (.0578 kg/sec), maximum, at one atmosphere of pressure. Rotometer inlet air temperature and pressure are measured and used to determine the corrections for flow rate at actual inlet conditions.

Seal upstream air pressure is measured by a 0 to 500 psig (345 N/sq cm) Heise gage.

Seal air inlet temperature is measured by two (2) thermocouples located in the high pressure plenum. One thermocouple is located within 0.5 inch (1.3 cm) of the test seal in the seal air inlet flowpath. The second is located approximately 2 inches (5 cm) radially outward and 90 degrees circumferentially from the first.

Seal Dynamic Analysis

Gas Film Forces

An analysis was made of each of the three self-acting gas bearing seal configurations (see Figure 6) to determine the theoretical gas film clearance

Located in Carbon Face

Bearing Radial Width	.29 inch
Bearing Step Length	1.048 inches
Bearing Total Length	1.563 inches
Rail Radial Width	.025 inch
Step Depth	.0007 inch
Number of Bearings	18

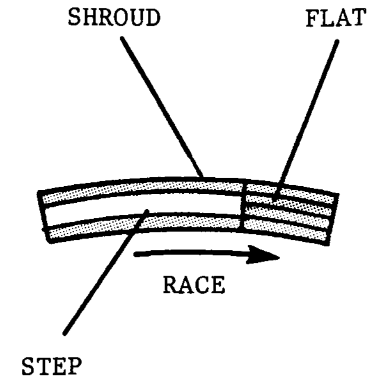

Figure 6a. Stepped Pad Geometry.

Located in Carbon Face

Bearing Radial Width	.29
Bearing Taper Length	1.386 inches
Bearing Total Length	1.512 inches
Rail Radial Width	.03 inch
Bearing Taper Depth	.009 inch
Number of Bearings	18

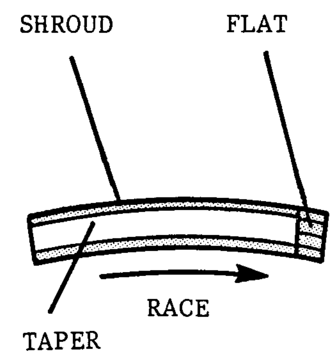

Figure 6b. Composite Slider Geometry.

Located in Face of Race

Carbon Pad Radial Width	0.29 inch
Arc Radius	4.97 inches
Arc Center Distance	1.99 inches
Number of Grooves	90
Groove to Land Ratio	.69
Groove Depth	.0007 inch
End Land Radial Width	.05 inch

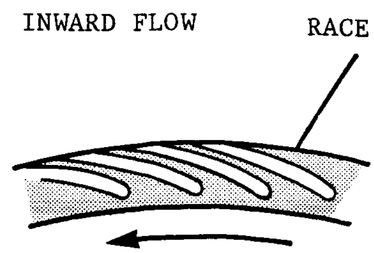

Figure 6c. Spiral Groove Geometry.

generated at the interface of the stationary seal and rotating race and to determine theoretical air leakage rates. Gas bearing load capacities and forces reacted by the gas bearings were calculated for the following two (2) cycles:

		Pressure**		Air Temp		Speed		
Cycle	Point	Psig	N/sq cm	F	K	RPM	ft/sec*	m/sec*
A	1	9	6.2	260	400	1181	48.2	14.7
A	2	202	139.3	940	777	7935	323.9	98.7
A	3	125	86.2	820	711	7480	305.3	93.1
B	1	23	15.9	600	589	6000	244.9	74.6
B	2	290	199.9	950	783	10500	428.6	130.6
B	3	270	186.2	950	783	9300	379.6	115.7

*At mean diameter of gas bearing, 9.355 inches (23.762 cm).
**Pressure downstream of the seal is equal to one (1) atmosphere.

Points A1, A2 and A3 are representative of ground idle, take-off and cruise conditions for a low pressure turbine thrust balance seal for a geared fan engine. Points B1, B2 and B3 are representative of a reduced temperature cycle for a core rotor compressor discharge seal in a large commercial fan engine.

Calculated hydrodynamic forces generated in the gas bearings are shown in Figures 7a and 7b, for Cycles A and B, respectively, for the composite slider, stepped pad and spiral groove configurations. Gas bearing dimensions are shown on Figure 6a, 6b and 6c for the three configurations tested. Bearing load capacity is based on the assumption of perfect geometry and parallelism at the transverse interface of the gas film.

Forces plotted on Figures 7a and 7b, 8a, 8b and 8c, 9 and 10 are total forces divided by the circumference of the seal balance diameter (force per inch of circumference).

The minimum, nominal and maximum net axial pressure closing forces (Figure 8a) are relative to drawing dimensional tolerances. Calculated forces for Figure 8a are based on the assumption that pressure distribution is a

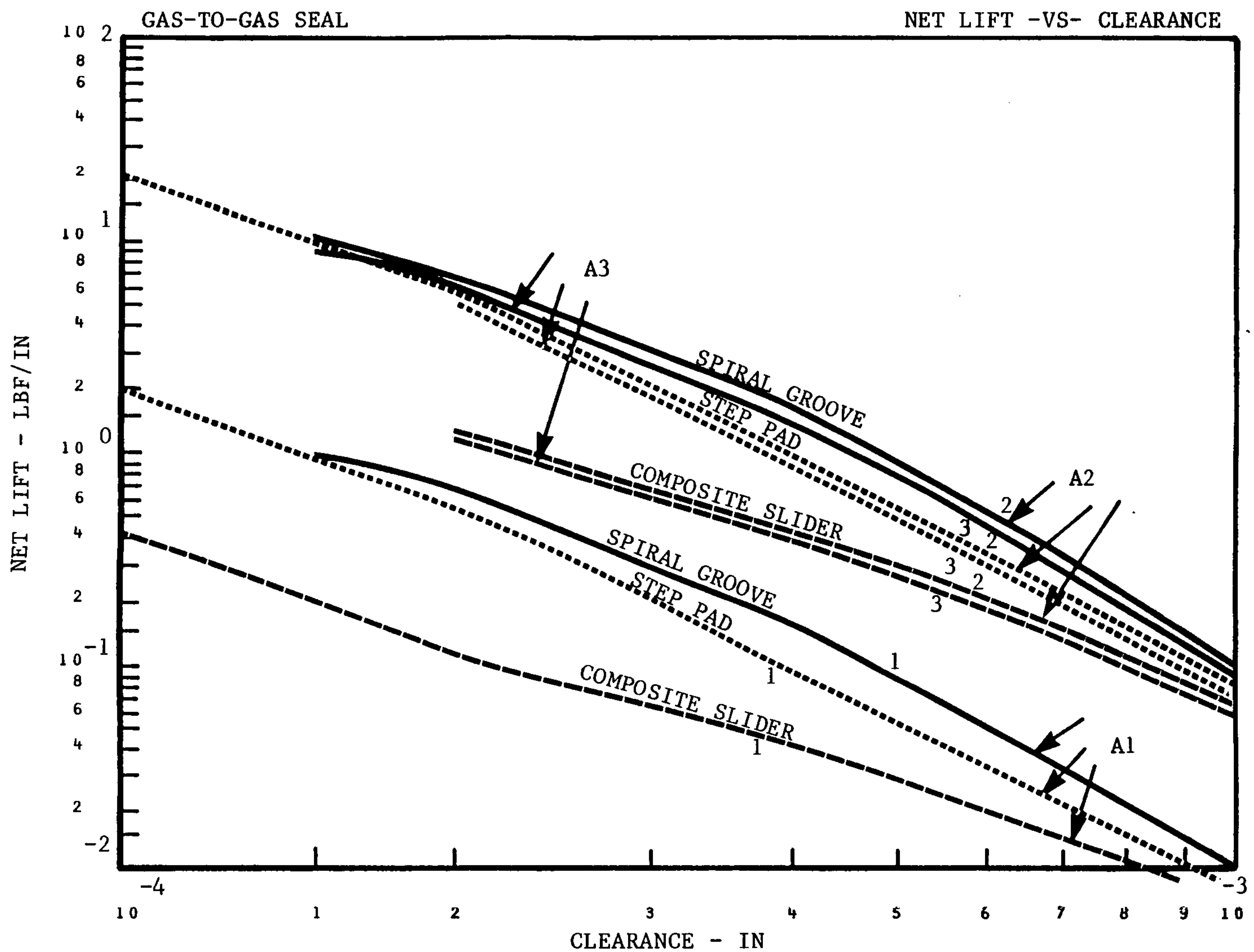

Figure 7a. Gas Bearing Capacity - Cycle A.

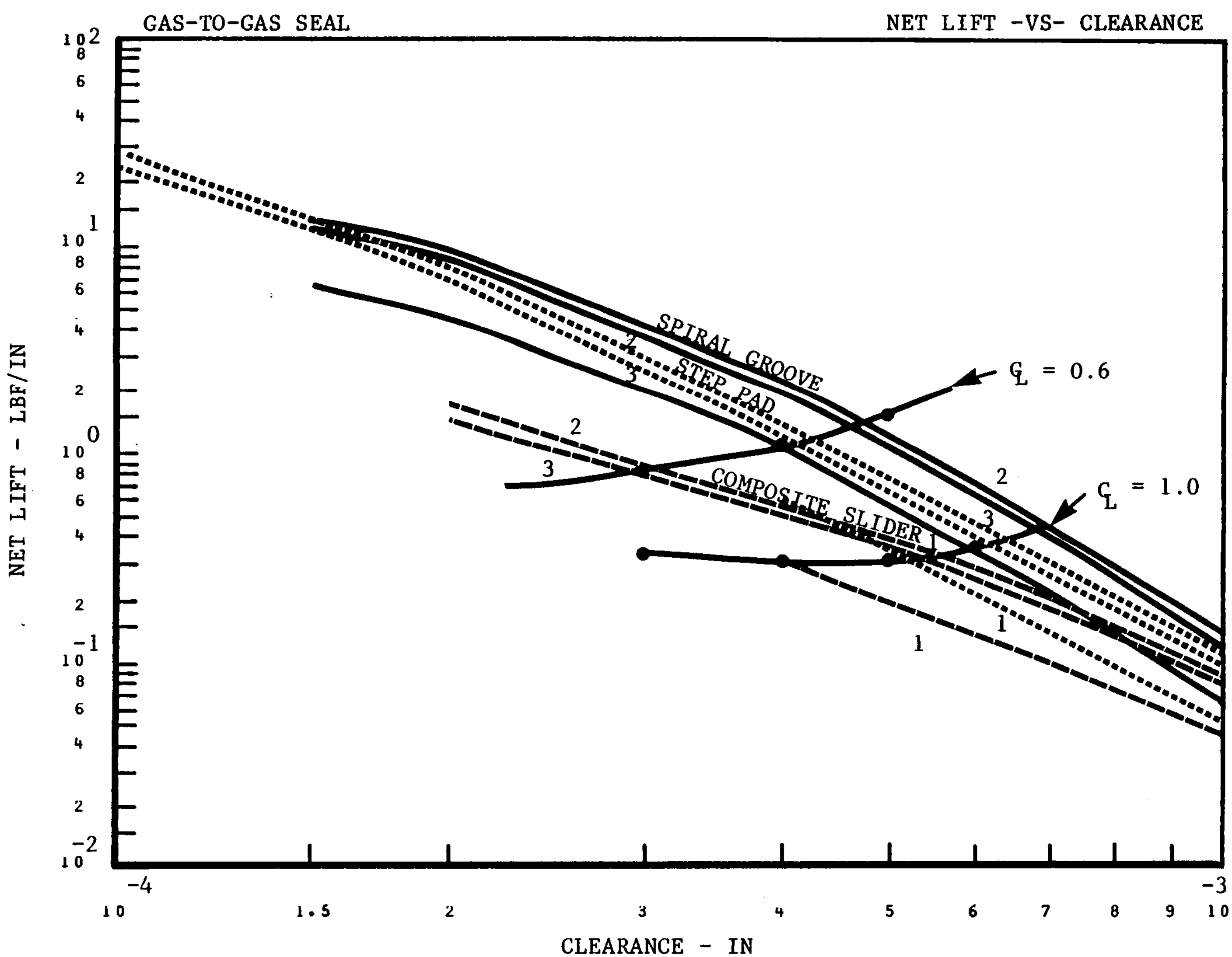

Figure 7b. Gas Bearing Capacity - Cycle B.

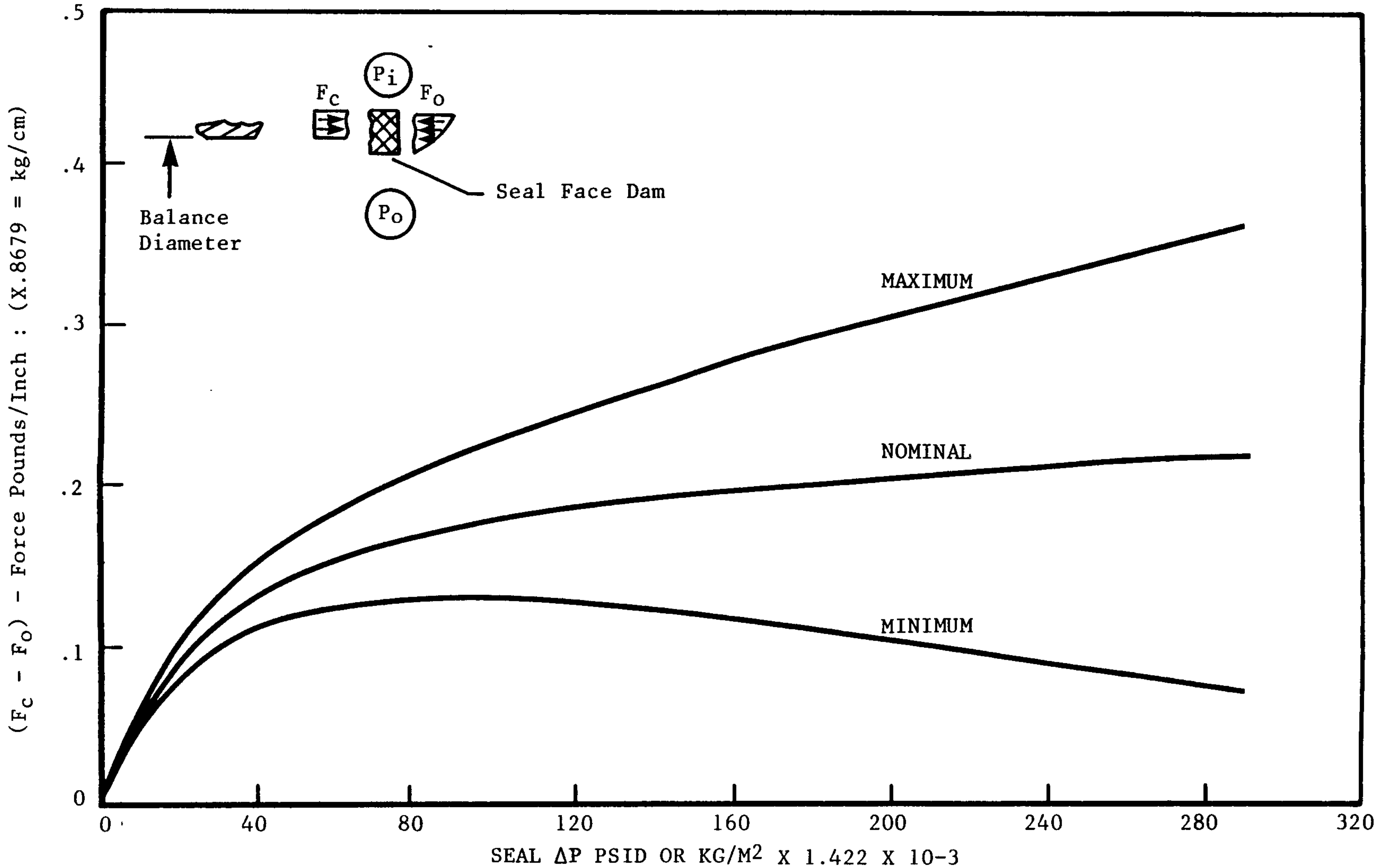

Figure 8a. Net Axial Gas Pressure Closing Force Versus Seal/ΔP.

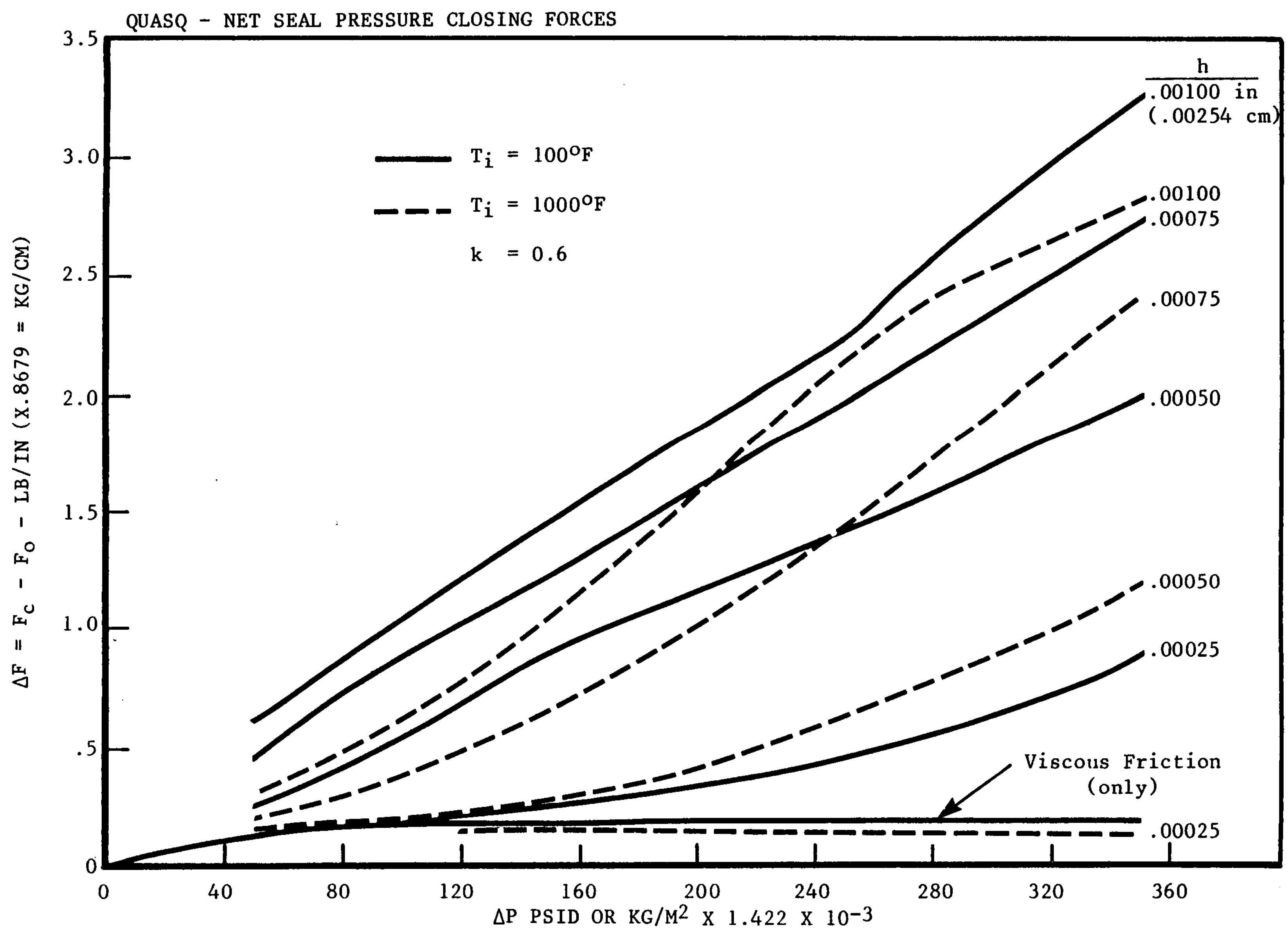

Figure 8b. Net Axial Gas Pressure Force vs. Seal ΔP (QUASQ, k = .6).

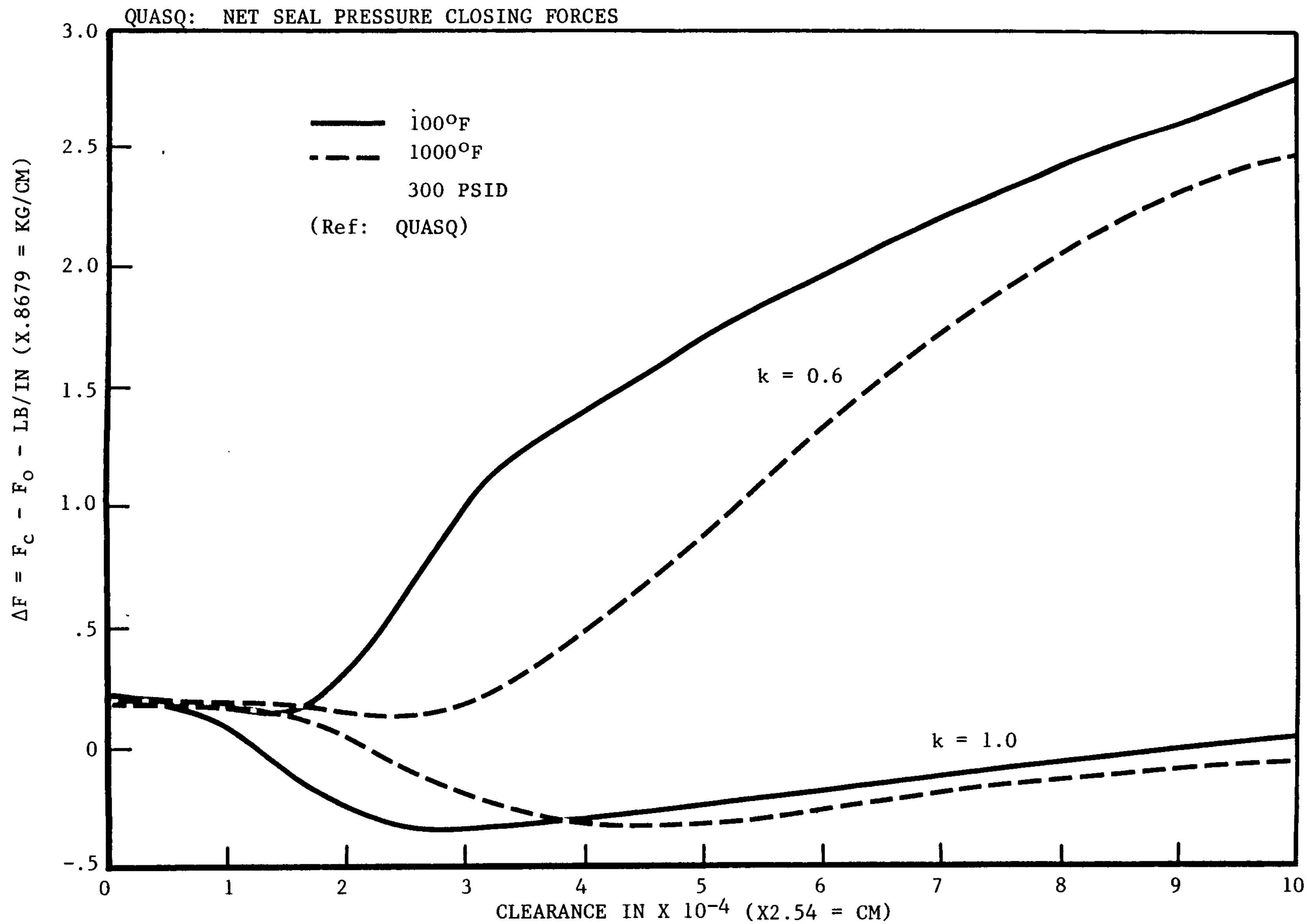

Figure 8c. Net Axial Gas Pressure Force @ 300 psid vs. Loss Coefficient.

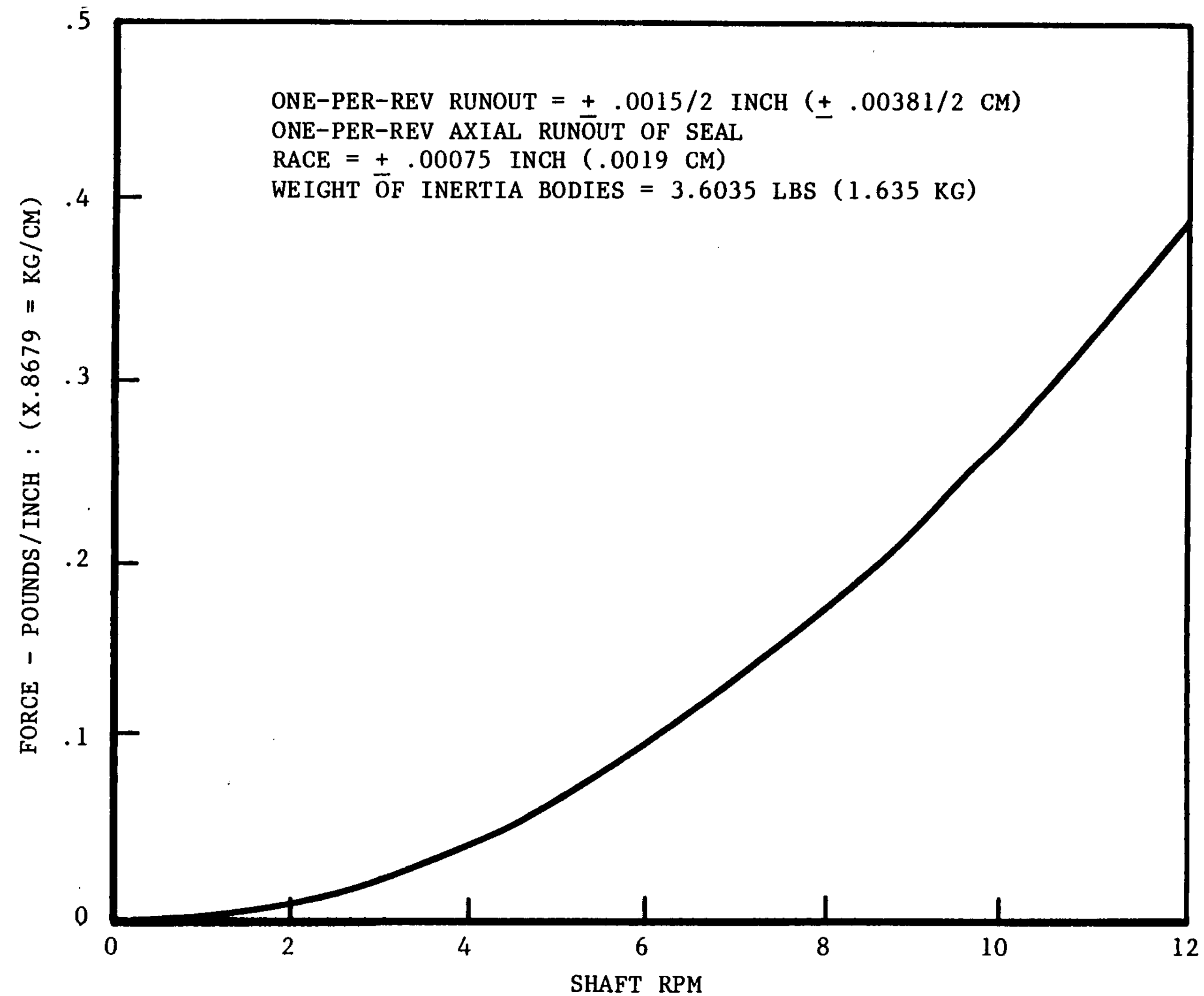

Figure 9. Inertia of Seal Face Assembly Versus Shaft RPM.

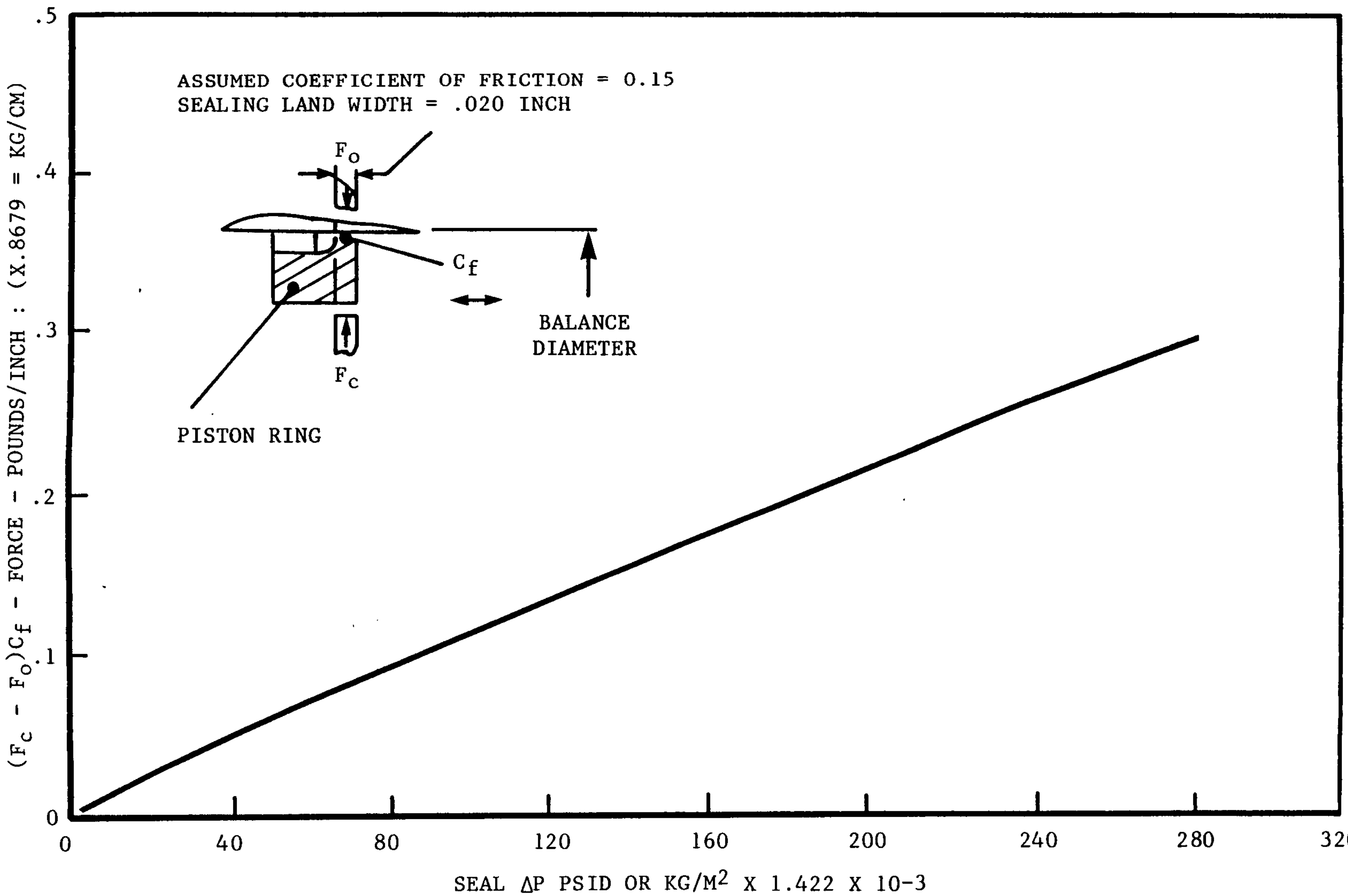

Figure 10. Piston Ring Sliding Friction Force Versus Seal ΔP.

function of viscous flow with friction, only. It is also assumed that the gas flow velocity is low enough to neglect dynamic losses at the entrance and exit of the seal face dam. Forces shown on Figure 8b are calculated via computer program QUASQ (Reference 1) with loss coefficient equal to 0.6, and with all dimensions at drawing nominal. Data shown on Figure 8c are for a high pressure condition (300 psig/206.84 N/sq cm) and compare seal pressure closing forces with loss coefficients at 0.6 an 1.0. Comparing results of Figures 8a, b, and c imply the significance of including dynamic losses and of knowing the loss coefficient relative to gas film clearance, leakage flow rate and sealing forces.

Angular misalignment of the rotating seal race with respect to perpendicularity with the center axis of the rotating shaft will generate a circumferential variation in gas film clearance and hydrodynamic force. This variation is a result of mass inertia and friction in the stationary seal face assembly. Inertia is proportional to mass and magnitude of misalignment. Figure 9 shows the inertia of the test seal face assembly if total misalignment results in one-per-revolution axial motion of 0.0015 inch (.00381 cm). Friction force is generated as the piston ring secondary gas seal and the rotation lock of the stationary seal assembly slide axially against their relative mating surfaces in response to seal race misalignment or other causes of relative axial motion. Friction force is shown on Figure 10 for the piston ring secondary seal with an assumed constant coefficient of friction equal to 0.15. Rotation lock friction force is negligible when the seal operates with a gas film at the seal to race interface. At 10,000 RPM the air shear gradient in the interface film generates a torque less than 7 in-lbs (8.07 kg-cm) with clearance as low as 0.00015 inch (0.00038 cm), or approximately 0.008 pounds/inch (1.43 gms/cm) of circumference friction force for an assumed rubbing coefficient of friction equal to 0.15 at the rotation lock interfaces.

Seal Air Flow Rates

Computer program QUASQ (Reference 1) was used to determine theoretical flow rates through the clearance at the interface of the seal face dam and the

rotating seal race. Results are shown for three air temperatures with loss coefficient equal to 0.6 (Figure 11) and 1.0 (Figure 12). Parallel face film clearance and air leakage flow rates projected to maximum condition (Cycle B-2) are approximately the following:

Loss Coefficient	Bearing Configuration	Clearance Inches	Clearance cm	Air Flow Rate SCFM	Air Flow Rate lbs/sec	Air Flow Rate kg/sec
0.6	Comp. Slider	.00031	.00079	9.0	.0115	.0052
1.0	Comp. Slider	.00054	.00137	31.0	.0395	.0179
0.6	Stepped Pad	.00042	.00107	16.5	.0210	.0096
1.0	Stepped Pad	.00063	.00160	40.2	.0512	.0232
0.6	Spiral Groove	.00046	.00117	19.5	.0249	.0113
1.0	Spiral Groove	.00069	.00175	46.4	.0592	.0269

Air leakage rates through the secondary piston ring seal are not included in the above and are assumed to be negligible in comparison to seal face flow rates. Those piston rings tested with open end gaps would have a maximum gap flow clearance area of approximately .00066 sq in (.0043 sq cm) resulting in theoretical leakage rates of approximately 3.1 scfm (.0018 kg/sec) at 300 psid (207 N/sq cm) and 70 deg F (294 deg K) and 1.9 scfm (.0011 kg/sec) at 1000 deg F (811 deg K) using orifice flow equations as a basis for calculations.

Test Results and Discussion

Summary

Twenty-five (25) recorded assemblies were made in the dynamic test rig (Figure 4) in an effort to complete the specified tests. Static testing only was completed in thirteen (13) of these builds primarily because of efforts to the determine a source(s) for higher than expected air leakage rates. Two hundred fifty-four (254) hours, twenty-nine (29) minutes of dynamic testing were completed as a result of the other twelve (12) builds on three gas bearing seal configurations as follows:

Configuration	Build Number	Test Time Hrs:Min
Shrouded Composite Slider	2, 3, 4, 7, 20, 22	119:33
NASA Shrouded Step Pad	5, 8, 21	15: 8
NASA Spiral Groove	23, 24, 25	119:48

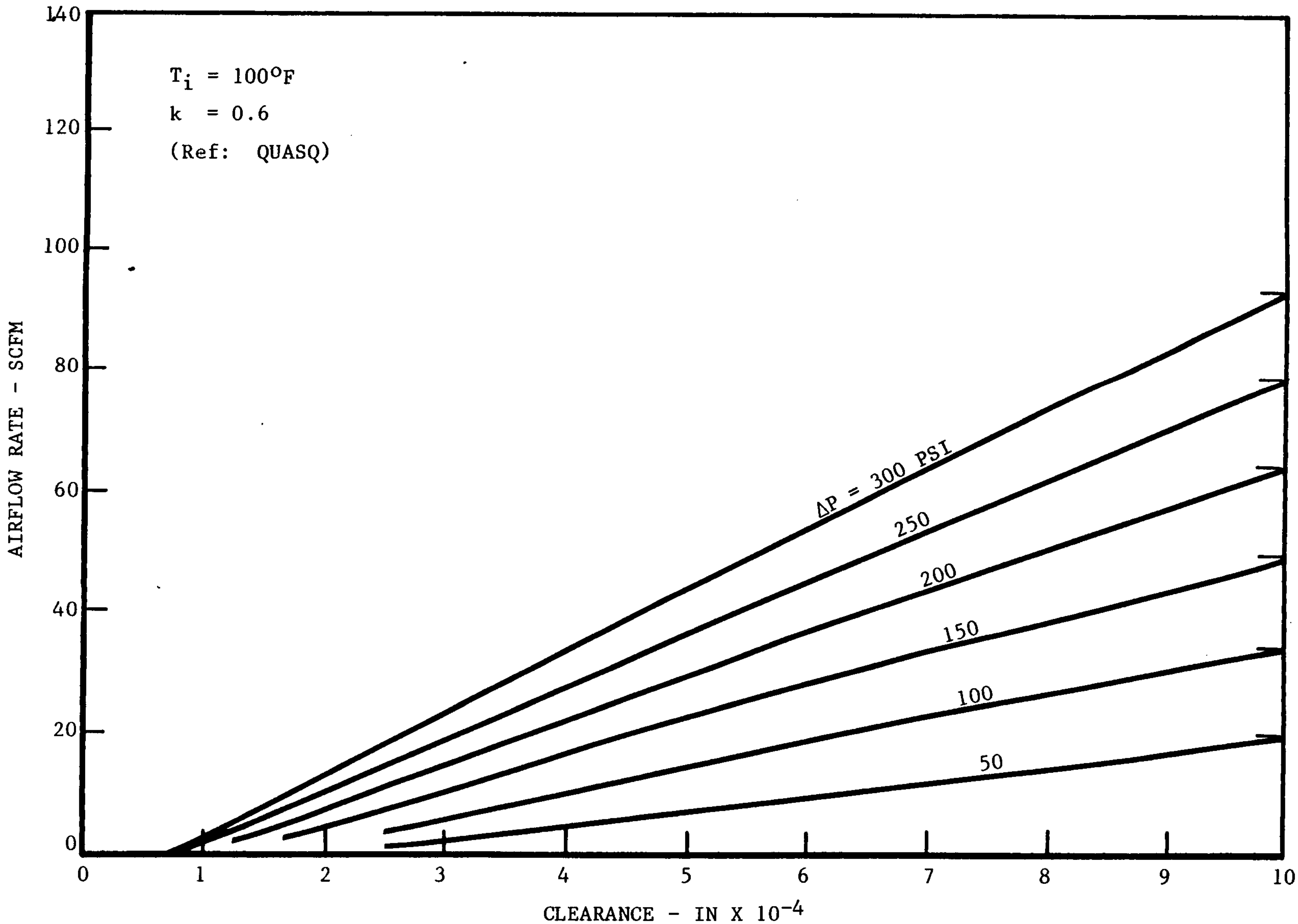

Figure 11a. Seal Dam Flow Rate vs. Clearance, T = 100F, k = .6.

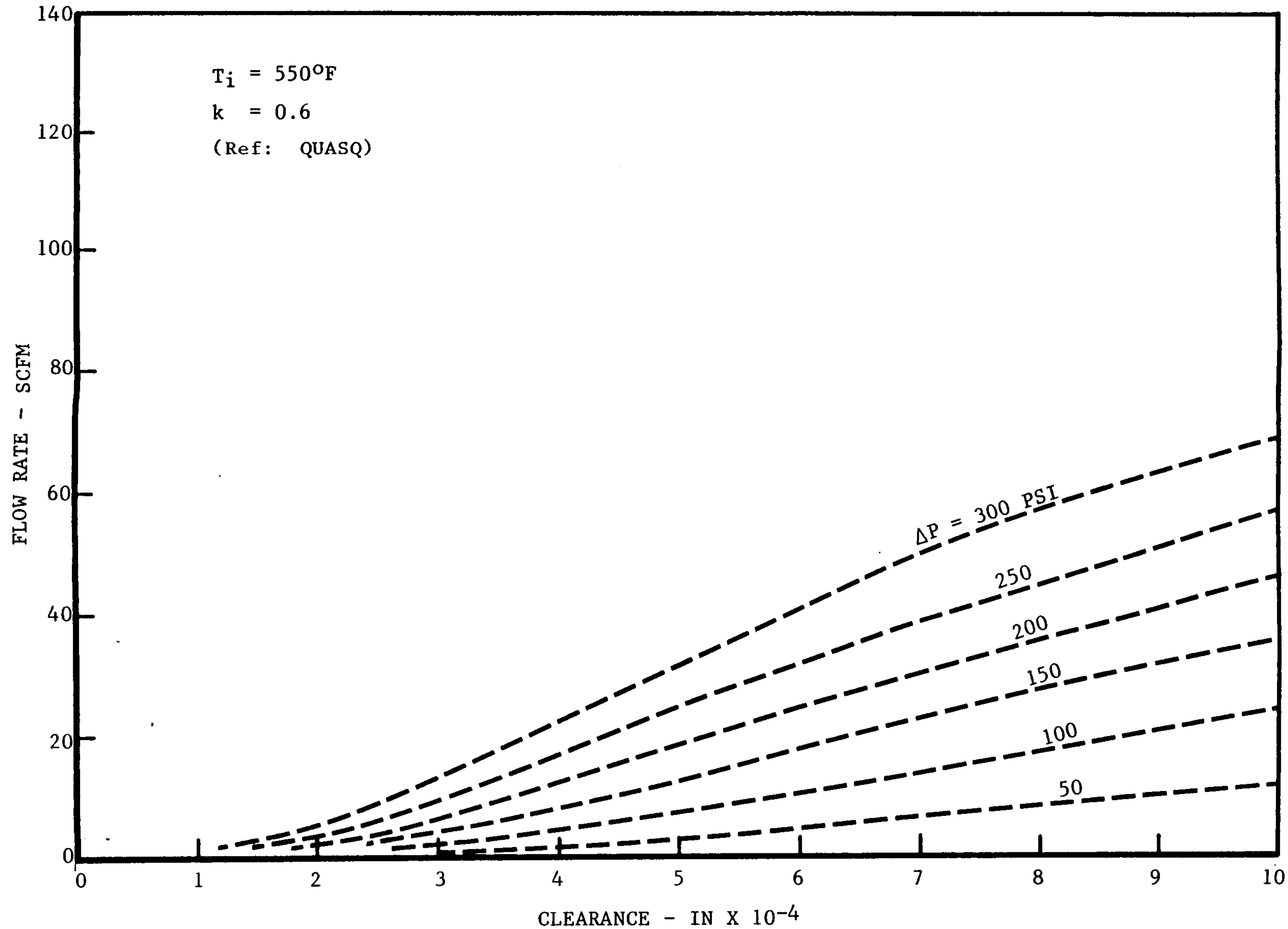

Figure 11b. Seal Dam Flow Rate vs. Clearance, T = 550F, k = .6.

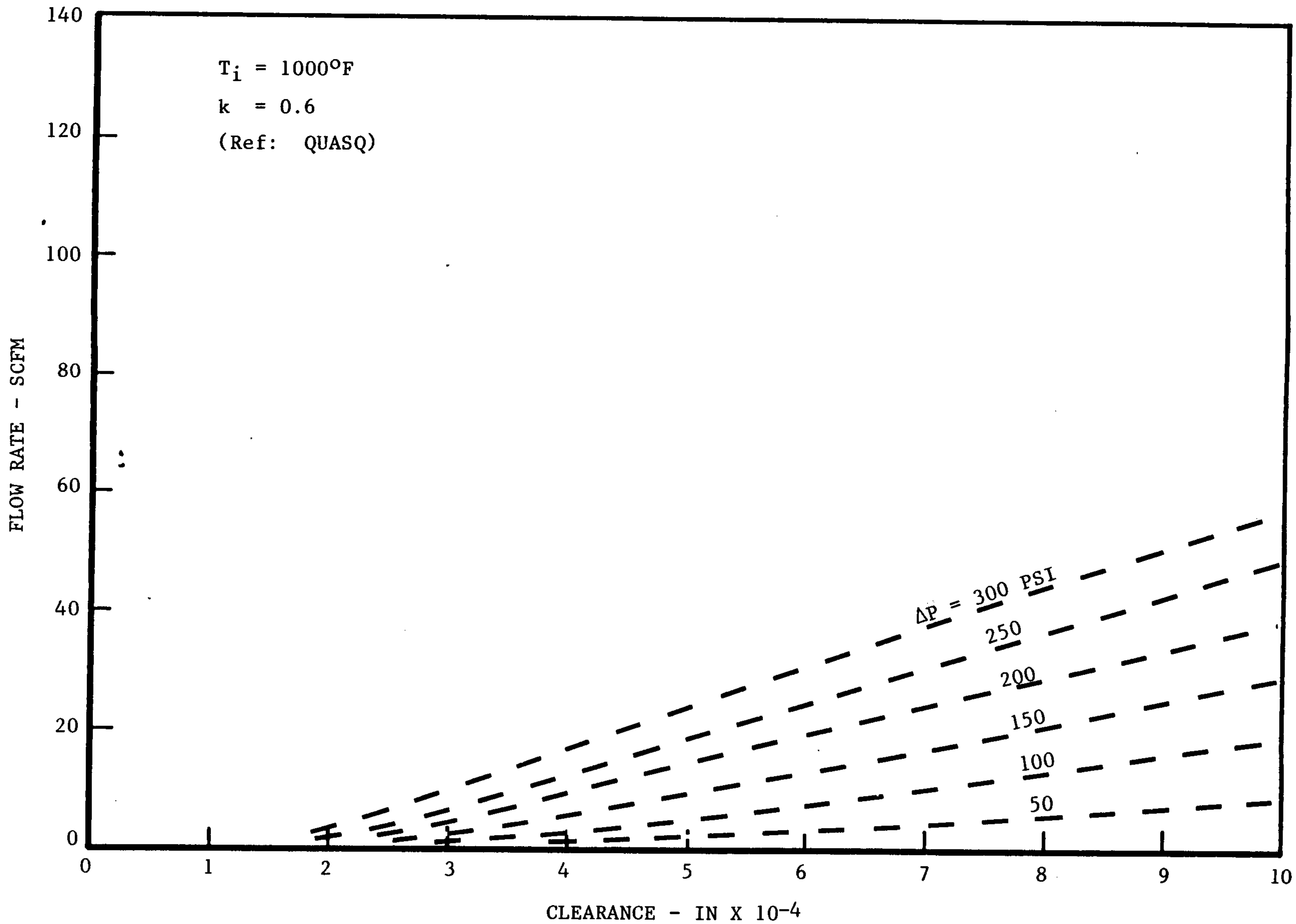

Figure 11c. Seal Dam Flow Rate vs. Clearance, T = 1000F, k = .6.

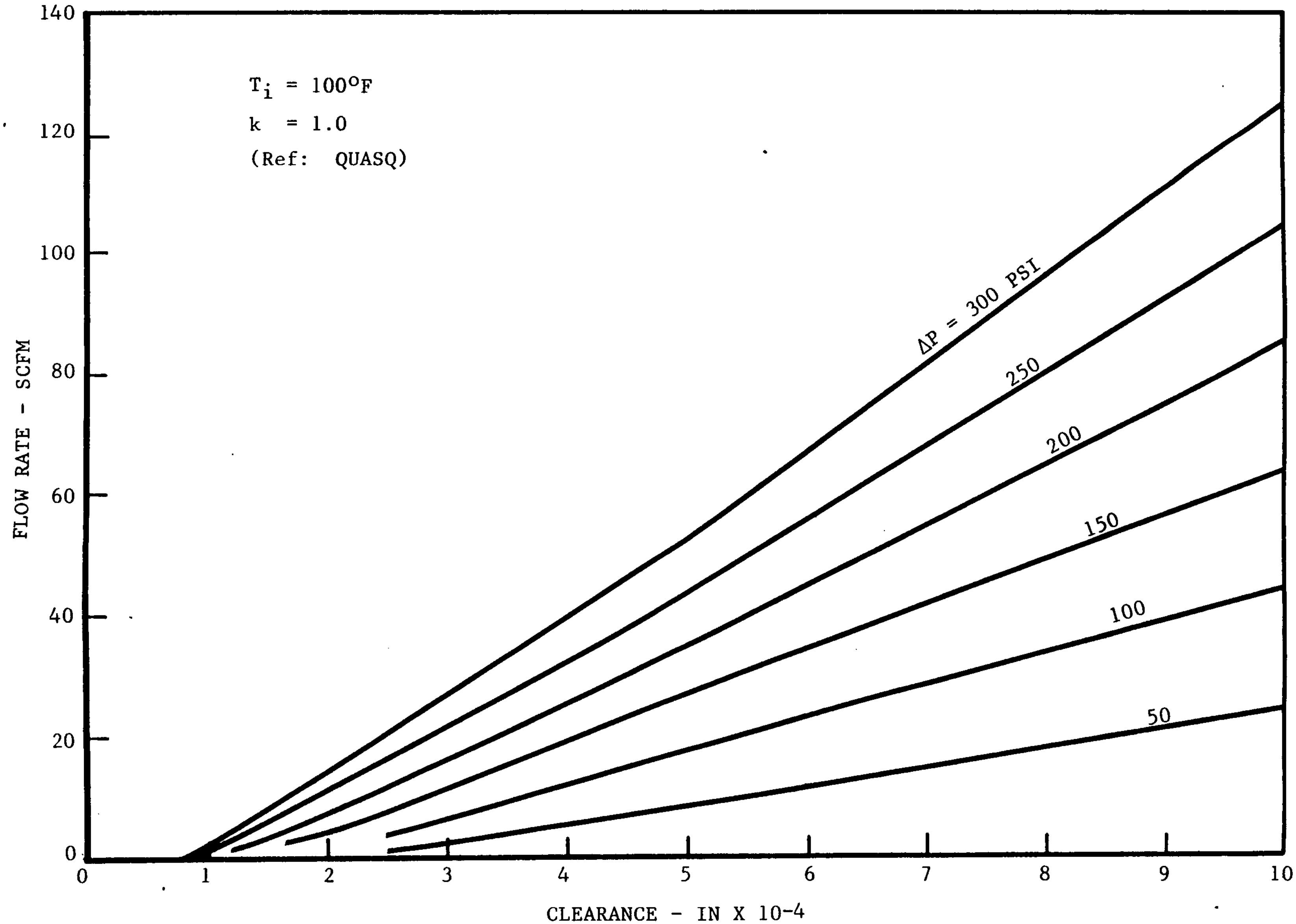

Figure 12a. Seal Dam Flow Rate vs. Clearance, T = 100F, k = 1.0.

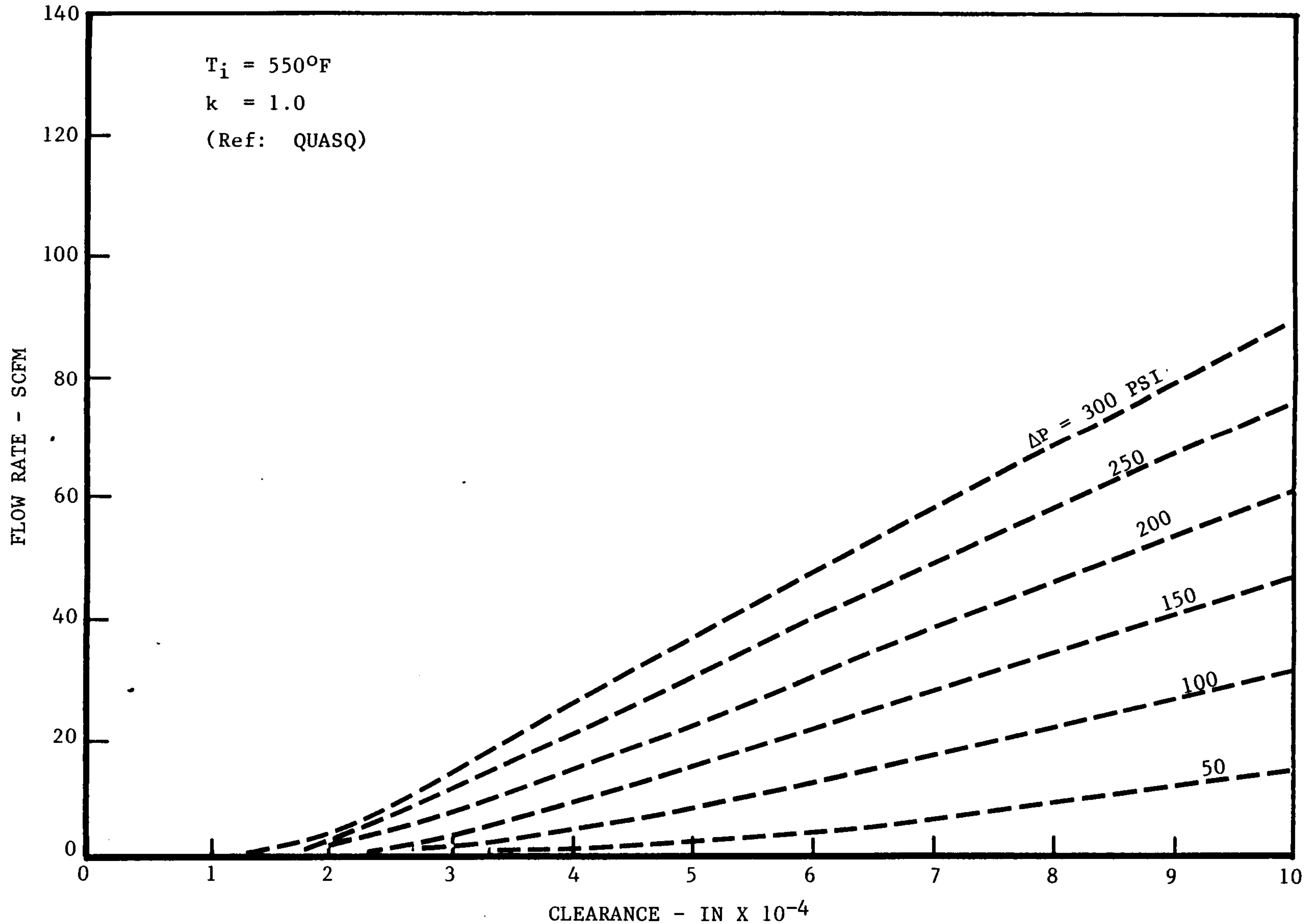

Figure 12b. Seal Dam Flow Rate vs. Clearance, T = 550F, k = 1.0.

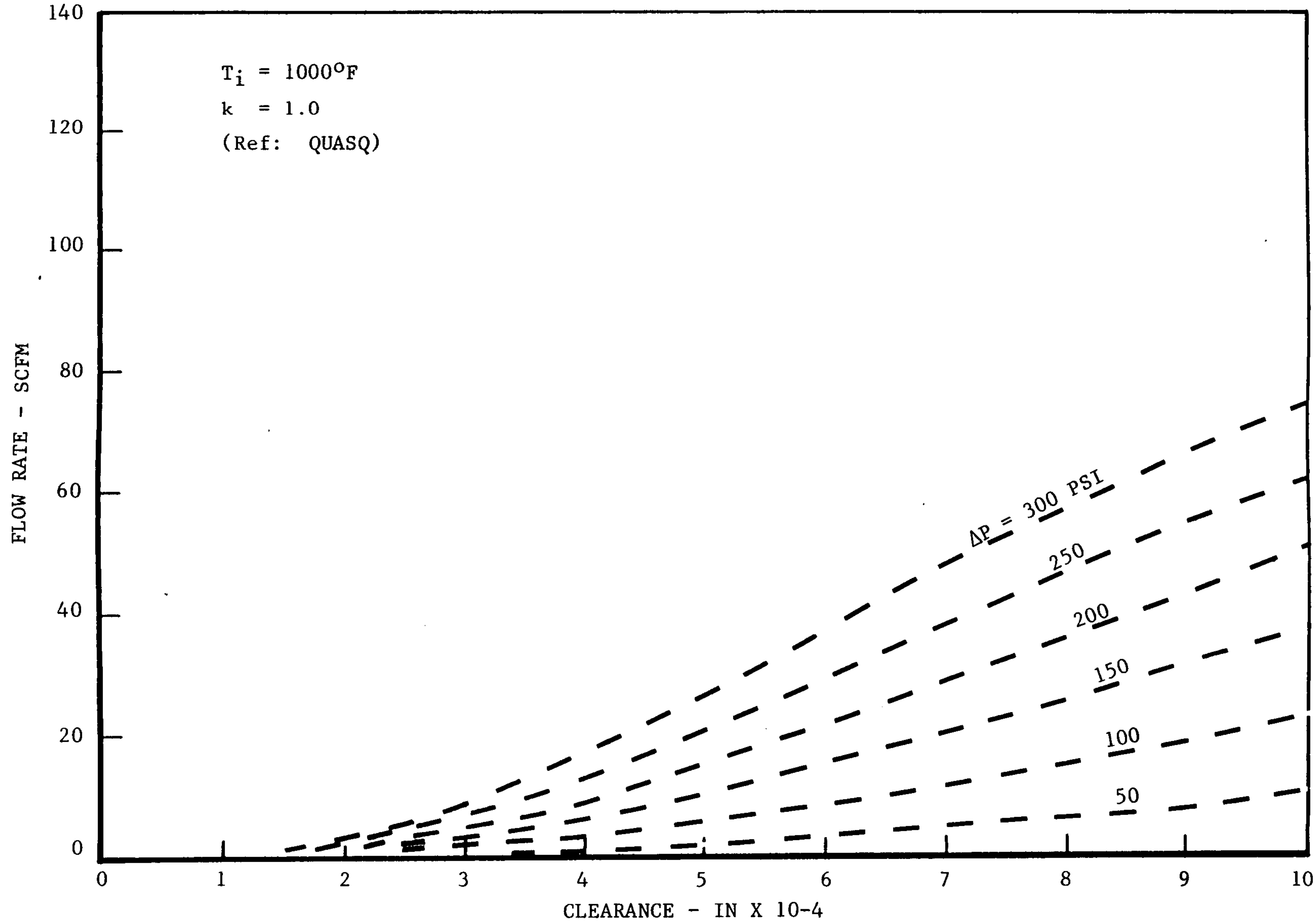

Figure 12c. Seal Dam Flow Rate vs. Clearance, T = 1000F, k = 1.0.

Several other builds were made in the static test fixture (Figures 2 and 3), also in efforts to isolate leakage sources.

A build-by-build summary of static and dynamic testing conducted in the dynamic rig is as follows:

<u>Test Build No. 1 - Static Test of Composite Slider Seal Assembly</u>

Shrouded composite slide wafer Serial Number (SN) 4 in seal housing SN 4 with 10.44 pounds (4.74 kg) spring force closing the seal face axially against the face of the seal race was static tested in the dynamic test rig to determine air leakage rates as a function of pressure drop. Data (Table 1.1) showed abnormally high leak rates, reaching 68.79 scfm (0.04 kg/sec) at 225 psid (155 N/sq cm). The cause was traced to the metal piston ring outside diameter sealing land. Per drawing, the land projects .002-.006 inch (.0051-.0152 cm) above the outside diameter of the main cross-section of the ring. Portions of the land, however, were flush with the outside diameter of the main section of the ring. This condition severely unbalances the radial pressure forces and results in "hanging" of the ring O.D. on the seal balance diameter with leakage occurring through the forced separation at the transverse interface of the ring and gland.

<u>Test Build No. 2 - Static and Dynamic Test of Composite Slider Seal</u>

A new piston ring was installed in place of the discrepant part from Build No. 1. Static air leakage rates (Table 2.1) were approximately 60 percent less than measured in Build No. 1. Although greatly reduced, the rates were still approximately 5 to 10 times higher than expected, implying the possibility of other geometric discrepancies. The second column on this table shows small changes in leak rates induced by vibrating the rig (striking the hat piece air plenum cover with a lead mallet), implying that friction at sealing interfaces was affecting leakage rates, but not significantly.

Dynamic tests were subsequently run to map leakage performance and to determine temperature rise in the seal carbon face wafer. Results are shown on Table 2.2.

TABLE 1.1

STATIC TEST
(Build 1)

Seal ΔP		Seal Air Flow		
psi	N/cm^2	kg/sec	SCFM	lb/sec
50	34.5	.0097	16.78	.0214
75	51.7	.0129	22.36	.0285
100	68.9	.0179	30.86	.0393
126	86.9	.0216	37.26	.0475
161	111.0	.0281	48.54	.0619
200	137.9	.0355	61.29	.0781
225	155.1	.0398	68.79	.0877

TABLE 2.1

STATIC TEST
(Build 2)

Seal ΔP		Seal Air Flow			(Vibrate Rig) Seal Air Flow		
N/cm^2	psid	kg/sec	SCFM	lb/sec	kg/sec	SCFM	lb/sec
11.9	25	.0014	2.47	.0031	.0009	1.64	.0021
34.5	50	.0024	4.20	.0054	.0024	4.20	.0054
51.7	75	.0043	7.41	.0094	.0036	6.18	.0079
68.9	100	.0065	11.17	.0142	.0065	11.17	.0142
86.2	125	.0089	15.41	.0196	.0071	12.33	.0157
103.4	150	.0107	18.41	.0235	.0097	16.74	.0213
120.7	175	.0124	21.55	.0275	.0104	17.96	.0229
137.9	200	.0111	19.10	.0244	.0132	22.93	.0292
158.6	230	-	-	-	.0118	20.40	.0260
160.0	232	.0130	22.53	.0287	-	-	-
103.4	150	.0078	13.39	.0171	.0078	13.39	.0171
68.9	100	.0049	8.38	.0107	.0057	9.78	.0125
34.5	50	.0018	3.15	.0040	.0018	3.15	.0040

*New Piston Ring Secondary Seal Installed

TABLE 2.2

BUILD 2 PERFORMANCE TESTING (Sheet 1 of 2)

Test Time		Sealed Air Pressure		Shaft	Seal Air				Carbon				Air Flow Rate			% of Labyrinth
					T/C #5		T/C #6		T/C #15		T/C #16					
Hrs	Min	psid	kg/cm^2	RPM	°F	°K	°F	°K	°F	°K	°F	°K	SCFM	lb/sec	kg/sec	Flow
	0	10	.7	0/5150	–	–	–	–	–	–	–	–	–	–	–	–
	5	10	.7	5150	84	302	84	302	90	305	95	308	–	–	–	–
	9	45	3.2	5150	87	303	87	303	97	309	100	311	5.08	.0065	.0029	4.04
	12	80	5.6	5150	91	306	91	306	100	311	102	312	15.30	.0195	.0088	7.72
	15	115	8.1	5150	94	307	94	307	102	312	103	312	28.32	.0361	.0164	10.46
	17	150	11.0	5150	94	307	94	307	102	312	103	312	40.29	.0514	.0233	12.30
	20	185	13.0	5150	96	309	96	309	102	312	103	312	59.12	.0754	.0342	14.21
	22	220	15.5	5150	96	309	96	309	102	312	104	313	70.07	.0894	.0405	14.33
	27	10	.7	10300	113	318	114	319	140	333	150	339	5.24	.0067	.0030	10.34
	30	45	3.2	10300	126	325	129	327	164	346	172	351	14.23	.0182	.0082	11.76
	32	80	5.6	10300	140	333	143	335	182	356	188	360	20.41	.0260	.0118	10.76
	33	115	8.1	10300	151	339	154	341	197	365	202	367	29.82	.0380	.0172	11.59
	34	150	11.0	10300	163	346	166	347	213	374	218	376	36.93	.0471	.0213	11.42
	37	185	13.0	10300	176	353	180	355	229	382	233	385	51.73	.0660	.0299	13.32
	39	220	15.5	10300	186	359	188	360	240	389	243	390	62.07	.0792	.0359	13.70
	45	100	7.0	0	150	339	180	355	190	361	206	370	8.42	.0107	.0049	3.77
	48	220	15.5	0	139	332	178	354	163	346	186	359	28.03	.0358	.0162	6.05
	52	10	.7	5150	–		–		–		–		–	–	–	–
1	8	10	.7	5150	380	466	396	475	306	425	316	431	2.62	.0033	.0015	6.29
1	12	45	3.2	5150	357	454	372	462	353	451	360	455	12.19	.0156	.0070	11.94
1	28	45	3.2	5150	388	471	401	478	380	466	385	469	14.22	.0181	.0082	14.18
1	39	80	5.6	5150	371	461	380	466	394	474	400	477	29.34	.0374	.0170	18.24
2	7	115	8.1	5150	372	462	382	467	382	467	386	470	47.71	.0609	.0276	21.67
2	18	150	11.0	5150	385	469	392	473	399	477	401	478	67.15	.0856	.0388	24.18
2	23	164	11.5	5150	373	462	380	466	390	472	392	473	80.42	.1026	.0465	26.50
2	27	167	11.8	10300	390	472	398	476	432	395	437	398	70.12	.0894	.0405	22.96
2	54	185	13.0	10300	384	469	383	468	430	494	432	495	77.60	.0990	.0448	22.98

TABLE 2.2 (Concluded)

BUILD 2 PERFORMANCE TESTING (Sheet 2 of 2)

Test Time		Sealed Air Pressure		Shaft	Seal Air				Carbon				Air Flow Rate			% of Labyrinth
					T/C #5		T/C #6		T/C #15		T/C #16					
Hrs	Min	psid	kg/cm^2	RPM	°F	°K	°F	°K	°F	°K	°F	°K	SCFM	lb/sec	kg/sec	Flow
3	6	150	11.0	10300	398	476	401	478	442	501	446	503	60.43	.0771	.0349	21.90
3	13	115	8.1	10300	370	461	372	462	417	487	422	490	46.22	.0590	.0267	20.92
3	22	80	5.6	10300	380	466	383	468	424	491	430	494	28.06	.0358	.0162	17.50
3	24	45	3.2	10300	383	468	386	470	428	493	434	496	14.23	.0182	.0082	14.10
3	26	10	.7	10300	386	470	390	472	426	492	437	498	6.55	.0084	.0038	15.72
3	37	10	.7	10300	656	620	686	636	508	537	520	544	2.62	.0033	.0015	7.26
3	45	45	3.2	10300	667	626	683	635	726	659	738	665	10.16	.0130	.0059	11.67
3	54	80	5.6	10300	645	614	663	624	686	636	695	641	30.62	.0391	.0177	21.98
4	22	115	8.1	10300	646	614	659	621	688	637	693	640	53.72	.0685	.0310	28.13
4	42	150	11.0	10300	Lost Power to Air Heater Bank											
4	46	10	.7	5000	Cannot Maintain Air Temperature											
5	17	10	.7	5000/0	Shut Down											

*"Best" configuration labyrinth of equivalent diameter, six slanted, stepped teeth against 1/16 honeycomb seat, operating at .008 inch radial clearance with no seat grooving opposite the labyrinth teeth, $(W\sqrt{T})/(P_1 A) = .28$.

Note: T/C = thermocouple, T/C #5 and 6 measure seal air inlet temperature approximately 0.5 to 1.0 inch upstream of the labyrinth seal clearance (see Figure 1). Circumferential locations are 12 o'clock and 3 o'clock (in the direction of shaft rotation). T/C #15 and 16 are embedded in the seal carbon wafer .16 inch from the sealing face (axially) and .20 inch deep from the carbon bore (radially).

The last column of Table 2.2 compares the test seal leakage with leakage rates through a "best configuration" labyrinth seal of the same diameter operating under the same conditions. Although test seal leakage is considered excessive, it is important to note that the flow rates are, in the worst case, approximately seventy-two (72) percent lower than the comparable "best configuration" labyrinth seal (see Table 2.2 for labyrinth seal description).

Carbon temperature rise relative to pressurizing air temperature showed very little change with air inlet temperatures when seal delta-P was greater than approximately 10 psi (6.9 N/sq cm). At 10 psid, with very low seal air leakage rates and immediately following a temperature transient (Table 2.2, 1 hour 8 minute point and 3 hour 57 minute point), carbon temperature is substantially lower than air inlet. Carbon temperature rise does show the effect of surface rubbing velocity, as shown in the following summary:

Shaft	Seal Delta-P		Average Temperature				(Carbon-Air) Temperature		
			Air		Carbon		Degrees F		
RPM	PSIG	N/sq cm	F	C	F	C	Min	Avg	Max
5150	10-220	7-152	92	33	100	38	7	9	12
5150	45-164	31-113	379	193	385	196	- 8	6	22
10300	10-220	7-152	152	67	198	92	33	46	55
10300	10-185	7-128	386	197	431	222	41	45	49
10300	45-150	31-103	661	349	704	374	37	44	43

Inspection following test showed average carbon face contour as shown on Figure 13. The source of this generated contour was not known at this point. If, however, it were a result of thermal section roll of the carbon face wafer assembly, generated by relative axial displacement of the centers of stiffness of the carbon and steel members of the assembly, it would be a source of increased air leakage rate past the seal face dam. Photos of the seal and race following test are shown on Figure 14.

Also observed was absence of piston ring outside diameter sealing land radial heighth adjacent to both ends of the piston ring end gap (Figure 15). Inspection of a second unused piston ring showed the same discrepancy, implying a manufacturing problem as opposed to a dynamic wear problem.

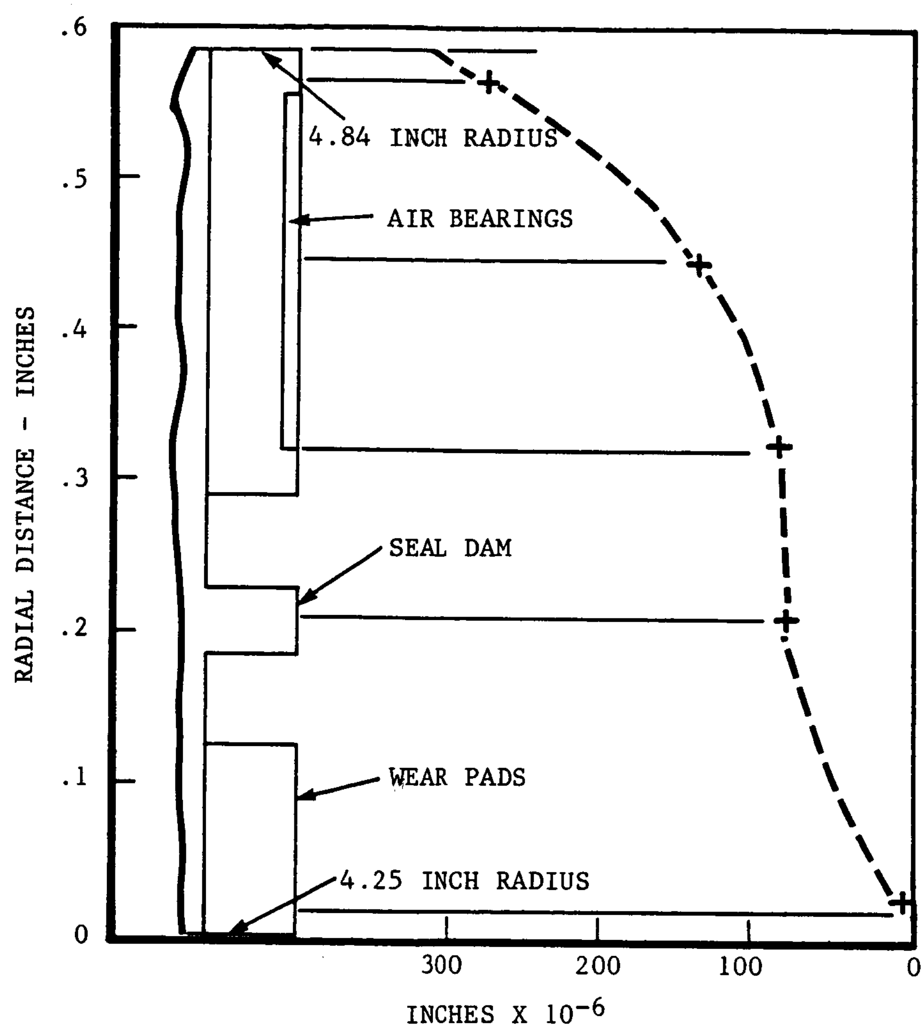

Figure 13. Composite Slider Face Contour, After Build 2.

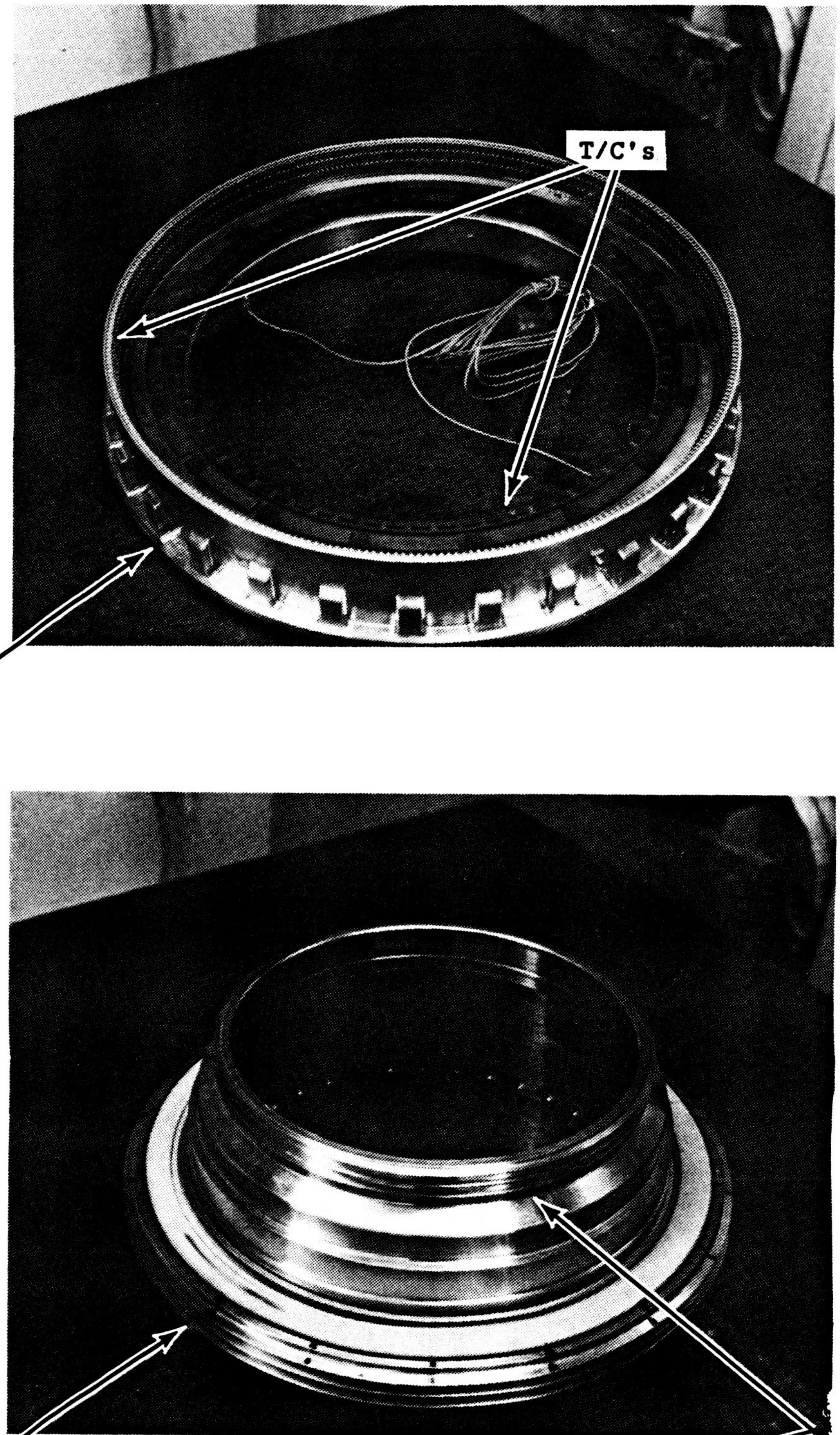

Figure 14. Seal and Race Assemblies, After Build 2.

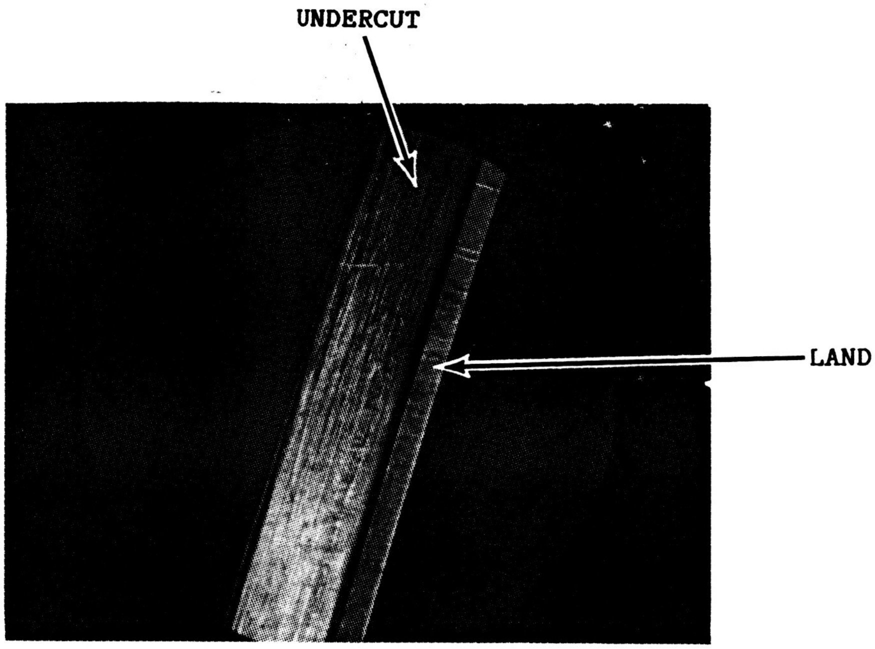

PISTON RING AFTER
R/W AFTER BUILD 2

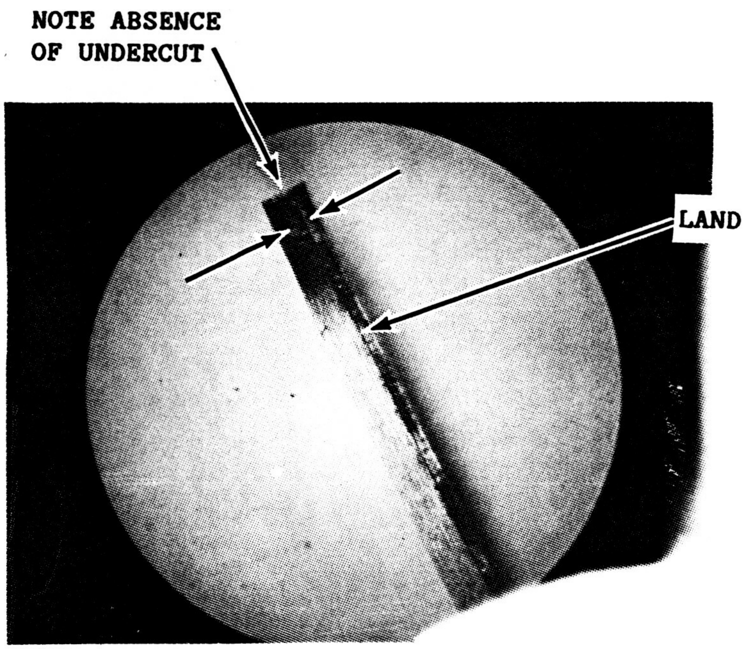

PISTON RING
AFTER BUILD 2

Figure 15. Piston Ring, After Build 2.

Test Build No. 3 - Static and Dynamic Test with Elastomer Secondary Seal

For this testing the seal face spring closing force was increased from 10.44 pounds (4.55 kg) to 17.4 pounds (7.58 kg), and an elastomeric O-ring was fitted at the secondary seal position in place of the discrepant metal piston ring. The purpose for these changes was to identify the contribution of the discrepant piston ring and/or mass inertia to excessive air leakage rates. Static test results in the dynamic rig prior to dynamic testing showed essentially zero air leakage rates throughout the test pressure range to 225 psid (155 N/sq cm). Dynamic air leakage at 115 psid (79 N/sq cm), 10,300 RPM and air inlet temperatures from 170 to 600 degrees F (77 to 316 degrees C) are shown on Table 3.1. These leakage rates are approximately 75 percent lower than experienced with the piston ring. Static leakage rates following test (Table 3.2) show a slightly erratic pattern but generally are near zero at 115 psig dynamic test pressure.

Figure 16 shows a typical area of the carbon face following test. Figure 17 shows the measured contour of the seal carbon face following Build 3 and wear measurements of the carbon face for the total of dynamic testing accumulated to date. Note that the contour has changed from approximately .000330 inch (.000838 cm) low toward the outside radius to .000100 inch (.000254 cm) high at the outside following Build 3. This represents a total contour change of approximately .00043 inch (.00109 cm) while measured wear in this area is only .00011 inch (.00028 cm). This may imply an instability in the shrink-line of the face wafer assembly, resulting from the difference in thermal expansion rates between the carbon and steel materials comprising the assembly, combined with the relatively low modulus of elasticity of the carbon material. For example, at an operating temperature of 600 degrees F the steel will expand axially approximately .0015 inch (.0038 cm) more than the carbon which may cause the carbon to be stretched and compressed axially in the vicinity of the shrink line while responding to thermal changes.

Test Build No. 4 - Static and Dynamic Test with Elastomer Secondary Seal

Transverse faces of the test adapters between the seal race and shaft were inspected and machined as necessary to assure low total axial runout

TABLE 3.1

BUILD 3 PERFORMANCE TESTING (O-RING SECONDARY)

Test Time		Sealed Air Pressure		Shaft	Seal Air				Air Flow Rate			% of Labyrinth	
					T/C #5		T/C #6						
Hrs	Min	psid	kg/cm²	RPM	°F	°K	°F	°K	SCFM	lb/sec	kg/sec	Flow*	Remarks
	0	100	7.0	0	-	-	-	-	-	-	-	-	
	3	115	8.1	5150	-	-	-	-	≈0	≈0	≈0	≈1.00	
	10	115	8.1	10300	170	350	175	352	8.95	.0114	.0052	3.53	
	18	115	8.1	10300	217	376	223	379	23.85	.0304	.0138	9.76	
	20	115	8.1	10300	226	381	230	383	14.91	.0190	.0086	6.14	
	22	115	8.1	10300	235	386	239	388	8.95	.0114	.0052	3.71	
	24	115	8.1	10300	238	387	242	390	5.96	.0076	.0034	2.48	
	32	115	8.1	10300	250	394	256	397	8.95	.0114	.0052	3.75	
	38	115	8.1	10300	267	404	273	407	8.95	.0114	.0052	3.80	
	44	115	8.1	10300	280	411	286	414	8.95	.0114	.0052	3.83	
	54	115	8.1	10300	310	427	316	431	10.44	.0133	.0060	4.56	
1	3	115	8.1	10300	345	447	350	450	11.93	.0151	.0069	5.32	
1	9	115	8.1	10300	378	465	385	469	11.93	.0151	.0069	5.43	
1	16	115	8.1	10300	401	478	409	482	11.93	.0151	.0069	5.51	
1	24	115	8.1	10300	424	491	432	495	13.42	.0171	.0078	6.28	
1	31	115	8.1	10300	452	506	462	512	11.93	.0151	.0069	5.67	
1	39	115	8.1	10300	500	533	510	539	11.93	.0151	.0069	5.82	
1	44	115	8.1	10300	520	544	532	551	13.42	.0171	.0078	6.62	
1	49	115	8.1	10300	544	557	555	564	13.42	.0171	.0078	6.69	
1	54	115	8.1	10300	569	571	581	578	11.93	.0151	.0069	6.03	
2	1	115	8.1	10300	592	584	603	590	13.42	.0171	.0078	6.85	
2	7	115	8.1	10300	454	507	456	509	40.25	.0513	.0233	19.11	
2	20	115	8.1	10300	371	461	371	461	31.31	.0399	.0181	14.17	
3	1	115	8.1	10300	330	439	330	439	34.29	.0437	.0198	15.13	

TABLE 3.2

STATIC TEST
(Build 3)

Seal ΔP		Air Temp		Seal Air Flow			
N/cm^2	psid	°F	°C	kg/sec	SCFM	lb/sec	Remarks
69	100	RT		0	0	0	Before Dynamic Test
155	225	RT		–	*	–	Before Dynamic Test
7	10	100	38	–	–	–	After Dynamic Test
14	20	100	38	–	–	–	After Dynamic Test
21	30	100	38	–	–	–	After Dynamic Test
28	40	100	38	–	–	–	After Dynamic Test
35	50	100	38	–	–	–	After Dynamic Test
41	60	100	38	–	–	–	After Dynamic Test
48	70	100	38	–	–	–	After Dynamic Test
55	80	100	38	–	–	–	After Dynamic Test
62	90	100	38	–	–	–	After Dynamic Test
69	100	100	38	–	–	–	After Dynamic Test
76	110	100	38	–	–	–	After Dynamic Test
83	120	100	38	–	–	–	After Dynamic Test
90	130	100	38	–	–	–	After Dynamic Test
97	140	100	38	.0038	6.51**	.0083	After Dynamic Test
103	150	100	38	.0039	6.71	.0085	After Dynamic Test
110	160	100	38	.0040	6.91	.0088	After Dynamic Test
117	170	100	38	.0062	10.66	.0136	After Dynamic Test
124	180	100	38	.0063	10.95	.0139	After Dynamic Test
131	190	100	38	.0065	11.22	.0143	After Dynamic Test
138	200	100	38	.0066	11.49	.0146	After Dynamic Test
145	210	100	38	.0068	11.76	.0150	After Dynamic Test
155	225	100	38	.0070	12.14	.0155	After Dynamic Test

*Too low to read on rotometer.

**Readings are below calibrated scale on rotometer. All readings are visually extrapolated.

ORIGINAL PAGE IS
OF POOR QUALITY

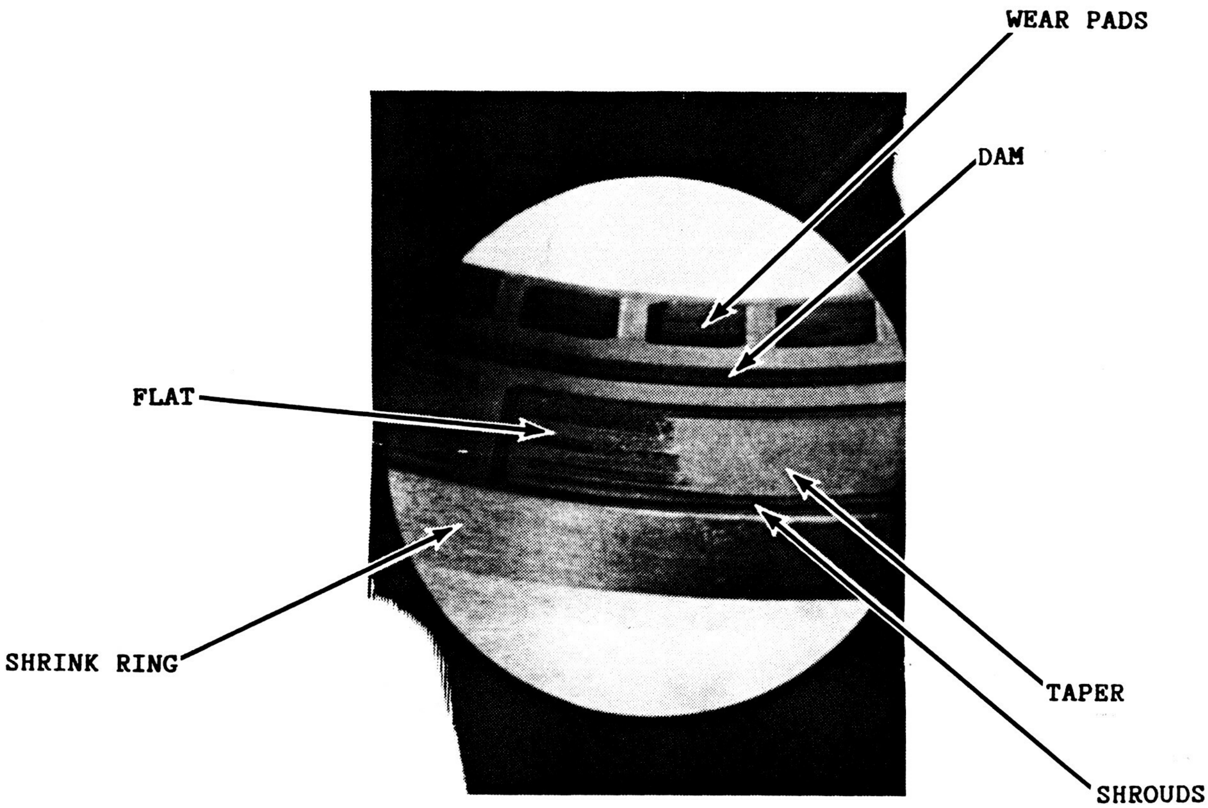

Figure 16. Carbon Face, After Build 3.

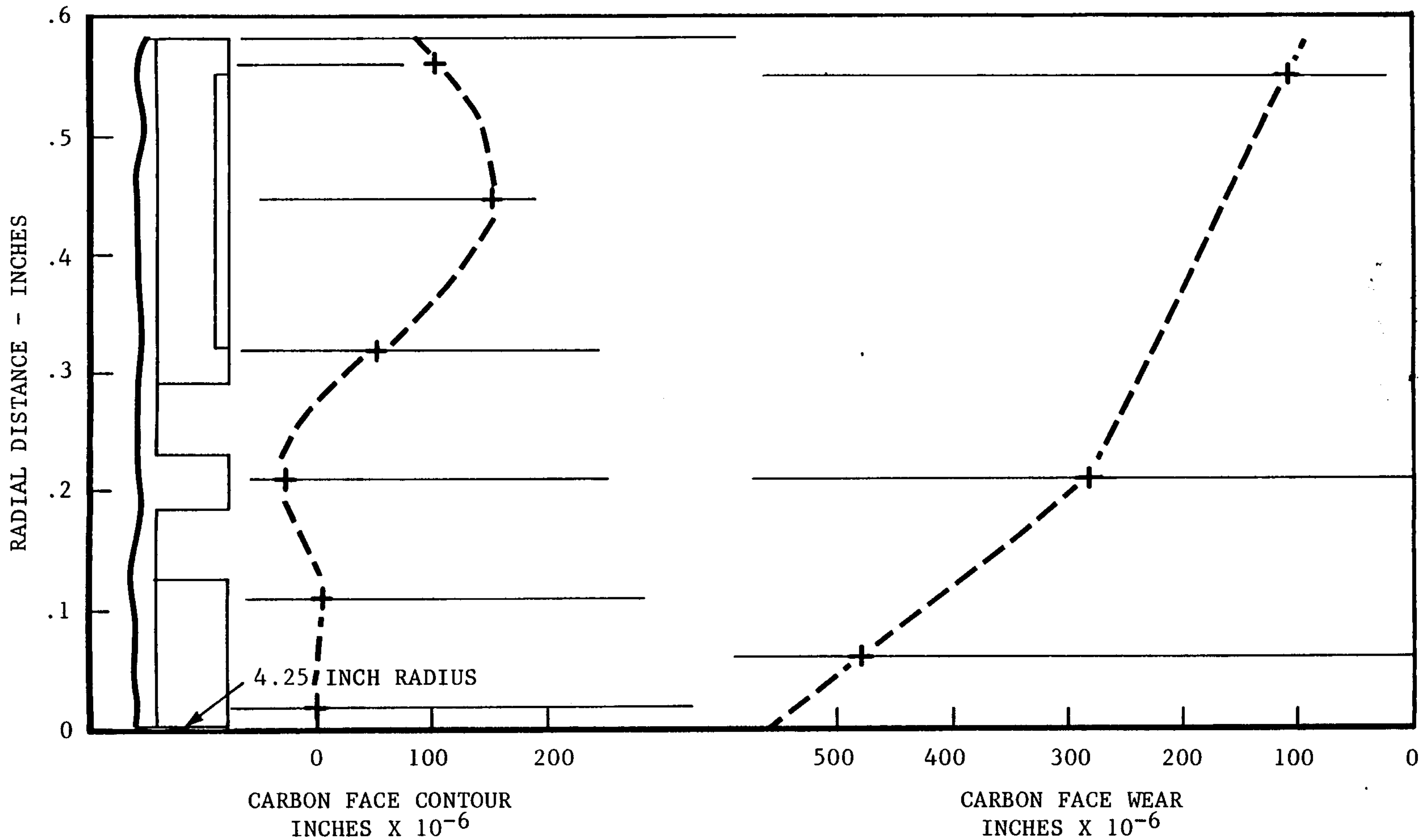

Figure 17. Carbon Face Measurements, After Build 3.

[<.001 inch (.00254 cm)] of the face of the seal race. Bench measurements also showed that excessive radial pilot interference at the seal housing interface to the dynamic rig adapter flange, and rig flange out-of-flatness, was forcing a .004 inch (.01 cm) reduction in the size of the seal balance diameter. This condition, which would affect an additional pneumatic closing force on the seal equal to 6.44 lbs (2.92 kg) at 115 psid (79.3 N/sq cm), was corrected by reworking the rig adapter flange.

The axial spring closing force in the seal assembly was reduced from 17.44 lbs (Build 3) to the design force of 10.44 lbs. Static testing was conducted to determine seal air leakage rates.

Static leakage rates as measured before and after dynamic testing are shown on Table 4.1. Comparing dynamic leakage rates from this test (Table 4.2) to the previous test (Table 3.1), where the sum of spring and gas pressure closing force was approximately 13.4 lbs (6.08 kg) greater, shows no significant change. Results may imply that seal inertia in conjunction with reasonably low race face runout does not contribute significantly to increases in seal air leakage rates; however, no conclusion with respect to operating with a piston ring secondary seal should be drawn due to the possible damping affect of the elastomer O-ring used in this test.

Figure 18 shows the measured contour of the seal carbon face following dynamic test. Comparing the contour to that shown in Figure 17 shows little change. This may imply that the wafer assembly has stabilized significantly after completion of the first thermal cycle (see Build 3). Air leakage during this test was approximately five (5) percent of that expected through a labyrinth of equivalent diameter.

Test Build No. 5 - NASA Design Stepped Pad Bearing and O-Ring Secondary

This was the first build made with a seal carbon wafer containing the NASA designed shrouded step lift pad air bearings. All other hardware was the same as Build 4. Seal spring force was 10.44 lbs, total. In addition to the change in lift pad configuration, the temperatures of the seal components at

TABLE 4.1

STATIC TEST
(Build 4)

Seal ΔP psid	Seal ΔP kg/cm^2	Sealed Air Temp °F	Sealed Air Temp °C	Air Flow Rate kg/sec	Air Flow Rate SCFM	Air Flow Rate lb/sec	Remarks
10	.7	80	27	.0010	1.71	.0022	Before Dynamic Test
25	1.8	80	27	.0010	1.66	.0021	Before Dynamic Test
50	3.5	80	27	.0018	3.17	.0040	Before Dynamic Test
75	5.3	80	27	.0022	3.73	.0048	Before Dynamic Test
100	7.0	80	27	.0032	5.61	.0071	Before Dynamic Test
125	8.7	80	27	.0036	6.19	.0079	Before Dynamic Test
150	11.0	80	27	.0048	8.39	.0107	Before Dynamic Test
175	12.3	80	27	.0059	10.18	.0130	Before Dynamic Test
200	14.1	80	27	.0066	11.49	.0146	Before Dynamic Test
225	15.8	80	27	.0082	14.16	.0180	Before Dynamic Test
100	7.0	104	40	.0016	2.81	.0036	After Dynamic Test
125	8.7	104	40	.0018	3.09	.0039	After Dynamic Test
150	11.0	104	40	.0019	3.36	.0043	After Dynamic Test
175	12.3	104	40	.0031	5.40	.0069	After Dynamic Test
200	14.1	104	40	.0066	11.49	.0146	After Dynamic Test
225	15.8	109	43	.0070	12.14	.0155	After Dynamic Test

TABLE 4.2

DYNAMIC TESTS
(Build 4)

Lapsed Time		Shaft	Air Temp		Seal ΔP		Air Flow Rate			% of Labyrinth	
Hrs	Min	RPM	°C	°F	kg/cm^2	psid	kg/sec	SCFM	lb/sec	Flow	Remarks
	3	0/10300		-	7.037	100	-	-	-	-	Accelerate to 10300 RPM
	6	10300	54	130	8.093	115	.0052	8.95	.0114	3.14	
	17	10300	79	175	8.093	115	.0052	8.95	.0114	3.54	
	29	10300	101	214	8.093	115	.0052	8.95	.0114	3.65	
	39	10300	121	250	8.093	115	.0052	8.95	.0114	3.74	
	51	10300	149	300	8.093	115	.0052	8.95	.0014	3.87	
	60	10300	179	354	8.093	115	.0060	10.44	.0133	4.68	
1	10	10300	207	404	8.093	115	.0060	10.44	.0133	4.82	
1	16	10300	235	455	8.093	115	.0052	8.95	.0114	4.25	
1	25	10300	277	531	8.093	115	.0060	10.44	.0133	5.16	
1	30	10300	304	579	8.093	115	.0052	8.95	.0114	4.53	
1	34	10300	321	610	8.093	115	.0060	10.44	.0133	5.36	
1	39	10300		-	8.093	115	-	-	-	-	Heaters Off
1	53	10300		-	8.093	115	-	-	-	-	
2	0	10300		-	8.093	115	-	-	-	-	Shutdown

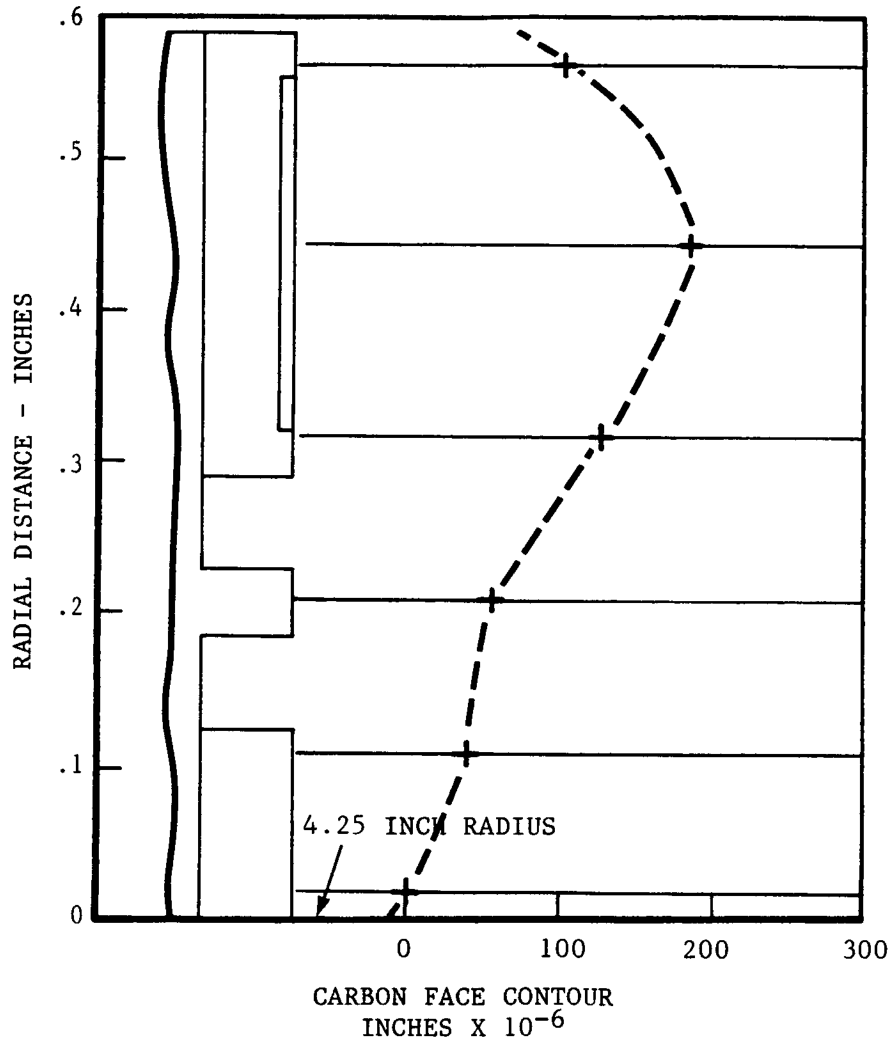

Figure 18. Carbon Face Contour, After Build 4.

the piston ring carrier and housing balance diameter were measured. The purpose of the measurements was to determine if significant thermal clearance changes are generated in the radial gap between these seal components. It should be noted that thermally generated interference would contribute to carbon face wear and leakage, and additional clearance could contribute to pneumatic force unbalance and frictional "hanging" of the piston ring with subsequent affect on leakage rates.

The test consisted of one (1) thermal cycle while increasing air inlet temperature from room temperature to 612 degrees F (322 degrees C), with the seal pressurized to 115 psid (79.3 N/sq cm) and shaft speed at 10,300 RPM. Seal dynamic performance results are shown on Table 5.1. Static air leakage rates were below the readable scale of the rotometer (approximately zero leakage) throughout the test pressure range to 225 psid (155 N/sq cm) prior to dynamic testing.

Dynamic air leakage rates were low in the air temperature range through 612 degrees F, not exceeding 17.9 scfm (.0104 kg/sec). As air inlet temperature was reduced, however, leakage increased and reached 77 scfm (.045 kg/sec) at 270 degrees F (132 degrees C). This was a result of thermal failure of the elastomer O-ring, which bonded firmly onto the seal housing balance diameter and totally lost its sealing integrity (see Figure 19). Static leakage after cooling to room temperature was 70 scfm (.04 kg/sec) at 10 psid (6.895 N/sq cm).

Recorded temperatures of the seal housing and piston ring carrier vs. air inlet temperature are shown on Table 5.2. No significant thermal differences relative to air leakage rates or seal face wear were observed.

Following test, all hardware with the exception of the elastomer O-ring were in good condition (see Figures 19 and 20).

Test Build No. 6 - Static Tests with Reworked Metal Piston Ring

Static testing was conducted with a metal piston ring (Design 1) which had been reworked to provide a .01 inch (.0254 cm) radial relief on the

TABLE 5.1

DYNAMIC TEST/O-RING SECONDARY
(Build 5)

Test Time		Pressure		Shaft	Air Temp		Air Flow Rate			% of Labyrinth	
Hrs	Min	psid	N/cm^2	RPM	°F	°K	SCFM	lb/sec	kg/sec	Flow	Remarks
	13	115	79	0/10300	–		–	–	–	–	
		(Shutdown to Calibrate Speed Pickup)									
	20	115	79	0/10300	–		–	–	–	–	
		(Shutdown to Rework Speed Pickup)									
	28	115	79	10300	153	340	5.96	–	–	2.32	
	30	115	79	(Heater Power On)							
	36	115	79	10300	200	366	8.9	.0076	.0034	3.59	
	44	115	79	10300	236	386	8.9	.0076	.0034	3.69	
	51	115	79	10300	268	404	10.4	.0133	.0060	4.41	
1	1	115	79	10300	323	435	11.9	.0152	.0069	5.23	
1	10	115	79	10300	396	475	11.9	.0152	.0069	5.47	
1	18	115	79	10300	450	505	13.4	.0171	.0077	6.35	
1	26	115	79	10300	500	533	16.4	.0209	.0095	7.98	
1	38	115	79	10300	556	564	16.4	.0209	.0095	8.21	
1	41	115	79	10300	604	591	14.9	.0190	.0086	7.63	
1	47	115	79	(Heaters Off)	612	595	17.9	.0228	.0103	9.20	
1	58	115	79	10300	593	585	16.4	.0209	.0095	8.35	
2	6	115	79	10300	544	557	26.8			–	*O-Ring Bonded to Seal
2	14	115	79	10300	480	522	43.2			–	Balance Diameter
2	26	115	79	10300	424	491	56.6			–	Because of Thermal
2	36	112	77	10300	380	466	67.7	*		–	Deterioration Causing
2	49	70	48	10300	298	420	74.8			–	Leakage Rate Increase
2	56	62	43	10300	270	405	77.0			–	
2	58			(Shutdown)	200	366	–			–	

TABLE 5.2

HARDWARE TEMPERATURES
(Build 5)

12 o'clock	3 o'clock	Carrier	Housing	Housing	Carrier	Remarks
150	153	172	177	5		Data Taken from Sandborn Trace Build 5
175	200	220	219	– 1		
220	236	246	242	– 4		
250	268	272	279	7		
300	323	318	320	2		
382	396	379	382	3		
440	450	433	437	4		
490	500	480	480	0		
548	556	538	537	– 1		
598	604	582	579	– 3		
602	612	612	602	–10		
580	593	584	582	– 2		
527	544	552	552	0		
460	480	487	493	6		
402	424	422	430	8		
359	380	376	383	7		
268	298	298	287	–11		
238	270	265	282	17		
200	200	250	258	8		

(°F)

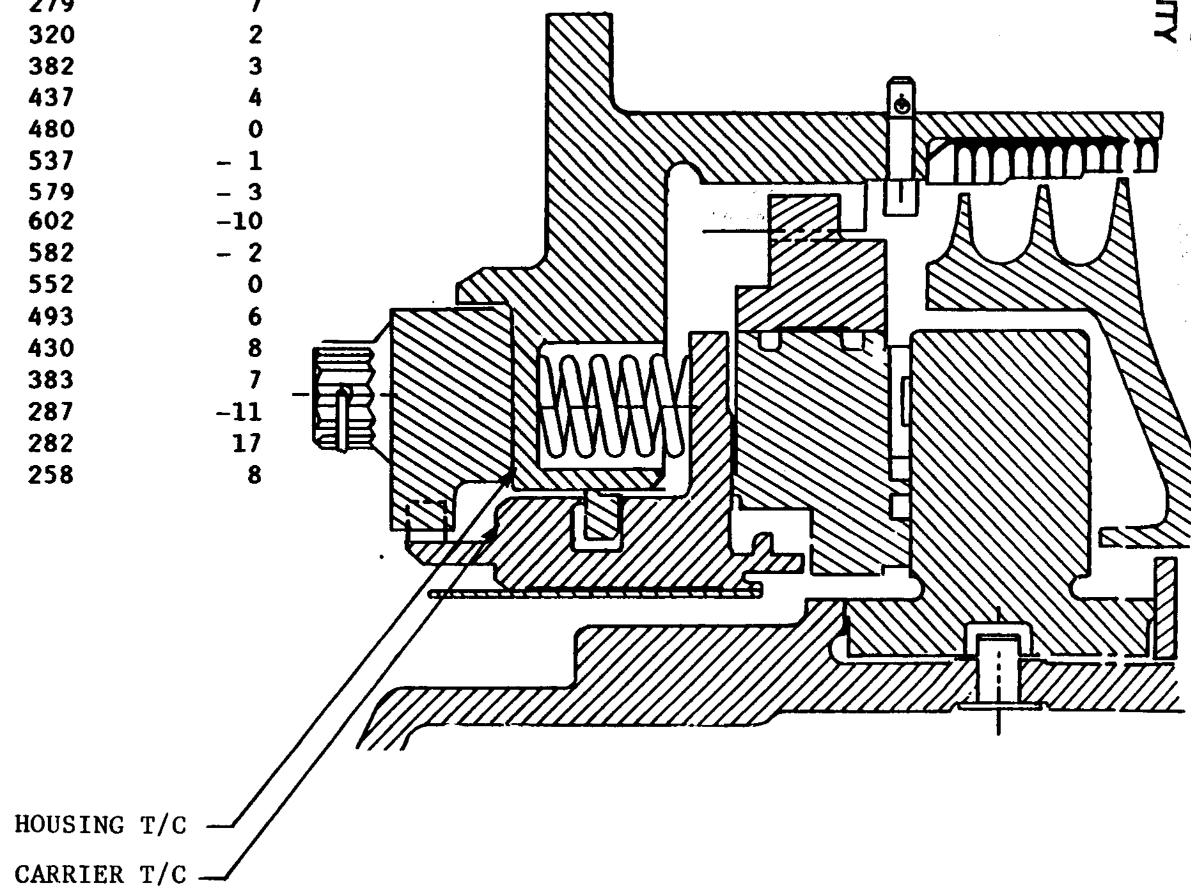

ORIGINAL PAGE IS
OF POOR QUALITY

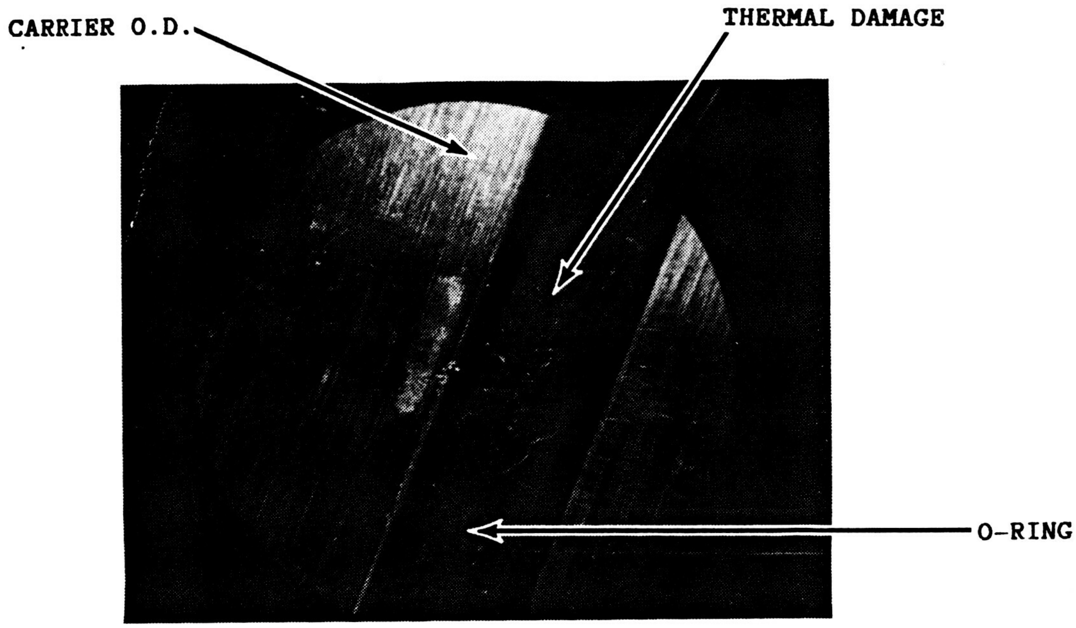

Figure 19. O-Ring Secondary, After Build 5.

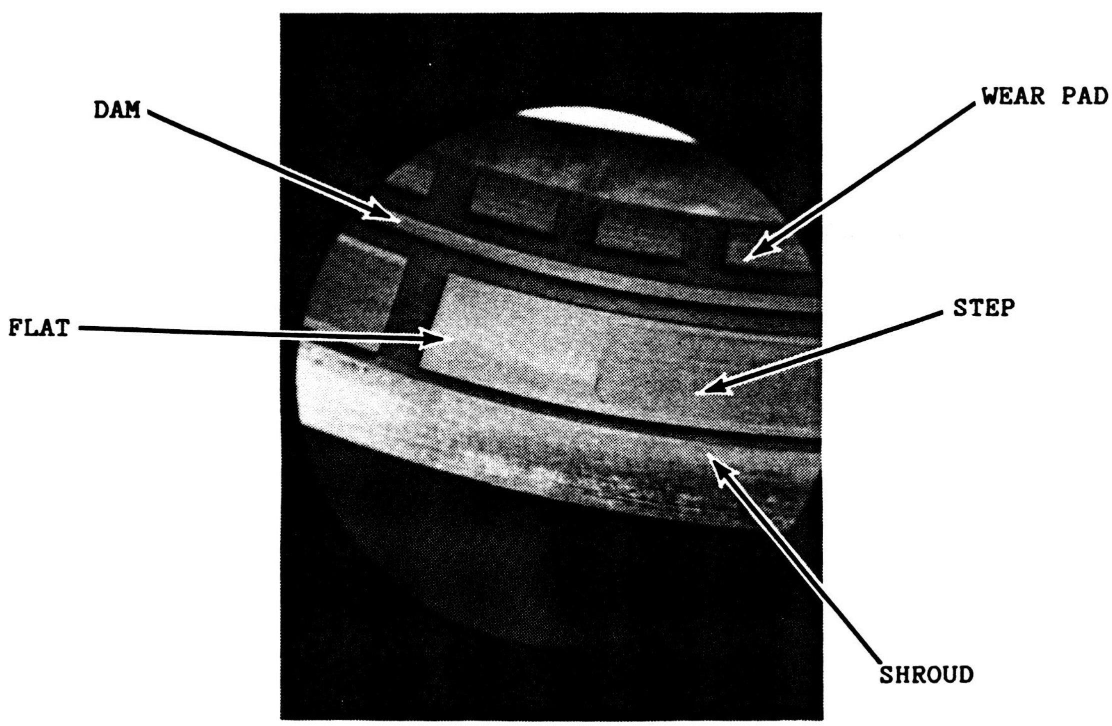

Figure 20. Typical Face Pad Area, After Build 5.

outside diameter adjacent to the sealing land. Results (Table 6.1) show no improvement in air leakage rates when compared to data on Table 2.1 (prior to rework of piston ring), and were two to three times the rates with an elastomer O-ring secondary seal (Tables 3.2 and 4.1). The secondary was inspected and found not light-tight at the housing balance diameter to piston ring interface, and the piston ring sealing land in the piston ring carrier was found to be .00032 inch (.00081 cm) out-of-flat circumferentially. Inspection of the other available housing and piston ring carriers also gave poor results and one housing (serial number 2) and two piston ring carriers (S/N 1 and 4) were scheduled for rework. One housing (S/N 4) and one piston ring carrier (no S/N) were retained for further testing on Builds 7 and 8.

Carrier sealing land circumferential flatness per drawing is .000030 inch (.000076 cm). Measured flatness showed the following:

Carrier S/N	Flatness (Circumferential)
(No S/N)	.000080 inch (.00020 cm)
1	.000110 inch (.00028 cm)
4	.000320 inch (.00081 cm)

Test Build No. 7 - Static and Dynamic Tests with Hardware Changes

Testing was conducted with the shrouded composite slider air bearing with 10.44 pounds spring closing force and metal piston ring secondary. Static testing (Table 7.1) shows high air flow rates which are nearly identical to the flow rates measured in Build 6 which had a different housing and piston ring carrier.

Results of three (3) hours, twenty-two (22) minutes of dynamic testing are shown on Table 7.2. The maximum pressure during testing was 185 psid (127.6 N/sq cm), and maximum sealed air temperature was 990 degrees F (532 degrees C). Higher pressures could not be run because of flow rate limitation of the air supply compressor.

Figure 21 shows seal face contour and wear through all testing to date. It is noted that face contour has changed during this test (see Figure 18, Build 4), but no additional average wear has occurred:

TABLE 6.1

STATIC TEST
(Build 6)

Seal ΔP		Seal Air Flow			
N/cm^2	psid	kg/sec	SCFM	lb/sec	Remarks
138	200	.0133	22.98	.0293	Air Temperature ≃ 80°F (27°C)
121	175	.0115	19.81	.0252	
103	150	.0106	18.47	.0235	
86	125	.0089	15.47	.0197	
69	100	.0081	14.03	.0179	
52	75	.0057	9.94	.0127	
35	50	.0049	8.46	.0108	
11	25	.0032	5.56	.0071	
7	10	.0019	3.31	.0042	

TABLE 7.1

STATIC TEST
(Build 7)

Seal ΔP		Seal Air Flow			
N/cm^2	psid	kg/sec	SCFM	lb/sec	Remarks
7	10	.0008	1.31	.0017	Air Temperature ≃ 80°F (27°C)
17	25	.0019	3.33	.0042	Prior to Dynamic Testing
28	40	.0034	5.84	.0074	Prior to Dynamic Testing
35	50	.0049	8.46	.0108	Prior to Dynamic Testing
52	75	.0057	9.94	.0127	Prior to Dynamic Testing
69	100	.0065	11.22	.0143	Prior to Dynamic Testing
86	125	.0072	12.38	.0158	Prior to Dynamic Testing
103	150	.0078	13.43	.0171	Prior to Dynamic Testing
121	175	.0114	19.81	.0252	Prior to Dynamic Testing
138	200	.0133	22.98	.0293	Prior to Dynamic Testing
155	225	.0140	24.28	.0309	Prior to Dynamic Testing
7	10	.0053	9.17	.0117	After Dynamic Testing
31	45	.0153	26.42	.0337	After Dynamic Testing
55	80	.0258	44.65	.0569	After Dynamic Testing
79	115	.0362	62.62	.0798	After Dynamic Testing

TABLE 7.2

BUILD 7 (Sheet 1 of 2)

Test Time		Sealed Air Pressure			Temperature								
				Shaft	Seal Air				Air Flow Rate			% of Labyrinth	
					T/C #5		T/C #6						
Hrs	Min	psid	N/cm²	RPM	°F	°K	°F	°K	SCFM	lb/sec	kg/sec	Flow	Remarks
	0	115	79	0	83	301	83	301	14.91	.0190	.0086	5.46	
	2	115	79	5150	88	304	84	302	20.87	.0266	.0121	7.66	
	19	115	79	10300	164	346	167	348	23.85	.0304	.0138	9.37	
	12	115	79	10300	375	364	375	464	26.84	.0342	.0155	10.55	
1	14	115	79	5150	372	362	374	463	26.84	.0342	.0155	12.16	
2	31	115	79	10300	681	634	682	634	32.80	.0418	.0190	17.40	
3	1	115	79	5150	692	640	698	643	26.84	.0342	.0155	14.32	
–	–	10	7	0	77	298	76	297	5.83	.0074	.0034	11.13	
–	–	25	17	0	77	298	76	297	9.86	.0126	.0057	11.71	
–	–	50	34	0	77	298	76	297	12.59	.0161	.0073	9.18	
–	–	75	52	0	77	298	76	297	19.87	.0253	.0115	10.45	
–	–	100	69	0	77	298	76	297	23.85	.0304	.0138	9.18	
–	–	125	86	0	77	298	76	297	27.84	.0355	.0161	9.40	
–	–	150	103	0	77	298	76	297	31.90	.0406	.0184	9.14	
–	–	175	121	0	77	298	76	297	39.62	.0505	.0229	9.85	
–	–	200	138	0	78	299	74	296	61.29	.0790	.0354	13.46	
3	32	115	79	10300	258	399	259	399	29.82	.0380	.0172	12.55	
3	51	115	79	10300	356	453	356	453	34.29	.0437	.0198	15.38	
4	27	115	79	10300	449	505	450	505	35.78	.0456	.0207	16.94	
4	42	115	79	10300	552	562	552	562	35.78	.0456	.0207	17.87	
5	8	115	79	10300	651	617	653	618	35.78	.0456	.0207	18.73	
5	9	150	103	10300	639	610	640	611	52.04	.0664	.0301	21.33	
5	10	185	128	10300	617	598	617	598	66.51	.0848	.0384	22.26	
5	12	80	55	10300	646	614	648	615	20.41	.0260	.0118	14.60	
5	14	45	31	10300	676	630	678	632	12.19	.0155	.0704	14.25	
5	16	10	7	10300	712	651	716	653	5.24	.0067	.0030	14.80	

TABLE 7.2 (Concluded)

BUILD 7 (Sheet 2 of 2)

Test Time		Sealed Air Pressure		Temperature								% of Labyrinth	
				Shaft	Seal Air				Air Flow Rate				
					T/C #5		T/C #6						
Hrs	Min	psid	N/cm²	RPM	°F	°K	°F	°K	SCFM	lb/sec	kg/sec	Flow	Remarks
5	21	115	79	5150	715	652	720	655	29.82	.0308	.0172	16.07	
5	24	150	103	5150	681	634	684	635	43.65	.0557	.0252	18.24	
5	26	185	128	5150	661	622	662	623	55.43	.0707	.0320	18.93	
5	28	80	55	5150	664	624	669	627	22.96	.0293	.0133	16.57	
5	30	45	31	5150	677	631	680	633	10.16	.0130	.0059	11.69	
5	31	10	7	5150	687	637	689	638	3.93	.0050	.0023	10.98	
6	7	80	55	10300	946	781	944	780	20.41	.0260	.0118	16.45	
6	9	115	79	10300	948	782	949	782	32.80	.0418	.0190	19.33	
6	12	150	103	10300	824	713	825	714	47.00	.0599	.0272	20.83	
6	14	45	31	10300	795	697	799	699	12.19	.0155	.0070	14.74	
6	16	10	7	10300	805	702	808	704	3.93	.0050	.0023	11.53	
(Shutdown to Repair Heater Circuit)													
8	13	80	55	10300	935	775	939	777	29.34	.0374	.0170	23.58	
8	15	45	31	10300	954	785	962	790	16.26	.0207	.0094	20.89	
8	17	115	79	10300	944	780	947	781	41.75	.0532	.0241	24.57	
8	19	150	103	10300	908	760	909	760	58.75	.0749	.0339	26.87	
8	21	10	7	10300	929	771	930	772	3.93	.0050	.0023	12.08	
8	25	80	55	5150	977	798	986	803	24.24	.0309	.0140	19.79	
8	26	115	79	5150	984	802	990	805	37.27	.0475	.0215	22.26	
8	28	150	103	5150	949	782	956	786	50.36	.0642	.0291	23.40	
8	30	185	128	5150	890	750	893	751	64.66	.0825	.0374	24.24	
8	31	45	31	5150	898	754	904	757	12.19	.0155	.0070	15.34	
8	33	10	7	5150	913	762	921	767	3.93	.0050	.0023	12.02	
9	38	45	31	5150	367	459	367	459	16.29	.0208	.0094	15.98	

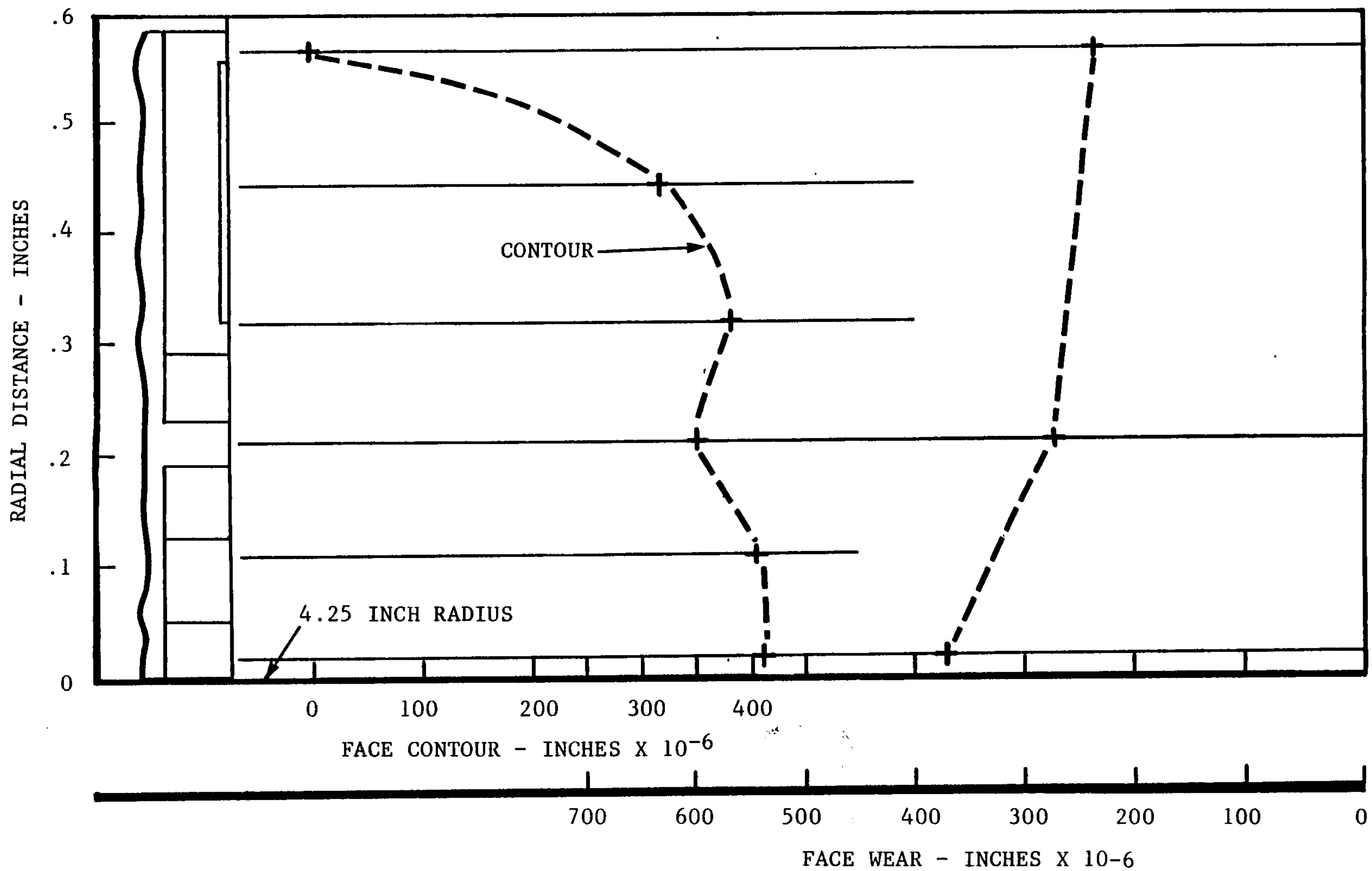

Figure 21. Carbon Face Measurements, After Build 7.

	Cumulative Test Time	Cumulative Average Face Wear
After Build 4	10 hrs, 19 min	.000290 inch (.000737 cm)
After Build 7	19 hrs, 57 min	.000290 inch (.000737 cm)

Test Build No. 8 - Static and Dynamic Tests, NASA Designed Step Bearing

Static and dynamic testing was conducted with a seal wafer containing the NASA designed shrouded stepped pad air bearing, with 10.44 lbs (4.74 kg) total spring force and metal piston ring secondary. With the exception of the carbon wafer, all hardware was the same as used in Build 7.

Dynamic test results are shown on Table 8.1. Maximum air temperature and pressure achieved during dynamic testing were 970 degrees F (521 degrees C) and 223 psid (154 N/sq cm). Static air leakage rates prior to and following dynamic tests are shown on Table 8.2.

Figure 22 shows carbon face contour and wear for all stepped pad seal testing to date (Build 5 plus Build 8) after a total operating time of 6 hours 53 minutes. Seal face contour and wear show a similarity. Average wear is .000287 inch (.000729 cm) and at this point is nearly identical to wear on the wafer with the GE designed shrouded tapered gas bearings (.000290 inch average), which again may imply an axial differential thermal expansion instability in the carbon to steel shrink line of the seal face wafer assembly (see Build 3).

Test Builds 9 through 13 - Static Leakage Evaluation

This sequence of builds and static testing was done in an effort to isolate the cause for the abnormally high air leakage rates experienced with seals tested utilizing metal piston ring secondary seals. Results are compared to data from Build 8 and are summarized on Table 9.1 and as follows:

Build 9 - Installed seal housing S/N 2 with newly lapped balance diameter and changed the carbon wafer and piston ring carrier. Otherwise the hardware was the same as in Build 8. Air leakage was still excessive.

TABLE 8.1

BUILD 8 (Sheet 1 of 2)

Test Time Hrs	Test Time Min	Sealed Air Pressure psid	Sealed Air Pressure N/cm^2	Shaft RPM	Temperature Seal Air T/C #5 °F	T/C #5 °K	T/C #6 °F	T/C #6 °K	Air Flow Rate SCFM	Air Flow Rate lb/sec	Air Flow Rate kg/sec	% of Labyrinth Flow*	Remarks
	1	10	7	5150	83	301	83	301	1.31	.0017	.0008	2.51	
	2	45	31	5150	88	304	88	304	8.13	.0104	.0047	6.49	
	3	80	55	5150	89	305	89	305	16.58	.0211	.0096	8.35	
	5	115	79	5150	92	306	92	306	32.80	.0418	.0190	12.10	
	6	150	103	5150	93	307	93	307	50.36	.0642	.0291	14.64	
	8	185	128	5150	96	309	96	309	68.36	.0872	.0395	16.44	
	-	220	152	5150	-		-		-	-	-	-	
	10	10	7	10300	98	310	98	310	1.96	.0025	.0011	3.82	
	13	45	31	10300	110	316	110	316	8.13	.0104	.0047	6.62	
	15	80	55	10300	127	326	127	326	15.31	.0195	.0088	7.98	
	16	115	79	10300	139	332	139	332	29.82	.0380	.0172	11.46	
	17	150	103	10300	153	340	153	340	40.29	.0514	.0233	12.33	
	18	185	128	10300	164	346	164	346	55.43	.0707	.0320	14.12	
	23	215	148	10300	185	358	185	358	65.37	.0833	.0378	14.22	
1	35	80	55	10300	365	458	368	460	16.58	.0211	.0096	10.25	
1	37	115	79	10300	365	458	366	459	26.33	.0361	.0152	12.78	
1	38	150	103	10300	359	455	359	455	40.29	.0514	.0233	14.28	
1	40	45	31	10300	363	457	365	458	9.14	.0117	.0053	8.95	
1	42	10	7	10300	370	461	374	463	5.24	.0067	.0030	12.46	
1	43	185	128	10300	363	457	364	457	59.12	.0754	.0342	17.29	
1	45	195	134	10300	354	452	354	452	58.68	.0748	.0339	16.28	
1	49	80	55	5150	348	449	348	449	7.86	.0100	.0045	4.80	
1	55	80	55	5150	365	458	368	460	7.86	.0100	.0045	4.86	
1	57	115	79	5150	364	457	365	458	31.31	.0399	.0181	14.12	
1	58	150	103	5150	355	452	355	452	48.68	.0621	.0281	17.18	
2	0	45	31	5150	363	457	367	459	9.14	.0116	.0053	8.95	
2	2	10	7	5150	376	464	381	467	2.62	.0033	.0015	6.25	

TABLE 8.1 (Concluded)

BUILD 8 (Sheet 2 of 2)

Test Time		Sealed Air Pressure		Shaft	Temperature Seal Air T/C #5		Temperature Seal Air T/C #6		Air Flow Rate			% of Labyrinth	Remarks
Hrs	Min	psid	N/cm^2	RPM	°F	°K	°F	°K	SCFM	lb/sec	kg/sec	Flow*	
2	4	185	128	5150	372	462	374	463	60.97	.0778	.0352	17.94	
2	45	80	55	5150	655	619	675	630	19.14	.0244	.0111	13.80	
2	47	115	79	5150	650	616	667	627	32.80	.0418	.0190	17.22	
2	49	150	103	5150	620	600	632	606	53.72	.0685	.0310	21.89	
2	51	45	31	5150	618	598	636	609	10.16	.0130	.0059	11.43	
2	55	185	128	5150	645	614	657	620	55.43	.0707	.0320	18.84	
2	57	10	7	5150	654	619	671	628	2.62	.0033	.0015	7.24	
2	58	195	134	5150	665	625	680	633	54.90	.0700	.0317	17.94	
3	6	115	79	10300	685	636	696	642	34.29	.0437	.0198	18.26	
3	8	150	103	10300	669	627	678	632	45.32	.0578	.0262	18.87	
3	10	185	128	10300	644	613	650	616	59.12	.0754	.0342	20.05	
3	11	80	55	10300	653	618	667	624	20.41	.0258	.0117	14.69	
3	12	45	31	10300	683	635	699	644	11.18	.0143	.0065	12.94	
3	15	10	7	10300	718	654	736	664	5.24	.0067	.0030	14.88	
3	28	45	31	10300	933	774	962	790	12.19	.0155	.0070	15.60	
3	29	80	55	10300	942	779	964	791	19.14	.0244	.0111	15.47	
3	30	115	79	10300	923	768	942	779	29.82	.0380	.0172	17.47	
3	32	10	7	10300	922	767	948	782	5.24	.0067	.0030	16.14	
3	33	150	103	10300	921	767	946	781	33.57	.0428	.0194	15.55	
3	35	185	128	10300	873	740	886	747	51.73	.0660	.0299	19.31	
3	46	80	55	5150	942	779	970	794	17.86	.0228	.0103	14.45	
3	48	115	79	5150	945	780	969	794	26.84	.0342	.0155	15.86	
3	49	150	103	5150	928	771	947	781	38.61	.0492	.0223	17.84	
3	50	45	31	5150	934	774	958	787	8.13	.0104	.0047	10.40	
3	52	185	128	5150	925	769	943	779	48.04	.0613	.0278	18.28	
3	54	10	7	5150	920	766	943	779	1.31	.0017	.0008	4.03	
3	55	223	154	5150	848	726	858	731	64.47	.0822	.0373	20.01	

TABLE 8.2

STATIC TEST
(Build 8)

Seal ΔP		Air Temp		Seal Air Flow			
N/cm^2	psid	°K	°F	kg/sec	SCFM	lb/sec	Remarks
7	10	302	85	.0030	5.24	.0067	Before Dynamic Test
17	25	302	85	.0058	9.98	.0127	Before Dynamic Test
34.5	50*	302	85	.0098	16.91	.0215	Before Dynamic Test - *(Rig Vibrated)
		302					
58	75	302	85	.0057	9.94	.0127	Before Dynamic Test
69	100	302	85	.0081	14.03	.0179	Before Dynamic Test
86	125	302	85	.0107	18.56	.0236	Before Dynamic Test
103	150	302	85	.0167	28.86	.0368	Before Dynamic Test
121	175	302	85	.0187	32.42	.0413	Before Dynamic Test
138	200	302	85	.0232	40.22	.0512	Before Dynamic Test
35	50*	302	85	.0055	9.51	.0121	Before Dynamic Test - *(Rig Vibrated)
35.5	50	302	85	.0054	9.40	.0120	Before Dynamic Test
17	25	302	85	.0024	4.16	.0053	Before Dynamic Test
7	10	302	85	.0015	2.62	.0033	Before Dynamic Test
7	10	306	92	.0011	1.96	.0025	After Dynamic Test
17	25	306	92	.0029	4.99	.0064	After Dynamic Test
35	50	306	92	.0043	7.40	.0094	After Dynamic Test
52	75	306	92	.0057	9.94	.0127	After Dynamic Test
69	100	306	92	.0089	15.43	.0197	After Dynamic Test
86	125	306	92	.0125	21.66	.0276	After Dynamic Test
103	150	306	92	.0213	36.93	.0470	After Dynamic Test
121	175	306	92	.0271	46.82	.0596	After Dynamic Test
138	200	306	92	.0354	61.29	.0781	After Dynamic Test

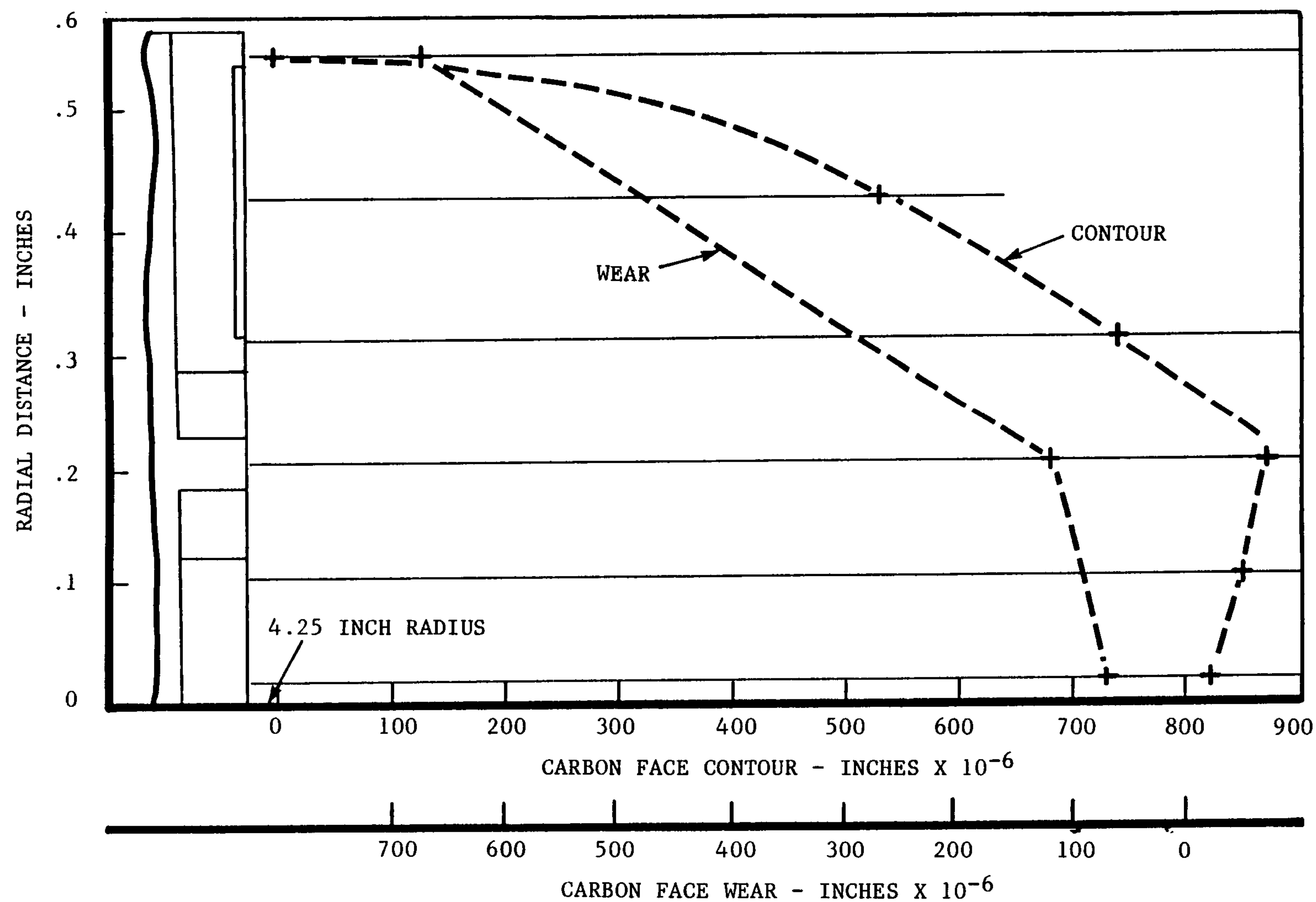

Figure 22. Carbon Face Measurements, After Build 8.

TABLE 9.1

STATIC TEST SUMMARY, BUILDS 8 THROUGH 13

Sealed Air Pressure PSIG	Build 8 Before Dynamic Test	Build 8 After Dynamic Test	Build 9	Build 10	Build 11	Build 12	Build 13
10	5.24	1.96	2.62	–	.65	–	1.31
25	9.98	4.99	6.66	–	1.66	–	3.33
50	16.91	7.40	8.46	–	4.23	–	7.40
75	9.94*	9.94	13.66	–	7.45	–	11.18
100	14.03	15.43	16.83	–	11.22	–	14.03
125	18.56	21.66	20.11	–	13.92	–	18.56
150	26.86	36.93	25.18	–	16.79	–	23.50
175	32.42	46.82	32.42	–	25.21	–	30.62
200	40.22	61.29	40.22	68.00	45.97	7.66	38.31
50	9.51						
50	9.40*						
25	4.16						
10	2.62						
	(SCFM)						

(*Vibrate Rig)

	Build 8 Before Dynamic Test	Build 8 After Dynamic Test	Build 9	Build 10	Build 11	Build 12	Build 13
Housing Serial No.	4	4	2	2	2	2	2
Lapped Balance Diameter	No	No	Yes	Yes	Yes	Yes	Yes
Piston Ring Relief (O.D.)	.01	.01	.01	.01	.01	–	.01
Relapped Piston Ring	No	No	No	Yes	Yes	–	Yes
O-Ring Secondary	–	–	–	–	–	–	–
Piston Ring Carrier Serial Number	None	None	1	1	1	1	1
Seat Lapped in Piston Ring Carrier	No	No	Yes	Yes	Yes	Yes	Yes
Carbon Face Wafer Serial Number	1	1	4	3	3	3	3
Carbon Face Wafer Design	NASA	NASA	GE	GE	GE	GE	GE
Carbon Face Wafer Condition	New	Used	Used	New	New	New	New
Seal Mounted Squareness	?	?	?	?	?	.0009 to .0023/in	.00024 /in
Flange Out-of-Flatness (Rig)	?	?	?	?	?	?	.00045/ in saddle

Build 10 - Changed to a new carbon wafer and a relapped piston ring. Otherwise same as Build 9. Leakage very excessive.

Build 11 - No hardware change. Teardown and rebuild, only. Leakage excessive but significantly reduced from Build 10.

Build 12 - Same as Build 11 except that an elastomer O-ring was installed in place of the piston ring in the seal secondary. As shown in past tests, leakage was again very significantly reduced.

Following the above test the face squareness of the test rig seal mounting flange was measured while installed on the test rig. It was found to vary from .0009 to .0023 in/in (cm/cm) of diameter, depending on the circumferential orientation. Since this would directly affect squareness of the piston ring to its radial and axial seats, it could also affect air leakage.

Build 13 - The seal housing rig adapters were shimmed at appropriate locations to reduce face out-of-squareness to .00024 in/in (cm/cm) of diameter. Air leakage was still excessive.

Following the above static test, the two rig adapters were removed from the test rig and measured while bolted together to determine seal housing adapter flange flatness. The flange surface was found to be saddled in the magnitude of .00045 in/in (cm/cm) of radius. This could distort the seal housing balance diameter (piston ring radial seat) in the form of a saddle.

Test Build Nos. 14 through 19 - Static Hardware Leakage Evaluation

Following Build 13 the seal housing rig adapters were reworked to provide .0004 inch (.001 cm) flatness and parallelism between flange faces. In addition, the seal housing flange (S/N 2) was measured and found to have a .003 to .004 inch (.0076 to .0102 cm) radial taper across the flange width. Since this could also distort the seal housing balance diameter when bolted to the seal adapter flange in the test rig, it was also reworked to obtain

flatness within .0004 inch (.00102 cm). Selective assembly was made in the ensuing six builds to try again to isolate the cause of excessive air leakage rates. Again, no cause was clearly identified. Results are shown on Table 14.1 and are described as follows:

Build 14 - This build was made after reworking the test rig flange and seal housing adapter flange as described above. Leakage rate was reduced from 38.31 scfm (.0488 lbs/sec) in Build 13 to 30.65 scfm (.0391 lbs/sec) with seal air pressure at 200 psid (137.9 N/sq cm). This rate, however, is still excessive.

Build 15 - A different carbon face wafer assembly and piston ring were installed. The piston ring was made from carbon steel with flash chrome plated surfaces and did not contain the aluminum oxide inlay on the transverse sealing face as did all other piston rings previously tested. The piston ring is not completely light tight when assembled inside the balance diameter of seal housing serial number 2. Leakage was very excessive.

Build 16 - This build was otherwise the same as Build 15 with the exception that a light tight piston ring (S/N 1) was installed. Leakage improved from Build 15 but was higher than Build 14 where a new carbon face wafer was used.

Build 17 - This build was otherwise the same as Build 16 except that piston ring carrier S/N 1 was substituted for S/N 4. This resulted in increased leakage over Build 16.

Build 18 - This build was otherwise the same as Build 16 except that a piston ring with vented wear pads on its outside diameter was substituted for piston ring S/N 1 (light tight piston ring). This piston ring was not light tight when installed inside the balance diameter of seal housing S/N 2. Minimum leakage at 200 psid (137.9 N/sq cm) is the same as Build 16 but is not stable, and maximum leakage exceeded Build 16.

TABLE 14.1

STATIC TEST SUMMARY, BUILDS 14 THROUGH 19

Sealed Air Pressure PSIG	Build 14	Build 15	Build 16	Build 17	Build 18	Build 19
10	-	-	-	-	-	-
25	-	-	-	-	-	1.66
50	2.11	-	4.23	5.29	2.11	4.23
75	3.73	-	7.45	6.21	4.97	7.45
100	7.02	-	11.22	9.82	8.42	9.82
125	12.33	-	13.92	12.38	10.83	10.83
150	15.11	-	18.47	16.79	15.11	13.43
175	21.61	-	25.21	28.81	21.61	21.61
200	30.65	53.63	38.31	45.97	38.31/44.05	30.64/45.97
	(SCFM)					

	Build 14	Build 15	Build 16	Build 17	Build 18	Build 19
Housing Serial Number	2	2	2	2	2	2
Lapped Balance Diameter	Yes	Yes	Yes	Yes	Yes	Yes
Piston Ring Relief (O.D.)	.01	.01	.01	.01	.01	.01
Relapped (Light Tight) Piston Ring O.D.	Yes	No	Yes	Yes	No	Yes
Piston Ring S/N (or Identification)	1	Flash Chrome	1	1	O.D. Pads	1
Piston Ring Carrier Serial Number	3	3	3	1	3	3
Seat Lapped in Piston Ring Carrier	Yes	Yes	Yes	Yes	Yes	Yes
Carbon Face Wafer Serial Number	2	4	4	4	4	4
Carbon Face Wafer Design	NASA	GE	GE	GE	GE	GE
Carbon Face Wafer Condition	New	Used	Used	Used	Used	Used
Seal Flange Rework	Yes	Yes	Yes	Yes	Yes	Yes
Rig Flange Rework	Yes	Yes	Yes	Yes	Yes	Yes

Build 19 - This build was otherwise the same as Build 16 except that the radial clearance between the seal housing balance diameter and the piston ring carrier outside diameter was shimmed to promote concentricity between the balance diameter and the piston ring carrier. This reduced the minimum leakage compared to Build 16 at higher pressures but was unstable and the maximum leakage exceeded that from Build 16.

Following the above sequence of unsuccessful static tests conducted in an effort to isolate a source of abnormally high air leakage rates, a meeting was held with the NASA Technical Program Director. This meeting resulted in a recommendation to proceed with endurance testing per Cycle A wherein maximum seal delta-P is 202 psi (139.3 N/sq cm) since the limited available flow rate capacity of the air supply would otherwise continue to preclude testing at higher pressures.

Test Build No. 20 - Endurance Test, Shrouded Composite Slider Bearing

Sixty-three and one-half (63.5) hours of endurance testing was completed at Cycle A operating conditions using seal face carbon wafer assembly S/N 4 with the GE designed shrouded composite slider gas bearings. Prior to this test 13.28 test hours had been accumulated on this same carbon wafer during Builds 2, 3, 4 and 7. The wafer was not reworked prior to test.

Actual hours and percent time at Cycle A conditions were as follows:

	Cycle Point	Hours	% Time
Ground Idle	A-1	18.8	29.61
Take-off	A-2	11.9	18.74
Cruise	A-3	32.8	51.65

Static air leakage rates measured before test are shown on Table 20.1. Table 20.2 gives data, including air leakage rates, taken during dynamic testing.

TABLE 20.1

STATIC TEST
(Build 20)

Seal ΔP		Seal Air Flow			Remarks
N/cm^2	psid	kg/sec	SCFM	lb/sec	
7	10	0	≈0	0	(Room Temperature)
17	25	0	≈0	0	
35	50	.0012	2.11	.0027	
52	75	.0036	6.21	.0079	
68	100	.0057	9.82	.0125	
86	125	.0089	15.47	.0197	
103	150	.0116	20.14	.0256	
121	175	.0156	25.21	.0321	
138	200	.0221	38.31	.0488	

TABLE 20.2

BUILD 20 (Sheet 1 of 2)

Test Time		Sealed Air Pressure		Shaft	Temperature: Seal Air T/C #5		Temperature: Seal Air T/C #6		Air Flow Rate			% of Labyrinth	
Hrs	Min	psid	N/cm^2	RPM	°F	°K	°F	°K	SCFM	lb/sec	kg/sec	Flow	Remarks
3	0	9	6	1180	450	505	–		≃0	–	–	–	
18	48	9	6	1180	200	366	200	366	≃0	–	–	–	
21	12	125	86	7480	280/	411	280/	411(1)	24.0	.0306	.0139	12.32	(1) See Note 1.
					780	689	780	689					
22	12	125	86	7440	780	689	780	689	21.0	.0268	.0121	10.78	
22	42	125	86	7460	800	700	800	700	21.0	.0268	.0121	10.87	
23	12	125	86	7440	825	714	815	708	52.4	.0668	.0303	27.33	
23	42	125	86	7420	835	719	830	716	21.0	.0268	.0121	10.99	
24	12	125	86	7460	825	714	820	711	22.5	.0287	.0130	11.73	
24	48	125	86	7440	840	722	830	716	21.0	.0268	.0121	11.02	
25	42	125	86	7410	860	733	870	739	24.6	.0314	.0142	13.05	
26	49	125	86	7420	880	744	880	744	24.6	.0314	.0142	13.13	
27	12	125	86	7420	785	691	783	690	22.0	.0281	.0127	11.31	
41	42	125	86	7440	754	674	750	672	21.0	.0268	.0121	10.66	
42	12	125	86	7460	720	655	720	655	20.0	.0255	.0116	10.01	
42	42	125	86	7470	815	708	810	705	20.09	.0255	.0116	10.40	
43	12	125	86	7460	785	691	780	689	20.0	.0255	.0116	10.28	
44	12	125	86	7460	815	708	820	711	21.0	.0268	.0121	10.94	
44	18	125	86	7460	960	789	–		22.0	.0281	.0127	12.08	
44	30	202	139	7460	920	766	–		46.0	.0587	.0266	16.06	
44	42	202	139	7935	920	766	–		–	–	–	–	
–	–	202	139	7960	914	763	910	761	46.0	.0587	.0266	16.16	
45	12	202	139	7960	865/	736	–	(2)	–	–	–	–	(2) See Note 2.
					920	766							
–	–	202	139	7960	913	762	–		46.0	.0587	.0266	16.17	
46	12	202	139	7960	876/	742	–		46.0	.0587	.0266	16.29	
					934	774							
46	42	202	139	7960	946	781	942	779	46.0	.0587	.0266	16.20	
–	–	202	139	7960	955	786	–		–	–	–	–	
47	12	202	139	7960	910	761	908	760	46.0	.0587	.0266	15.99	
47	42	205	141	7960	890	750	887	748	46.0	.0587	.0266	15.66	
48	30	202	139	7960	920	766	918	765	49.0	.0625	.0283	17.10	
49	48	202	139	7960	942	779	939	777	59.0	.0752	.0341	20.75	

TABLE 20.2 (Concluded)

BUILD 20 (Sheet 2 of 2)

Test Time Hrs	Test Time Min	Sealed Air Pressure psid	Sealed Air Pressure N/cm²	Shaft RPM	Temperature Seal Air T/C #5 °F	T/C #5 °K	T/C #6 °F	T/C #6 °K	Air Flow Rate SCFM	Air Flow Rate lb/sec	Air Flow Rate kg/sec	% of Labyrinth Flow	Remarks
50	12	202	139	7960	950	783	948	782	30.0	.0383	.0173	10.58	
50	42	202	139	7950	940	777	938	776	48.0	.0612	.0277	16.87	
51	12	200	138	7960	935	775	933	774	48.0	.0612	.0277	17.00	
51	42	200	138	7960	945	780	943	779	48.0	.0612	.0277	17.06	
52	12	200	138	7960	944	780	942	779	54.0	.0689	.0312	19.18	
53	12	202	139	7960	960	789	954	785	46.0	.0587	.0266	16.27	
53	42	200	138	7960	945	780	943	779	47.0	.0600	.0272	16.70	
54	12	202	139	7960	940	777	938	776(3)	46.0	.0587	.0266	16.17	(3) See Note 3.
54	42	200	138	7960	920	766	–		58.0	.0740	.0335	20.44	
55	12	200	138	7960	930	772	–		48.0	.0612	.0277	16.97	
55	42	200	138	7950	935	775	–		48.0	.0612	.0277	17.00	
56	12	200	138	7920	920	766	–		49.0	.0625	.0283	17.26	
–	–	(One Heater Bank Out)											
56	42	125	86	7480	820	711	860	733	21.5	.0274	.0124	11.30	
57	12	125	86	7510	810	705	–		22.0	.0281	.0127	11.43	
57	42	125	86	7350	810	705	–		22.0	.0281	.0127	11.43	
63	30	125	86	7400	813	707	–		22.0	.0281	.0127	11.43	Test Stopped, Bearing Failure. See Note 4.

Notes: (1) Seal leakage increased to ≃ 93 SCFM for a few seconds then returned to normal.

(2) Leakage cycled to 85 SCFM and returned over a 5 minute period, then cycled to 65 SCFM in about 3 minutes. Cycling continued to occur with diminishing variation in flow rate over the next six hours. Increased flow rate was accompanied by decrease in air inlet temperature and pressure. Raising air inlet temperature appears to increase the cyclic air flow rate.

(3) Rig seems to be running rougher, possibly bearing noise.

(4) Duplex bearing failed, shaft shifted axially causing the seal to bottom out against the seal race. Torque increased and drive belt disengaged from shaft. Seal pressure dropped from 125 to 70 PSIG and seal leakage (static) increased to 76 SCFM.

It is noted in the log sheets (Table 20.2) that there was a tendency towards cyclic flow rates when stabilizing at high temperature and pressure. This may imply a cyclic axial thermal gradient in the seal assembly, particularly at the interface of carbon wafer and race where the resulting thermal deflection can force a change in the seal dam to race clearance. This situation may be aggravated by the configuration of test apparatus since any small change in air flow rate affects a change in air temperature because the air heaters are set at a constant power input. This is unlike the situation in an engine installation.

Failure of the duplex thrust bearing assembly while endurance testing the lift pad seal resulted in heavy wear on the face of seal carbon wafer (S/N 4) and resulted in moderate rub tracks in the hard plated surface of the seal race. The failure caused damage to the bearing journals on both the shaft and rig housing such that both were in non-serviceable condition. (See photographs on Figures 23, 24 and 25.)

Table 20.3 shows carbon wear rates following the thrust bearing failure 63.5 hours after initiation of the endurance test. When the duplex bearing failed, the rotor shifted axially until the seal bottomed in its housing and the entire gas pressure thrust force was supported at the dynamic interface of the seal carbon and race. Operating pressure at initiation of the failure was 125 psid (86.2 N/sq cm) and decreased to 70 psid (48.3 N/sq cm) at time of rig shutdown. The thrust force at these pressures is 7776 and 4355 pounds (3387 and 1897 kg), respectively. The resulting carbon specific load is in the order of 500 to 1000 psi (345 to 689 N/sq cm), which, of course, is an extremely high wearing load.

Inspection of the wear rates shown on Table 20.3 implies that the seal was functioning with minimum wear until the bearing failure. The wear pattern on the carbon face is symmetrical, with the maximum wear occurring approximately 180 degrees from the minimum, where no wear occurred. The uniform, symmetrical wear pattern may be the result of out-of-squareness at internal interfaces of the seal assembly in the compressed position following bearing failure.

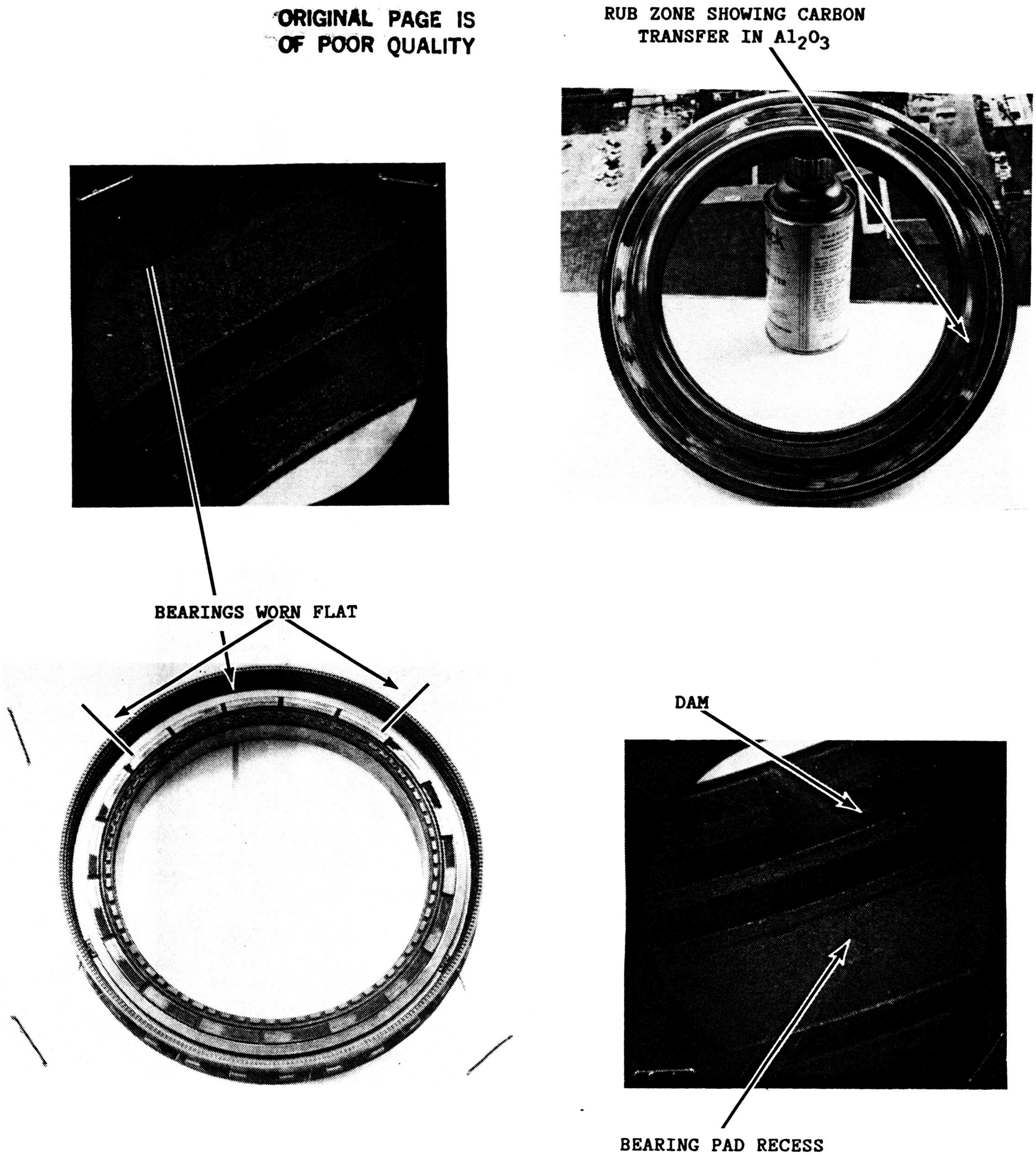

Figure 23. Seal Face and Race After Bearing Failure, Build 20.

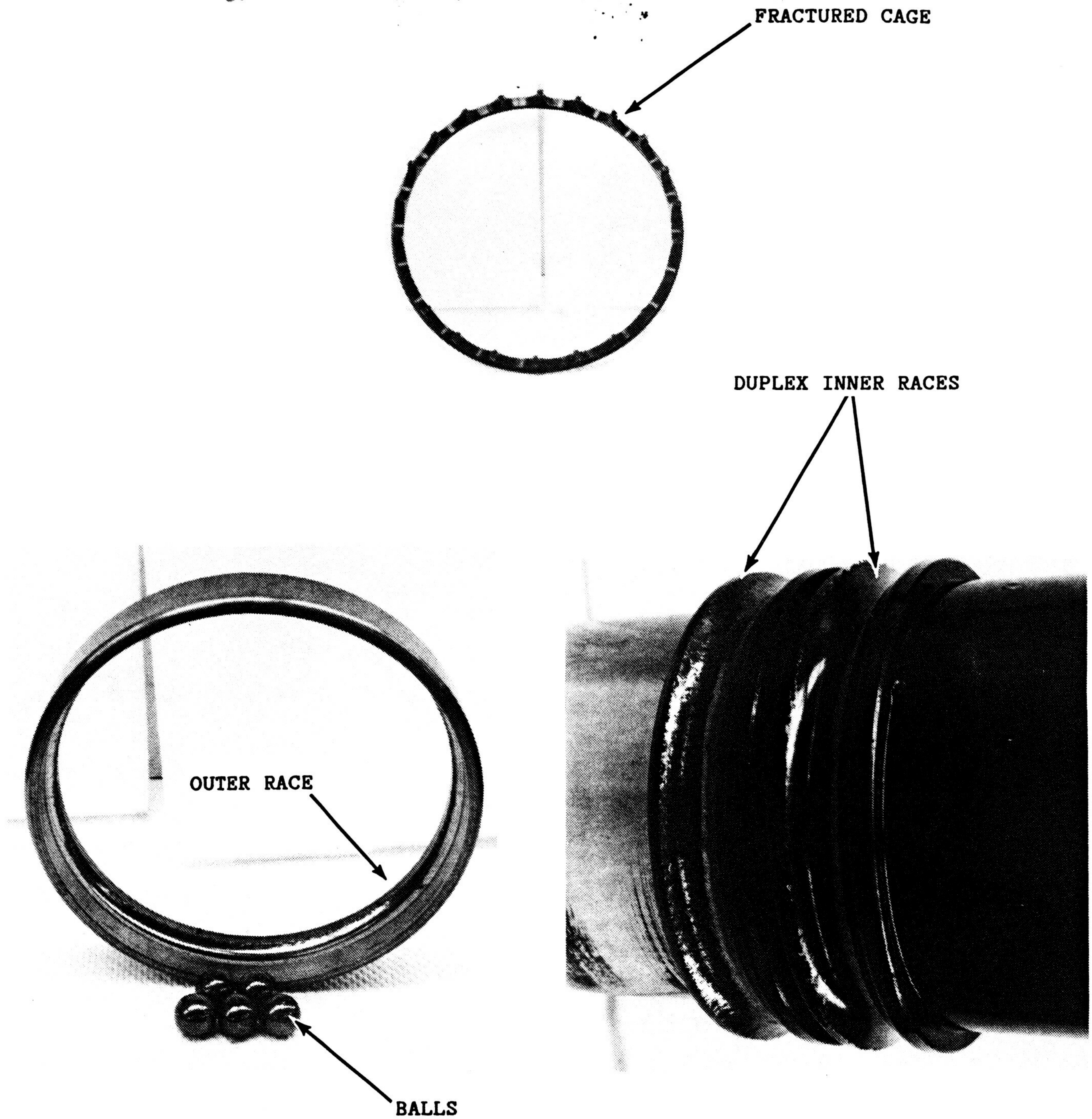

Figure 24. Failed Thrust Bearing, Build 20.

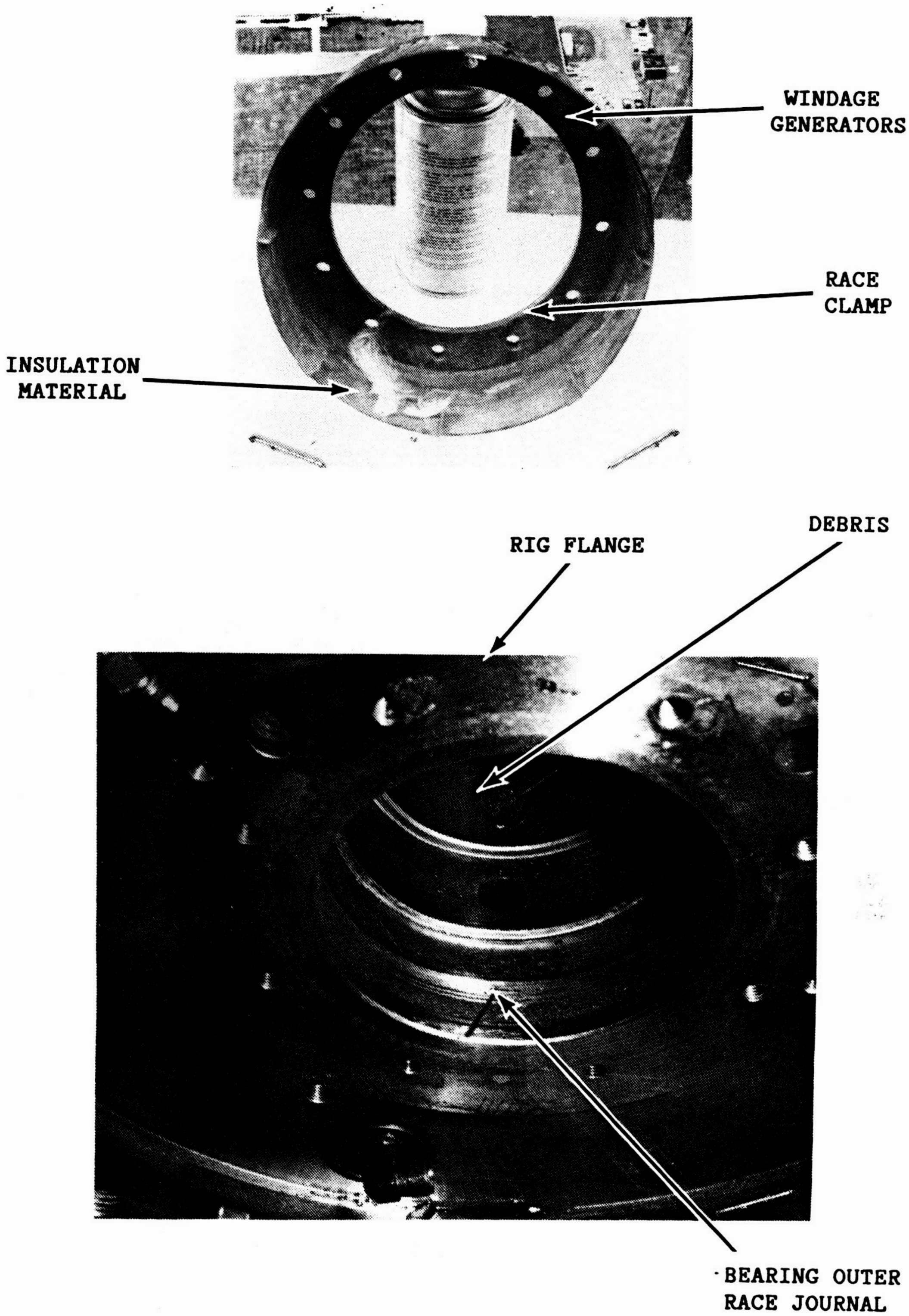

Figure 25. Rig Hardware After Bearing Failure, Build 20.

TABLE 20.3

CARBON FACE WEAR FROM BUILD 20 (WAFER SERIAL NO. 4)

Circumferential Position (Degrees)	Air Bearing O.D.		Sealing Dam		Wear Pads I.D.		Average	
	inch	cm	inch	cm	inch	cm	inch	cm
0	.0010	.0025	.0006	.0015	.0013	.0033	.000967	.0246
40	.0026	.0066	.0045	.0114	.0057	.0145	.004267	.0108
80	.0081	.0205	.0092	.0234	.0088	.0224	.008700	.0220
120	.0095	.0241	.0111	.0282	.0100	.0254	.010200	.0259
160	.0053	.0135	.0070	.0179	.0077	.0196	.006667	.0169
200	.0018	.0046	.0015	.0038	.0020	.0051	.001767	.0045
240	.0013	.0033	.0010	.0025	.0009	.0023	.001067	.0027
280	.0005	.0013	.0003	.0008	0	0	.000267	.0007
320	.0004	.0010	.0003	.0008	.0003	.0008	.000333	.00084
Average	.003389	.0086	.003944	.0100	.004078	.0140	.003800	.0120
Maximum	.0095	.0241	.0111	.0282	.0100	.0254	.010200	.0259
Minimum	.0004	.001	.0003	.0008	0	0	.000233	.0007

It is noted that the seal did not fail, and it is probable that it would still be serviceable, albeit at a higher gas leakage rate. The ruggedness of the seal design as demonstrated by results of this test is significant in that it implies the potential for saving an engine in the event of a catastrophic rotor thrust bearing failure. This particular advantage has been inadvertently demonstrated in a test engine with a similar face type carbon seal assembly.

Steady state air leakage rates for the lift pad seal configuration at conditions of test was 80 to 90 percent lower than an equivalent "best" configuration labyrinth seal. For the NASA/QCSEE geared fan engine rotor thrust balance seal, of which the conditions are representative, this reduction in flow rate would improve engine SFC by approximately one (1) percent and would allow reduction of turbine inlet temperature by approximately 20 degrees F.

Test Build No. 21 - Performance Mapping, NASA Design Step Pad Bearing

Performance mapping was initiated using seal carbon face wafer S/N 2 containing NASA designed shrouded stepped gas bearing pads, seal housing S/N 4, and a new carbon piston ring secondary seal with overlapping tongue and socket end gap. All testing was done at 5000 RPM shaft speed. Total operating time at speed was 8 hours 15 minutes, with 6 hours 53 minutes at performance points. Test data is shown on Table 21.1. The seal assembly is shown on Figure 26.

While operating at 150 psid (103.4 N/sq cm) and seal air temperature at approximately 700 degrees F (371 degrees C), the seal air heater system malfunctioned. The test was stopped to facilitate repair of an electrical problem in the heater system. After restarting the rig, seal air pressure was set at 220 psid (151.7 N/sq cm) and air temperature was increased to 662 degrees F (350 degrees C). Air leakage rate at this point was 7.99 scfm (.0102 lbs/sec), which is normal. After 7 minutes at this point, seal air leakage rate suddenly increased to approximately 49 scfm (.0625 lbs/sec) and pressure decreased to 75 psid (51.7 N/sq cm). The test was shut down at this point.

TABLE 21.1

BUILD 21, PERFORMANCE MAPPING (Sheet 1 of 2)

Test Time		Sealed Air Pressure		Shaft	Sealed Air Temperature		Air Flow Rate			% of Labyrinth
Hrs	Min	psig	N/cm^2	RPM	°F	°K	SCFM	lb/sec	kg/sec	Flow
	0	30	21	0/5000	84	303	0	0	0	0
	13	90	62	5000	84	303	4.0	.0051	.0023	1.80
	17	153	106	5000	89	305	10.13	.0129	.0059	2.80
	28	215	148	5000	104	314	7.9	.0101	.006	1.64
	29	200	136	5000	106	315	7.6	.0097	.0044	1.69
	32	255	176	5000	105	314	17.1	.0218	.0099	3.02
	35	245	169	5000	107	315	14.7	.0187	.0085	2.69
	37	290	200	5000	108	316	20.5	.0261	.0118	3.21
	40	290	200	5000	108	316	22.8	.0291	.0132	3.57
	55	230	159	5000	124	325	10.2	.0130	.0059	2.02
1	10	230	159	(Stop Test to Replace Failed Rig Drive End Bearing)						
1	50	25	17	5000	118	322	2.46	.0031	.0014	2.95
2	0	25	17	5000	121	323	1.64	.0021	.0009	2.00
2	3	50	35	5000	123	324	3.14	.0040	.0018	2.34
2	11	50	35	5000	124	325	2.09	.0027	.0012	1.58
2	14	75	52	5000	129	328	2.47	.0031	.0014	1.32
2	24	75	52	5000	128	327	2.47	.0031	.0014	1.32
3	44	85	59	5000	370	462	5.2	.0066	.0030	2.99
3	49	53	37	5000	445	503	4.29	.0055	.0025	3.84
4	0	150	103	5000	370	462	20.75	.0264	.0120	7.25
4	5	185	128	5000	327	438	21.37	.0272	.0123	6.00
4	12	220	152	5000	370	462	15.98	.0240	.0092	4.63
4	19	215	148	5000	394	475	15.81	.0202	.0091	4.04
4	23	256	177	5000	371	462	26.6	.0339	.0154	5.67
4	28	255	176	5000	334	442	26.55	.0339	.0153	5.56
4	35	290	200	5000	372	463	19.12	.0244	.0110	3.63
4	40	280	193	5000	401	479	18.8	.0240	.0109	3.75

TABLE 21.1 (Concluded)

BUILD 21, PERFORMANCE MAPPING (Sheet 2 of 2)

Test Time		Sealed Air Pressure		Shaft	Sealed Air Temperature		Air Flow Rate			% of Labyrinth Flow
Hrs	Min	psig	N/cm^2	RPM	°F	°K	SCFM	lb/sec	kg/sec	Flow
5	36	80	55	5000	662		12.6	.0161	.0073	8.94
5	42	85	59	5000	694		5.2	.0066	.0030	3.53
5	50	150	103	5000	665		13.38	.0171	.0077	5.47
6	26	144	99	5000	632		13.79	.0176	.0080	5.75
(Lost heater Power at Air at ≃ 700°F - Stop Test)										
6	43	30	21	5000	-		-			
(Stop Test - Heater Failure)										
7	13	30	21	5000	-		-			
(Stop Test - Another Heater Failure)										
7	43	220	152	5000	662		7.99	.0102	.0046	2.28
(Stop Test - Repair Drive)										
8	15	30	21	5000	-		-			
(Stop Test - Excessive Air Flow Rate) (Found Spalled Plating on Seal Race)										

ORIGINAL PAGE IS
OF POOR QUALITY

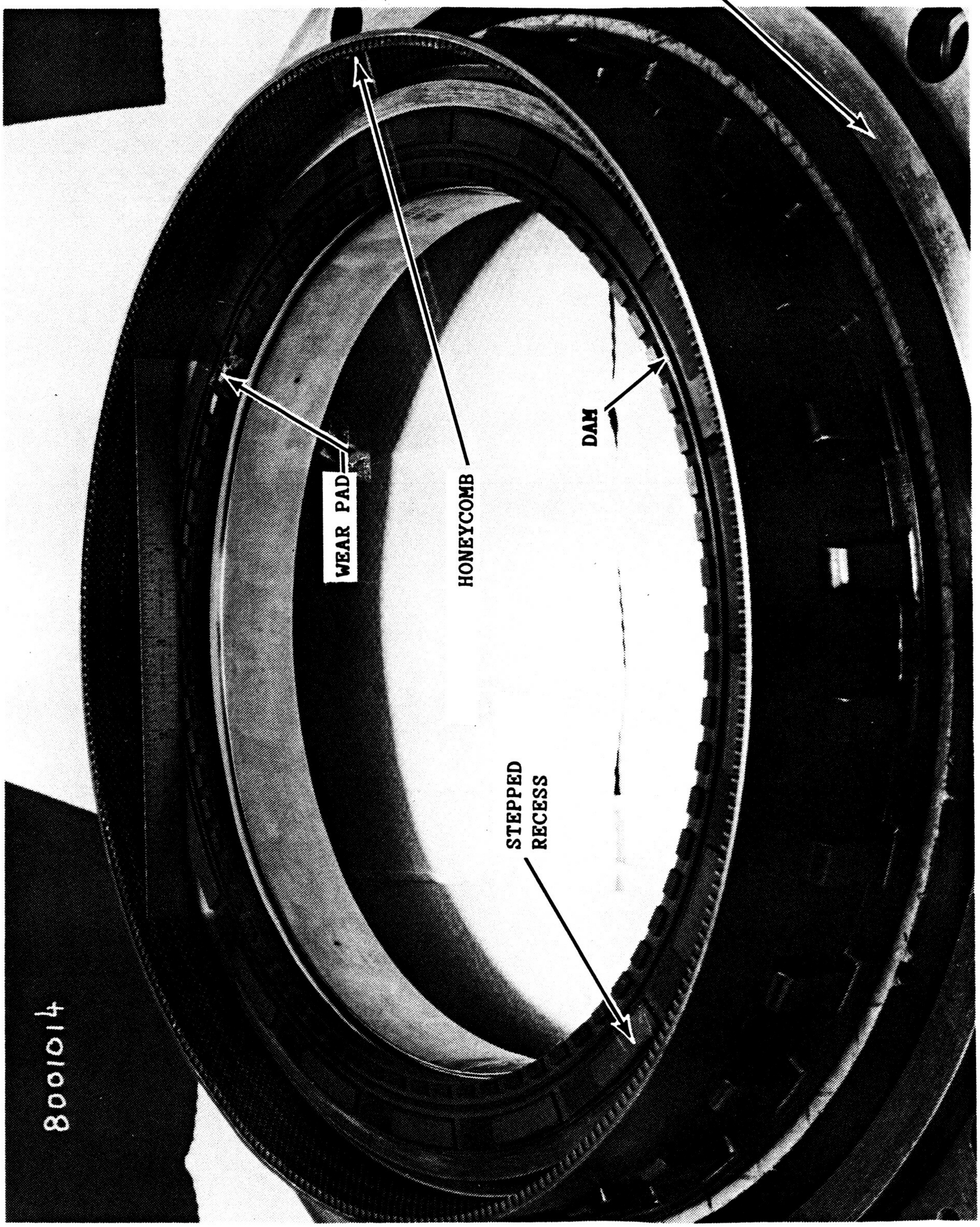

Figure 26. Stepped Pad Seal Assembly, Before Build 21.

The seal was removed from the test rig for inspection, and the following was noted:

- Several spalls from the aluminum oxide coating on the face of the seal race in the area that contacts the inner wear pads of the seal carbon wafer face (see Figures 27 and 28). The plated surface in the circumferential band of this same area was grooved with a "phonograph" finish, evidently resulting from race plating particles imbedded in the leading edges of the carbon face inner wear pad vent grooves.

- Approximately .0035 inch wear in the carbon face sealing dam and gas bearing pads. The gas bearing pad recesses, initially approximately .001 inch (.00254 cm) deep (Figure 26), were completely removed (Figure 29). Face wear on the inner wear pads was approximately .0075 inch (.029 cm).

- Burnishing on the outer surfaces of the carbon inserts (Figure 30) in the rotation locks on the outside diameter of the seal carbon wafer assembly. A matching burnish on the outer radius surface of the rotation lock slots on the inside diameter of the seal housing. A dimensional check with shim stock showed radial clearance between the insert and housing at one location equal to .0015 inch as compared to part drawing dimensions which would provide .014-.023 inch clearance.

The probable cause for the sudden increase in air leakage rate, as described above, was the spalled platelets of hard coating (aluminum oxide) from the seal race passing through and damaging the interfaces of the carbon seal and seal race.

The sequence resulting in plating spalls, based on test evidence, implies that the problem may have resulted from thermally generated radial interference between the outer radius of the seal wafer rotation lock and the bottom of the lock slot in the seal housing. At one rotation lock location (where measured radial clearance was .0015 inch), a 25 degree F delta-T

ORIGINAL PAGE IS
OF POOR QUALITY

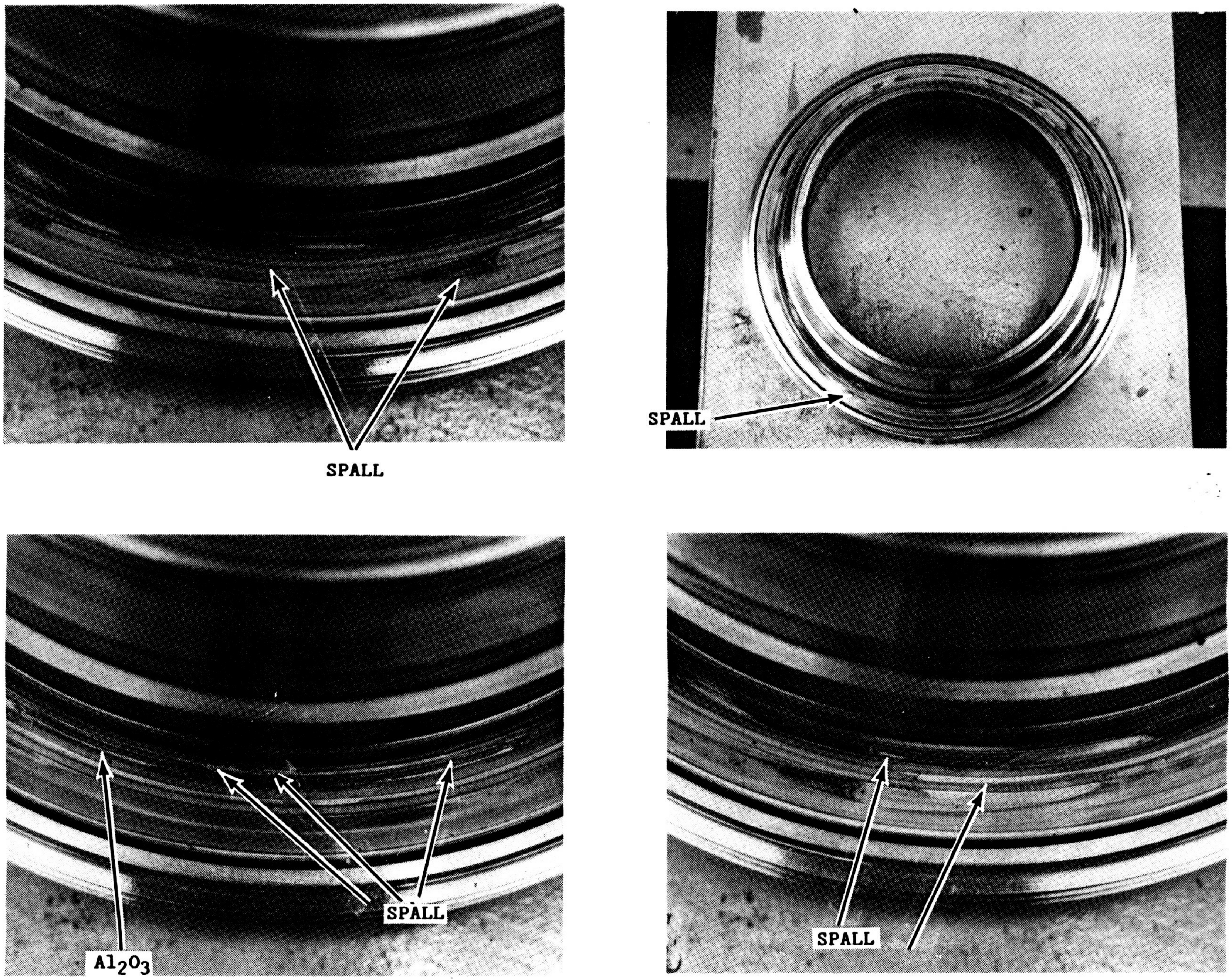

Figure 27. Seal Race Coating Spalls, After Build 21.

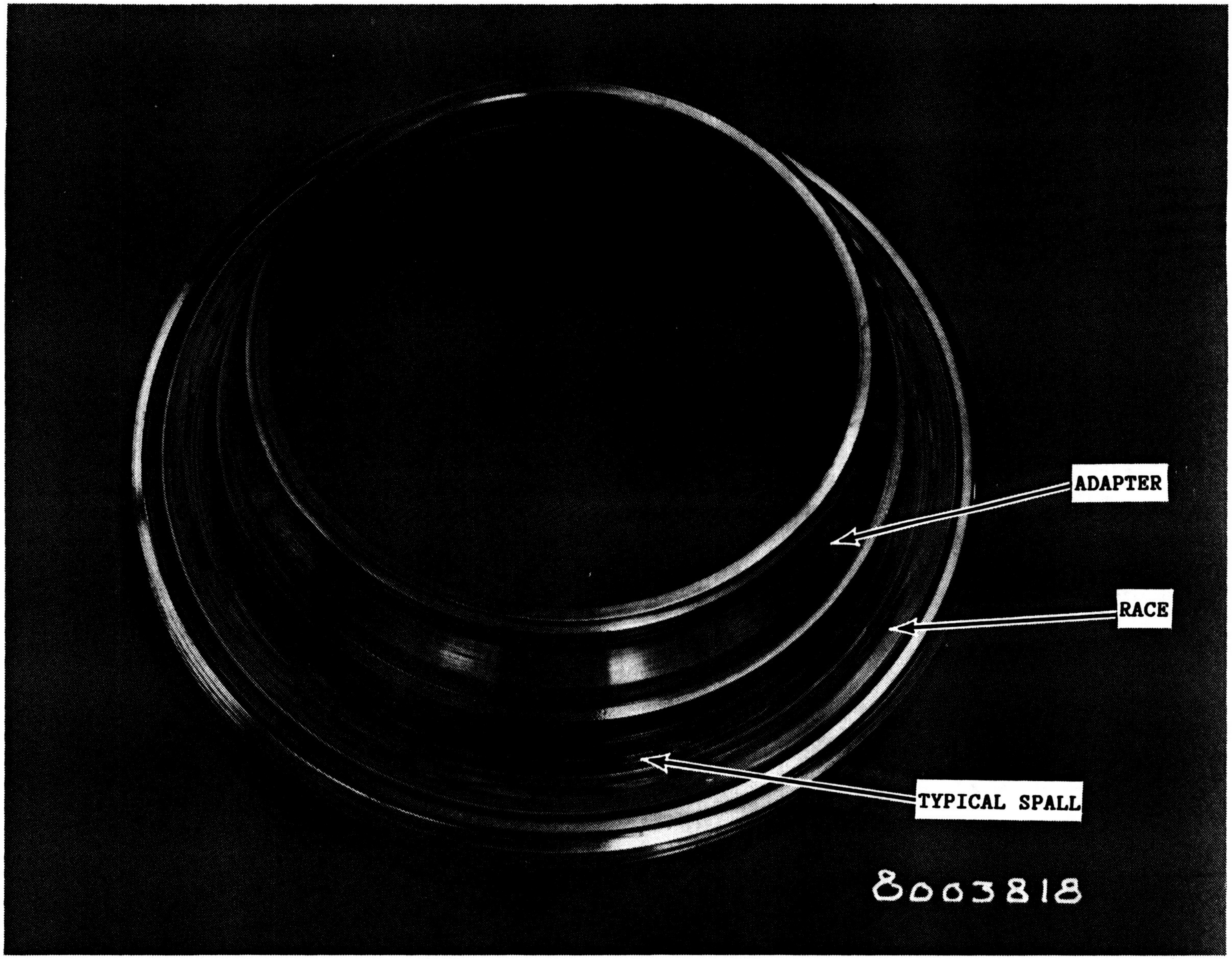

Figure 28. Seal Race and Adapter, After Build 21.

ORIGINAL PAGE IS
OF POOR QUALITY

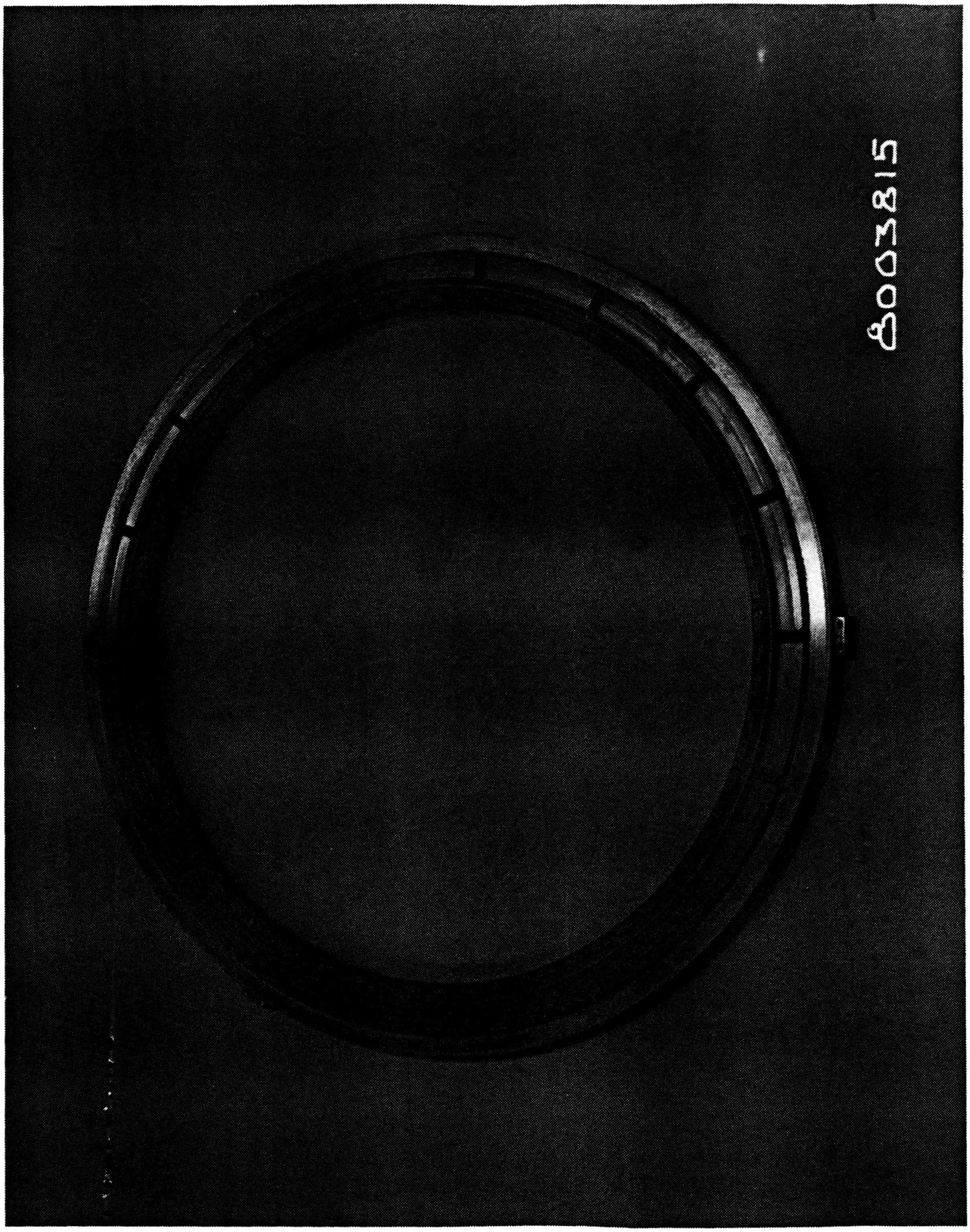

Figure 29. Carbon Wafer Face, After Build 21.

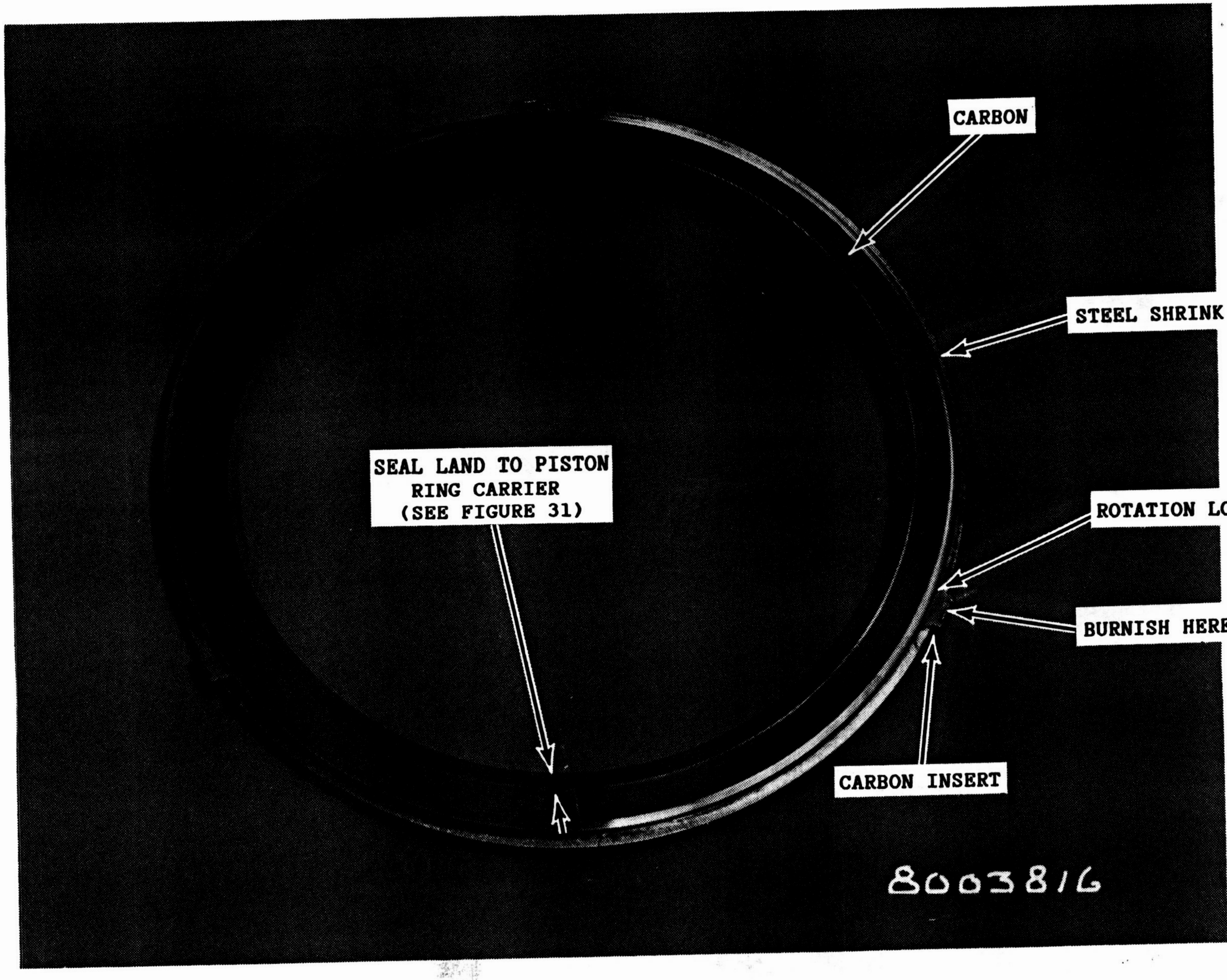

Figure 30. Carbon Wafer Aft Face, After Build 21.

ORIGINAL PAGE IS
OF POOR QUALITY

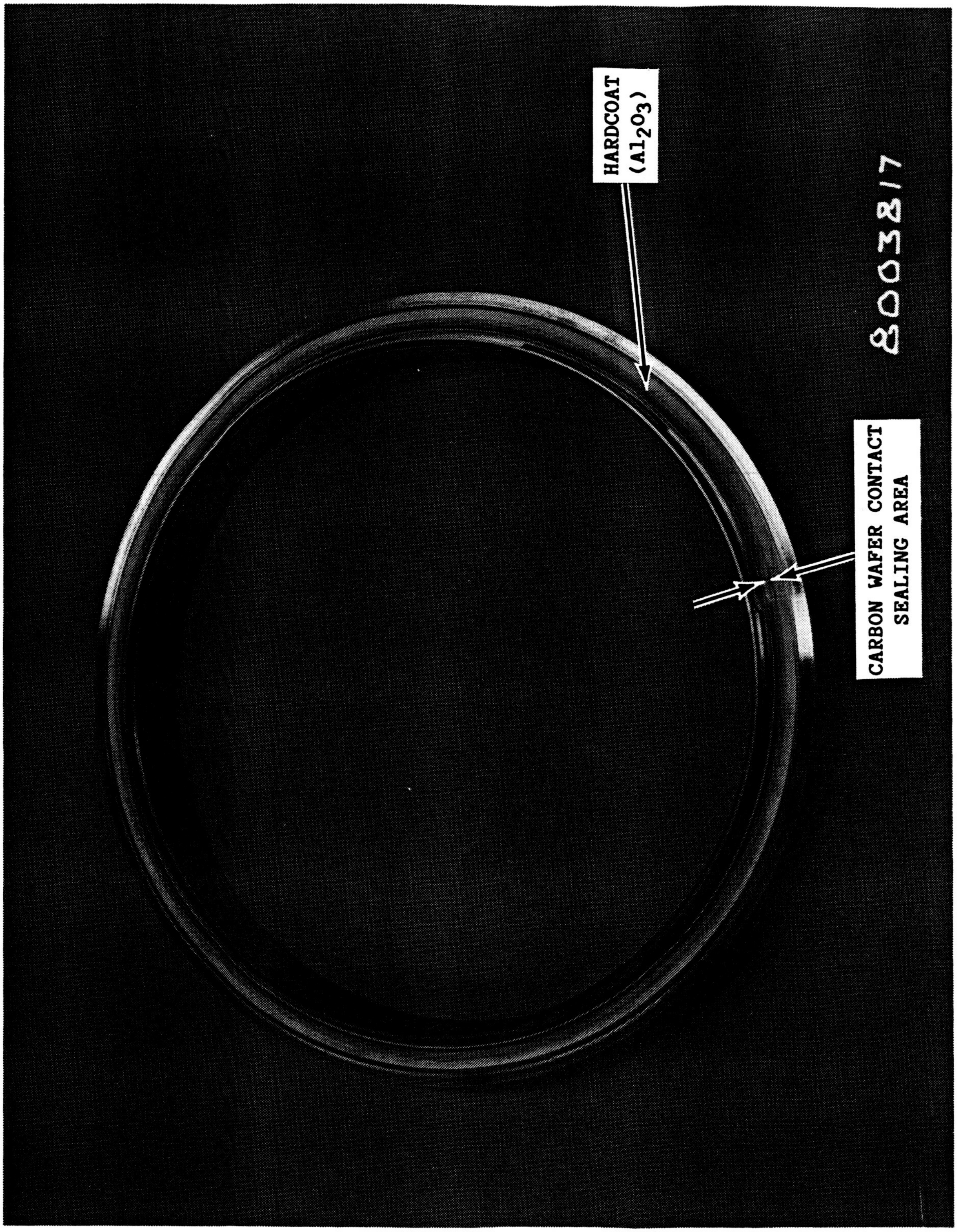

Figure 31. Piston Ring Carrier, After Build 21.

C-2

between the seal wafer and housing would result in radial interference. Interference at this interface would generate a high friction drag force which would prevent the seal from freely following the axial motion of the rotating seal race. This would cause a substantial increase in rubbing loads, and the resulting heat generated in the dynamic sealing interface could result in thermal spalling of the hard coating.

Test Build No. 22 - Performance Mapping, Composite Slider Bearings

Performance mapping was completed using seal carbon wafer S/N 3, containing the GE designed shrouded composite slider gas bearings, seal housing S/N 4, and a carbon piston ring secondary seal.

Prior to testing, the inside radius of the seal dam on the face of the carbon wafer assembly was reworked, changing the radial width of the dam from .045 inch (.1143 cm) to .0336 inch (.0853 cm), to provide additional pressure force to seat the seal face against the race. The carbon inserts at the wafer assembly rotation locks were also reworked to provide drawing specified radial clearance to the seal housing (see Build No. 21). In addition, the carbon wear pads at the inside radius of the primary seal face were removed.

Static leakage rates measured in the dynamic test rig prior to dynamic testing are shown on Table 22.1. Leakage rate at 290 psi (200 N/sq cm) delta-P was 10.02 scfm (.0058 kg/sec).

Data from dynamic testing is shown on Table 22.2. Total operating time was 36 hours 6 minutes. Seal performance was excellent throughout the testing. All hardware was in excellent condition after test (see photos, Figures 32, 33, 34, and 35). Average carbon wear on the face of the primary wafer assembly (see Table 22.3) was approximately .000850 inch (.002159 cm). No wear occurred in the hard coating on the face of the seal race.

Test Build No. 23 - Performance Mapping, Spiral Groove Seal

Static and dynamic testing was conducted using seal carbon wafer S/N 2, seal housing S/N 1, and a carbon piston ring secondary seal. The seal race

TABLE 22.1

STATIC TEST
(Build 22)

Seal ΔP		Seal Air Flow			Remarks
N/cm^2	psid	kg/sec	SCFM	lb/sec	
7	10	.0002	.26	.0003	Air Temperature ≈ 80°F (43°C)
17	25	.0002	.33	.0004	
35	50	.0002	.42	.0005	
69	100	.0003	.56	.0007	
103	150	.0004	.67	.0009	
138	200	.0004	.76	.0010	
172	250	.0024	4.24	.0054	
200	290	.0058	10.02	.0128	

TABLE 22.2

BUILD 22, PERFORMANCE MAPPING, SHROUDED COMPOSITE SLIDER (Sheet 1 of 4)

Lapsed Time		Sealed Air Pressure		Shaft	Sealed Air Temperature		Air Flow Rate			% of Labyrinth
Hrs	Min	psig	N/cm^2	RPM	°F	°K	SCFM	lb/sec	kg/sec	Flow
	36	8	6	1355	88	304	0.248	.0003	.0001	0.51
	54	6	4	1598	275	408	0.237	.0003	.0001	0.62
1	18	8	6	1631	262	401	0.248	.0003	.0001	0.59
1	36	12	8	1647	249	394	0.269	.0003	.0002	0.54
1	48	8	6	1660	265	402	0.248	.0003	.0001	0.59
2	06	10	7	1590	272	406	0.259	.0003	.0001	0.57
2	24	9	6	1590	267	404	0.253	.0003	.0001	0.58
2	36	9	6	1590	263	401	0.253	.0003	.0001	0.57
2	54	9	6	1586	263	401	0.253	.0003	.0001	0.57
3	18	9	6	1580	264	402	0.253	.0003	.0001	0.57
					(Shut Down)					
4	0	125	86	7440	260	400	0.617	.0008	.0004	0.23
4	24	125	86	7441	784	691	0.617	.0008	.0004	0.31
5	06	125	86	7437	827	715	18.50	.0236	.0107	9.51
5	36	125	86	7439	830	716	19.11	.0243	.0110	9.82
					(Shut Down)					
6	24	125	86	7390	710	650	0.617	.0008	.0004	0.30
6	42	125	86	7422	809	705	15.41	.0196	.0089	7.86
7	18	125	86	7401	829	716	17.88	.0228	.0103	9.19
7	48	125	86	7410	834	719	17.88	.0228	.0103	9.21
8	12	200	138	7921	917	765	38.22	.0467	.0221	13.21
8	42	200	138	7914	925	769	42.04	.0536	.0243	14.58
9	12	200	138	7916	924	769	38.98	.0497	.0225	13.51
9	42	200	138	7907	932	773	30.57	.0389	.0177	10.63
10	18	200	138	7907	940	777	38.98	.0497	.0225	13.59
10	42	200	138	7900	951	784	45.86	.0584	.0265	16.05
11	12	200	138	7916	922	767	40.13	.0511	.0232	13.90
11	42	200	138	7914	928	771	45.86	.0584	.0265	15.91

TABLE 22.2 (Continued)

BUILD 22, PERFORMANCE MAPPING, SHROUDED COMPOSITE SLIDER (Sheet 2 of 4)

Lapsed Time		Sealed Air Pressure		Shaft	Sealed Air Temperature		Air Flow Rate			% of Labyrinth
Hrs	Min	psig	N/cm^2	RPM	°F	°K	SCFM	lb/sec	kg/sec	Flow
11	54	125	86	7884	750	672	15.41	.0196	.0089	7.67
12	12	125	86	6867	649	616	12.95	.0165	.0075	6.17
12	30	125	86	6873	595	586	5.55	.0071	.0032	2.58
12	45	125	86	7882	561	567	6.17	.0079	.0036	2.82
13	06	125	86	7869	522	545	12.95	.0165	.0075	5.81
13	24	125	86	6877	475	519	11.71	.0149	.0068	5.13
13	36	125	86	6862	438	499	3.7	.0047	.0021	1.58
					(Shut Down)					
14	12	25	17	6044	312	429	0.328	.0004	.0002	0.46
14	36	26	18	6057	609	594	1.66	.0021	.0010	2.67
15	6	25	17	6069	614	596	2.96	.0038	.0017	4.89
15	36	20	14	6066	602	590	2.77	.0035	.0016	4.55
16	6	25	17	6060	618	600	2.96	.0038	.0017	4.90
				(Shut Down - Loose Connection on Chip Detector)						
16	42	29	20	6040	595	586	0.862	.0011	.0005	1.28
17	12	24	17	6019	602	590	0.811	.0011	.0005	1.37
17	42	175	121	9311	726	659	17.96	.0229	.0104	6.52
17	54	110	76	9312	860	733	11.94	.0152	.0069	6.96
18	6	110	76	9310	907	759	17.18	.0219	.0105	10.19
18	36	275	190	9300	855	730	48.83	.0622	.0283	12.23
18	54	148	102	8567	640	611	20.63	.0263	.0119	8.41
19	6	150	103	8575	552	562	14.06	.0179	.0081	5.43
19	36	140	97	8659	500	533	12.65	.0161	.0073	5.07
19	54	137	94	8565	444	502	7.07	.0090	.0041	2.80
					(Shut Down)					
20	36	136	94	9300	679	632	4.80	.0061	.0028	2.15
21	0	225	155	9316	810	705	24.23	.0309	.0140	7.21
21	30	269	185	9322	831	717	43.93	.0560	.0254	11.13

TABLE 22.2 (Continued)

BUILD 22, PERFORMANCE MAPPING, SHROUDED COMPOSITE SLIDER (Sheet 3 of 4)

Lapsed Time		Sealed Air Pressure		Shaft	Sealed Air Temperature		Air Flow Rate			% of Labyrinth
Hrs	Min	psig	N/cm^2	RPM	°F	°K	SCFM	lb/sec	kg/sec	Flow
21	48	269	185	9320	847	726	44.81	.0571	.0259	11.42
22	6	269	185	9312	870	739	48.32	.0616	.0279	12.42
22	24	269	185	9319	878	743	50.52	.0643	.0292	13.03
22	48	269	185	9316	881	745	52.58	.0670	.0304	13.57
23	18	269	185	9306	831	717	52.72	.0672	.0305	13.39
24	0	269	185	9308	862	734	51.40	.0655	.0297	13.18
24	36	269	185	9305	860	733	49.20	.0627	.0284	12.60
25	6	269	185	9303	863	735	51.84	.0660	.0300	13.29
25	12	165	114	9254	663	624	27.27	.0347	.0158	10.17
25	30	130	90	9246	598	587	12.55	.0160	.0073	5.64
25	42	130	90	9246	484	524	11.92	.0152	.0069	5.06
(Shut Down) Drive Belt Problem										
26	0	124	85	9285	448	504	6.45	.0082	.0037	2.80
26	24	130	90	9294	627	604	12.55	.0160	.0073	5.72
26	42	130	90	9304	884	746	12.55	.0160	.0073	6.36
27	0	125	86	9317	869	738	15.41	.0196	.0089	8.04
27	24	115	79	9322	917	765	16.93	.0216	.0098	9.68
27	42	115	79	9308	948	782	18.12	.0231	.0105	10.49
27	48	275	190	9325	817	709	44.39	.0565	.0256	10.95
28	18	275	190	9324	814	707	26.64	.0339	.0154	6.56
28	42	275	190	9340	858	732	43.51	.0554	.0251	10.91
(Shut Down) Compressor Problem										
29	54	123	85	9304	646	614	9.18	.0117	.0053	4.43
30	12	125	86	9306	738	665	12.33	.0157	.0071	6.11
30	24	130	90	9295	807	704	13.18	.0168	.0076	6.48
30	42	125	86	9309	856	731	12.95	.0165	.075	6.73
30	54	128	88	9298	890	750	15.58	.0198	.0090	8.63

TABLE 22.2 (Concluded)

BUILD 22, PERFORMANCE MAPPING, SHROUDED COMPOSITE SLIDER (Sheet 4 of 4)

Lapsed Time		Sealed Air Pressure		Shaft	Sealed Air Temperature		Air Flow Rate			% of Labyrinth
Hrs	Min	psig	N/cm^2	RPM	°F	°K	SCFM	lb/sec	kg/sec	Flow
31	12	128	88	9287	917	765	17.14	.0218	.0099	8.91
31	24	128	88	9291	945	780	18.07	.0230	.0104	9.49
31	42	128	88	9294	970	794	18.07	.0230	.0104	9.58
31	54	177	122	9288	927	770	28.17	.0359	.0163	10.95
32	12	128	88	9288	984	801	16.82	.0214	.0097	8.96
32	36	285	196	10400	854	730	52.38	.0667	.0303	12.67
33	0	290	200	10387	875	741	55.54	.0707	.0321	13.32
33	6	290	200	10387	883	746	40.98	.0522	.0237	9.86
33	24	285	196	10387	898	754	1716	.0219	.0099	4.22
33	36	285	196	10391	866	736	18.96	.0242	.0110	4.61
33	54	285	196	10391	840	722	18.96	.0242	.0110	4.56
34	6	275	190	10391	865	736	13.32	.0170	.0077	3.35
34	18	282	194	10408	893	751	17.07	.0217	.0099	4.23
34	30	282	194	10411	893	751	17.07	.0217	.0099	4.23
34	42	135	93	8000	721	656	13.40	.0171	.0077	6.15
34	48	125	86	8000	664	624	11.71	.0149	.0068	5.62
35	0	125	86	8000	621	600	9.25	.0118	.0053	4.35
35	12	127	88	8000	579	577	9.31	.0119	.0054	4.24
35	24	125	86	8000	548	560	9.25	.0118	.0053	4.20
35	36	132	91	8000	518	543	7.58	.0097	.0044	3.23
35	42	126	87	8000	492	529	6.81	.0087	.0039	2.99
35	54	99	68	8000	471	517	5.28	.0067	.0031	2.83
36	1	80	55	8000	455	508	3.81	.0049	.0022	2.43
36	6	45	31	8000	442	501	2.02	.0026	.0012	2.03

(Shut Down - Inspect Seal)

ORIGINAL PAGE IS
OF POOR QUALITY

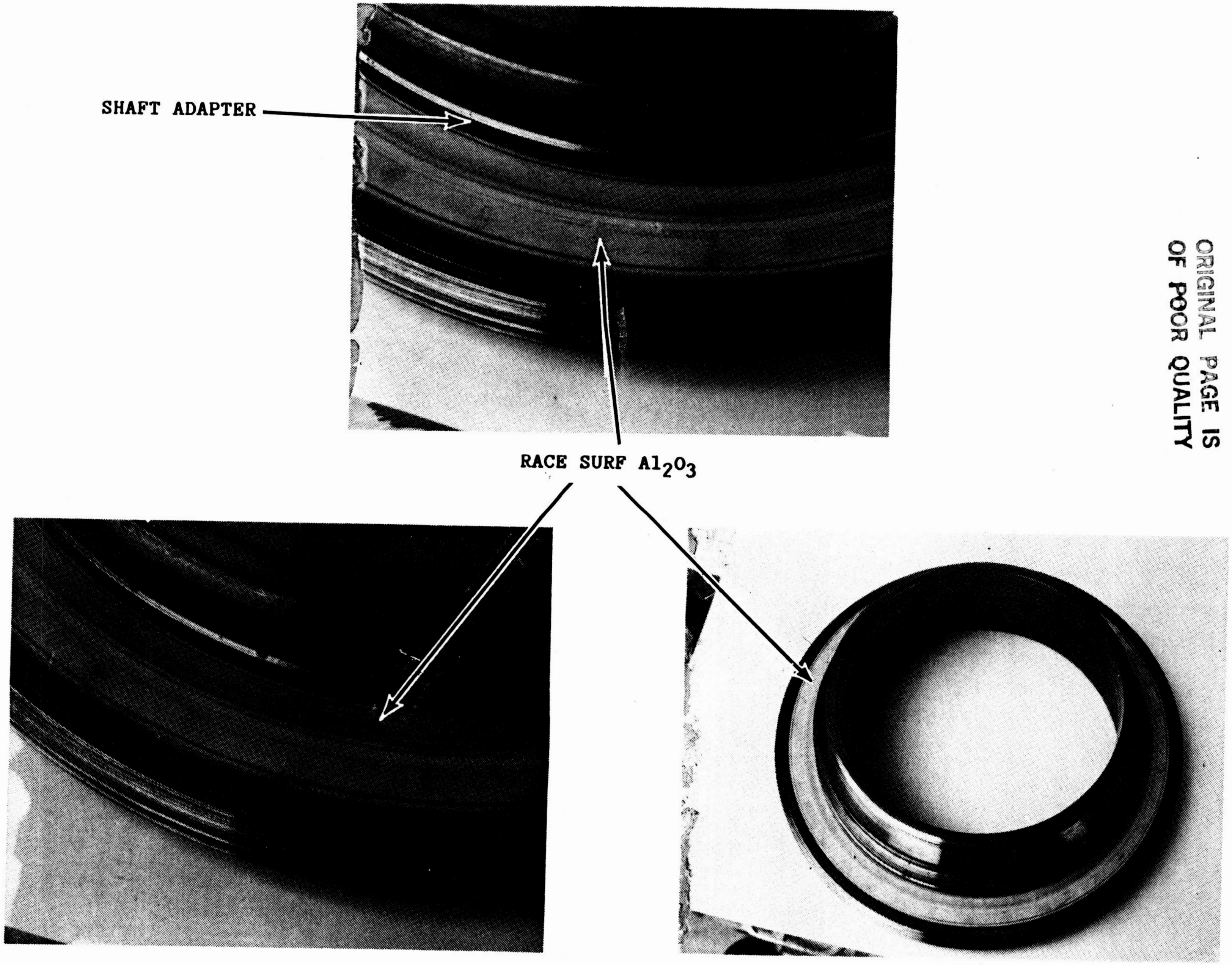

Figure 32. Seal Race, After Build 22.

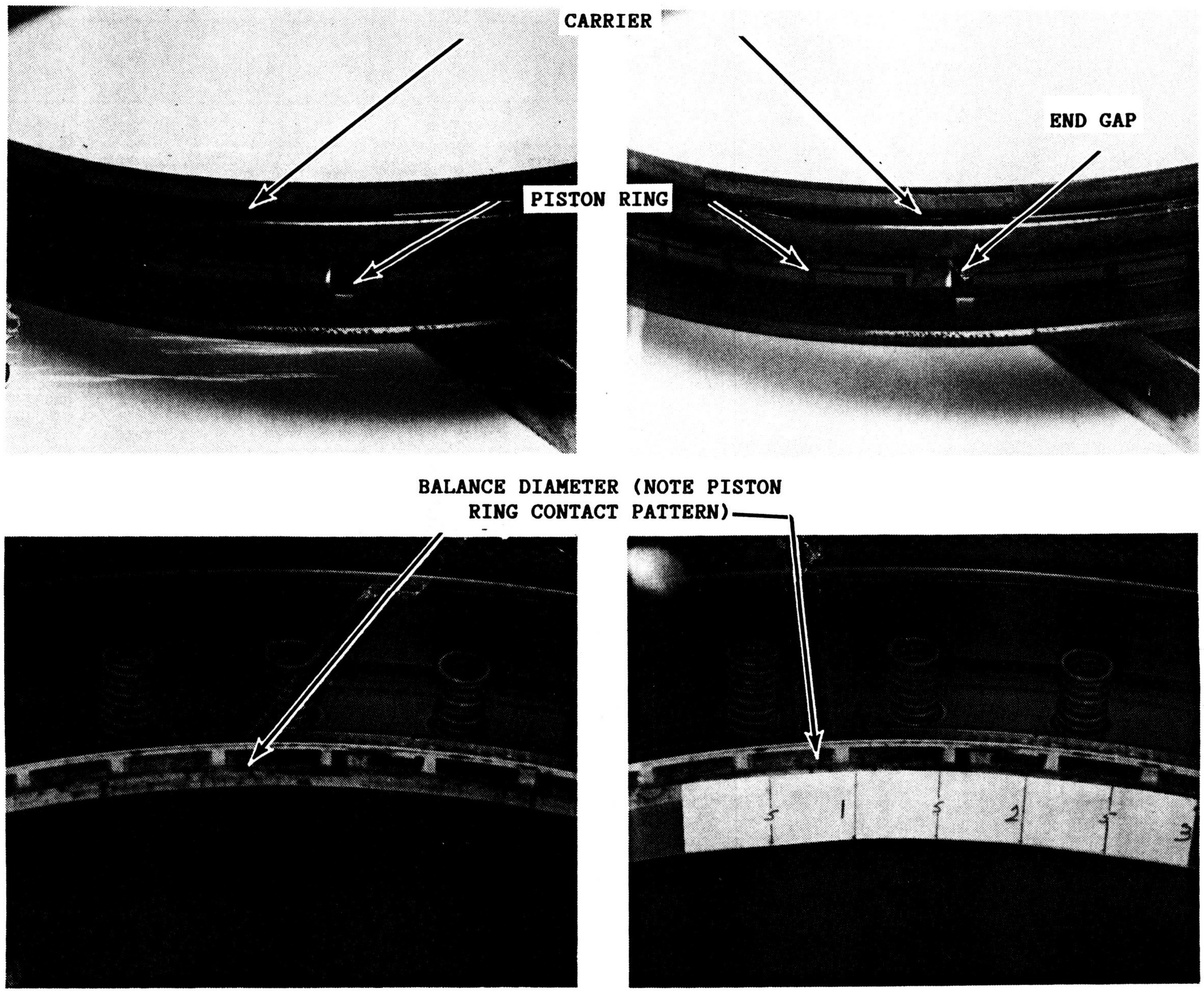

Figure 33. Piston Ring/Balance Diameter, After Build 22.

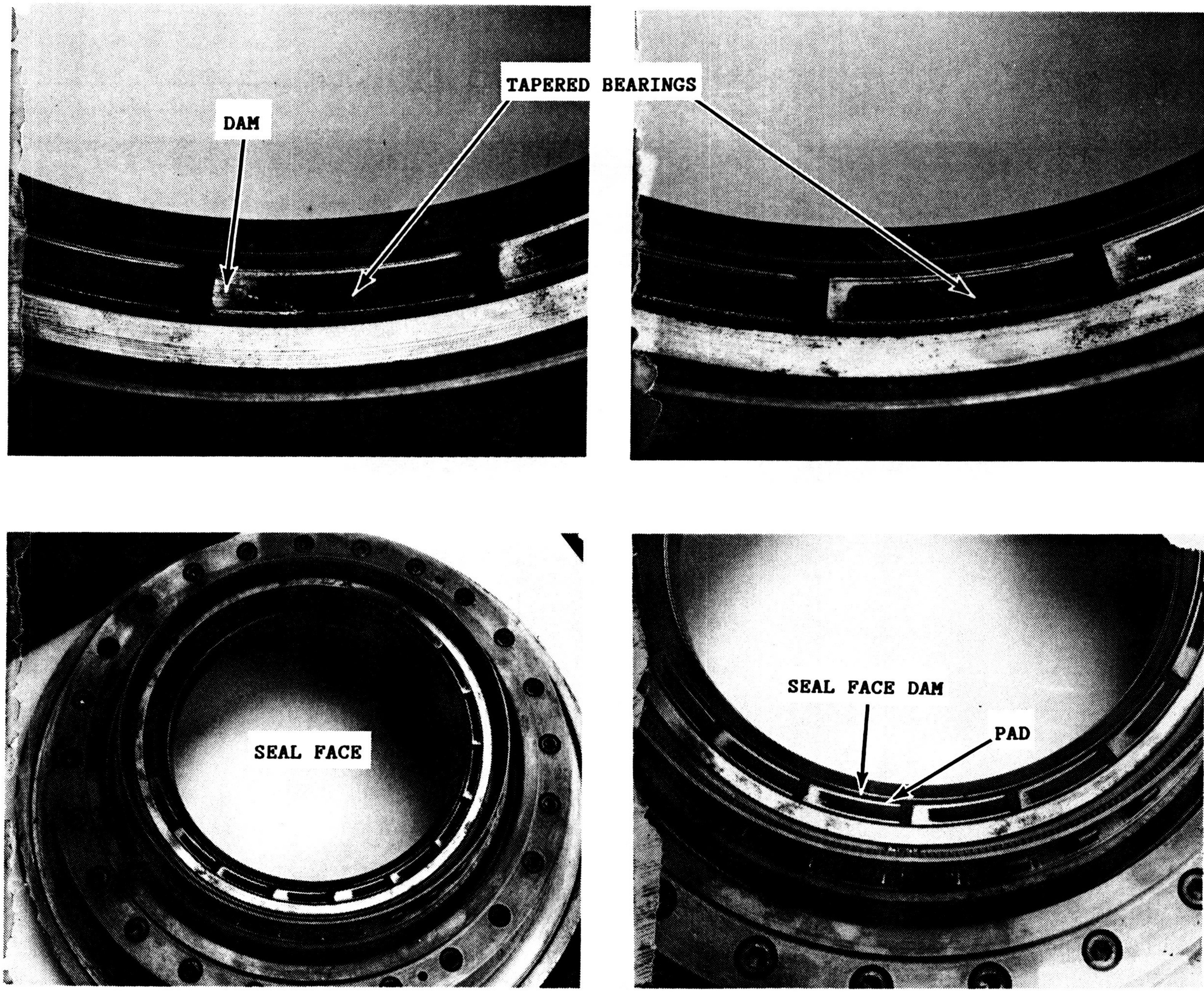

Figure 34. Carbon Face/Bearings, After Build 22.

ORIGINAL PAGE IS
OF POOR QUALITY

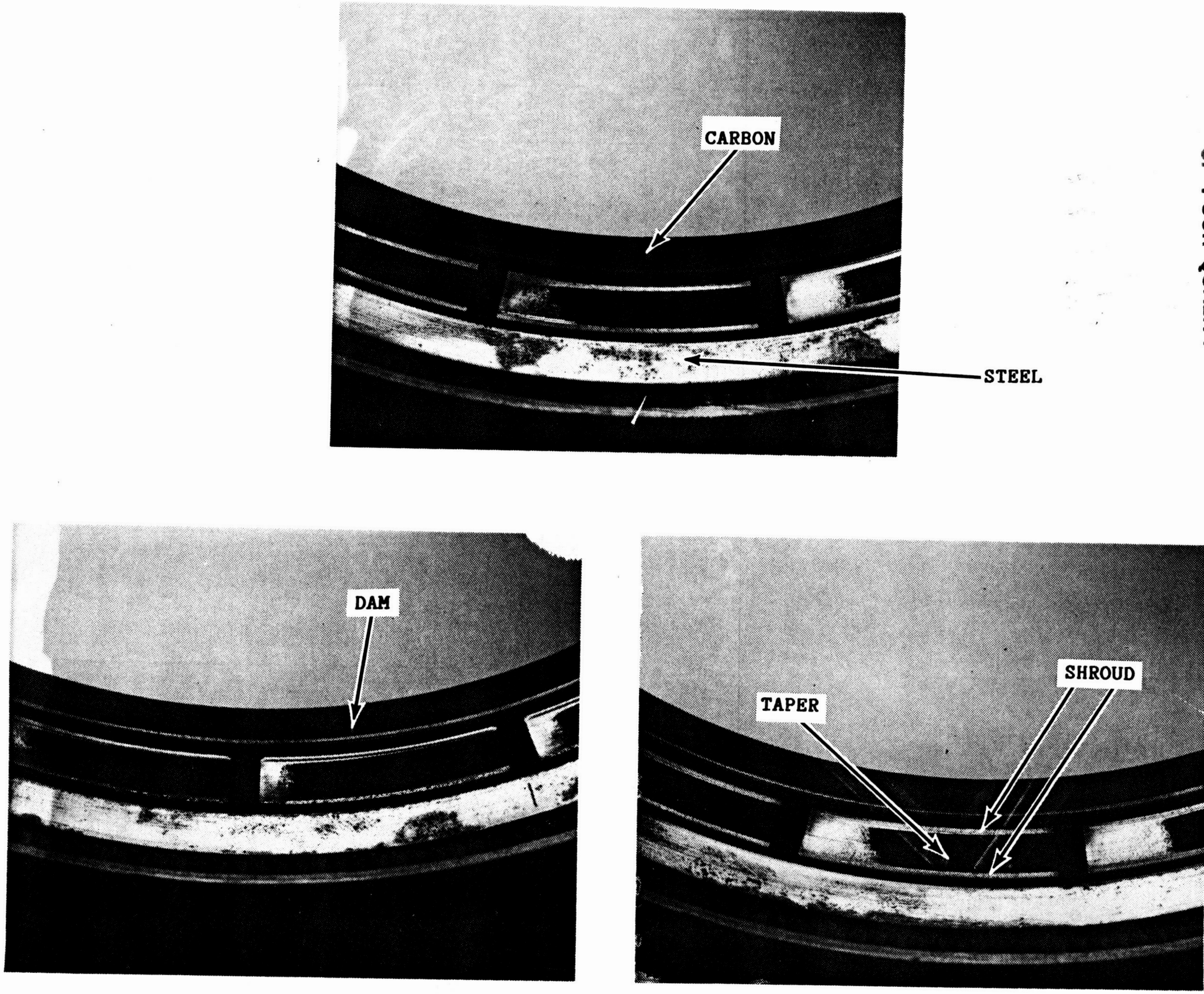

Figure 35. Gas Bearings, After Build 22.

TABLE 22.3

CARBON FACE WEAR MEASUREMENTS
(Shrouded Composite Slider)

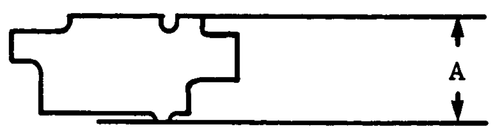

Point	Angular Location Degrees	Dimension A (inches) Before Test	After Test	Wear (inches)
1	0	.4843	.4839	.0004
2	40	.4843	.4830	.0013
3	80	.4837	.4830	.0007
4	120	.4837	.4830	.0007
5	160	.4833	.4829	.0004
6	200	.4839	.4831	.0008
7	240	.4840	.4825	.0015
8	280	.4841	.4829	.0012
9	320	.4840	.4833	.0007

Maximum Wear = .0015 inch (.00381 cm)

Minimum Wear = .0004 inch (.00102 cm)

Average Wear = .000855 inch (.00217 cm)

Total Time = 33 hrs, 44 min

Wear Rate = 25 x 10^{-6} inch/hr (64 x 10^{-6} cm/hr)

contained a total of 90 inward pumping spiral grooves with 75% groove, 25% land, in the aluminum oxide hard coating. The depth of each groove was measured, and average, minimum, and maximum depths were .00095 inch (.00241 cm), .00088 inch (.00224 cm), and .00118 inch (.00300 cm), respectively.

Prior to test, the radial width of the primary face carbon sealing dam was reworked from .045 inch (.1143 cm) to .0335 inch (.0851 cm) to increase the pressure force seating the seal face against the race. To accomplish this change, material was removed from the inner radius of the dam.

Two dynamic tests, consisting of 8.2 hours total operating time, were completed. Data from the first test (5 hours 13 minutes) is shown on Table 23.1. Results of the balance of testing (2 hours 59 minutes) is shown on Table 23.2. Wear on the carbon face was relatively high following Build 23.1, with a conical taper high at the outside diameter of the sealing face. This taper suggested the possibility of an axial offset of the centers of stiffness of the carbon cross-section and cross-section of the metal ring shrunk around its outside diameter.

To determine if the result was repeatable, a second test (Build No. 23.2) was conducted after lapping the carbon face to flatness within three (3) helium light bands. Following are wear and taper measurements for both tests:

			Average Carbon Face				Carbon Taper
	Time		Wear		Wear Rate		(High @ OD)
Build	Hrs	Min	inch	cm	in/hr	cm/hr	in/in
23.1	5	13	.000971	.002466	.000186	.000472	.00487
23.2	2	57	.000401	.001019	.000136	.000345	.00580

Based on analysis using nominal drawing dimensions, the carbon taper predicted at 1000 degrees F (538 degrees C) and 295 psid (203.4 N/sq cm) was .00154 inch/inch high at the inside diameter. Approximately 91% of the calculated taper results from offset of axial centers of gravity of the carbon ring and steel shrink-ring of the wafer assembly. The torsional moment generating this taper is 1.944 inch-pounds per inch of circumference. The axial offset generating this moment is .00458 inches (.01163 cm).

TABLE 23.1

BUILD 23, PERFORMANCE MAPPING, SPIRAL GROOVE SEAL (Sheet 1 of 2)

Time		Sealed Air Pressure		Shaft	Sealed Air Temperature		Air Flow Rate			% of Labyrinth
Hrs	Min	psig	N/cm²	RPM	°F	°K	SCFM	lb/sec	kg/sec	Flow
0	0	10	7	5000	85	302	.259	.0003	.0001	0.49
		45	31	5000	87	304	.403	.0005	.0002	0.32
		80	55	5000	95	308	.508	.0006	.0003	0.25
		115	79	5000	110	316	.594	.0008	.0003	0.22
		150	103	5000	117	320	3.347	.0043	.0019	0.98
		185	128	5000	134	330	5.528	.0070	.0032	1.35
		220	152	5000	167	348	13.985	.0178	.0081	2.98
		255	176	5000	144	335	33.409	.0426	.0193	6.09
1	24	290	200	5000	138	332	35.551	.0453	.0205	5.71
		10	7	5000	391	472	.648	.0008	.0004	1.53
		45	31	5000	390	472	4.230	.0054	.0024	4.13
		80	55	5000	384	469	8.883	.0113	.0051	5.45
		115	79	5000	378	465	12.474	.0159	.0072	5.57
		150	103	5000	390	472	16.735	.0213	.0097	5.93
		185	128	5000	382	467	21.373	.0272	.0123	6.21
		220	152	5000	384	469	23.970	.0305	.0138	5.93
		255	176	5000	390	472	25.698	.0327	.0148	5.56
2	24	290	200	5000	392	473	28.222	.0359	.0163	5.41
		10	7	5000	687	637	.648	.0008	.0004	1.78
		45	31	5000	687	637	6.045	.0077	.0035	6.86
		80	55	5000	669	627	10.660	.0136	.0062	7.57
		115	79	5000	675	630	14.256	.0182	.0082	7.41
		150	103	5000	666	625	20.080	.0256	.0116	8.18
		185	128	5000	634	607	26.164	.0333	.0151	8.67
		220	152	5000	634	607	35.955	.0458	.0208	10.13
		255	176	5000	614	596	43.686	.0556	.0252	10.62

TABLE 23.1 (Concluded)

BUILD 23, PERFORMANCE MAPPING, SPIRAL GROOVE SEAL (Sheet 2 of 2)

Time		Sealed Air Pressure		Shaft	Sealed Air Temperature		Air Flow Rate			% of Labyrinth Flow
Hrs	Min	psig	N/cm^2	RPM	°F	°K	SCFM	lb/sec	kg/sec	
3	30	290	200	5000	585	580	50.070	.0638	.0289	10.62
		10	7	5000	934	774	.249	.0003	.0001	0.75
		45	31	5000	981	800	.403	.0005	.0002	0.51
		80	55	5000	978	799	5.58	.0071	.0032	4.47
		115	79	5000	955	786	6.53	.0083	.0038	3.79
		150	103	5000	925	769	10.04	.0128	.0058	4.54
		185	128	5000	880	744	14.74	.0188	.0085	5.40
		220	152	5000	830	716	15.98	.0240	.0092	4.89
		255	176	5000	802	701	25.69	.0327	.0148	6.77
4	30	290	200	5000	777	687	45.52	.0580	.0263	10.51
		100	69	5000	560	566	25.14	.0320	.0145	14.00
		100	69	5000	413	485	30.72	.0391	.0178	15.83
		100	69	5000	348	449	33.52	.0427	.0194	16.62
5	13	100	69	5000	306	425	33.52	.0427	.0194	16.18

(Shut Down - Inspect for Cause of Increasing Leakage Rates)

TABLE 23.2

BUILD 23a, PERFORMANCE MAPPING, SPIRAL GROOVE SEAL

Time		Sealed Air Pressure		Shaft	Sealed Air Temperature		Air Flow Rate			% of Labyrinth Flow
Hrs	Min	psig	N/cm²	RPM	°F	°K	SCFM	lb/sec	kg/sec	
	12	25	17	5018	132	329	.329	.0004	.0002	0.40
	30	100	69	5022	355	452	.559	.0007	.0003	0.28
	42	110	76	5025	524	546	.583	.0007	.0003	0.29
1	0	100	69	5057	692	640	.559	.0007	.0003	0.33
1	30	90	62	5076	918	765	.534	.0007	.0003	0.38
1	36	115	79	5067	931	772	.594	.0008	.0003	0.34
1	42	290	200	5058	940	777	9.105	.0116	.0053	2.24
1	47	290	200	5068	729	660	35.505	.0452	.0205	8.04
1	54	290	200	5069	643	612	35.505	.0452	.0205	7.74
1	59	290	200	5071	573	574	35.505	.0452	.0205	7.49
2	5	255	176	5070	558	565	35.505	.0452	.0205	8.40
2	8	200	138	5080	560	566	19.109	.0243	.0110	5.69
2	15	100	69	5051	583	579	8.938	.0114	.0052	5.06
2	25	100	69	5034	478	521	16.758	.0213	.0097	8.95
2	30	100	69	5053	415	486	19.551	.0249	.0113	9.56
2	49	100	69	5045	327	437	19.551	.0249	.0113	9.56
2	59	15	10	5048	316	431	–			–

Since the above analysis did not correlate well with test results (measured taper is larger than calculated), the calculations were repeated based on actual physical measurements taken from the carbon wafer assembly. Results showed an axial offset of c.g.'s equal to .01563 inch (.03970 cm) generating a taper of approximately .00493 inch/inch at 1000 degrees F and 295 psid, which correlates exceptionally well with measurements taken from the seal carbon face following tests.

Data on Figure 36 shows calculated face seal dam to race clearance required to give the flow rates measured during Build 23.2 testing (Table 23.2). The circled numbers, 1 through 17, are in sequence from test start to stop. Calculated clearances were estimated based on the assumption of viscous, laminar, isothermal flow, with secondary piston ring flow assumed equal to zero. The curve suggests that the wafer section rolls in the direction to close the seal dam to race clearance as temperature is increased and in the process wear is generated on the seal face with the greater wear occurring at the seal dam. When temperature is decreased, the wafer section rolls in the opposite direction which moves the worn seal dam away from the race to generate a clearance which increases with decreasing temperature. This test data supports the results of analysis.

Figures 37, 38, and 39 show seal condition following test.

Test Build No. 24 - Performance Mapping, Spiral Groove Seal

Following the testing completed in Build 23, seal carbon wafer S/N 3 was reworked to align the axial c.g. of the carbon ring to the axial position of the c.g. of the metal shrink ring in the wafer assembly. Face taper measurements taken before and after rework confirmed that the accuracy of the calculations was within 10%. While taking measurements to determine if rework affected dimensions of the face sealing dam, the dam was fractured and was not repairable.

Carbon wafer S/N 1 was then measured, and the axial offset in carbon to shrink ring c.g.'s was determined by calculation to produce a section roll of

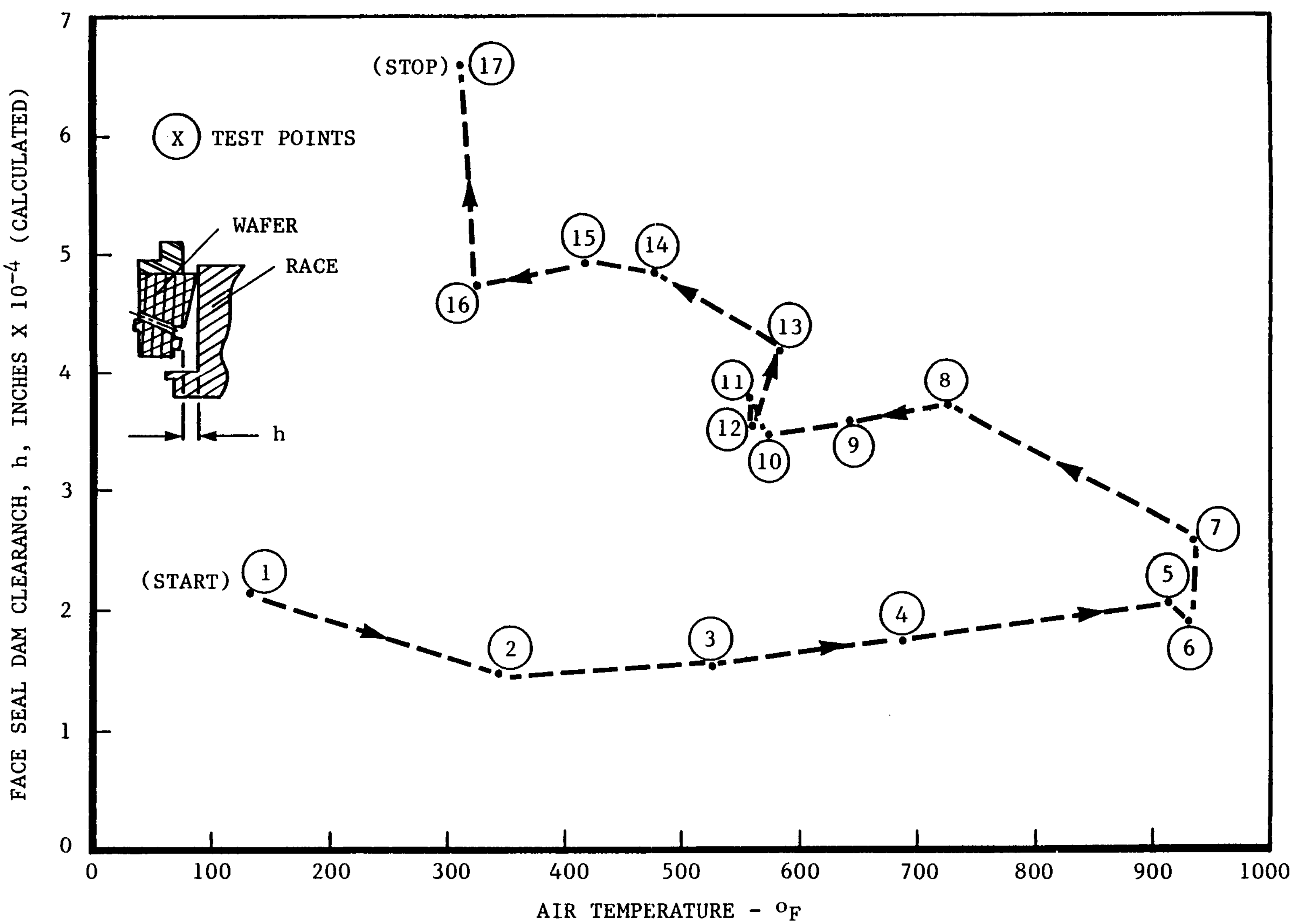

Figure 36. Calculated Seal Dam Clearance, Build 23.

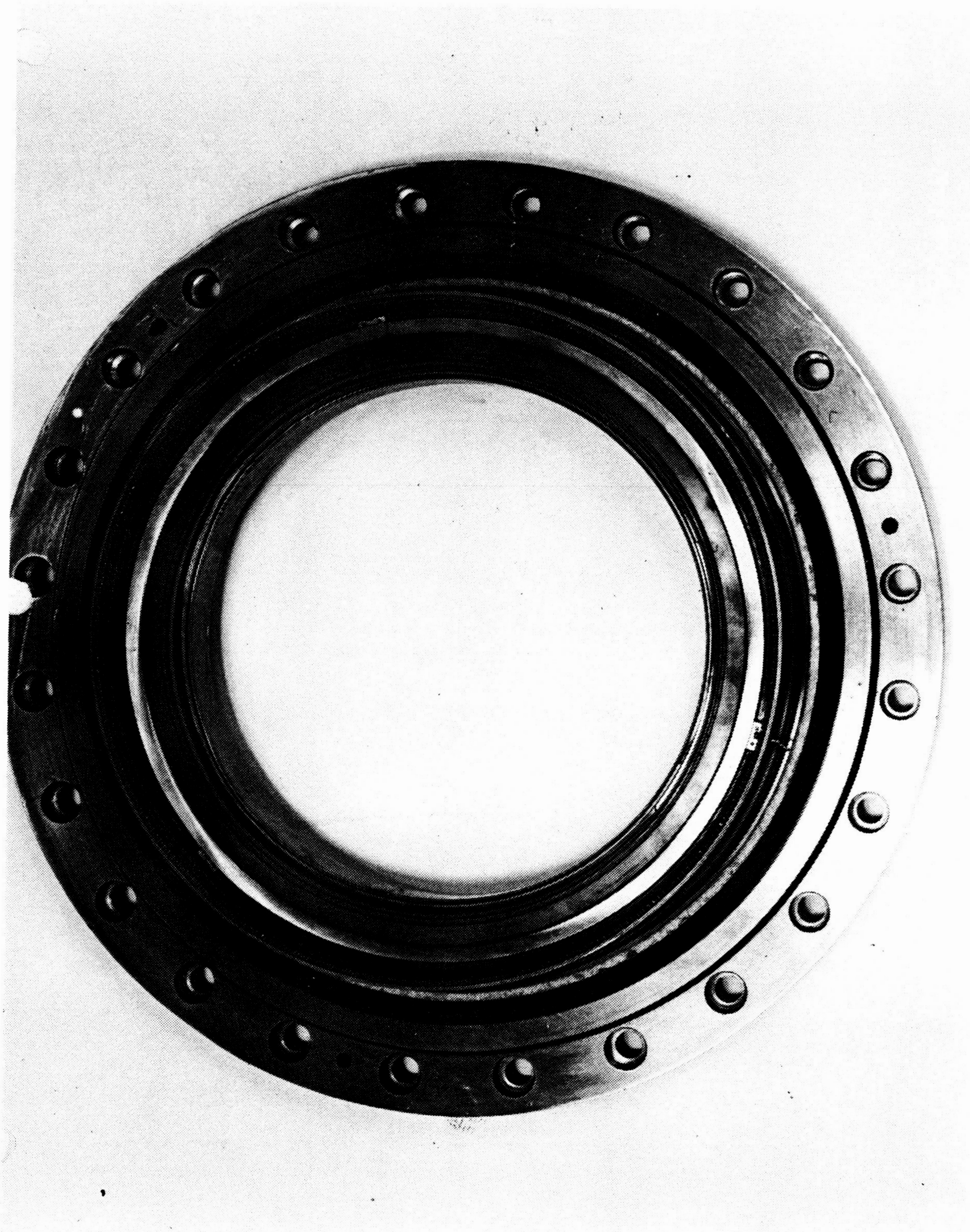

Figure 37. Seal Assembly Before Spiral Groove Bearing Tests, Build 23.

ORIGINAL PAGE IS
OF POOR QUALITY

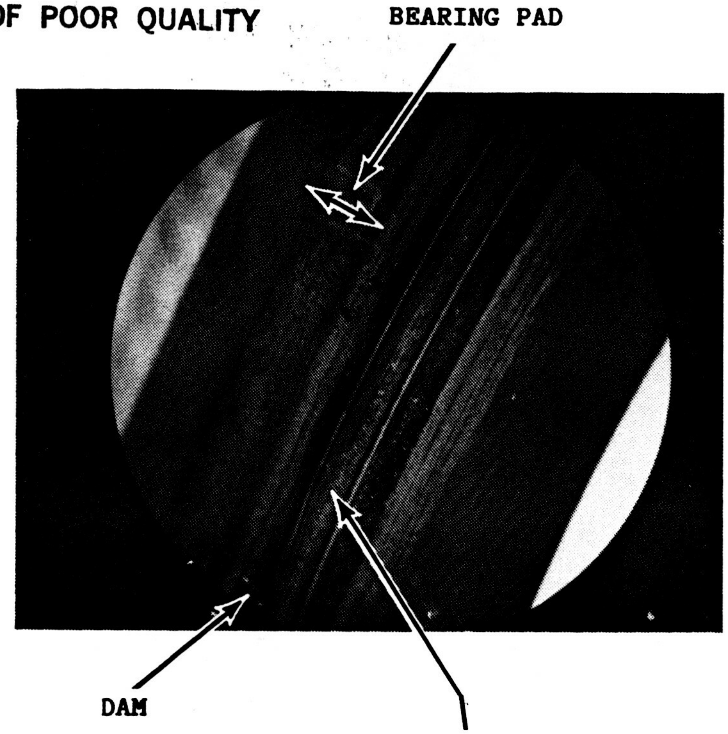

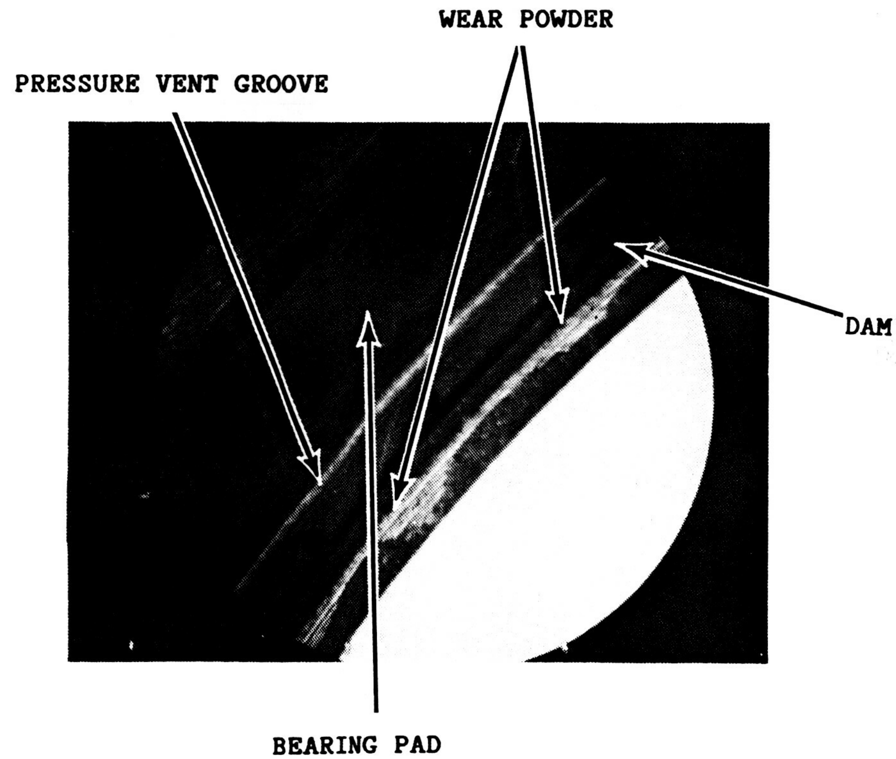

Figure 38. Carbon Face, After Build 23.

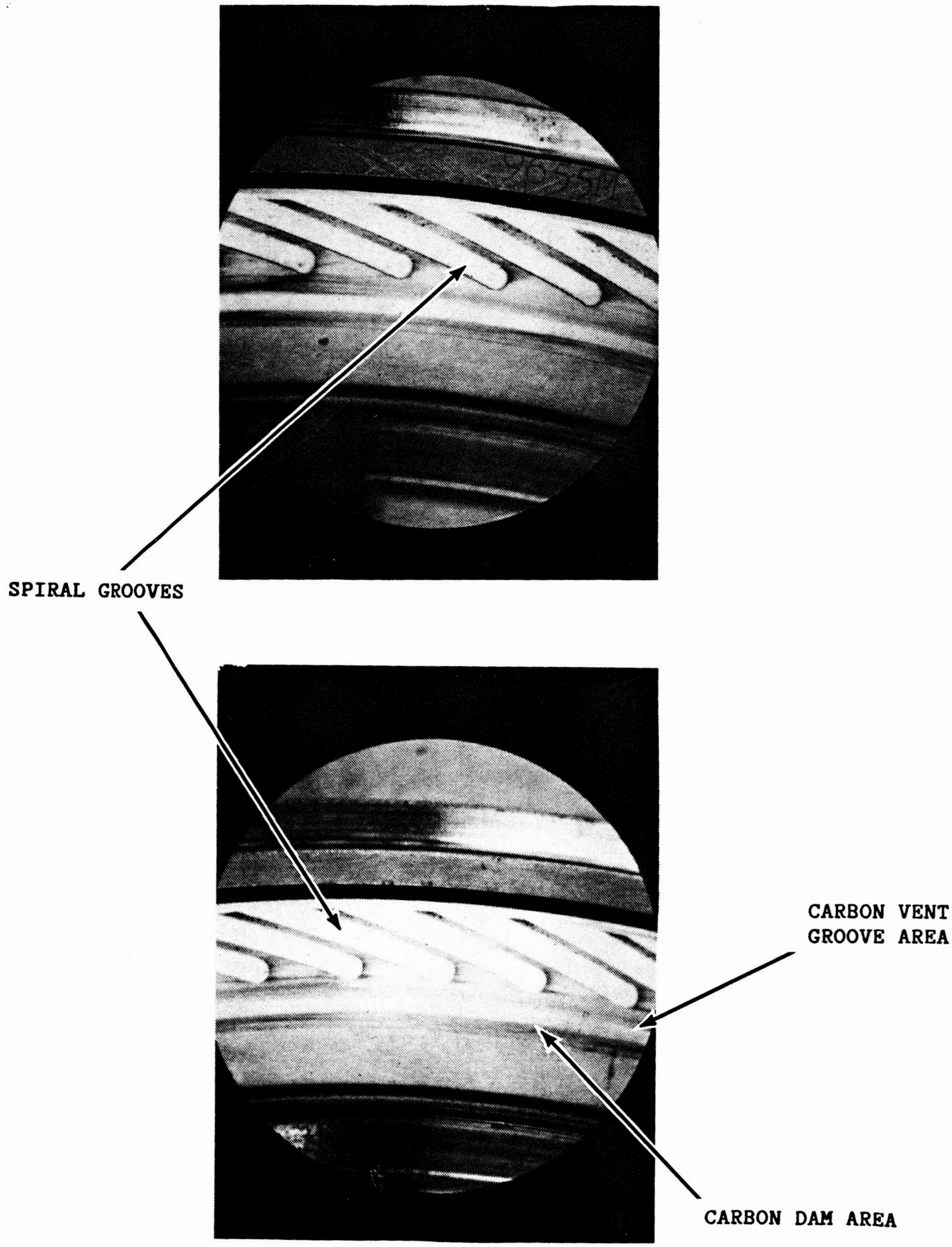

Figure 39. Spiral Groove Gas Bearings, After Build 23.

.001567 inch/inch at 1000 degrees F and 295 psid. Rework to align the c.g.'s again corroborated that the analytical prediction was within 10% of accuracy based on pre- and post-rework measurements of carbon face taper.

In addition to the above, the inside radius of the carbon face sealing dam was reworked to decrease the dam radial width from .045 inch (.0043 cm) to .0378 inch (.0960 cm) to increase the axial pressure force seating the seal against the race.

Seal wafer S/N 1, in seal housing S/N 1, with a carbon piston ring secondary seal was subsequently tested dynamically for 8 hours 26 minutes against the same spiral groove race used in Build 23. Test results are shown on Table 24.1. Average wear on the carbon face was .000546 inch (.001387 cm). Wear rate was .000067 inch (.000170 cm) per hour. Measured taper was .000128 inch (.000325 cm) with the high at the seal dam. No measurable wear occurred on the aluminum oxide hard coating of the spiral groove seal race. All hardware appeared to be in good condition (see photo, Figure 40).

Test Build No. 25 - Endurance Testing, Spiral Groove Seal

Spiral groove seal wafer S/N 1 was again reworked to increase the axial pressure force seating the seal against the race. Rework consisted of removing material from the inner radius of the carbon face sealing dam to reduce its radial width from .0378 to .0345 inch (.0960 to .0876 cm). The wafer assembly was not relapped or reconditioned in any other way (see Figure 41). The wafer was assembled in housing S/N 2 with a new carbon piston ring secondary seal prior to this endurance test.

One hundred three (103) hours thirty (30) minutes dynamic testing was subsequently completed at conditions and with air leakage rates shown on Table 25.1.

Seal carbon face wear for this test duration was as follows:

TABLE 24.1

BUILD 24, PERFORMANCE MAPPING, SPIRAL GROOVE SEAL (Sheet 1 of 2)

Time		Sealed Air Pressure		Shaft	Sealed Air Temperature		Air Flow Rate			% of Labyrinth
Hrs	Min	psig	N/cm^2	RPM	°F	°K	SCFM	lb/sec	kg/sec	Flow
	10	25	17	5000	87	304	3.29	.0042	.0019	6.23
	17	50	35	5000	96	309	4.20	.0054	.0024	3.06
	30	115	79	5000	108	315	5.94	.0076	.0034	2.18
	48	120	83	5000	116	320	9.08	.0116	.0052	3.24
1	15	140	97	5000	123	324	11.35	.0145	.0066	3.54
1	39	138	95	5000	304	424	6.45	.0082	.0037	2.33
1	55	130	90	5000	536	553	6.27	.0080	.0036	2.75
2	18	100	69	5000	588	582	8.38	.0107	.0048	2.37
2	25	95	65	5000	479	521	11.47	.0146	.0066	6.41
2	30	104	72	5000	372	462	16.48	.0210	.0095	8.01
2	48	112	77	5000	278	410	12.33	.0157	.0071	5.29
				(Shut Down to Repair Air Heaters)						
3	3	100	69	5000	112	317	5.30	.0068	.0031	2.21
3	13	125	86	5000	144	335	5.86	.0075	.0034	2.06
3	23	128	88	5000	172	351	6.23	.0079	.0036	2.20
3	33	125	86	5000	209	371	6.17	.0079	.0036	2.28
3	43	130	90	5000	287	415	5.96	.0076	.0034	2.25
3	53	125	86	5000	470	516	5.86	.0075	.0034	2.56
4	3	105	72	5000	574	574	5.71	.0073	.0033	3.07
4	13	100	69	5000	658	620	5.86	.0075	.0034	3.42
4	23	100	69	5000	734	663	8.37	.0107	.0048	5.04
4	33	120	83	5000	729	660	12.71	.0162	.0073	6.51
4	43	115	79	5000	768	682	11.88	.0151	.0067	6.42
5	8	108	74	5000	837	720	12.13	.0155	.0071	7.12
5	28	110	76	5000	877	742	12.23	.0156	.0071	7.17
5	33	115	79	5000	889	749	13.36	.0170	.0077	7.57

TABLE 24.1 (Concluded)

BUILD 24, PERFORMANCE MAPPING, SPIRAL GROOVE SEAL (Sheet 2 of 2)

Time		Sealed Air Pressure		Shaft	Sealed Air Temperature		Air Flow Rate			% of Labyrinth
Hrs	Min	psig	N/cm^2	RPM	°F	°K	SCFM	lb/sec	kg/sec	Flow
5	43	115	79	5000	887	749	17.23	.0219	.0100	9.75
5	53	151	104	5000	870	739	30.22	.0385	.0175	8.48
5	58	148	102	5000	829	716	31.61	.0403	.0183	13.95
6	8	150	104	5000	739	666	46.86	.0597	.0271	19.71
6	28	128	88	6500	840	723	19.32	.0246	.0111	9.76
6	37	117	81	5000	809	705	35.92	.0458	.0208	19.14
6	43	100	69	5000	800	700	20.95	.0267	.0121	12.97
6	47	105	72	5000	750	672	17.12	.0218	.0098	9.95
6	48	100	69	5000	700	645	16.76	.0213	.0093	9.95
6	49	98	68	5000	650	617	16.61	.0212	.0096	9.82
6	51	100	69	5000	600	584	16.76	.0213	.0097	9.52
6	54	100	69	5000	550	562	16.76	.0213	.0097	9.29
6	58	100	69	5000	500	533	16.76	.0213	.0097	9.06
7	5	100	69	5000	450	505	16.76	.0213	.0097	8.82
7	19	105	72	5000	400	478	16.27	.0207	.0094	7.97
7	23	105	72	5000	389	472	14.27	.0182	.0082	6.95
7	44	108	74	5000	350	450	14.45	.0184	.0083	6.70
7	52	108	74	5000	341	445	12.13	.0155	.0070	5.60
8	18	110	76	5000	300	423	11.65	.0148	.0067	5.15
8	26	110	76	5000	–		–			

(Shut Down)

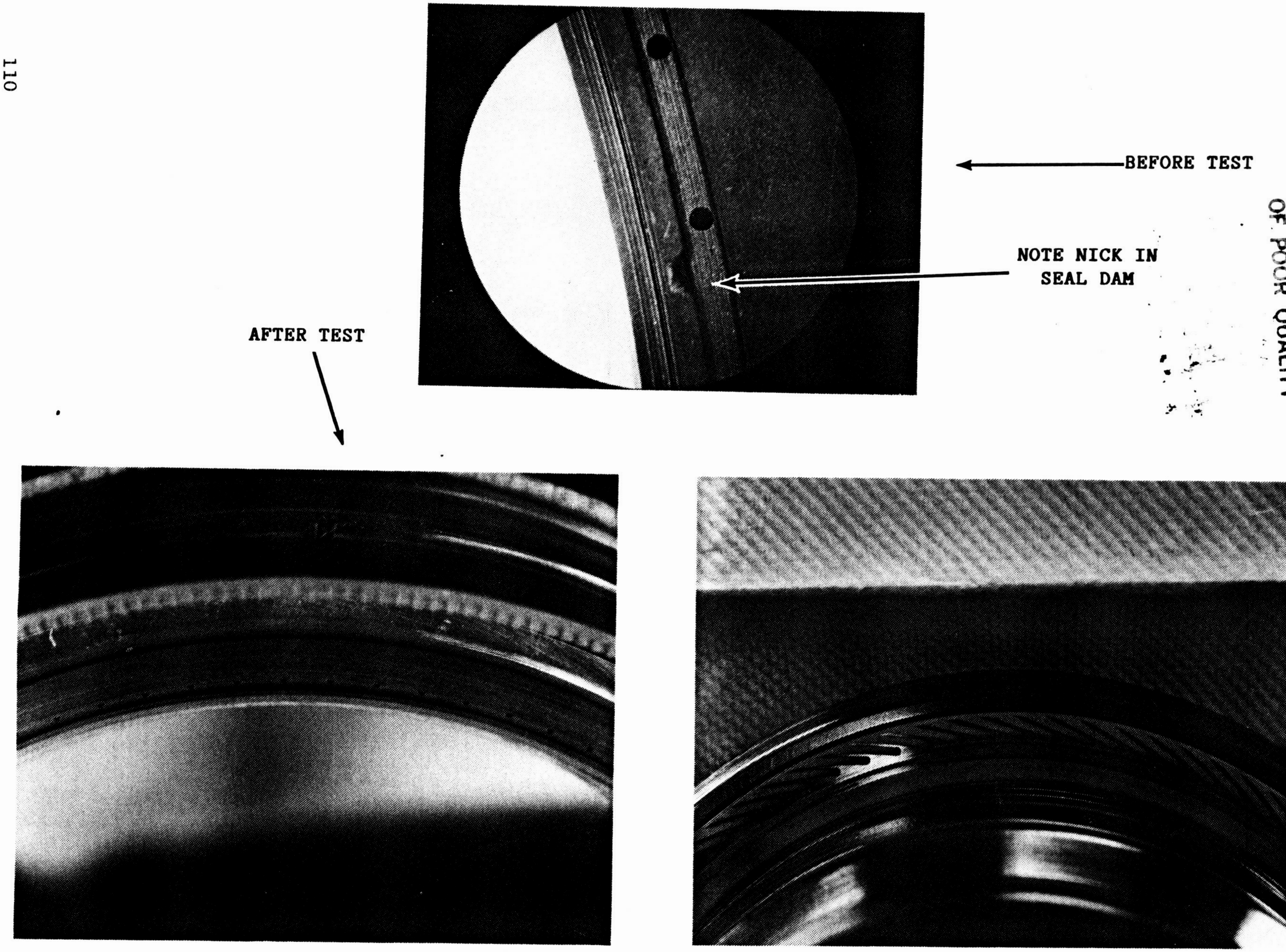

Figure 40. Seal and Race, After Build 24.

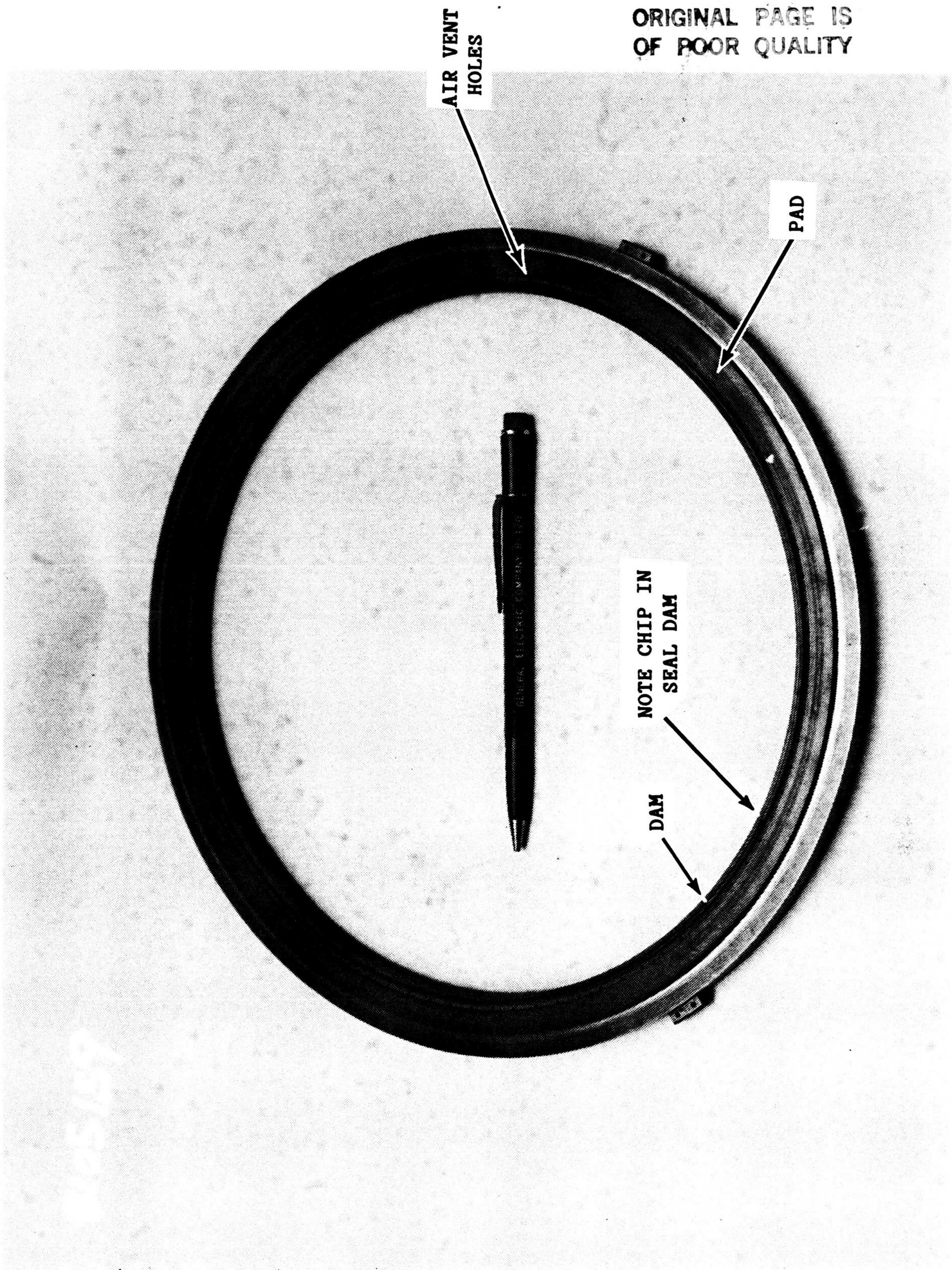

Figure 41. Spiral Groove Seal Wafer, Before Build 25.

TABLE 25.1

BUILD 25, ENDURANCE TEST, SPIRAL GROOVE SEAL (Sheet 1 of 5)

Time		Sealed Air Pressure		Shaft	Sealed Air Temperature		Air Flow Rate			% of Labyrinth
Hrs	Min	psig	N/cm²	RPM	°F	°K	SCFM	lb/sec	kg/sec	Flow
	15	5	3	5000	89	305	.232	.0003	.0001	0.55
	25	27	19	5000	98	310	.842	.0011	.0005	0.95
	35	127	88	5000	113	318	6.21	.0079	.0036	2.10
	40	127	88	5000	118	321	6.21	.0079	.0036	2.11
1	0	127	88	7400	193	362	6.21	.0079	.0036	2.24
1	21	125	86	7400	262	401	6.17	.0079	.0036	2.37
				(Shut Down - Replace Blown Fuse)						
1	31	127	88	7400	610	594	8.68	.0111	.0050	4.01
1	46	127	88	7400	728	660	11.78	.0150	.0068	5.73
2	1	123	85	7400	803	701	18.06	.0230	.0104	9.32
2	21	123	85	7400	818	710	27.55	.0351	.0159	14.31
2	41	123	85	7400	821	711	32.13	.0409	.0186	16.70
3	1	123	85	7400	840	722	32.13	.0409	.0186	16.83
3	21	135	93	7400	819	710	38.29	.0488	.0221	18.29
3	41	125	86	7400	835	719	33.91	.0432	.0196	17.60
4	1	125	86	7400	854	730	35.42	.0451	.0205	18.38
4	21	130	90	7400	862	734	37.65	.0480	.0218	18.92
4	41	126	87	7400	872	740	35.57	.0453	.0207	18.45
5	1	125	86	7400	881	745	35.42	.0451	.0205	18.57
5	21	123	85	7400	815	708	37.03	.0472	.0214	19.20
5	41	127	88	7400	832	717	34.10	.0434	.0197	17.30
6	1	125	86	7400	846	725	33.88	.0432	.0196	17.53
6	21	125	86	7400	840	722	33.88	.0432	.0196	17.49
6	41	123	85	7400	839	721	35.19	.0448	.0203	18.42
6	46	125	86	6250	840	722	33.88	.0432	.0196	17.49
6	49	125	86	5000	847	726	33.88	.0432	.0196	17.54
6	56	125	86	5000	750	672	43.12	.0549	.0249	21.48

TABLE 25.1 (Continued)

BUILD 25, ENDURANCE TEST, SPIRAL GROOVE SEAL (Sheet 2 of 5)

Time		Sealed Air Pressure		Shaft	Sealed Air Temperature		Air Flow Rate			% of Labyrinth
Hrs	Min	psig	N/cm^2	RPM	°F	°K	SCFM	lb/sec	kg/sec	Flow
7	2	126	87	5000	500	533	37.08	.0472	.0214	16.33
7	21	127	88	5000	397	476	34.10	.0434	.0197	14.09
7	48	127	88	5000	-		-			
(Test Aborted Due to In Plant Power Loss)										
8	0	135	93	2600	183	357	25.53	.0325	.0148	5.68
8	17	123	85	5500	195	364	30.61	.0390	.0177	11.38
8	50	135	93	6879	220	377	35.10	.0447	.0203	12.23
9	20	125	86	7350	313	429	33.91	.0432	.0196	13.50
10	20	125	86	7349	470	516	41.62	.0530	.0240	18.17
11	20	125	86	7356	689	638	40.08	.0511	.0232	19.45
12	12	125	86	7357	783	783	40.08	.0511	.0232	20.23
(Rig Shut Down - Lost Power to Roots Blower)										
12	45	130	90	7000	833	718	43.30	.0552	.0250	21.52
13	45	125	86	7000	883	746	42.54	.0542	.0246	22.32
14	42	120	83	7000	901	756	39.35	.0501	.0227	21.56
(Shut Down - Roots Blower Lost Power)										
15	27	132	91	7341	473	518	56.86	.0722	.0328	23.68
15	57	124	85	7180	637	609	49.15	.0626	.0284	23.48
16	30	129	89	7172	684	635	50.03	.0637	.0289	23.55
16	57	125	86	7179	748	671	48.71	.0620	.0281	24.24
17	27	125	86	7160	773	685	46.24	.0589	.0267	23.33
18	2	124	85	7159	842	723	44.54	.0567	.0257	23.17
18	55	124	85	7162	887	748	43.45	.0553	.0251	23.04
19	55	123	84	7162	791	695	44.50	.0567	.0257	22.86
20	52	115	79	7162	704	646	42.18	.0537	.0244	22.19
21	48	115	79	7148	689	638	41.59	.0530	.0240	21.74
22	32	115	79	7154	692	640	41.59	.0530	.0240	21.76

TABLE 25.1 (Continued)

BUILD 25, ENDURANCE TEST, SPIRAL GROOVE SEAL (Sheet 3 of 5)

Time		Sealed Air Pressure		Shaft	Sealed Air Temperature		Air Flow Rate			% of Labyrinth
Hrs	Min	psig	N/cm^2	RPM	°F	°K	SCFM	lb/sec	kg/sec	Flow
40	8	115	79	7144	675	630	41.59	.0530	.0240	21.61
(Rig Shut Down - Motor Failure)										
40	18	45	31	5968	100	311	24.18	.0308	.0140	19.17
40	53	45	31	6616	164	346	18.18	.0232	.0105	15.22
(Shut Down - Chip Detector)										
41	21	110	76	6956	148	337	46.30	.0590	.0268	18.31
(Shut Down - Belt Detector)										
41	25	35	24	6456	97	309	18.39	.0234	.0106	17.47
41	39	35	24	7171	101	311	16.56	.0211	.0096	15.79
42	0	55	38	7239	187	359	22.86	.0291	.0132	16.69
42	7	113	78	7239	293	418	46.57	.0593	.0269	20.02
42	53	118	81	7350	323	435	39.06	.0498	.0226	16.47
43	19	110	76	7381	509	538	43.69	.0557	.0252	21.81
43	38	110	76	7393	547	559	43.69	.0557	.0252	22.23
43	58	110	76	7406	603	590	43.07	.0579	.0249	22.52
44	18	110	76	7411	627	604	41.32	.0526	.0239	21.85
44	38	110	76	7416	643	612	43.69	.0557	.0252	23.27
44	58	110	76	7420	660	622	43.69	.0557	.0252	23.45
45	19	110	76	7423	671	628	43.69	.0557	.0252	23.57
45	39	110	76	7432	681	634	43.69	.0557	.0252	23.67
45	58	110	76	7430	691	639	43.69	.0557	.0252	23.77
46	18	108	74	7436	699	644	43.34	.0552	.0250	24.05
47	13	108	74	7445	743	668	40.45	.0515	.0234	22.87
47	24	90	62	7447	437	498	42.17	.0537	.0244	24.13
47	26	90	62	5263	384	469	42.17	.0537	.0244	23.40
(Shut Down)										

TABLE 25.1 (Continued)

BUILD 25, ENDURANCE TEST, SPIRAL GROOVE SEAL (Sheet 4 of 5)

Time		Sealed Air Pressure		Shaft	Sealed Air Temperature		Air Flow Rate			% of Labyrinth
Hrs	Min	psig	N/cm²	RPM	°F	°K	SCFM	lb/sec	kg/sec	Flow
47	38	-		7400	-		-			
(Shut Down - Water in Seal Air - Compressor Failure - Water/Oil in Supply Line)										
47	50	35	24	1300	92	306	-	-	-	-
48	10	115	79	7400	100	311	65.34	.0832	.0378	23.84
48	35	115	79	7400	107	315	53.46	.0681	.0309	19.63
48	50	110	76	7400	118	321	49.47	.0630	.0286	19.08
49	10	0	0	7400	(Adjust Air Compressor)					
49	14	110	76	7400	121	322	48.02	.0612	.0277	18.57
50	0	105	72	7400	297	420	42.80	.0545	.0247	19.68
50	34	115	79	7400	390	472	47.52	.0605	.0275	21.36
51	34	115	79	7400	514	541	44.55	.0567	.0257	21.44
54	24	115	79	7400	549	560	43.07	.0549	.0249	21.10
					(Shut Down)					
55	19	110	76	7000	126	325	45.98	.0586	.0266	17.85
55	44	125	86	7300	314	430	49.94	.0636	.0289	19.89
56	53	120	83	7300	525	547	45.45	.0579	.0263	21.18
57	37	120	83	7300	595	586	49.94	.0636	.0289	24.09
58	50	120	83	7300	630	605	43.03	.0548	.0249	21.09
59	15	110	76	7350	643	612	40.74	.0519	.0235	21.70
60	29	115	79	7350	666	625	42.17	.0537	.0244	21.82
61	19	120	83	7350	685	636	42.42	.0540	.0245	21.31
76	41	115	79	7400	736	664	46.93	.0598	.0271	25.03
78	14	110	76	7400	786	692	43.65	.0556	.0252	23.76
79	49	120	83	7400	823	712	45.45	.0579	.0263	24.17
81	24	115	79	7400	836	720	42.18	.0537	.0243	23.42
83	44	125	86	7400	835	719	46.24	.0589	.0267	23.80
84	59	125	86	7400	835	719	46.24	.0589	.0267	23.82

TABLE 25.1 (Continued)

BUILD 25, ENDURANCE TEST, SPIRAL GROOVE SEAL (Sheet 5 of 5)

Time		Sealed Air Pressure		Shaft	Sealed Air Temperature		Air Flow Rate			% of Labyrinth
Hrs	Min	psig	N/cm^2	RPM	°F	°K	SCFM	lb/sec	kg/sec	Flow
100	59	120	83	7400	733	662	62.69*	.0799	.0362	See Note*
101	52	125	86	7400	725	658	64.74*	.0825	.0374	See Note*
101	57	115	79	7400	599	588	62.37*	.0825	.0374	See Note*
102	3	120	83	7400	430	494	73.08*	.0825	.0374	See Note*
102	8	120	83	7400	393	474	73.08*	.0825	.0374	See Note*
102	13	129	89	7400	372	462	75.50*	.0961	.0436	See Note*
102	18	120	83	7400	355	452	75.50*	.0961	.0436	See Note*
102	23	120	83	7400	332	440	69.46*	.0961	.0436	See Note*
102	28	125	86	7400	323	435	75.46*	.0961	.0436	See Note*
102	33	125	86	7400	315	430	75.46*	.0961	.0436	See Note*
102	38	125	86	7400	309	427	75.46*	.0961	.0436	See Note*
102	43	125	86	7400	305	425	75.46*	.0961	.0436	See Note*
102	48	125	86	7400	294	419	75.46*	.0961	.0436	See Note*
103	15	125	86	7400	268	404	80.08*	.1020	.0463	See Note*
103	30	125	86	7400	263	401	77.00*	.1020	.0463	See Note*
–	–	118	81	0	254	396	81.12*	.1020	.0463	See Note*

Note: Air compressor will not pump this much flow (≃ 58 SCFM, maximum). Vapors were noted from discharge pipes downstream of seal. Source of vapors is air storage tank. Liquid through air rotometer gives high indicated false readings. Storage tank drain valve not open.

Radial Location	Average Wear inches	cm
Seal Dam	.002600	.006604
Bearing Pad I.D.	.000719	.001826
Bearing Pad Ctr.	.000665	.001689
Bearing Pad O.D.	.000696	.001768

The above wear data is based on the average of measurements taken at six (6) equally spaced circumferential locations sixty (60) degrees apart. Radial flatness remained within .000055 inch (.000140 cm), average, on the gas bearing pad implying good flatness during testing. Pad wear averaged .000693 inch (.001760 cm) for a wear rate of .0000068 inch/hour (.0000173 cm/hr). Based on an initial available depth of carbon wear material of .065 inch (.165 cm), this would extrapolate to a minimum carbon wear life of 9561 hours.

Wear on the seal face dam was approximately .0026 inches (.0066 cm), or approximately .00188 inch (.00478 cm) greater than at the inner radius of the gas bearing pad on the carbon face. The surface of the sealing dam was very rough and striated circumferentially, and the inner and outer radius of the dam, as well as the circumferential groove above the dam and the 90 air bleed holes that feed high pressure air to the groove, were coated with a reddish colored fine powder with the consistency of iron oxide. In referring to Table 25.1, Sheet 4, a failure was experienced in the supply air compressor approximately 56 hours 6 minutes prior to test completion. Oily water was found in the seal pressurizing air pipes after the compressor failure. Again, 2 hours 30 minutes before test completion vapors were observed exiting the seal downstream air plenum (see Table 25.1, Sheet 5), followed by a significant increase in seal air leakage rates. Inspection of the seal pressurizing air plenum showed all surfaces to be coated with red colored fine abrasive powder. The vapors were the result of failure to open the air storage tank drain line prior to testing. This allowed the tank to accumulate water and compressor oil. This mixture apparently flushed rust through the pressurizing air to the seal inlet air plenum (see photos, Figures 42 through 48).

The above implied that the seal dam wear was caused by ingestion of abrasive particles in the seal dam interface, causing the rapid wear and sudden increase in air leakage rates noted 2.5 hours prior to the end of test.

ORIGINAL PAGE IS
OF POOR QUALITY

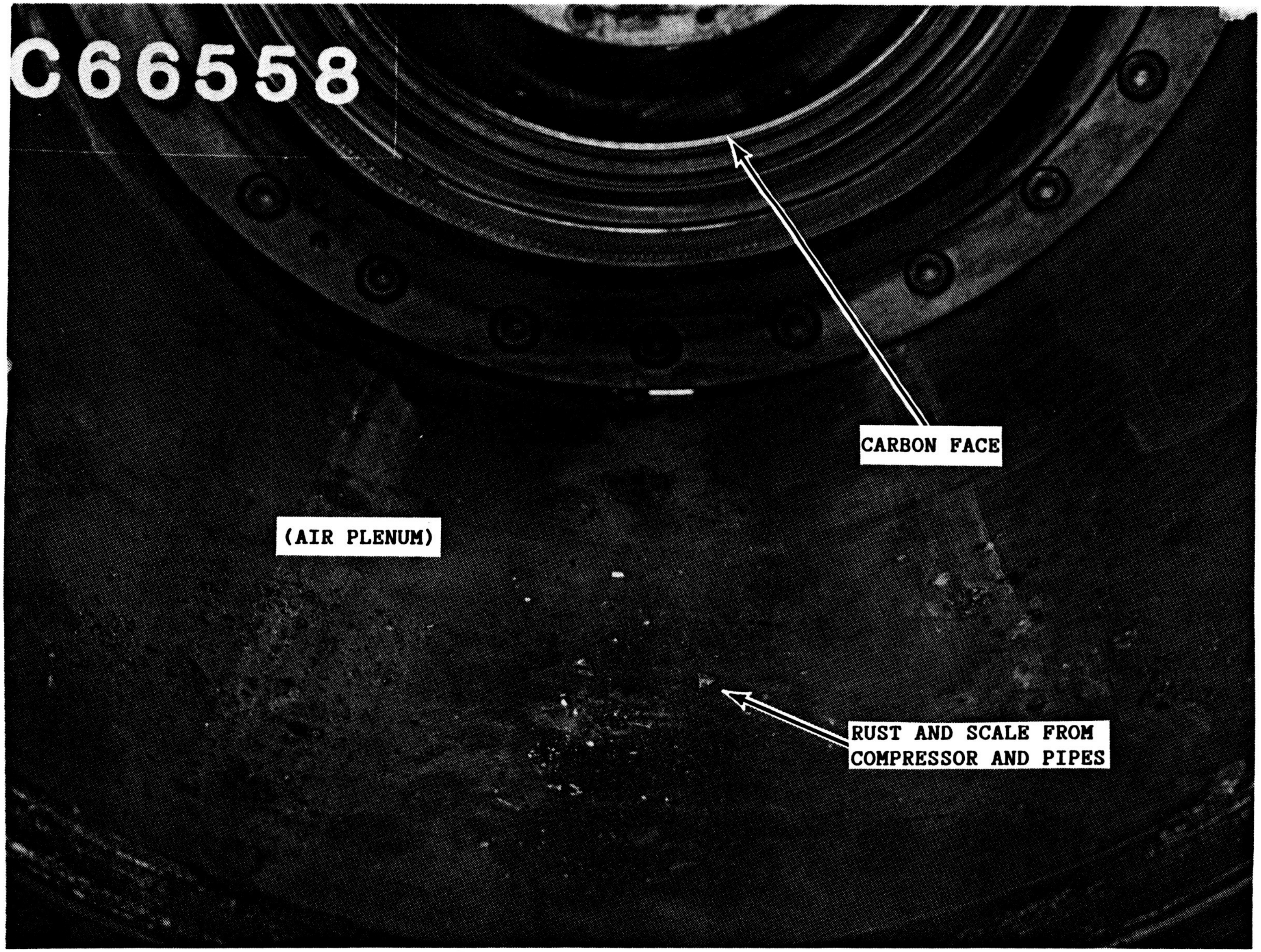

Figure 42. Seal and Air Plenum, After Build 25.

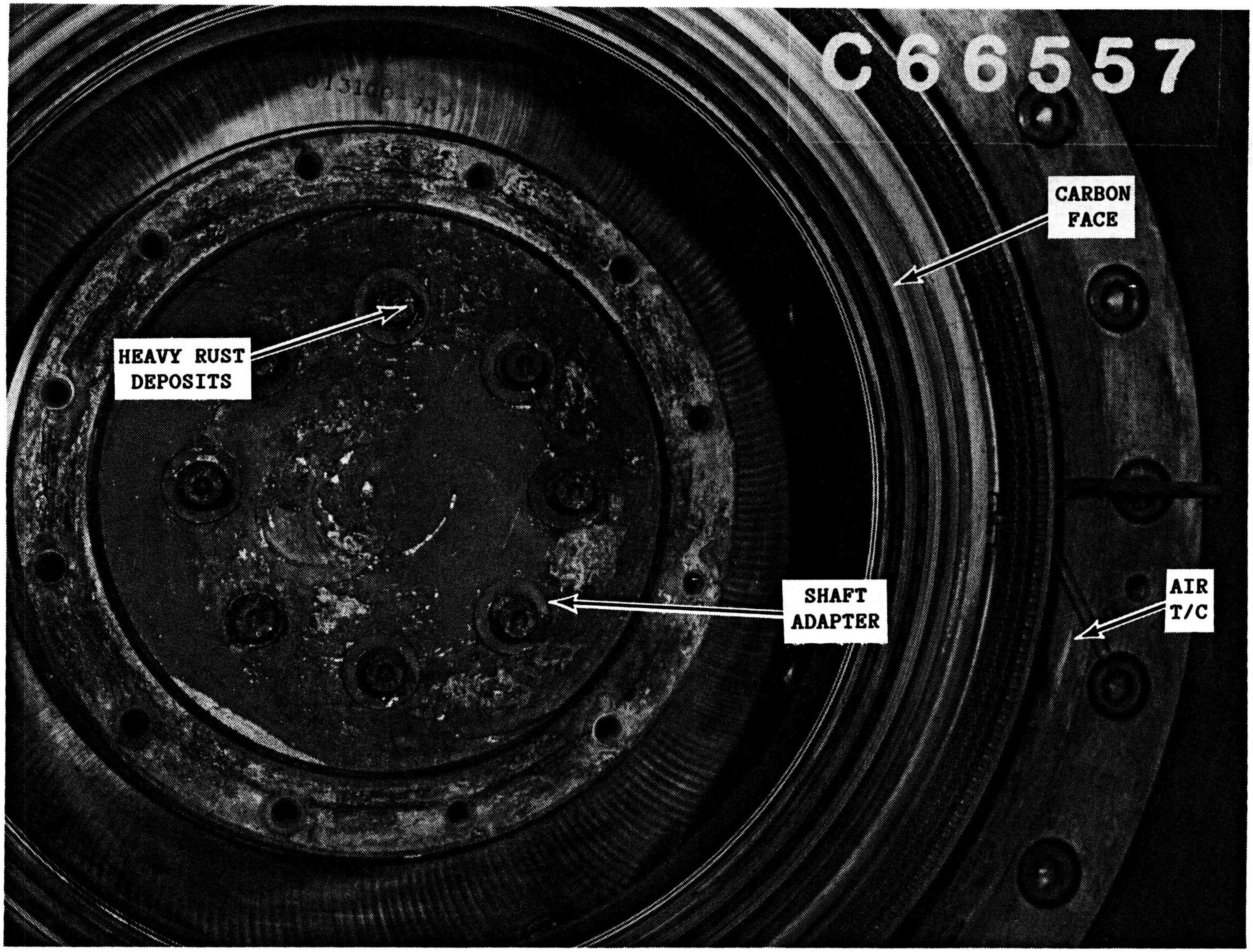

Figure 43. Shaft Face, After Build 25.

ORIGINAL PAGE IS
OF POOR QUALITY

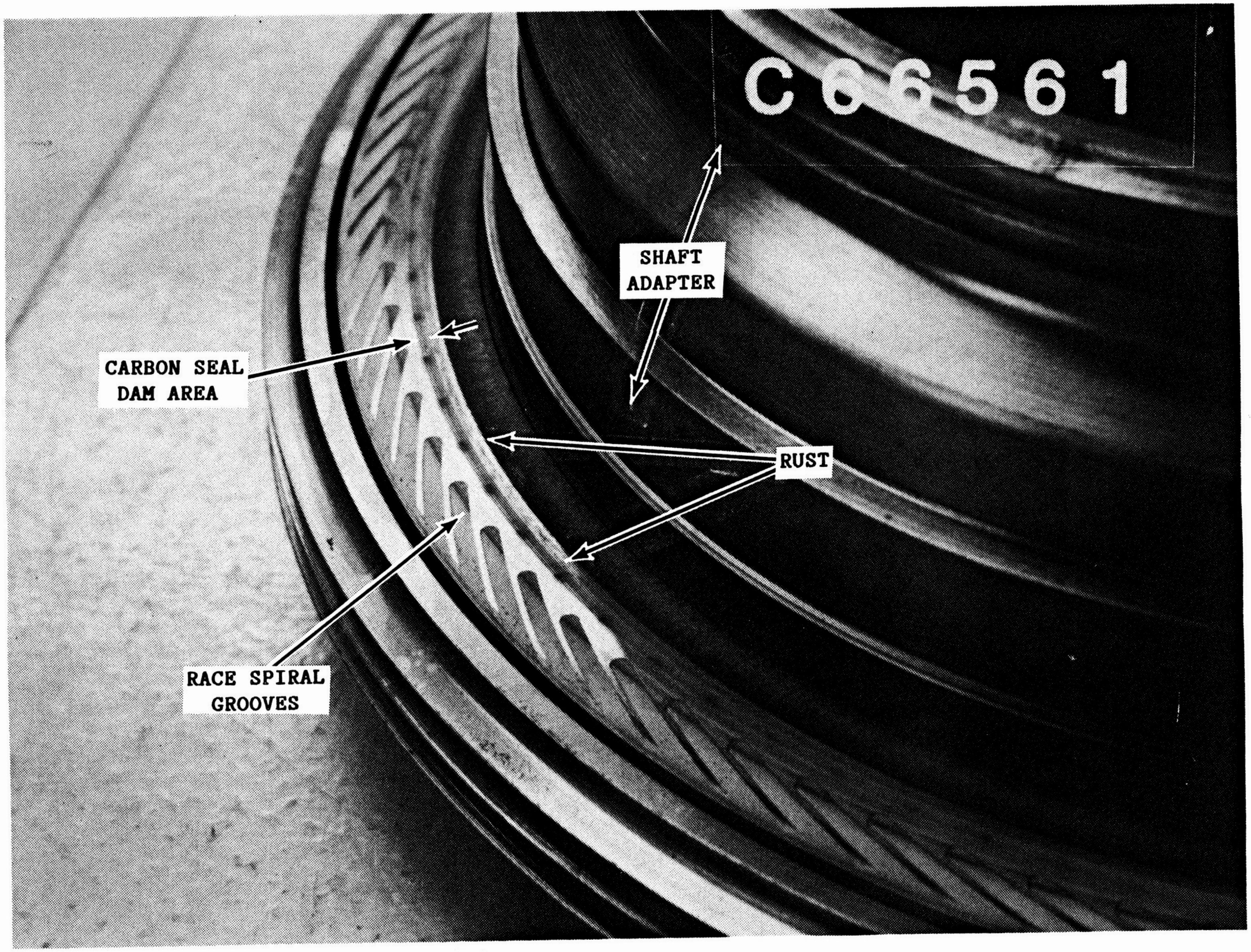

Figure 44. Spiral Groove Bearing Race, After Build 25.

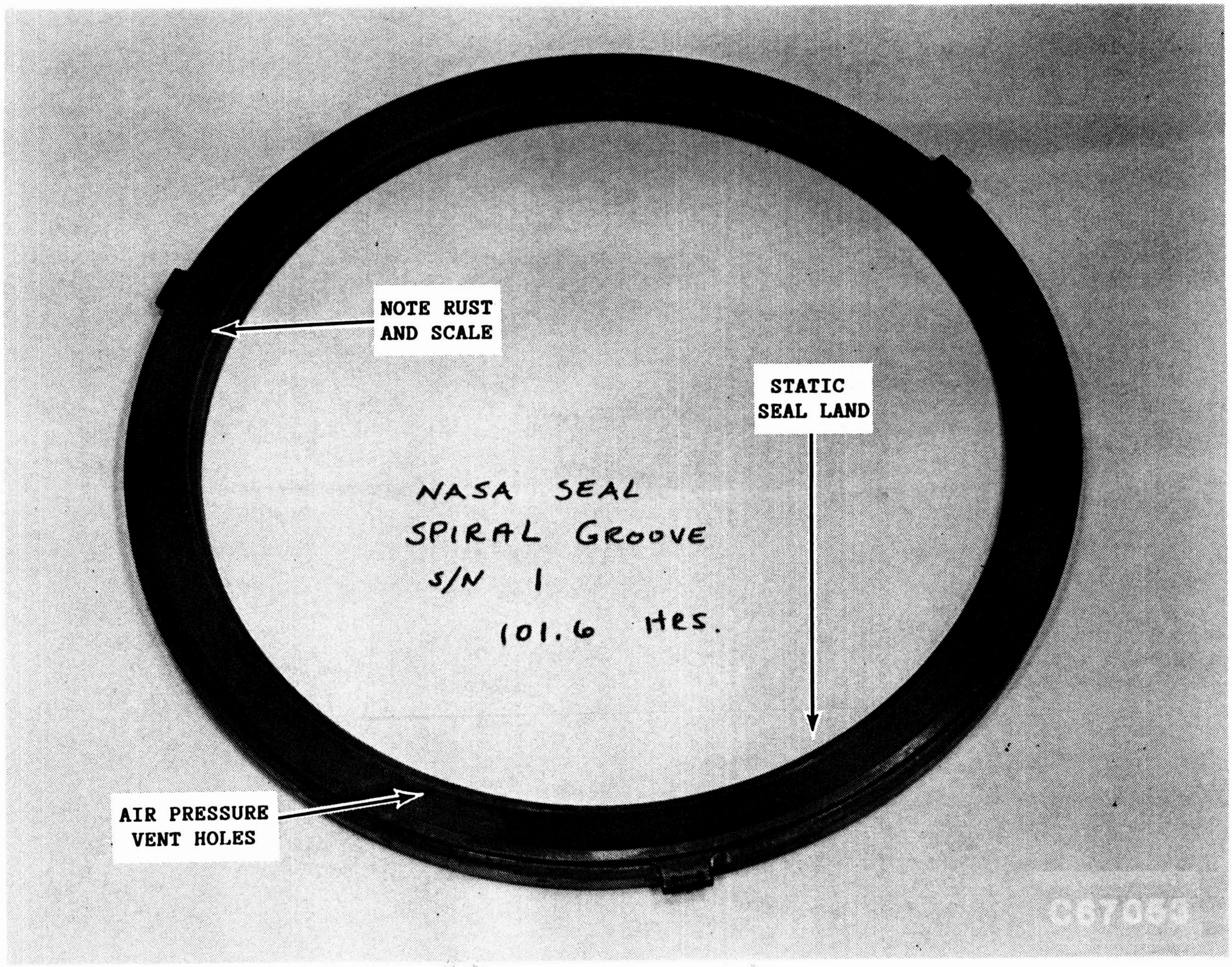

Figure 45. Wafer Aft Face, After Build 25.

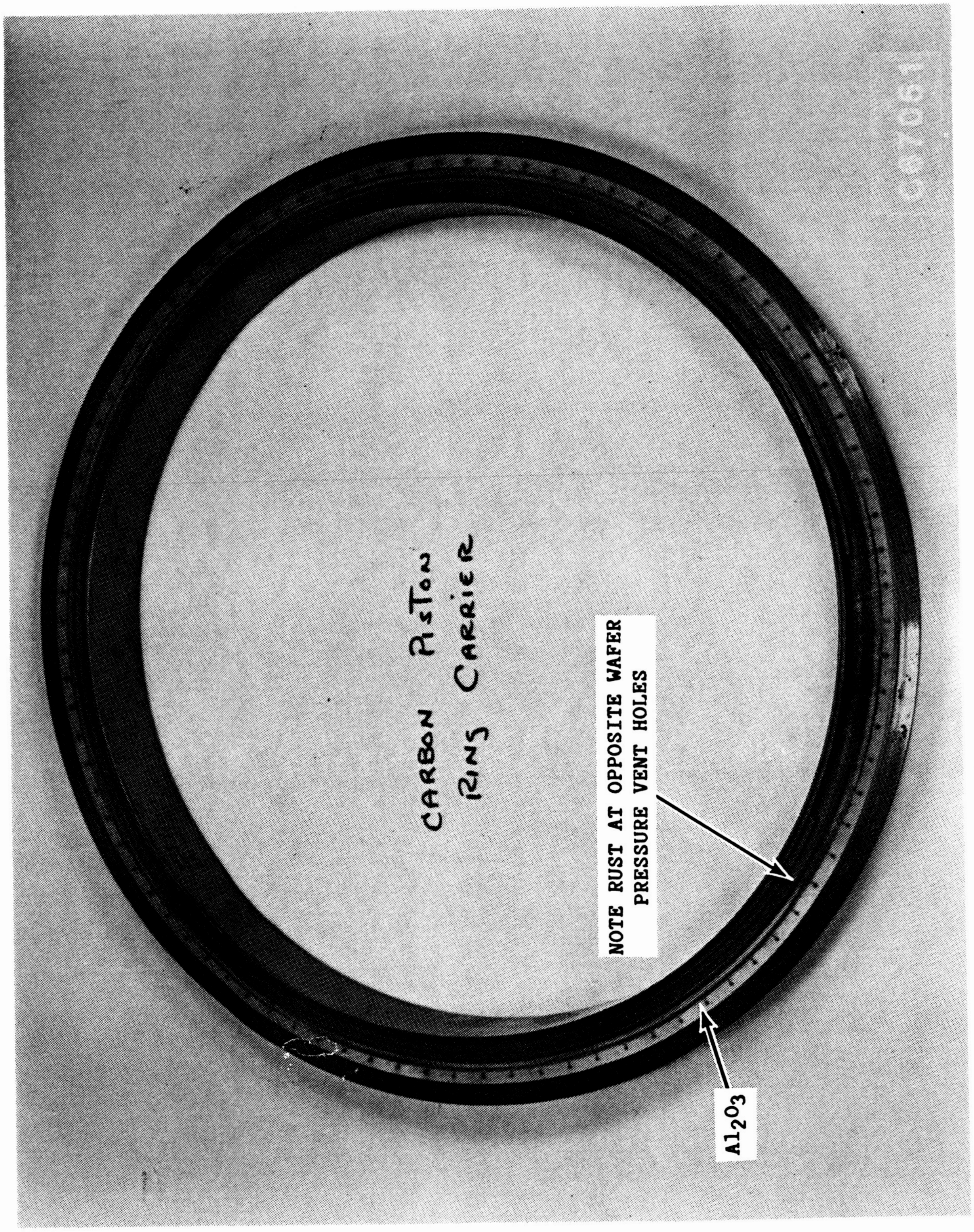

Figure 46. Carrier Face, After Build 25.

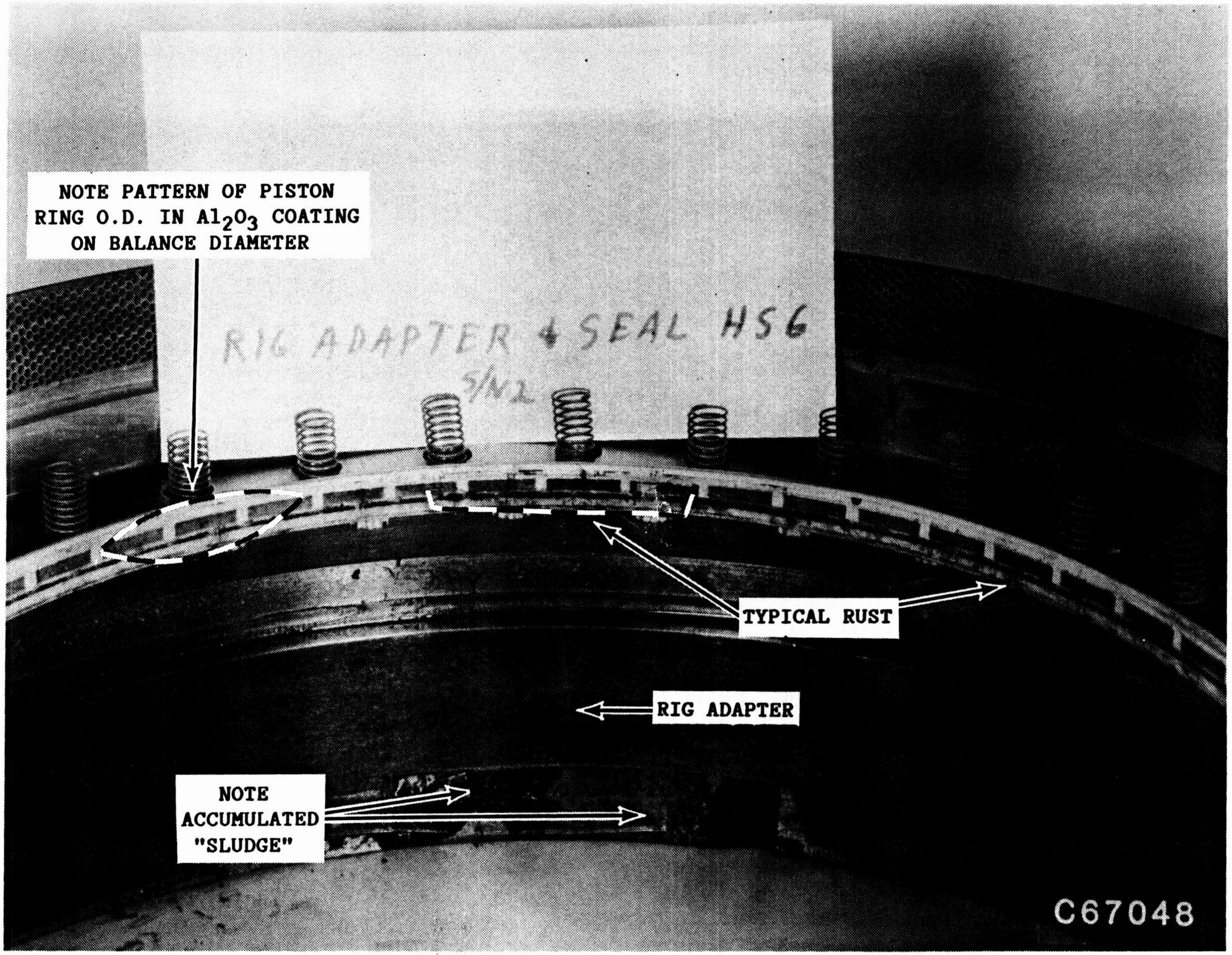

Figure 47. Seal Housing Balance Diameter, After Build 25.

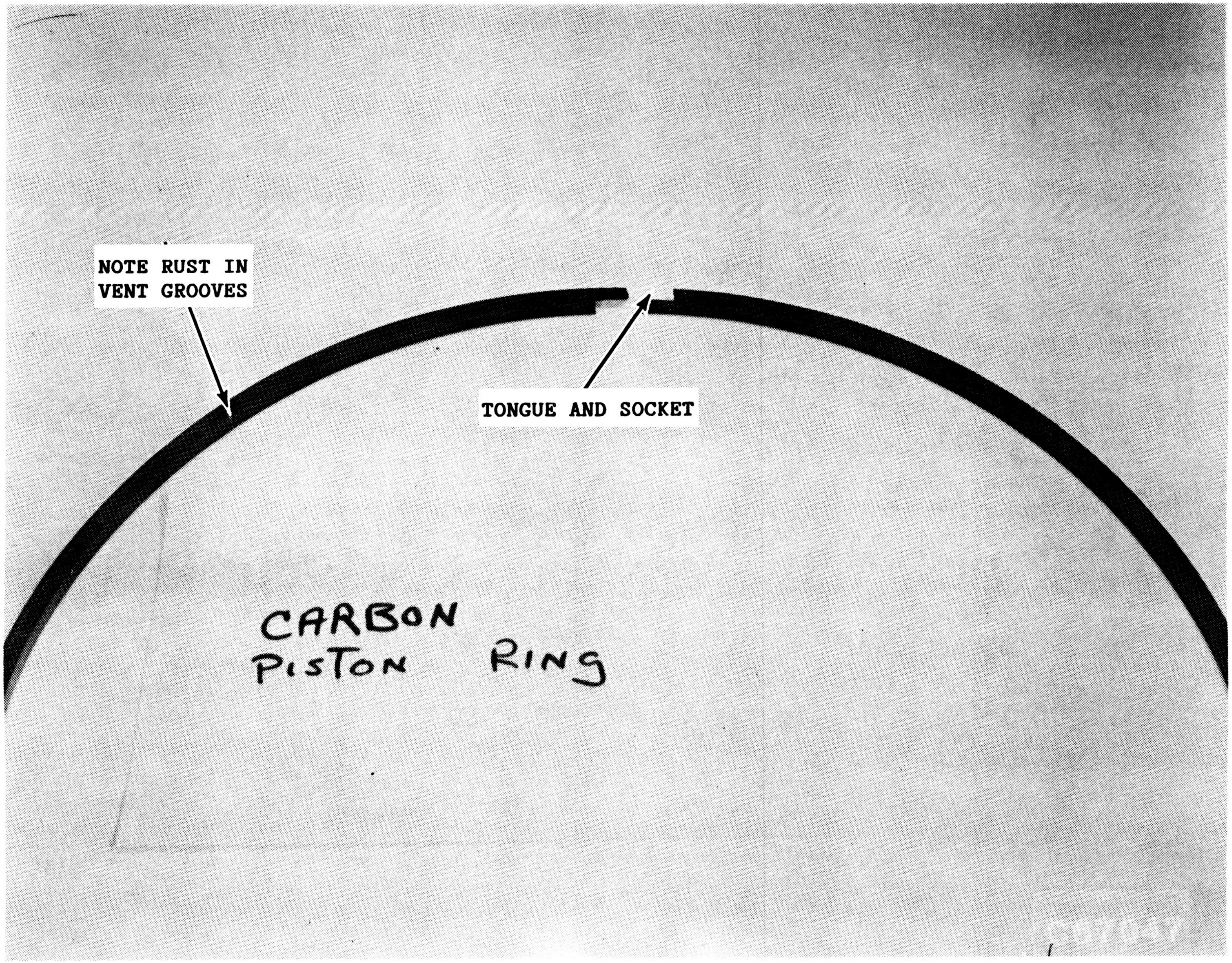

Figure 48. Carbon Piston Ring, After Build 25.

No measurable wear was observed in the hard coating (aluminum oxide) of the spiral groove race. Light striations were observed in the vicinity of the race opposite the carbon face sealing dam but not in the bearing pad area (see photo, Figure 44).

Conclusions and Recommendations

The three (3) lift pad gas bearing seal designs tested demonstrated adequate potential to encourage continuation of development for application to high pressure, high speed, energy conservative gas sealing applications.

The principal seal design problems experienced during this program were related to the structure of the seal face wafer assembly. The wafer lacked sufficient structural stiffness to control radial pressure dilation and thermally and pressure generated section torsional "roll." Strain gage measurements were made on several wafers to determine pressure induced deflection. These measurements showed that 300 psi pressure drop generated radial dilation in the order of 1500 micro-radians with circumferential variations in section roll in the order of 350 micro-radians. The radial dilation affects a change in total seal axial pressure closing force of minus 11.07 pounds at 300 psid due to the increased projected interface area between the seal face dam and the piston ring balance diameter. This affects a reduction in allowable friction coefficient at the piston ring to balance diameter interface from .275 to .085 with spring force equal to 10.44 pounds, used earlier in the program, and .394 to .204 with the later used 17.40 pound spring force. Both are marginal in providing the magnitude of force required to allow the seal to track the axial one per rev runout of the seal race. If mass inertia affects are added, the situation becomes more marginal. To compensate for this, the seal face dams were reworked to restore the pressure closing forces prior to the last several tests as described previously under Test Results and Discussion. The pressure induced torsional moments are of sufficient magnitude when compared to the calculated gas bearing film thickness to cause face wear and increased air leakage rates. In addition to the pressure-strain problems, the large differential thermal expansion rate between the carbon and the steel shrink ring is the source of significant

additional section roll when even small offsets exist between the axial centers of stiffness of the carbon and steel (see Figure 49). The relatively low thermal expansion rate of the carbon results in a shrink line force (F) of approximately 600 pounds per inch of circumference at room temperature in order that a sufficient fit is retained at part temperature of 1000 degrees F. This force varies almost linearly with temperature. The composite stiffness of the wafer section about the Y-Y plane is approximately .041 lb-inch squared. Using the equation, theta equals moment times radius squared divided by stiffness, the section roll at 1000 degrees F and .01 inch offset is approximately 3000 micro-radians or a deflection across the seal face of approximately .0018 inch. This affect was clearly demonstrated in Test Build No. 23. To correct these problems it became necessary to measure each individual wafer and, using the measured data, determine analytically the dimensional adjustments required to align the axial locations of the carbon with respect to the steel and the composite center of stiffness with respect to the center of radial pressure force. Material was then removed from appropriate areas of the shrink ring, carbon, or both to correct the problem.

The above described "stiffness" problem is detrimental in the manufacture of the part as well as in its operation. During manufacture the problem shows up in final machining and lapping operations where material removed from one face generates a section roll which shows up as a taper on the opposite face. During operation any face wear incurred changes the axial location of the center of stiffness of the carbon and affects a section roll of the wafer assembly. This is more pronounced on the spiral groove assembly wafers because the entire dynamic face of the carbon is part of the section hoop, whereas the stepped and tapered bearing wafers contain radial vent grooves in the dynamic faces which effectively interrupts the hoops except at the sealing dams.

In addition to the stiffness problem, other areas require improvement as follows:

1. <u>Spline Inserts</u> - The carbon inserts installed by rework at the male radial splines on the wafer assembly are too fragile. Several of these fractured during normal handling.

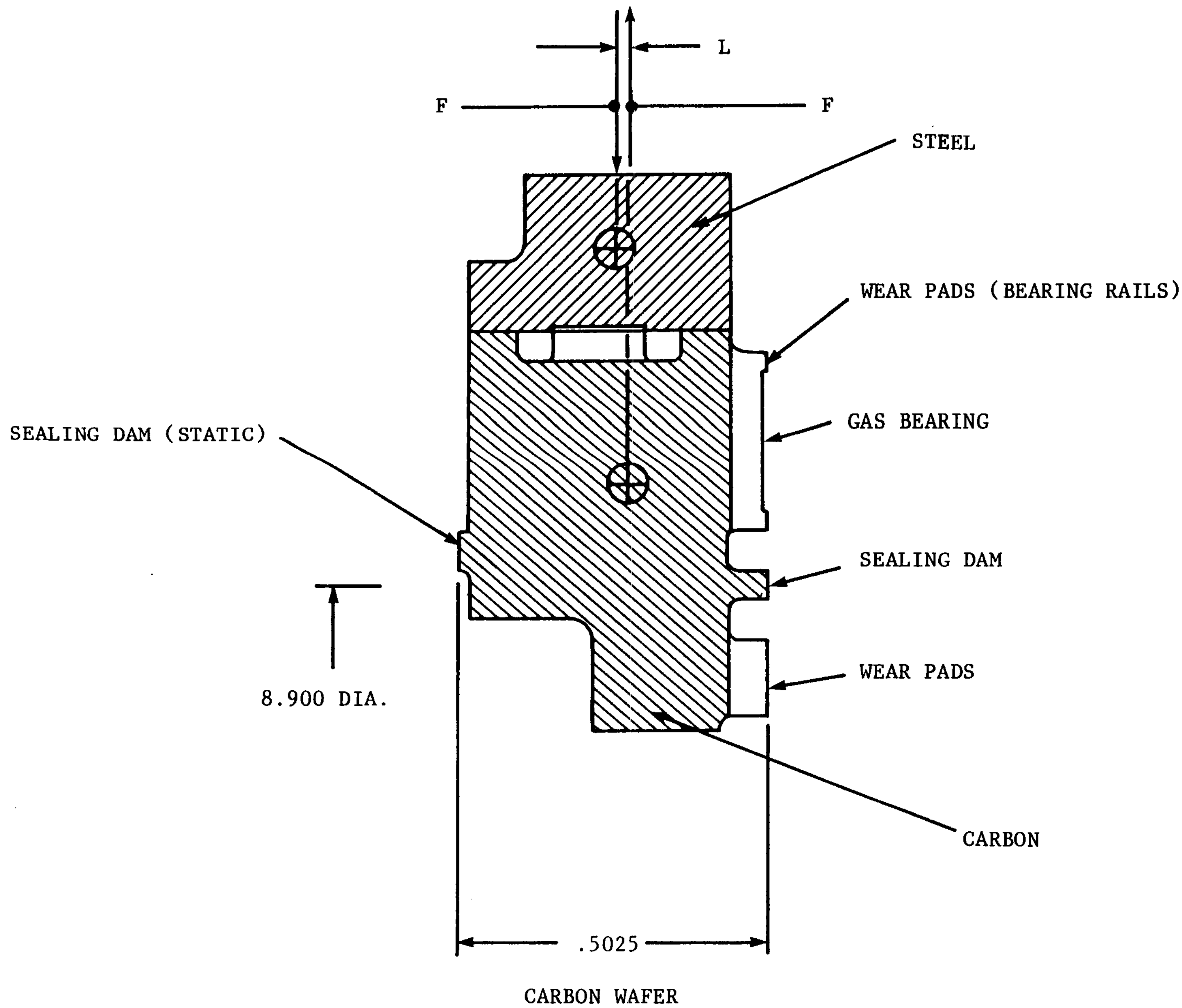

Figure 49. Wafer Shrink Line Forces and Moments.

2. Wafer Stabilization - Thermal cycling is recommended to relieve the axial and radial shrink line strains generated in the carbon wafer assembly while the steel shrink ring cools after heat assembly around the carbon ring.

3. Inner Wear Pads - The small vented wear pads located radially inward of the sealing dam on the face of the carbon wafer were removed during the later stages of the test program. This was done primarily because the integrity of the bond between the hard coating and the substrate on the seal race in the vicinity of these pads was in doubt. A pneumatic study of the affect of these pads should be done to understand if they are a requirement on gas bearing seal faces. They are used to reduce the seal dam pressure force variations resulting from convergence in the direction of gas flow. Since convergence affects an increase in pressure force as face clearance approaches zero, it may well be advantageous to ignore this convention on clearance type seals.

4. Race Plating - A plating spillover groove was provided in the design of the seal race at the intersection of the transverse face and inner flange of the race. The bond of the coating to the substrate in this area is in doubt, and spalling was experienced as a result of a hard rub during one test. This design should be changed to the flush machined "pocket" as is now the commonly accepted practice.

It is recommended that a configuration, revised approximately as shown on Figure 50, be designed, manufactured and tested. This design has the potential to substantially improve the problems described above. Torsional stiffness can potentially be increased in the Y-Y plane by a factor of between 10 and 18 to 1, in the X-X plane by 6 or 8 to 1, and radially between 2 and 3 to 1. It is also recommended that the spiral groove gas bearing configuration be continued as the prime design in follow-on development since it is more easily adapted to the hard coating of the seal race, allowing substantially greater carbon wear without loss of load capacity.

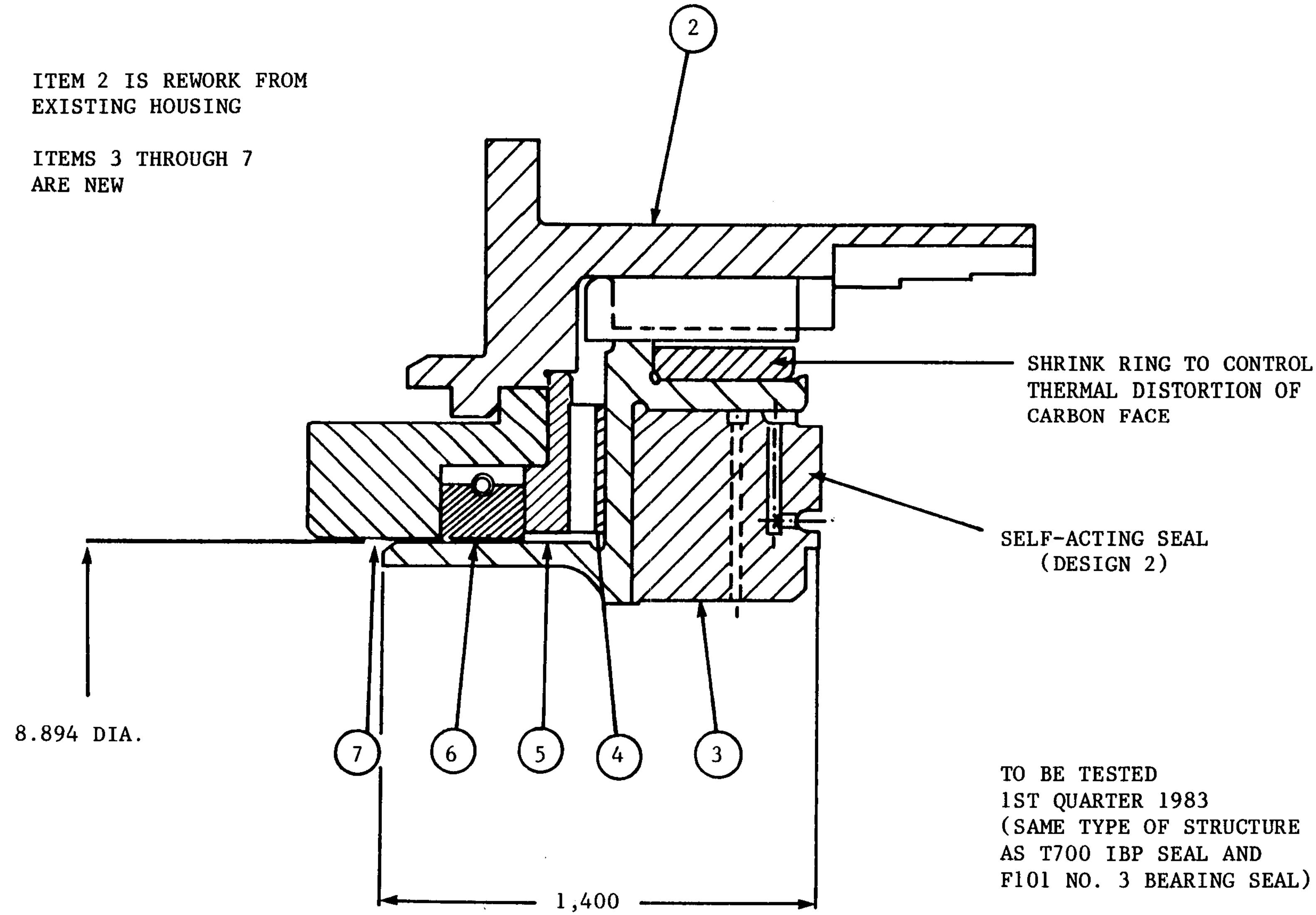

Figure 50. Recommended Configuration.

REFERENCES

1. Yuk, J. and Smith, P.J., " Quasi-One-Dimensional Compressible Flow Across Face Seals and Narrow Slots," NASA Technical Note NASA TN D-6787, August 1972.

2. Chow, C.V. and Wilcox, D.F., "Optimization and Design of Non-Contact Bearing Geometry," MTI CADENSE Program HS-7, Prepared for the General Electric Company, August 6, 1968.

3. Pugh, D.W., "Analysis of Spiral Groove Gas Bearings with Parallel Interfaces," SPIRAL, General Electric DRB No. 6161, Vol. I, June 6, 1980.

VOLUME II

ABSTRACT

This report covers an extension of the development of the gas-to-gas seal reported in Volume I. The original wafer design functioned well on test, but each seal required delicate and expensive rework to obtain the desired performance. The intent of the follow-on effort was to design a seal functionally equivalent to the original, but having design features amenable to production type hardware. This volume documents the design, manufacture, and testing of the follow-on seal.

SUMMARY

The gas-to-gas seal has been redesigned from a wafer type seal to a composite assembly design. The design and design analysis are described. Two sets of the composite seal assembly design were manufactured, and race hardware from testing reported in Volume I was used in testing.

After some difficulties in manufacturing the hardware, further problems were encountered in the static test phase. The hardware was returned to the vendor for rework and completion of the static testing. Acceptable leakage was obtained (10 scfm at 300 psid).

Startup problems were again encountered in the dynamic testing. A drive motor shutdown resulted in wear of the carbon and race faces. Further testing was attempted, but erratic leakage prevented successful completion of the performance mapping. Although backup hardware was available, some rework would have been required to proceed. Since funding for the program had been used up by unanticipated hardware rework and program delays associated with the rework, and because of other Government programs of higher priority using the test rig, the program has been stopped.

CONCLUSIONS

Due to the difficulties encountered in the test program, the basic adequacy of the composite design could not be determined.

It appears that the radial face of the insert where the secondary seal seats should have been finish ground after the press fit assembly in the housing. In addition, the axial taper on the bore of the secondary seal should be incorporated into the design (vendor designed secondary seal).

The need for undercutting the primary seal face above the seal dam is not understood. The vendor felt that the race was rotating counterclockwise under pressure loading, but that problem had not been encountered in testing reported in Volume I.

RECOMMENDATIONS

The design integrity of the composite design was not proved or disproved by the test program. Two sets of seal hardware are available for further testing. one of which would have to be reworked. Both sets of race hardware would be in need of rework.

There remains work to be done in providing reliable techniques for calculating flow across the seal dam. Entrance loss coefficients need to be defined experimentally.

If a need for an air-to-air seal of this type were identified, there is no reason to doubt the ability of the hardware designed in this program to function well. The hardware designed and manufactured under this program remains available for rework and testing.

1.0 SEAL DESIGN

The wafer seal design is shown in Figure 1. The initial configuration of the proposed composite design is shown in Figure 2.

1.1 WAFER SEAL DESIGN PROBLEMS

Assembly Interference Fit - A major problem in the wafer design was associated with the configuration of the seal. In this design. the seal carbon is compressed by the metal shrink ring, which is press-fitted over the carbon. A large press fit (0.060 inch diametral) is necessary since the thermal expansion coefficient the carbon is so much lower than the shrink ring (difference in alpha is approximately 5.8×10^{-6} in/in-° F). When the ring assembly is heated to 1000° F, there will still be a small press fit between the two rings. However, at room temperature, the fit load, or pressure, is 477 lbf/in of circumference. Although this presents no problem with stresses, if there is an initial axial offset in the centers of stiffness of the two rings, then the resultant moment will be the press fit load times the offset. For instance, if there were a 0.01 inch offset in the centers of stiffness and the parts were at 1000° F, the resultant moment would be 3.9 in-lbf/in circumference. The section roll would be 0.0021 in/in and the total taper on the seal face would be 0.00084 inch. Since the press fit load changes with temperature, it is clear that the seal and race faces will not be parallel across the seal operating range, partially resulting in wear and leakage.

In addition, since wear of the carbon changes the location of the center of stiffness of the carbon, two other problems arise. First, during the manufacturing process, as the seal face is lapped to achieve the required flatness, the assembly must occasionally be "rung." Ringing is a process wherein vibrating the assembly will relieve nonuniform shrink line forces. If the assembly is lapped without ringing, then as time goes by or as the seal is used, the nonuniform forces will naturally redistribute to relieve the unbalance, and subsequently the face flatness will change and seal performance will deteriorate significantly.

Second, as the seal is run, wear will naturally occur. As wear occurs, the center of stiffness of the carbon changes, and thus an offset is generated between the carbon and the carrier ring. If the offset in ring stiffness centers is in the disadvantageous direction, then as the seal wears it will tend to twist out of flat. This is a non-self-stabilizing process.

Balance Diameter - An additional problem with the wafer design is the fact that the seal dam and the balance diameter are located on different parts (see Figure 1). Since the axial force balance on the seal assembly is a function of the relative location of these two diameters, any eccentric mislocation or any relative change of these diameters will adversely affect seal performance (see Figure 3). During testing of this design, the seal dam was reworked to restore the relationship between these two diameters, thus

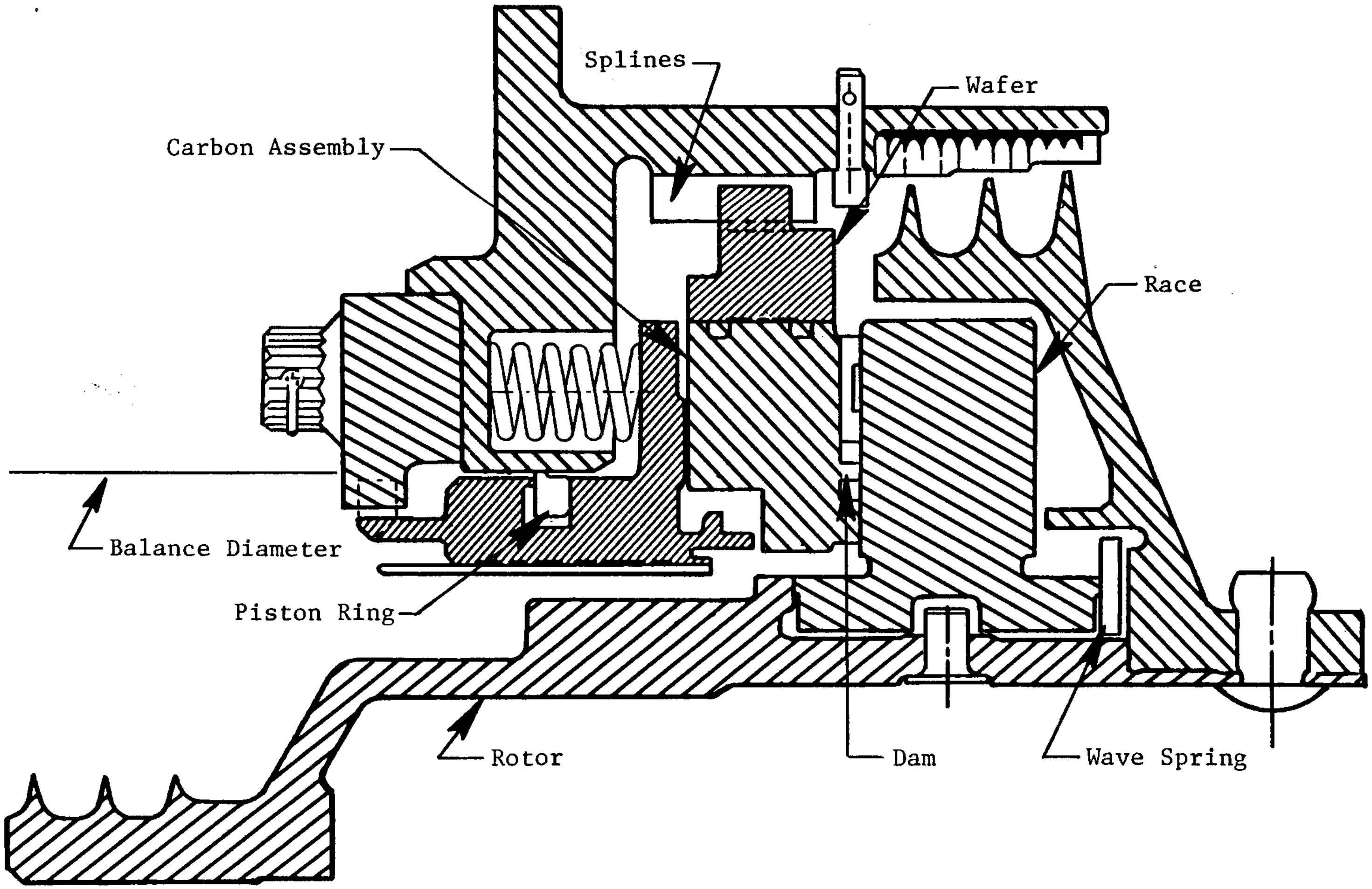

Figure 1. Wafer Design.

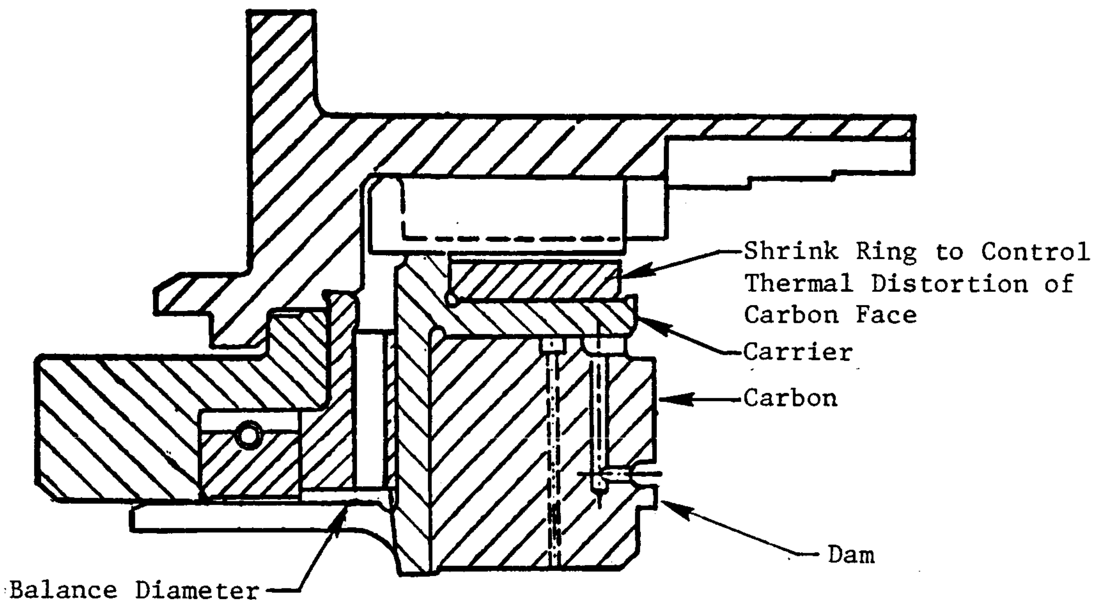

Figure 2. Composite Design.

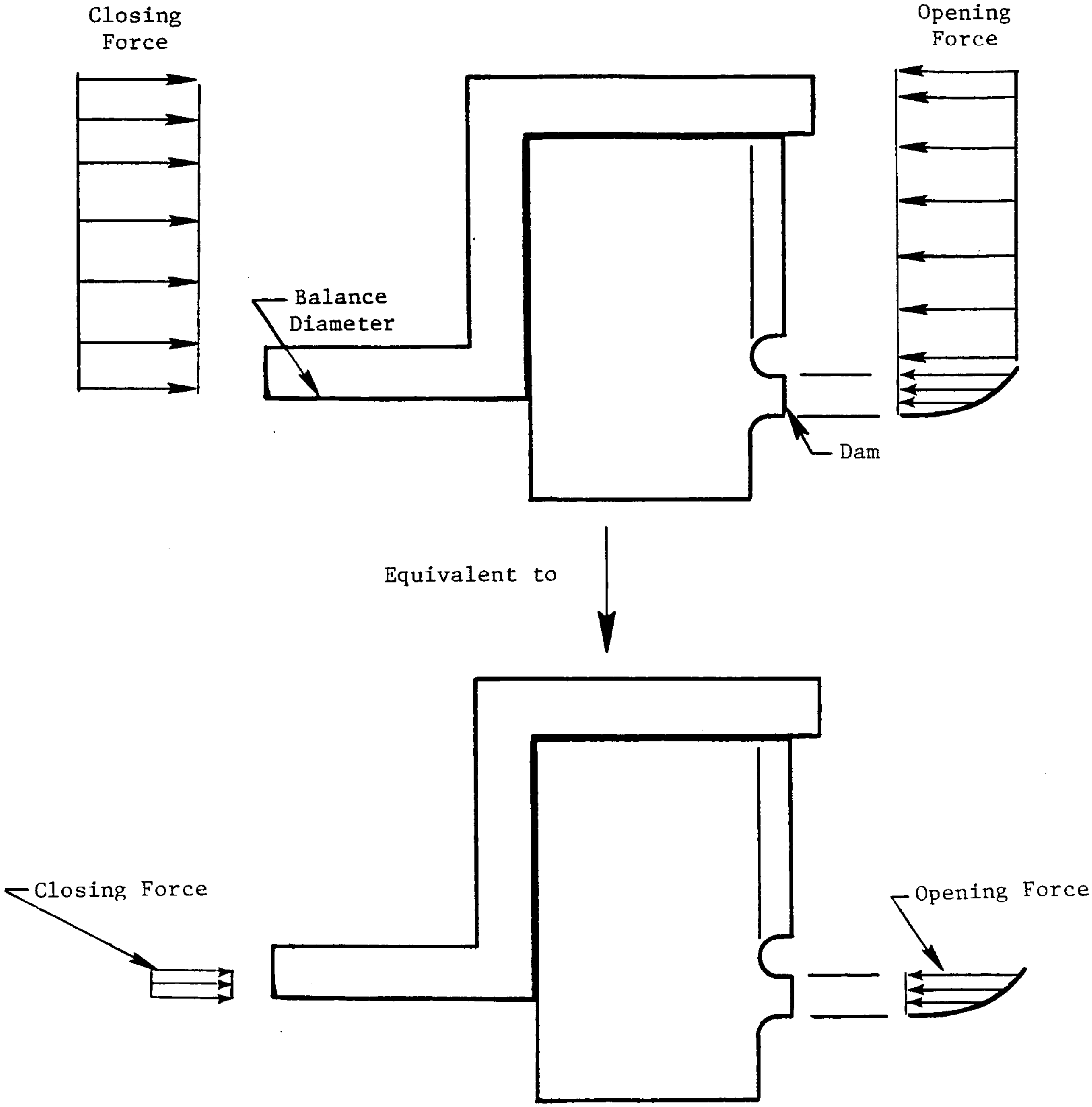

Figure 3. Axial Static Pressure Forces.

reducing the width of the dam. This had the effect of making the dam more fragile and also of causing increased leakage (+35%).

1.2 PROPOSED DESIGN

The intent of the composite design is to substantially reduce the problems inherent in the wafer design. Specifically, the design goals are as follows:

- Significantly increase the torsional stiffness of the carbon assembly
- Significantly increase the hoop transverse stiffness (resistance to forces producing out-of-roundness)
- Increase hoop stiffness
- Incorporate dam and balance diameter on the same press-fit assembly
- Increased envelope for secondary seal allowing a more-rugged, better-performing design.

The composite design is shown in Figure 2. It is similar in structure to seals used in the F101 engine (6.7 inch diameter) and one designed and tested on the T700 engine (3.4 inch diameter). In this design, the balance diameter and seal dam are located on the same press-fit assembly. Thus, when the structure grows or shrinks radially, the diameters grow or shrink together, preserving the axial force balance. This is true as long as the ring cross section does not roll as it grows or shrinks. Ring roll would also diminish the performance of the seal interface since lift forces are maximum for parallel seal/race faces. In order to ensure that the section does not roll, several steps were taken.

1. The axial location of the secondary seal is chosen such that the pressure forces generate zero net moment on the section (see Figure 4).

2. The three ring fit is designed such that, as the assembly temperature changes, the net result on applied section moment is minimized. This will be discussed later.

Also incorporated in the proposed design is a block and shoe rotation lock arrangement wherein both the block and shoe are replaceable (see Figure 5). This allows investigating various material combinations in this area.

The existing race hardware was used. The race face incorporates a spiral groove bearing that generates the lift required to separate the race and seal assemblies at operating conditions. The spiral groove details are shown in Figure 6.

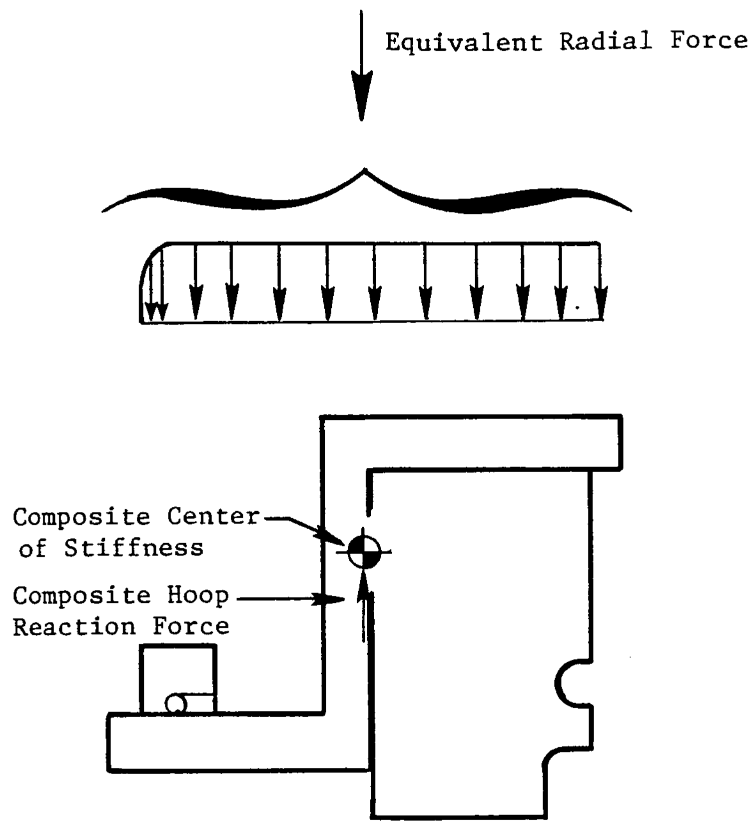

Figure 4. Radial Static Pressure Forces.

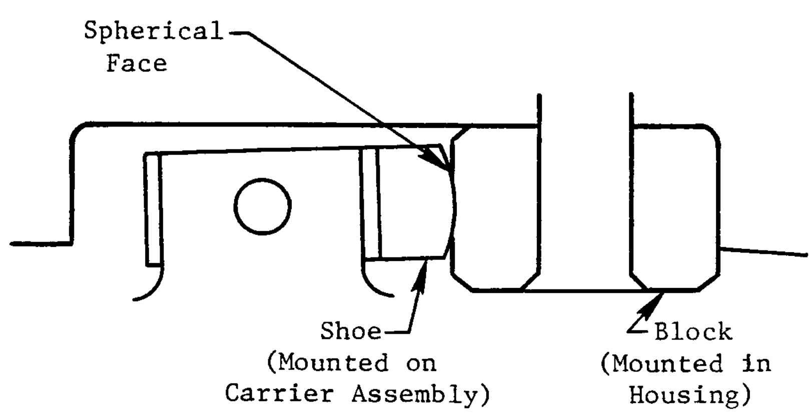

Figure 5. Block and Shoe Design.

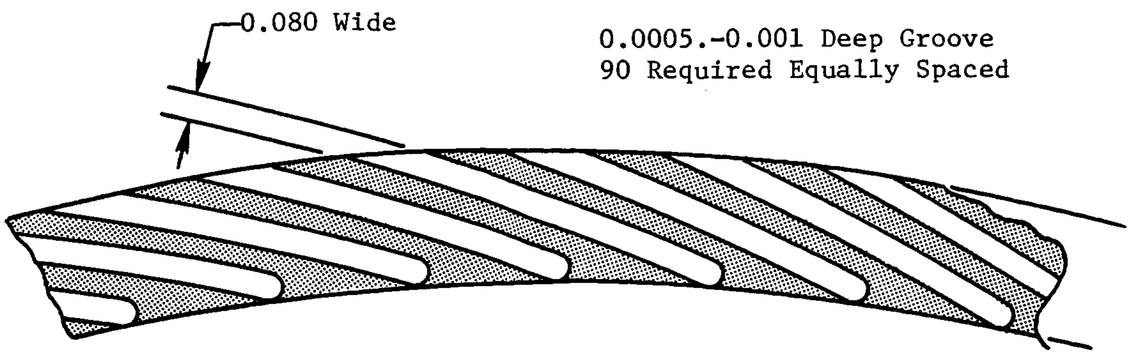

Figure 6. Spiral Groove Details.

1.3 SHRINK RING DESIGN

Problem - The carbon member of the seal, because of its flexible and fragile nature, must be constrained by a more rigid, rugged structure. The most reliable method of securing the carbon is by press fitting it into a more rigid carrier. Because of this, a couple of difficult problems arise. First, since the carrier is normally a metallic material, the coefficient of thermal expansion of the carrier is significantly higher than that of the carbon. Second, since a secondary seal must be incorporated (the primary seal is at the dam face on the carbon), the supporting structure is asymmetrical and the axial center stiffness of the carbon carrier is significantly offset from the center of stiffness of the carbon (see Figure 7). The net result is a substantial self-induced moment in the structure due to the press fit. As the temperature changes, the press fit load changes since the expansion coefficients are different. The face of the carbon is lapped at room temperature with a certain press fit load; therefore, at other temperatures the interference changes, the fit load changes, and the section will roll. As the section rolls, the face will no longer be flat.

Solution - To alleviate this problem, a third ring, the "shrink ring", is located above the carrier (Figure 7). The material and geometry of this ring are chosen so that the press fit load of the shrink-ring/carrier is the same as the carrier/carbon over as much of the operating range as possible.

Design Considerations - Among the considerations in the design are:

- The face of the carbon will be lapped at room temperature, with the carbon installed in the carrier assembly
- The operating temperature is 950° F, at which there must be a good press fit
- The material properties vary with temperature.

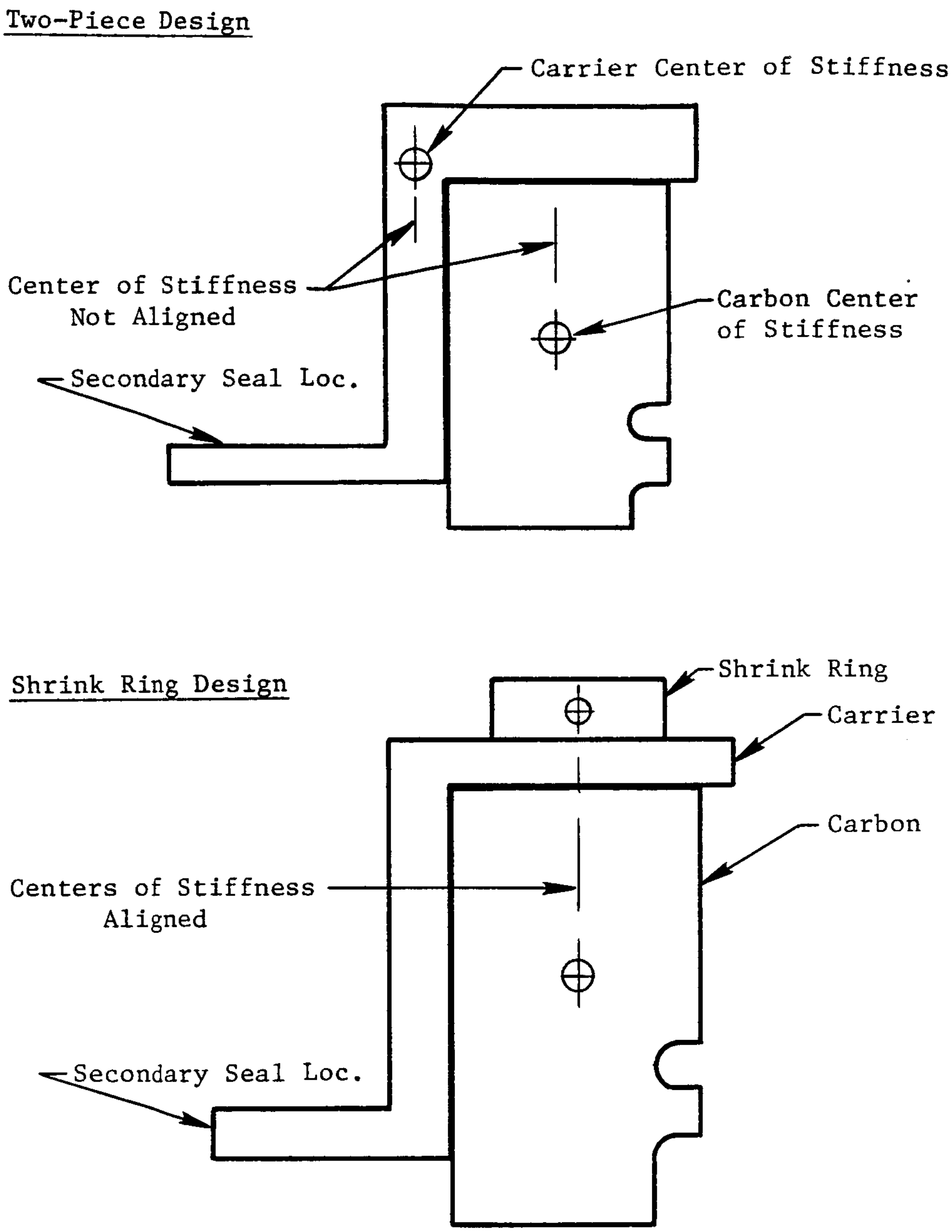

Figure 7. Two-Piece and Shrink Ring Designs.

Material Selection - A critical factor in the design process is the selection of the proper carbon type, carrier, and shrink ring materials.

The first material selected was the carbon. Desirable carbon mechanical properties are the following:

- Low Modulus of Elasticity: This will provide best conformity and lower stresses

- High Thermal Expansion Coefficient: This will lower the press fit loads since the expansion will be closer to the supporting structure

- High Strength: This will allow the large interference fit required because of the high operating temperature.

The following data summarize properties for the candidate carbon materials:

Grade	E ($\times 10^6$)	Alpha ($\times 10^{-6}$)	Composite Strength, psi
2980	1.8	2.3	15000
2690	1.4	3.5	23000
CJPS	2.1	1.7	26000
2866	1.75	2.6	18000
3048	1.8	2.3	15000

Based on this data, Grade 2690 was chosen for the carbon (low E, low alpha, high strength).

Given this information, a computer program was written to scan a material properties data base, and select candidate carrier and shrink ring combinations based on geometric envelope, alpha, and E. The program was given the following set of assumptions:

- Material properties were taken from the data base at 250° F to be representative of the operating range

- The shrink ring must fit in an envelope where the maximum outer diameter (OD) is 10.2 inches and the total length is less than 0.35 inch

- The shrink-ring/carrier fit is at 10.00 inches and the carrier/carbon fit is at 9.72 inches (diameters)

- The fits are line-to-line when the assembly is uniformly at 1200° F.

After the initial runs were made, several material combinations were found acceptable. To narrow the field, a further assumption was made that the carrier material thermal expansion coefficient should be near that of the existing housing, Inconel 718, so that the housing and carrier would grow

similarly and allow the balance diameter/housing bore clearance to be minimized. This narrowed the field to the following:

Shrink Ring	Carrier
A286	Cr-Mo-V
V57	Inco 722
	Inco X-750
	L605
	Waspaloy

From the above, A286 was chosen for the shrink ring and Inco X-750 for the carrier. This final selection was based primarily on availability.

Fit Load Analysis - Another computer program was written to compute the fit interference and load over a range of temperatures, from room temperature to 1200° F. The program accounts for the variation of properties with temperature. The program was also used to choose the cross-sectional area of the shrink ring. The results of this analysis are shown in Figures 8 and 9. Figure 8 shows a number of details of the fits, and Figure 9 shows the effect on the flatness of the carbon face. This curve shows that at the operating temperature, 950° F, the face will have a taper of 0.0002 inch total. In hindsight, the line-to-line fit at 1200° F requirement should be replaced by zero flatness error at the operating temperature.

Figure 8 also shows the stresses in the rings. The maximum compressive stress is 8 ksi in the carbon and 65 ksi in the shrink ring, both well within the allowable range for their respective materials.

1.3.1 Parameters Related to Axial Forces

A face seal is designed to operate with a gap between the carbon and the race. The force required to hold the carbon away from the race is generated by the spiral groove bearing in the race face. A typical curve showing the axial forces is presented in Figure 10(a). A spring is included in the assembly that provides a small closing force, principally to ensure that the seal is closed prior to startup. The balance diameter and the dam are related so as to generate a "bias" closing force as a pressure differential is applied to the seal. The two forces tending to close the seal (the bias and the spring) are added together and shown on Figure 10(a). When the race rotates, the inertia and friction forces shown in Figure 10(b) are developed.

To counteract the closing forces, spiral grooves are machined into the face of the race. These provide a lift force as the race rotates generating relative motion between the carbon and race faces. Since the lift force is a function of clearance, the carrier assembly will position itself so that the axial forces are in balance, and the operating gap is thus established. This system behaves very much like a servo device in that, if the gap increases, the lift force diminishes and the carrier assembly tends to return to the operating gap; similarly, if the gap decreases, the lift force increases and

ORIGINAL PAGE IS
OF POOR QUALITY

```
PROGRAM SHRINKD      DATE=12/11/81    TIME= 10.97
RA=  5.0000                RB=  4.9000
AJ= 0.36640                E3=  14.000E 05          RB3=  4.5847
RB2=  4.9300

SHRINK RING OUTSIDE RADIUS =  5.1000
SHRINK TEMP= 1200.
ZERO NET FORCE TEMP=   70.

SHRINK RING IS A 286
CARRIER IS INCO X-750

SHRINK RING IS A 286
CARRIER IS INCO X-750

SHRINK RING LENGTH =  0.4518     AREA = 0.04518
RBAR =  5.0500
```

TEMP (DEGF)	SR-CR FIT (IN)	SR-CR PRESS (LBF/IN)*	CR-CB FIT (IN)	CR-CB PRESS (LBF/IN)*	NET OUT PRESS (LBF/IN)*	STRESS (KPSI) SR (KPSI)	CARB (KPSI)
70.0	0.011733	596.7	0.026292	596.7	0.	65.1	8.0
100.0	0.011367	574.9	0.026023	590.6	15.6	62.7	7.9
200.0	0.010248	508.8	0.024849	563.9	55.1	55.5	7.6
300.0	0.009268	451.4	0.023284	528.4	77.0	49.3	7.1
400.0	0.008375	400.0	0.021376	485.1	85.2	43.6	6.5
500.0	0.007500	351.0	0.019215	436.1	85.0	38.3	5.9
600.0	0.006571	301.1	0.016937	384.4	83.3	32.9	5.2
700.0	0.005472	245.3	0.014461	328.2	82.9	26.8	4.4
800.0	0.004299	188.2	0.011900	270.1	81.8	20.5	3.6
900.0	0.003188	136.2	0.009227	209.4	73.2	14.9	2.8
1000.0	0.002190	90.8	0.006479	147.0	56.3	9.9	2.0
1100.0	0.001168	46.6	0.003474	78.8	32.2	5.1	1.1
1200.0	0.000000	0.0	0.000000	0.0	-0.0	0.0	0.0

* - PRESSURE IN LBF/IN CIRC AT RB2

Figure 8. Analysis Results Showing Details of Fits.

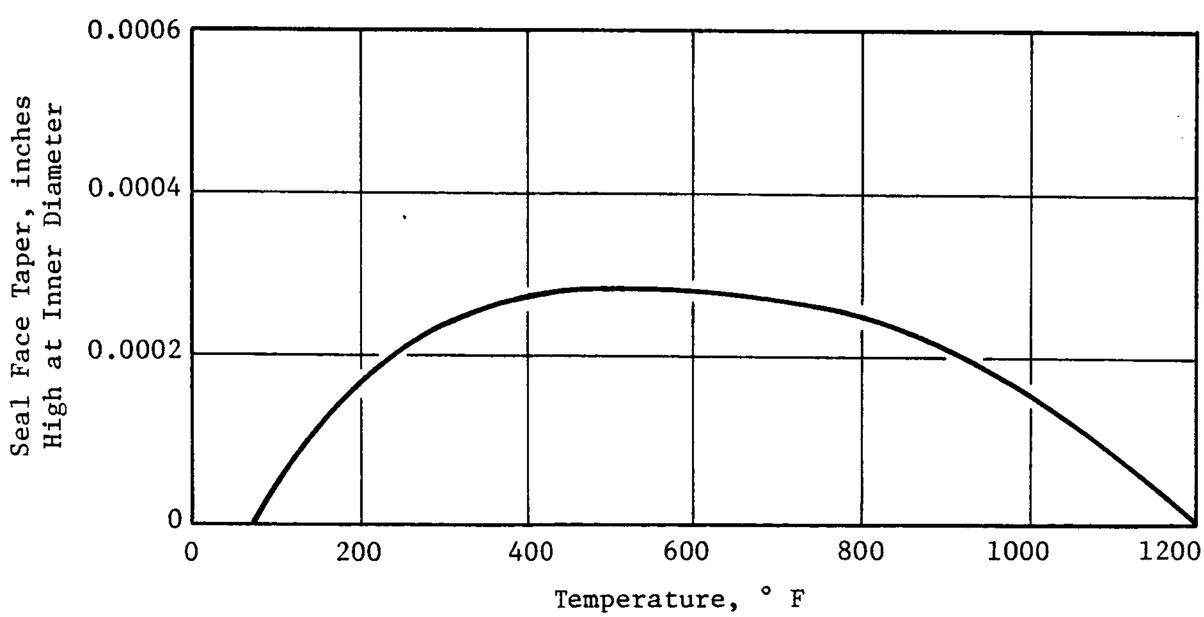

Figure 9. Thermally Generated Face Deflection.

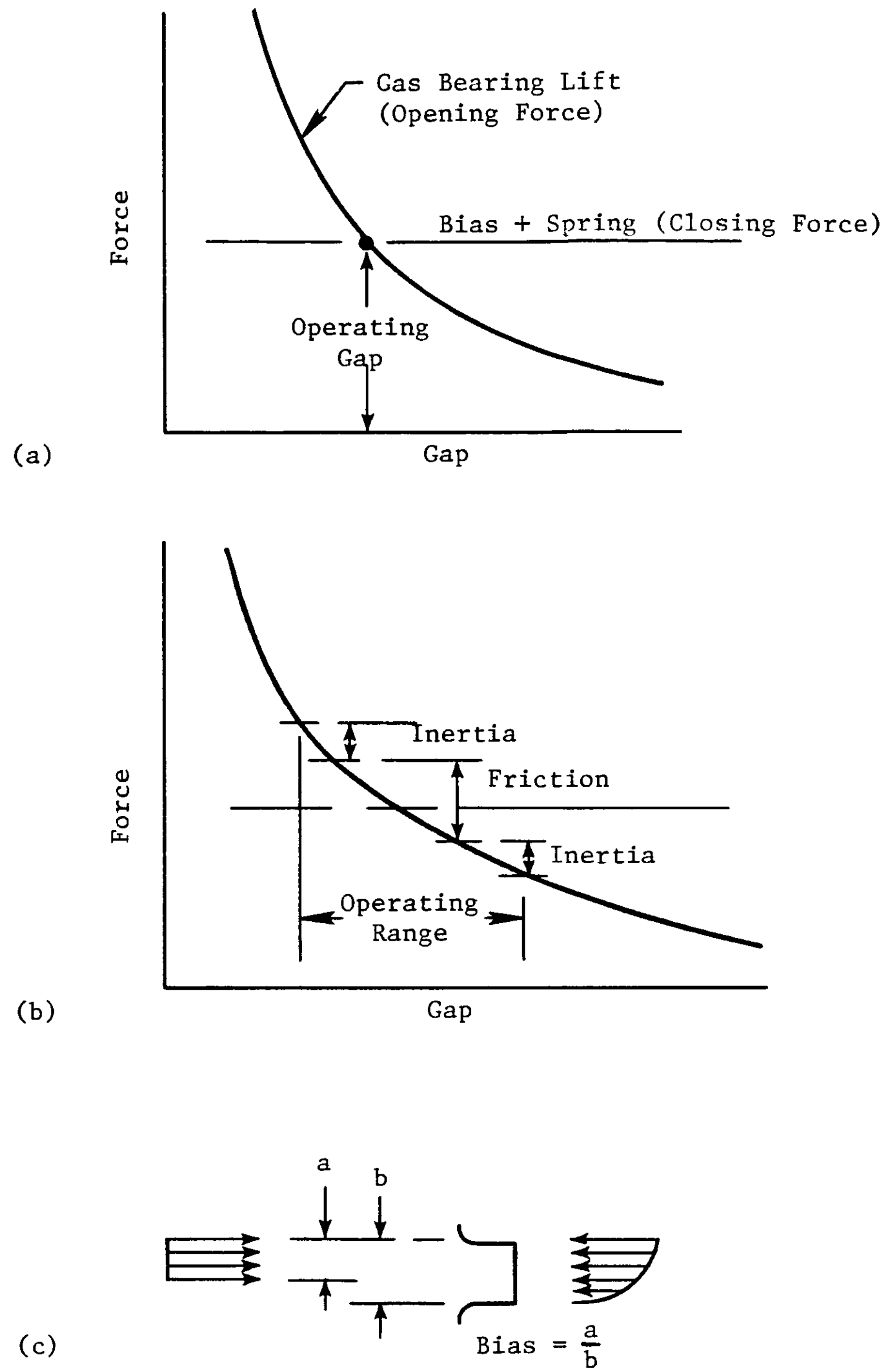

Figure 10. Axial Forces.

the carrier assembly tends to return again to the operating gap. Other operative forces are friction forces (between the secondary seal and the carrier) and inertia forces (if there is axial runout that makes the race oscillate axially). An additional criterion in choosing the operating gap is that the friction and inertia forces should not cause the gap to become zero, as shown in Figure 10(b).

For the current design, a spring force of 15 lbf was chosen to provide a light closing force. The bias chosen was 0.67, where bias is defined as in Figure 10(c). The axial forces can be calculated using the approximate equation for the dam lift force:

$$F = \lambda \Delta r \Delta p$$

Where:

$$\lambda = \frac{1}{3} \quad \frac{2+r}{1+r} \quad , \quad r = \frac{P_e}{P_i}$$

Δr = dam width

Δp = pressure drop across dam

F = lift force - lbf/in-circum.

Defining the bias as β, the equation for the bias force is:

$$F_\beta = (\beta - \lambda)\Delta r \Delta P \quad (+ = \text{opening})$$

To minimize the radial height of the seal, a narrow dam is desirable. However, too narrow a dam would be fragile, so to balance these requirements, a width of 0.060 inch was selected. Using this width, the above equation for bias force gives a value of 0.33 lbf/in circumference.

A more detailed analysis of the dam was performed later using the NASA program QUASC. These results are a function of the entrance loss parameter. Two values of this parameter were used, 0.6 and 1.0. Some of the results are shown in Figure 11. As indicated on the plots, the bias force depends on the temperature and the assumption regarding the loss coefficient. Note that at low clearance, the bias force tends toward the above calculated value. Because of the uncertainties regarding the loss coefficient, the approximate calculation was used in the design. Further experimental studies would be warranted regarding the flow through the seal dam.

Sprial Groove Bearing Lift - The lift generated by the spiral grooves was calculated; it is plotted in Figure 12. As shown, the total lift force for all assumptions of speed and temperature yields an operating clearance in excess of 0.0003 inch, if the above calculated closing force of 26.0 lbf is used.

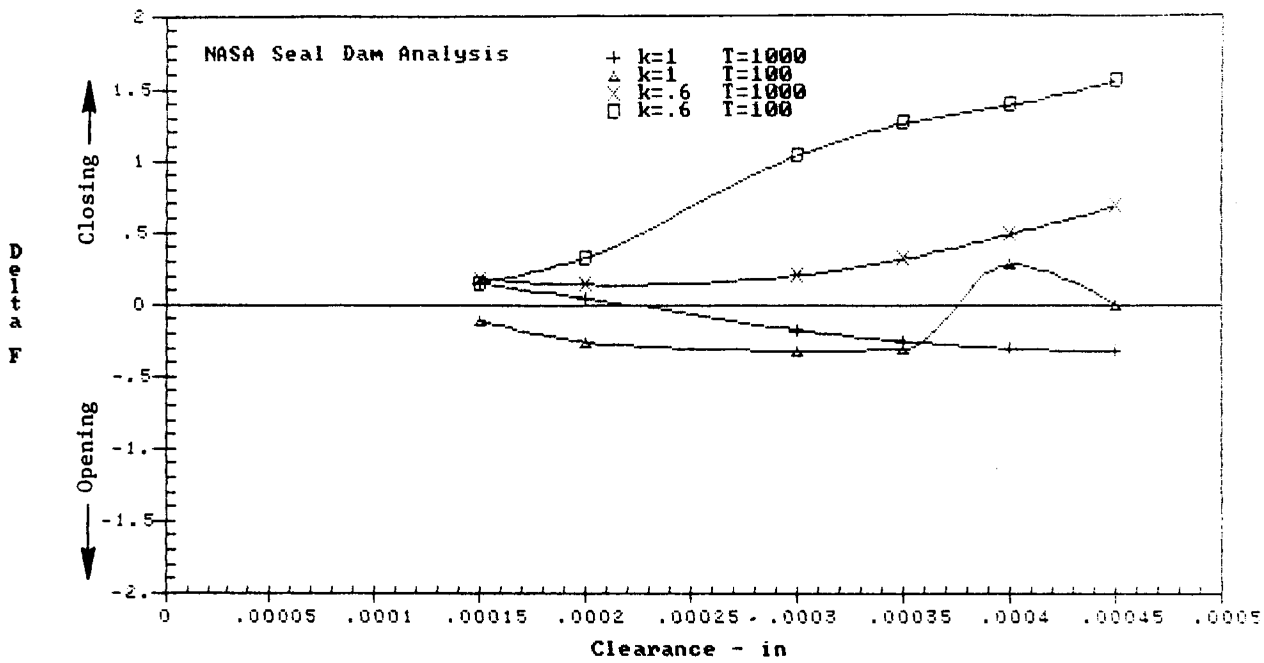

(a)

Figure 11. Results of Seal Dam Analysis Using QUASC.

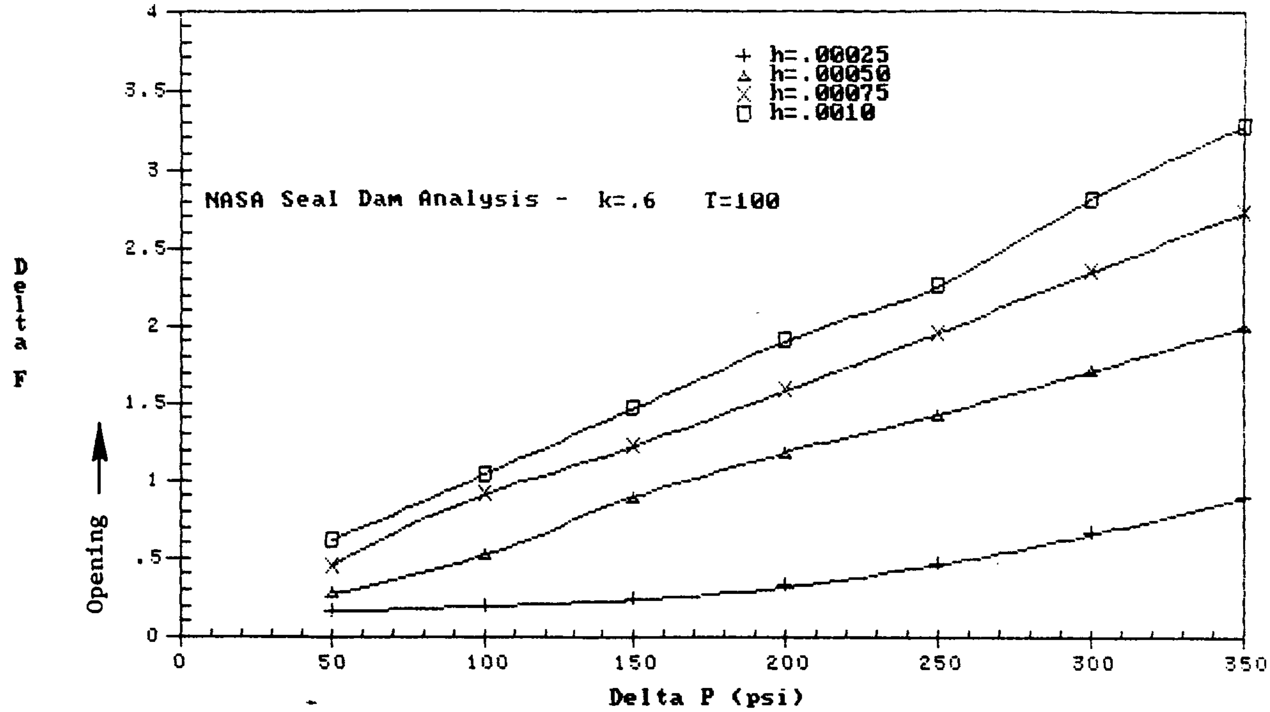

(b)

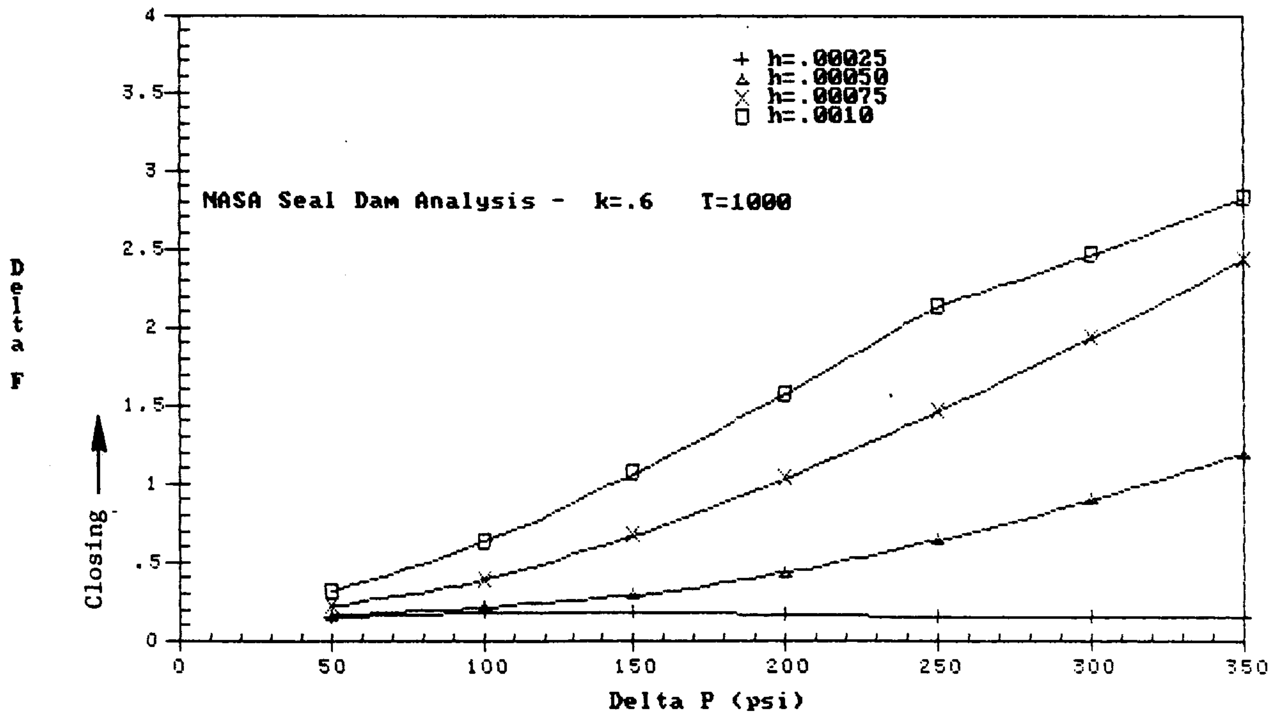

(c)

Figure 11. Results of Seal Dam Analysis Using QUASC. (Concluded)

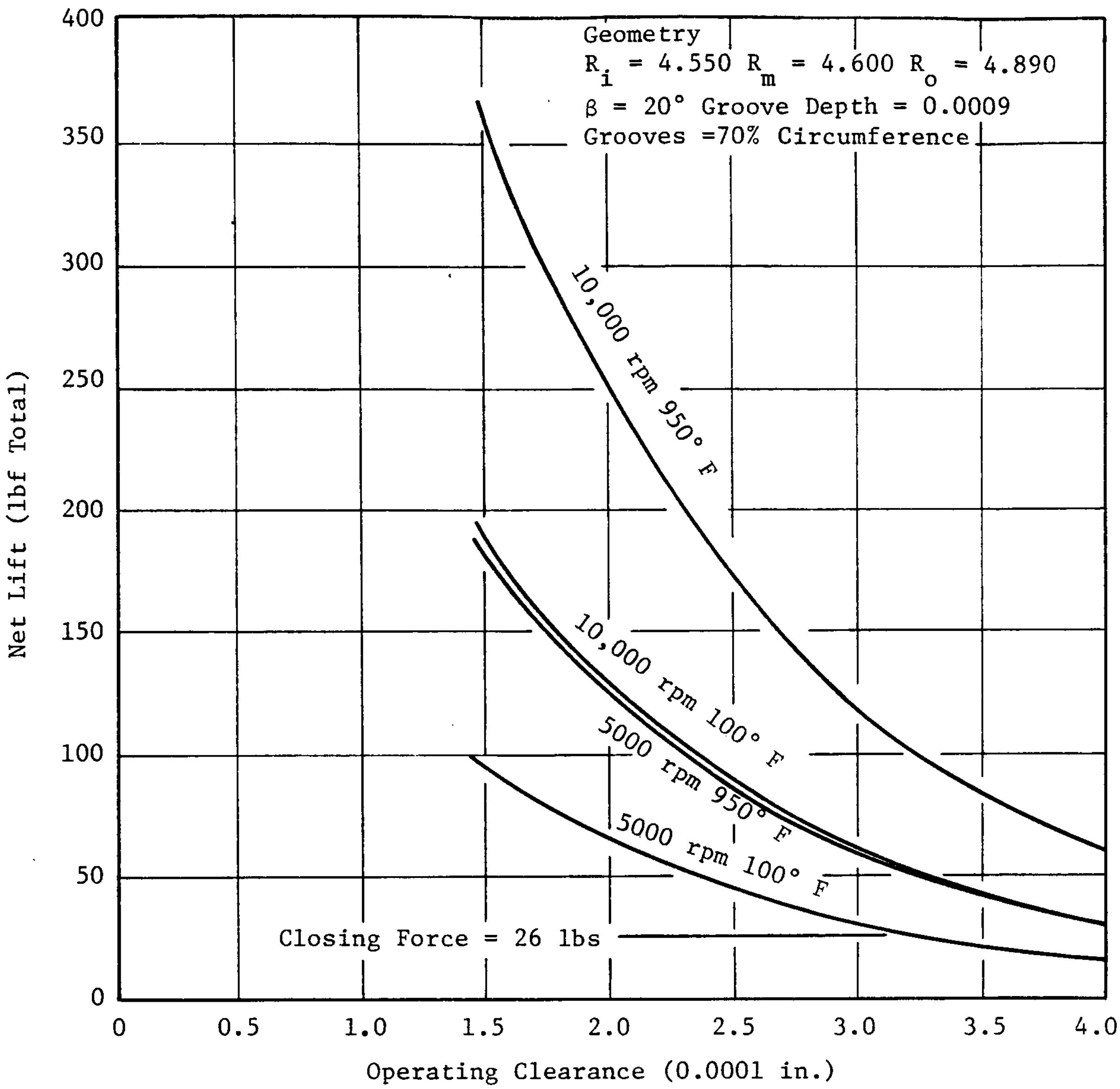

Figure 12. Net Lift Versus Operating Clearance.

1.3.2 Parameters Related To Radial Pressure Forces

Since the balance diameter and the dam are on the same assembly, radial deflections of the carrier assembly do not affect the seal performance. However, to minimize the twisting of the assembly about its section center of stiffness, the radial forces should be balanced. In calculating the moment applied to the assembly by the radial forces, it is assumed that the applied forces are reacted by a radial force acting at the assembly center of stiffness (the self-equilibriating force of the ring). The applied radial pressure forces are a function of the location of the secondary seal (see Figure 4) which was chosen so that the moment on the assembly is zero.

1.3.3 Design Details

The design is iterative. Details of the final results are summarized below and in Figures 13 and 14.

Carrier Assembly

Several of the detail values are:

Center of Stiffness

x = 0.5769

Balance diameter = 8.894

$\Sigma Ixx = 5.75 \times 10^{-5}$ lbf-in^2

$\Sigma Irr = 7.20 \times 10^{-5}$ lbv-in^2

Weight = 2.7 lbm (approximate)

Figure 13 shows:

- Location of Secondary Seal
- Bias of Balance Diameter and Seal Dam
- Location of Section Center of Stiffness
- Pressure Loading
- Spring Force Location
- Spiral Groove Lift Force Location.

The total moment on the assembly is 0.14 in-lbf/in, which generates a section roll of 0.004 milliradians.

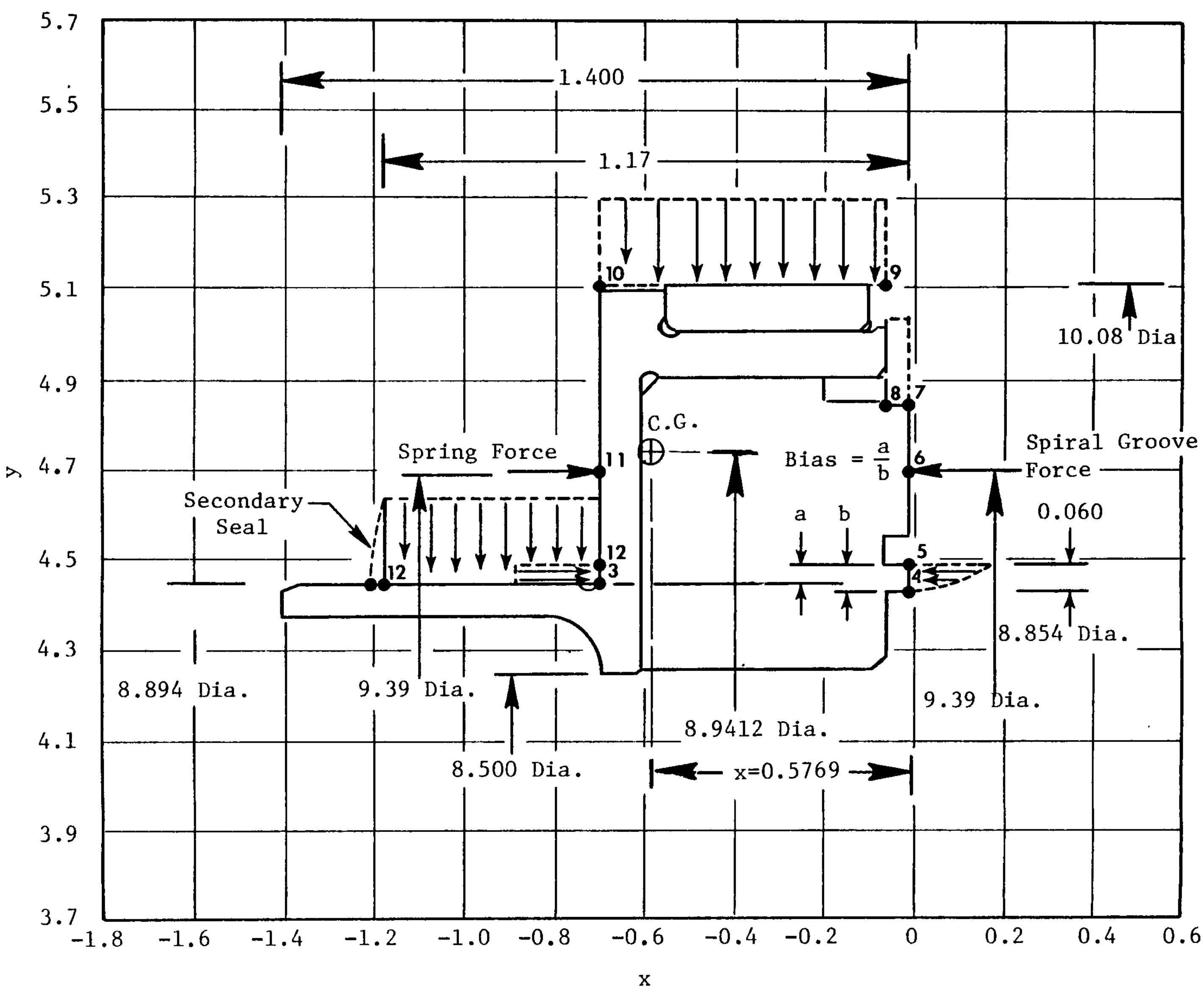

Figure 13. NASA Face Seal Carrier Assembly.

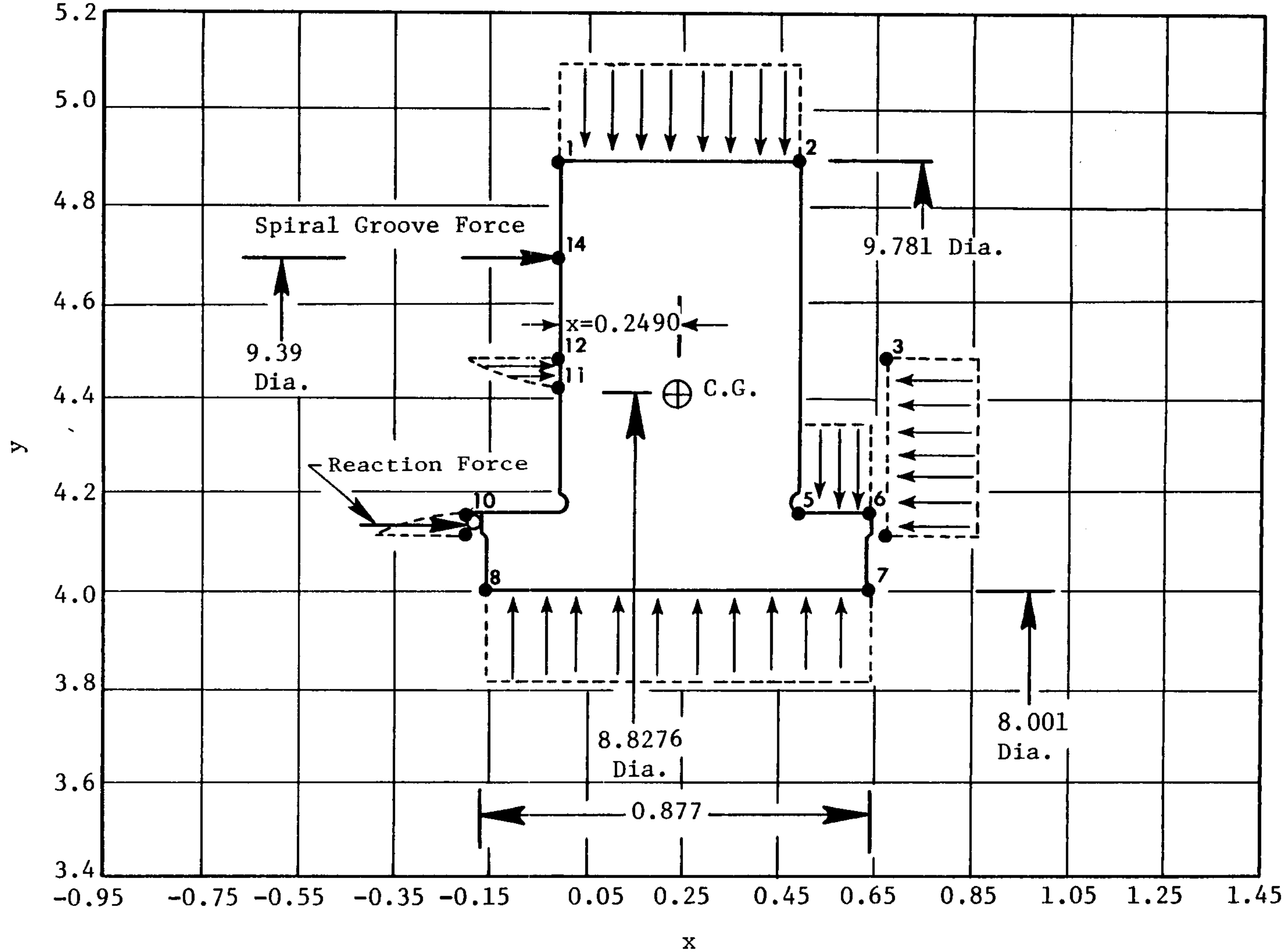

Figure 14. NASA Face Seal Race.

Race

Several of the race detail values are:

Center of Stiffness

x = 0.2490 in.

Diameter = 8.827 in

$\Sigma Ixx = 1.04 \times 10^{-6}$ lbf-in^2

$\Sigma Irr = 0.42 \times 10^{-6}$ lbf-in^2

Weight = 3.8 lbm.

Figure 14 shows:

- Center of stiffness
- Applied pressures.

The total moment on the race is 0.30 in-lbf/in, which generates a section roll of 0.014 milliradians.

1.3.4 Other Design Features

The final design is shown as assembled in the static test fixture in Figure 15. Several features of the design are described below.

Airflow - To provide equal pressure on both ends of the spiral groove region, the forward OD of the carbon is undercut to expose radial vent holes that feed a groove just above the dam OD (see Figure 13b). To ensure that the bore of the race is at high pressure, air flows through the wave spring and the race bore to the opposite end, where the race seats against the shaft shoulder and provides the secondary seal. The three seal locations, then, are the circumferential secondary seal on the carrier assembly, the primary seal dam, and the secondary seal on the race where it clamps against the shaft.

Secondary Seal - The secondary seal is a three-segment circumferential seal. The segments are loaded by a helical "garter" spring wrapped around the OD of the segments and are loaded axially by small coil springs. To be able to use the existing seal housing, modifications were required to accommodate the circumferential secondary seal. The insert and retainer were designed to capture the seal and provide a sealing surface. The retainer has a slightly tapered OD that is pressed into a similarly tapered bore of the housing, and is thus restrained by a press fit. The total section of the insert is relatively large to reduce deflections due to unbalanced pressure loading.

Race Plating/Spiral Grooves - The spiral grooves are incorporated in the plating on the face of the race. The plating, Linde LA2 aluminum oxide, is intended to reduce wear on the occasions when the carbon and race come into contact. The plating is 0.003 to 0.005 inch thick. The plating and the race

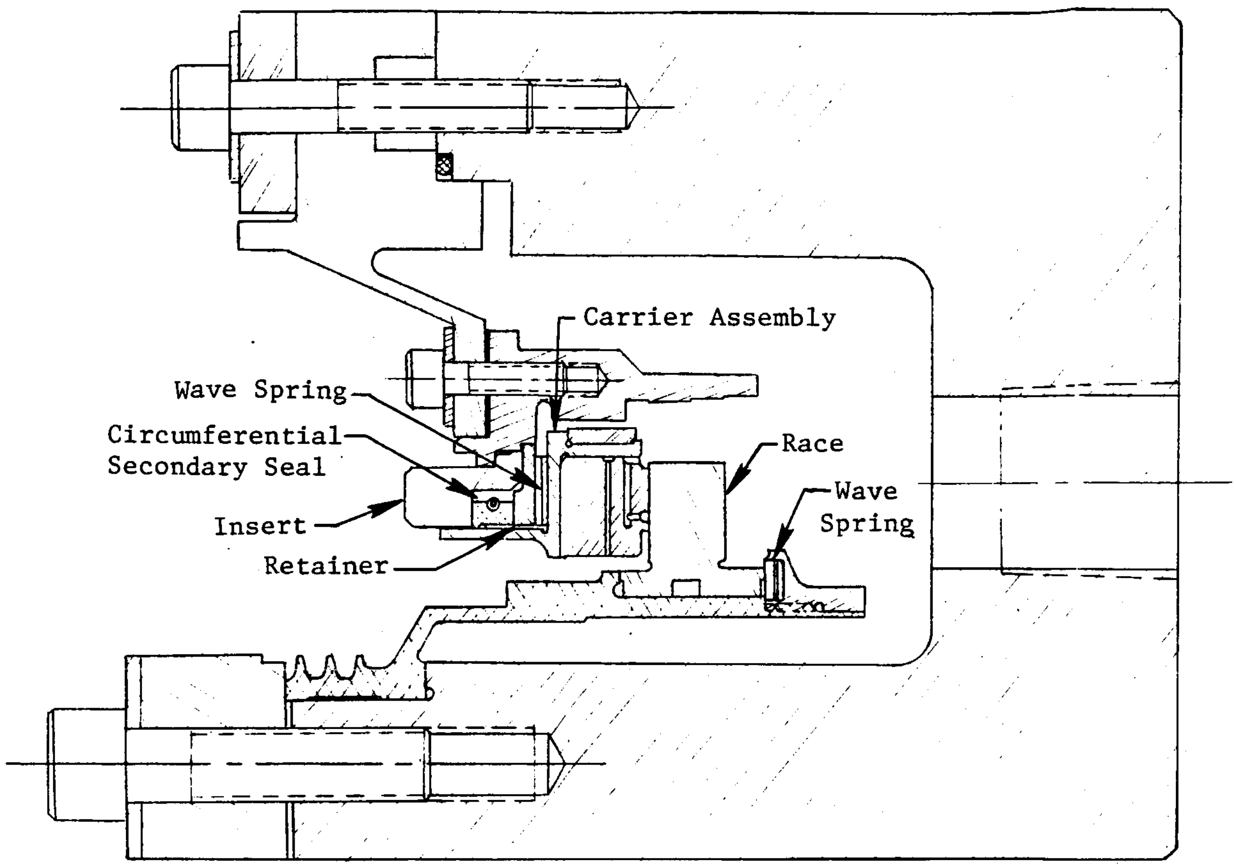

(a)

Figure 15. Final Design Assembled in Static Test Fixture.

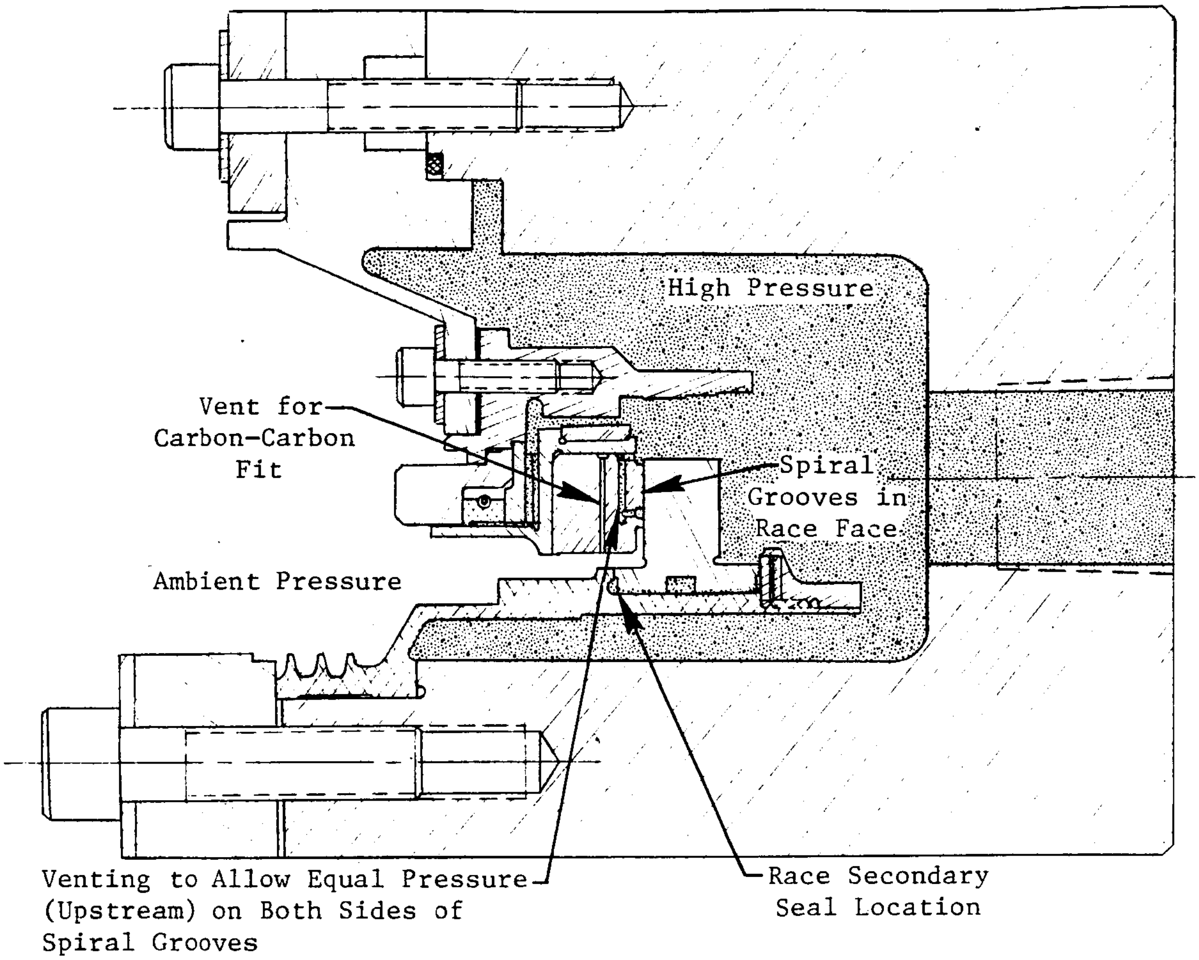

(b)

Figure 15. Final Design Assembled in Static Test Fixture. (Concluded)

materials have different thermal expansion coefficients, so that as the race heats, internal stresses are generated in the race. The stresses cause the race section to roll. The amount of face taper was calculated at different temperatures (assuming uniform race temperature) and is shown below:

	Face Taper, mils/inch		
Plating Thickness	0.003	0.004	0.005
600° F	0.167	0.222	0.278
1200° F	0.386	0.515	0.643

In the operating range, these distortions are of similar magnitude and direction as the carrier distortions (Figure 9). This being the case, there should be no problems caused by the differential thermal expansion.

2.0 MANUFACTURING

A couple of problems were encountered in the manufacturing phase. Although the problems were resolved, the net effect was a substantial delay in the program.

Carbon Blank - The carbon processing cycle is lengthy, about 13 weeks. The first set of blanks to be manufactured fractured during the cool-down cycle. New blanks had to be manufactured, delaying the procurement by about 26 weeks.

Shrink Ring - The A286 shrink ring is relatively highly stressed. It is critical that the ring have the proper strength. There is a requirement on the assembly drawing that the seal go through a heat (900°F)/cool (RT)/face lap cycle until the face flatness stabilizes from one heat cycle to the next. The vendor was unable to achieve stabilization, and investigation revealed that the A286 shrink ring had not been heat treated for strength prior to assembly. Thus, when the ring was shrunk onto the assembly, it was stressed beyond its yield strength and the tight fit thus loosened. In this condition, the ring would come loose at approximately 800°F. The ring would then shift position axially, and on subsequent cooling the face of the seal would be out of flat. The shrink ring had to be remanufactured, causing another 12 to 16 week delay.

Once received, however, the hardware was of excellent quality. Dimensions checked were within tolerance. The bias of the seal was checked and found to be 0.679 versus a drawing specification of 0.667. The face flatness of the carbon was checked and found to be within 6 He light bands.

3.0 STATIC LEAK TEST

Prior to dynamic testing, static leak tests were performed to establish a baseline and to determine the leakage characteristics of the seal. The test fixture is shown in Figure 16. Pressurization air is supplied as shown. Figure 17 shows the test setup, and Figure 18 is a photograph of the setup.

As shown in Figure 17, the static pressure within the test cavity is measured using a dial gage and the leakage is measured using a rotometer in the supply line.

Prior to assembling the rig, strain gages were applied to the test parts to be used to determine deformation of the parts during operation. The strain gage locations are shown in Figure 19 and photographs are shown in Figures 20 and 21.

Upon initial testing, substantial leakage was encountered. The leakage is plotted in Figure 22. As shown, the leakage starts at a relatively low ΔP and shows no sign of decreasing as the pressure is increased. It appeared that most of the leakage was occurring at the secondary seal location and the leakage varied circumferentially (see Figure 23). This indicates leakage at the end gaps of the segmented secondary seal. Dial indicators were located along the exposed radial face of the insert and the twist of the section calculated from the readings. The twist thus determined was 0.00256 radians when the cavity pressure was 248 psig. Structural analysis of the part shows that the twist of the section due to fit-only would be 0.00106 radians and the twist due to fit and pressure loading would be 0.00226 radians. The dial indicators would measure the difference, 0.00120 radians. Thus, the agreement between analytical and the measured twist is not very good. The analytical result would indicate a marginal design.

The secondary seal was designed by the vendor; however, the insert design was given to the vendor. The sealing surface of the insert should have been finish machined with the insert installed in the seal housing, thus eliminating the press fit deflection.

Considerable effort was expended to determine the exact cause of the static leakage. The strain gage information was difficult to analyze. Initially, there was substantial drift in the data. Some of the data are shown in Figure 24. Note that the carrier in the region of the secondary seal is deflecting counterclockwise a small amount and the carbon is deflecting clockwise a fair amount more. This suggests that the carrier assembly is bowing.

The chief problem during the testing was the drifting of the race strain gages, also shown in Figure 24. The arrows show the data as pressure was applied and then relieved. The gages were reapplied, but the problem persisted. A new bonding agent was used to mount the gages, and the gages were then coated to ensure that moisture would not cause problems. Further testing, however, resulted in data similar to that shown above.

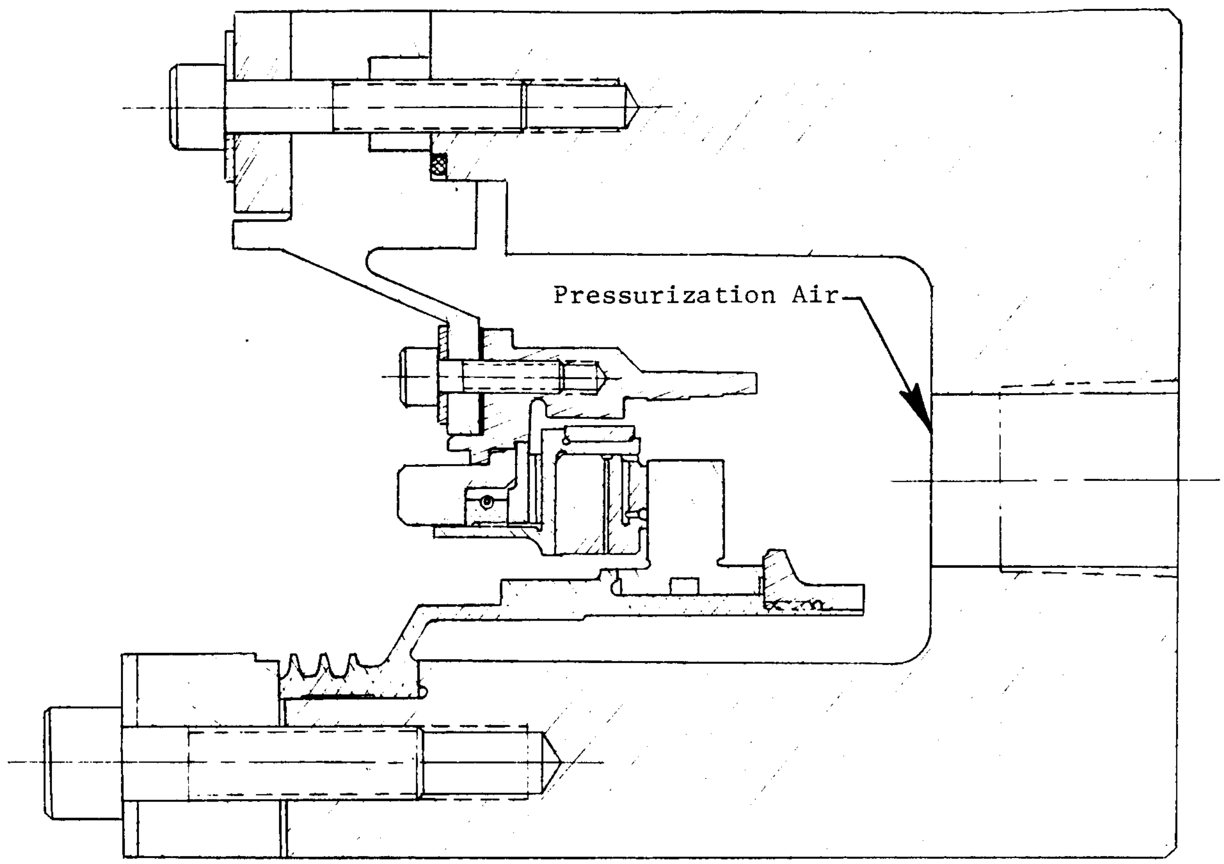

Figure 16. Static Test Assembly.

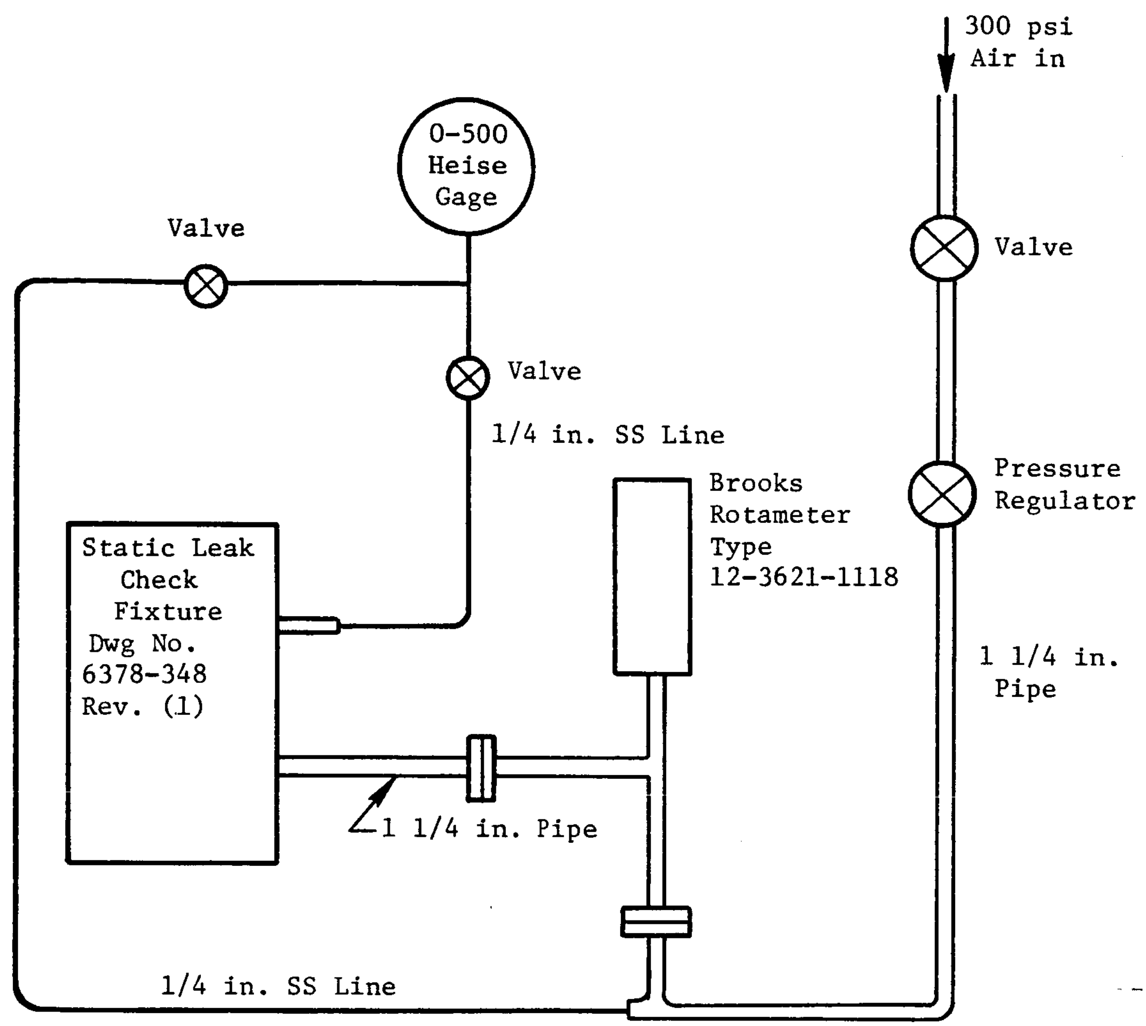

Figure 17. Schematic of Static Leak Check Setup.

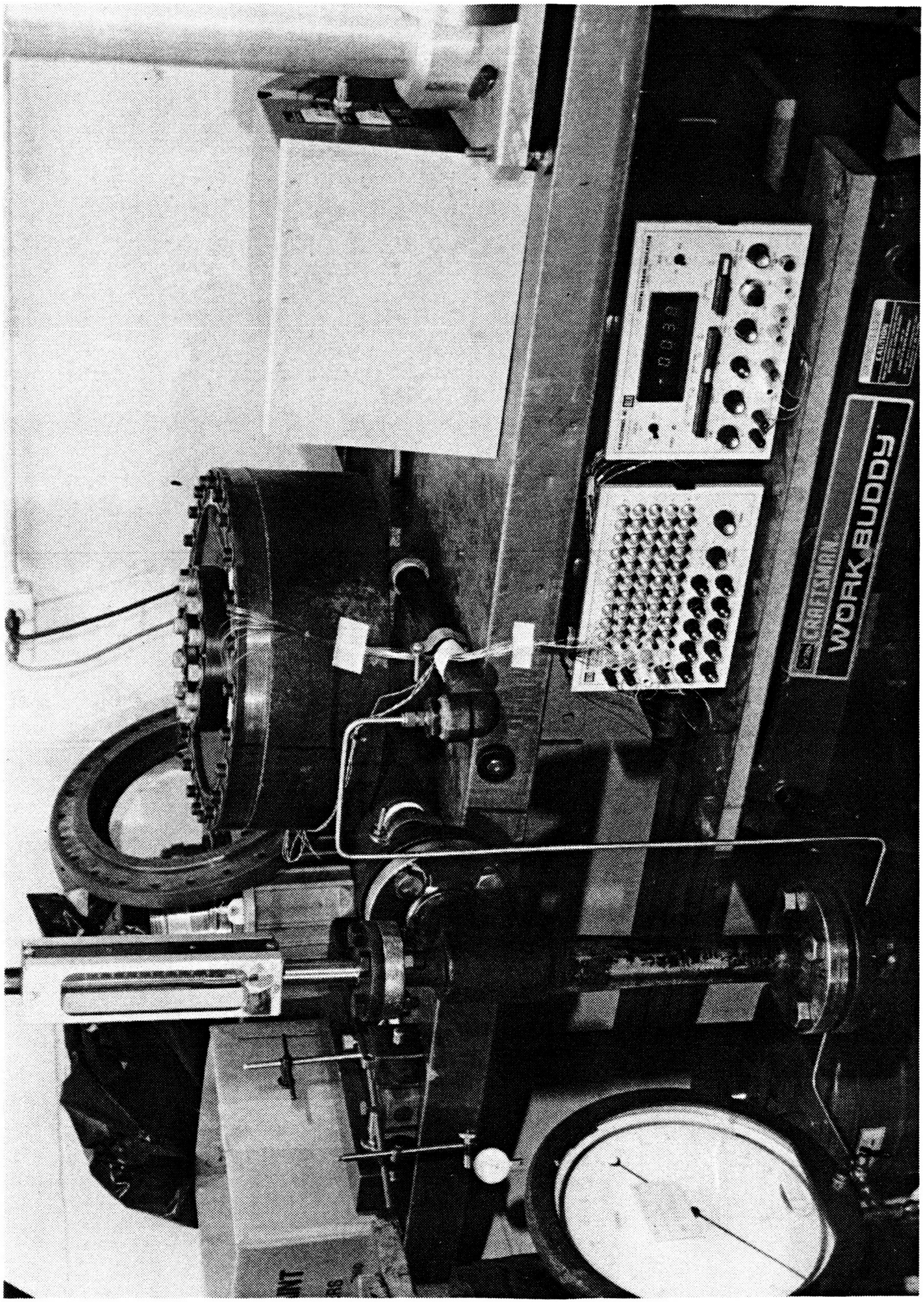

Figure 18. Photograph of Static Leak Check Setup.

Note
Gages Were Installed So That:
Gages 1, 2, 3, 4, 9, 10 Are in the 12 o'clock Position
Gages 5, 6, 7, 8, 11, 12 Are in the 6 o'clock Position

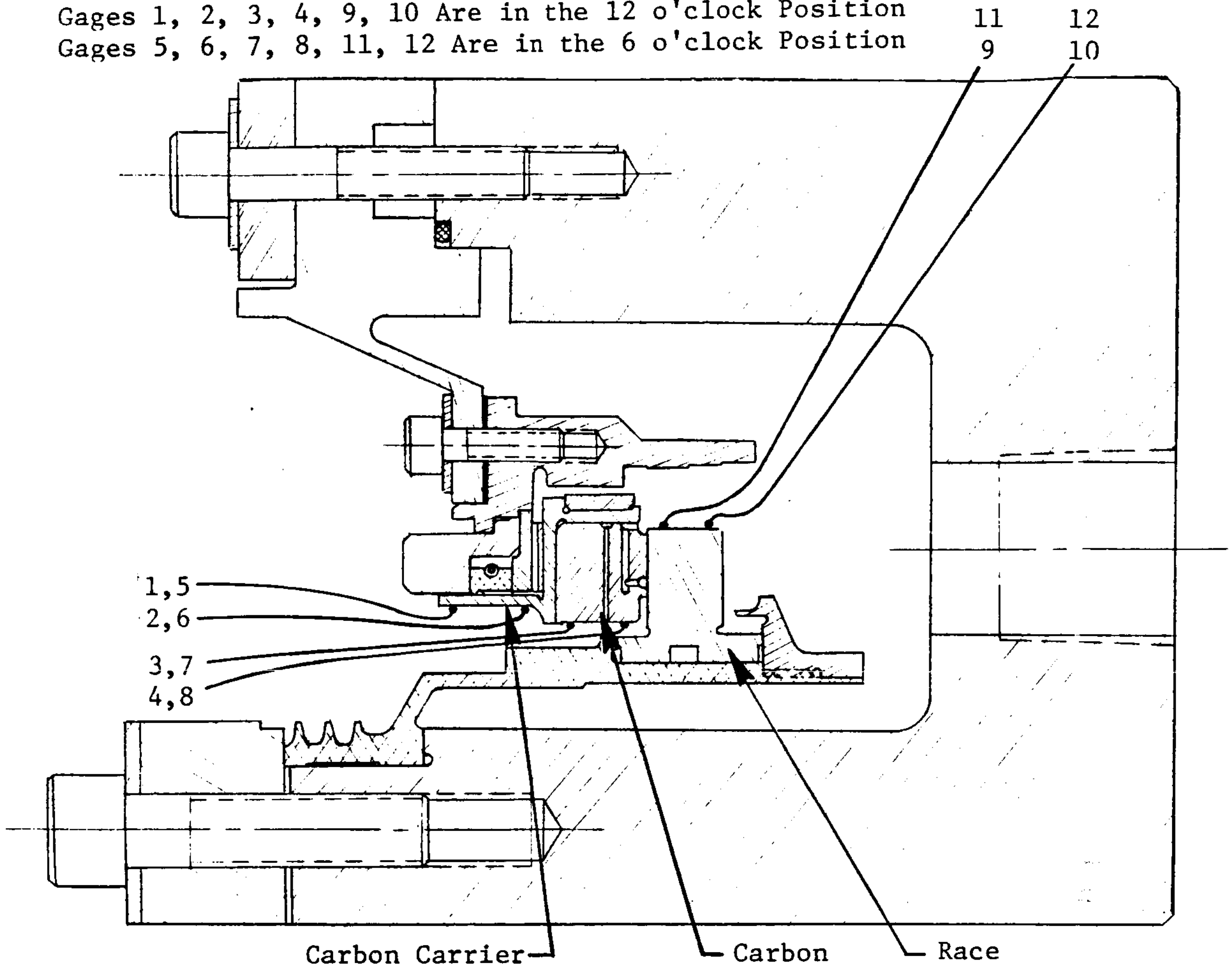

Figure 19. Test Assembly and Strain Gage Locations.

ORIGINAL PAGE IS OF POOR QUALITY

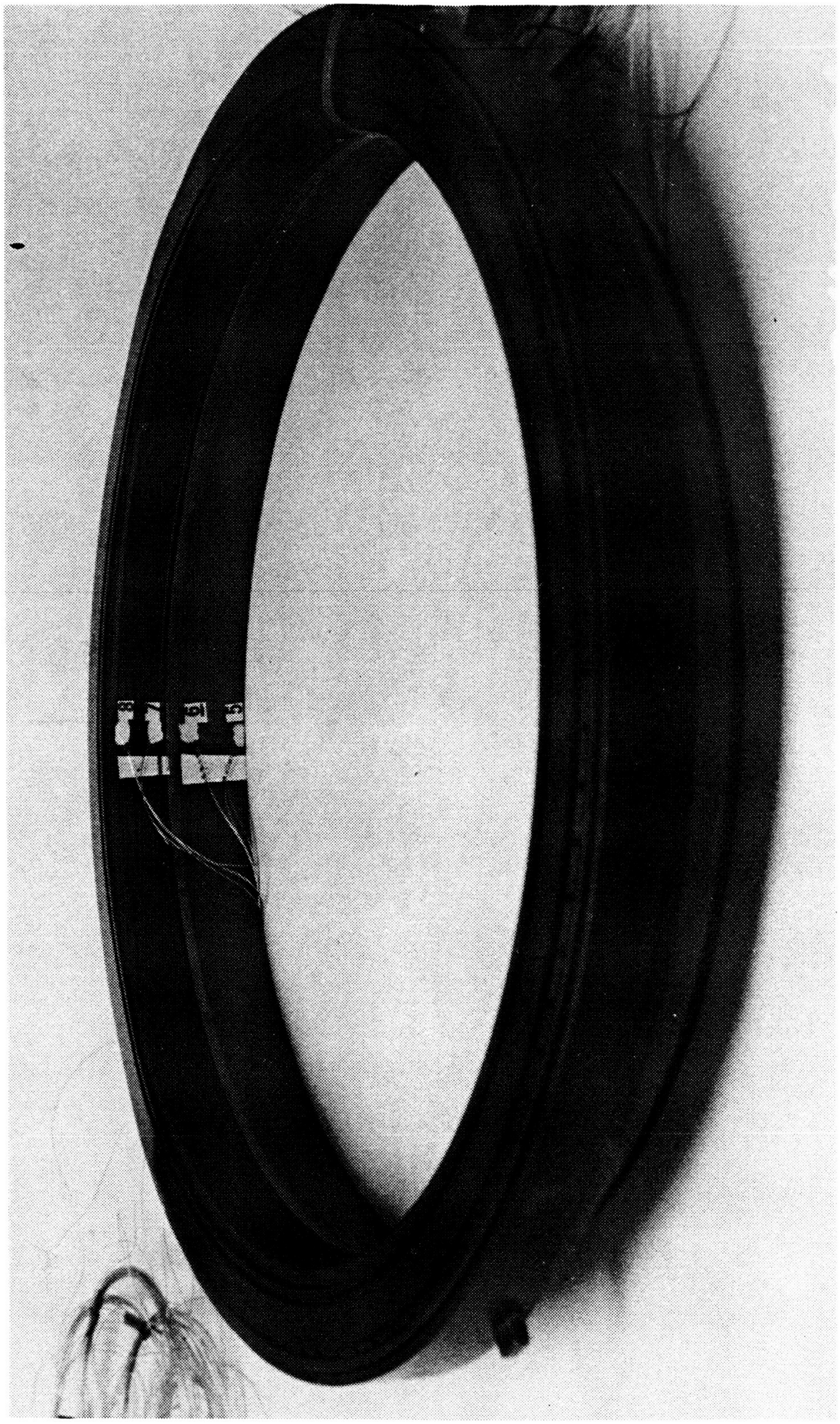

Figure 20. Photograph of Carbon Carrier Showing Strain Gage Locations.

ORIGINAL PAGE IS
OF POOR QUALITY

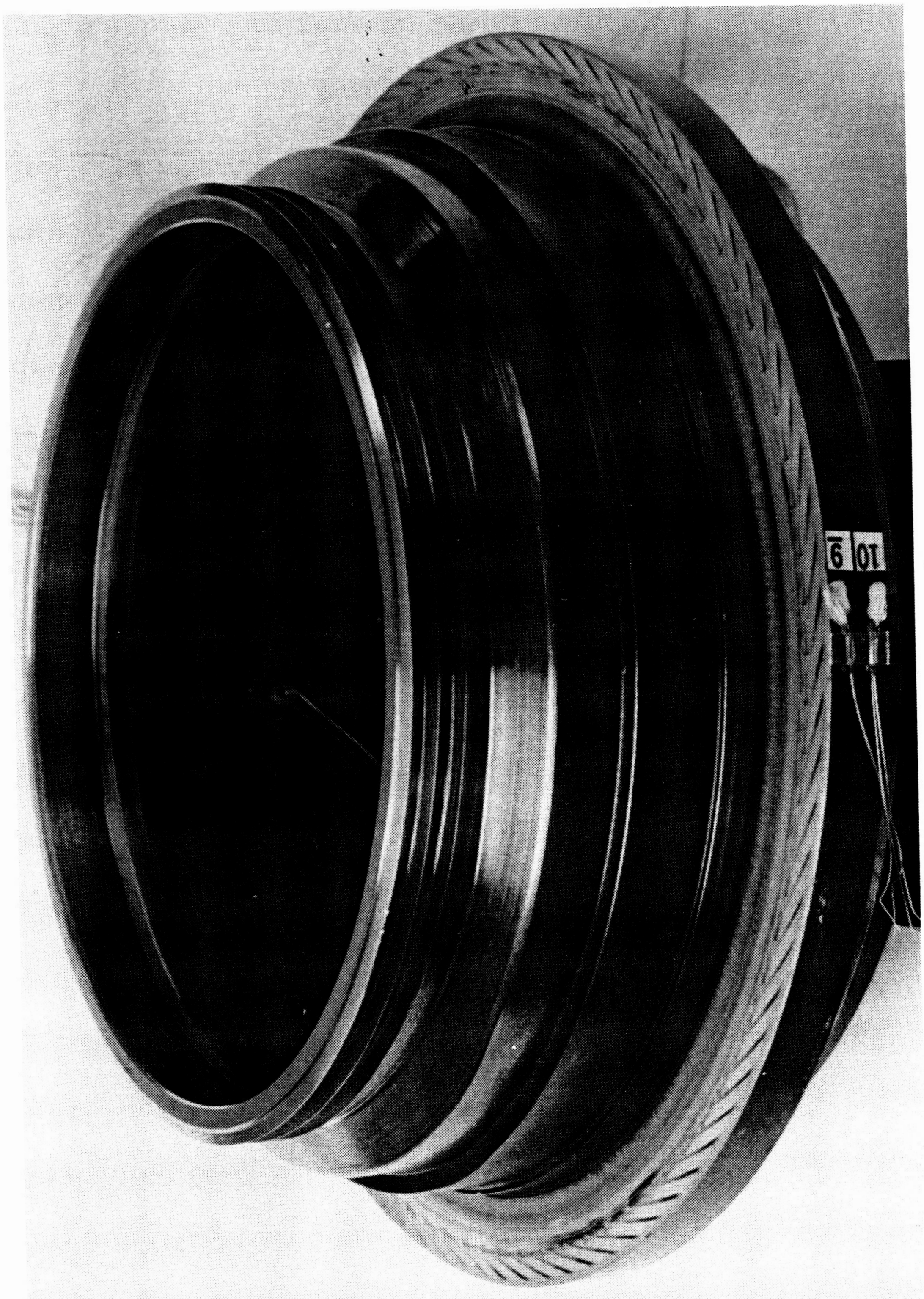

Figure 21. Photograph of Race Showing Strain Gage Locations.

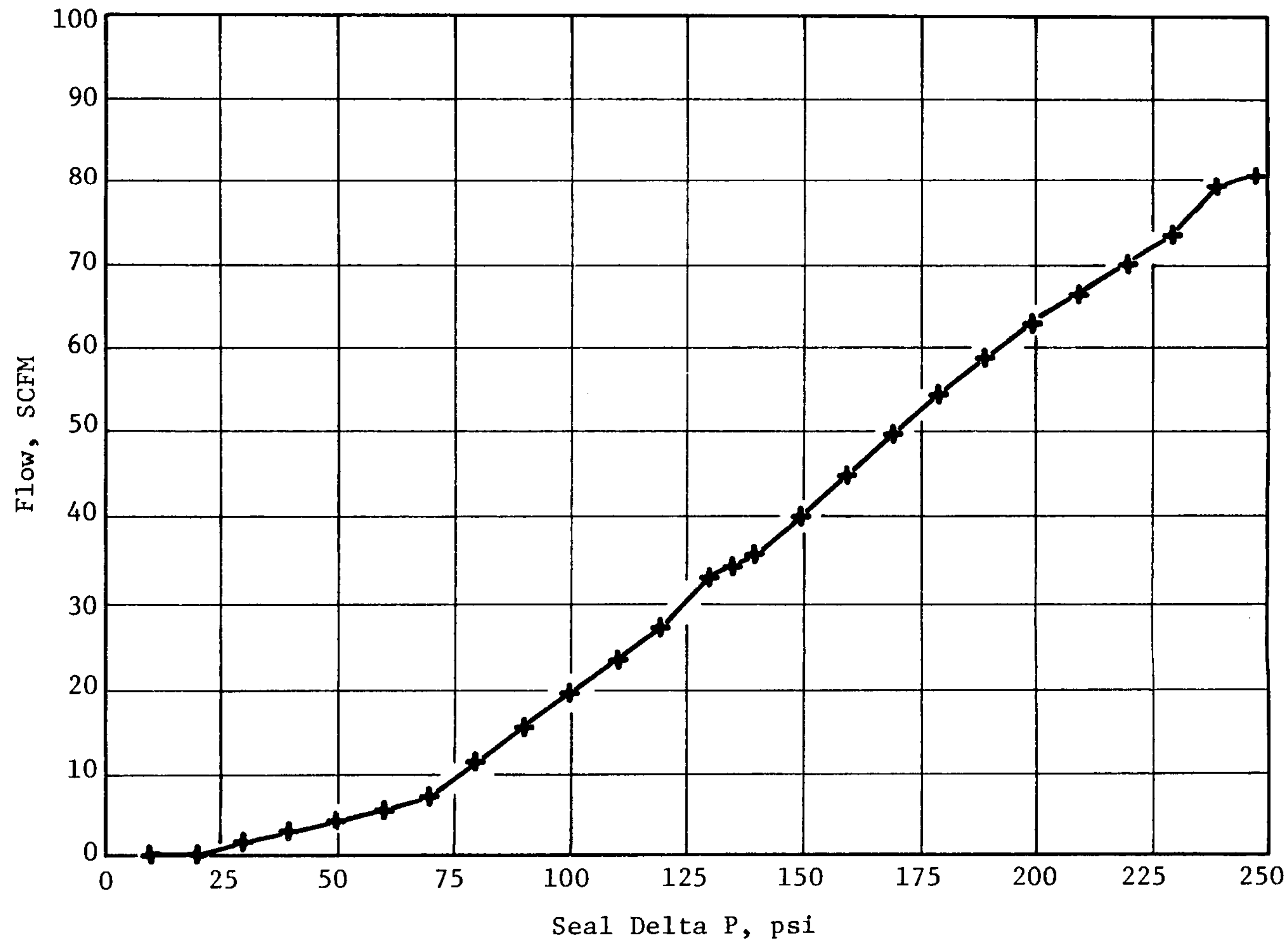

Figure 22. Gas-to-Gas Seal - Static Leak Test Leakage Flow Versus Seal Delta P.

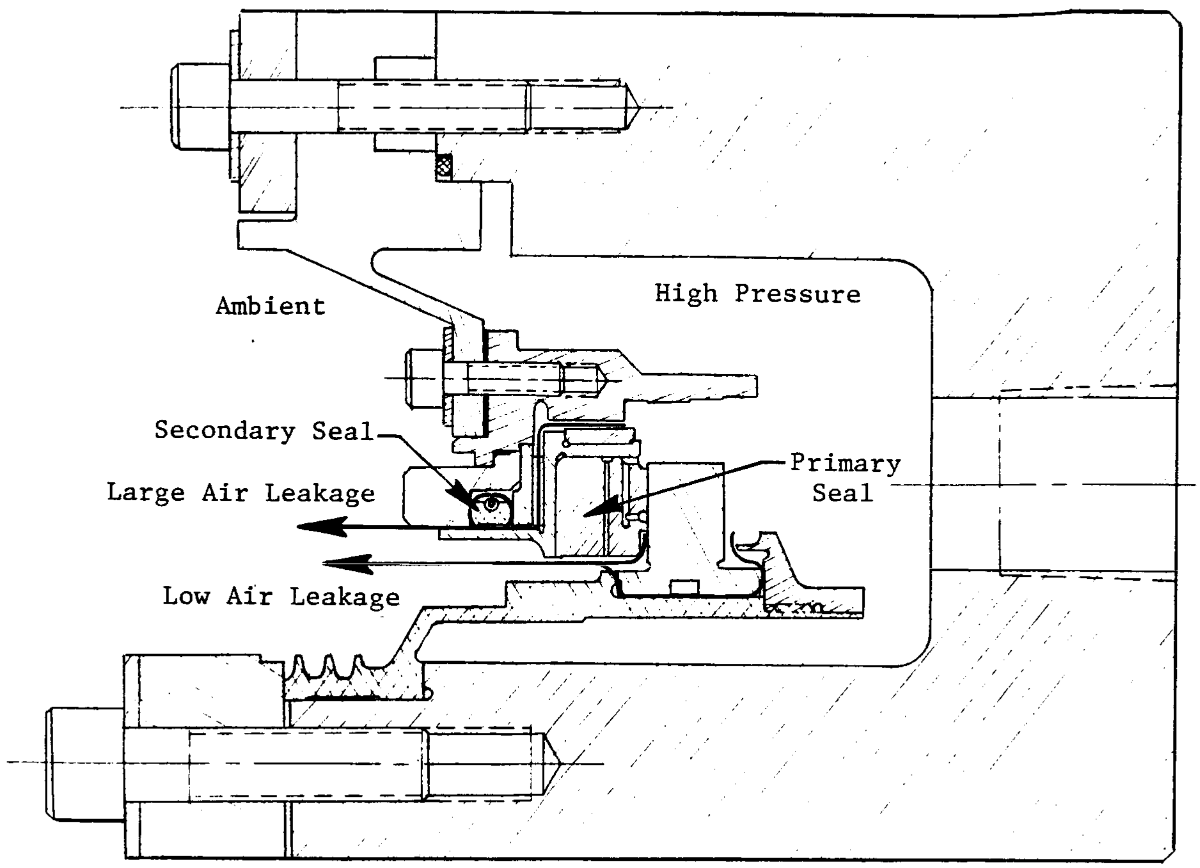

Figure 23. Flowpaths of Observed Air Leakage.

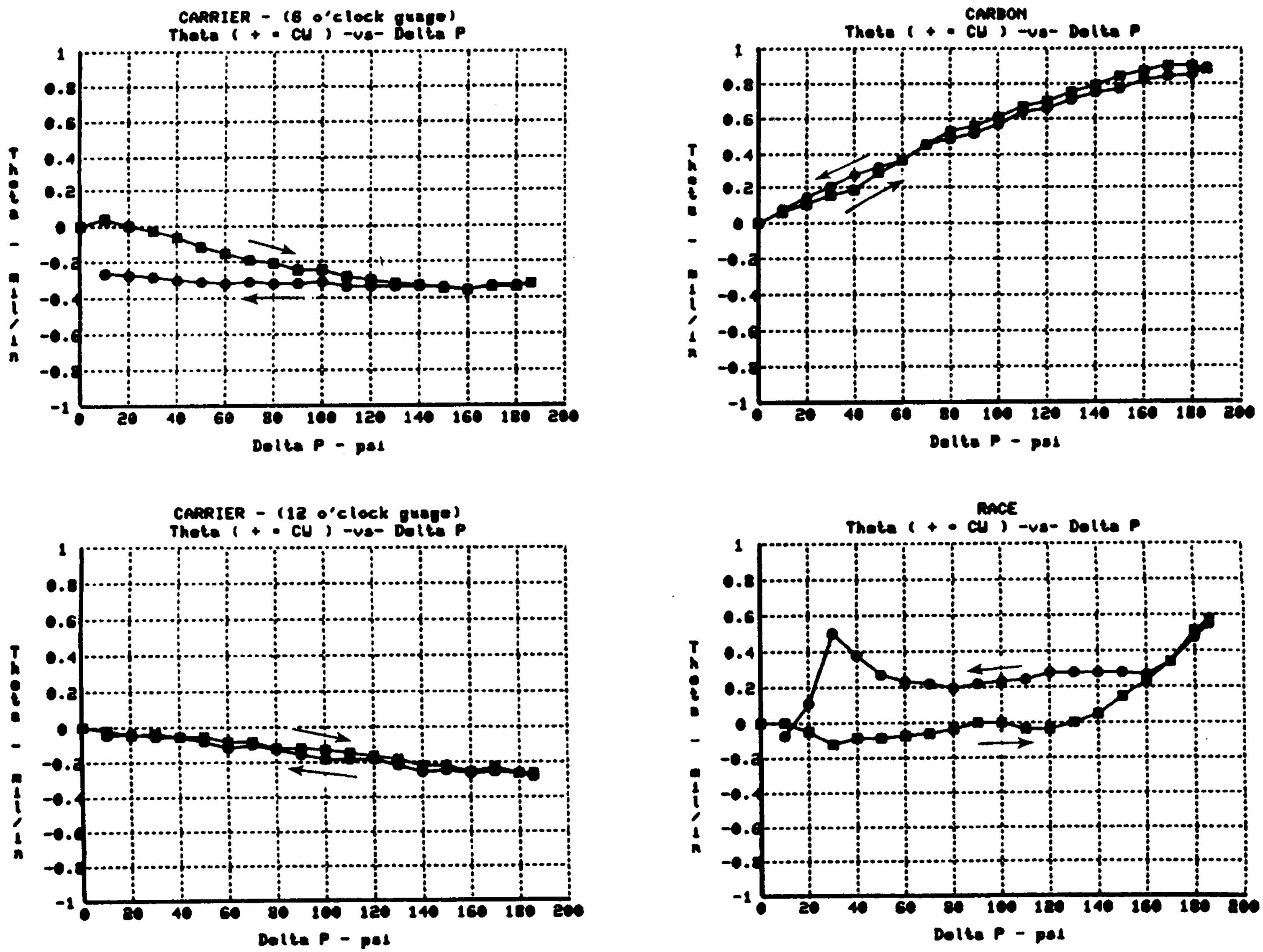

Figure 24. Local Twisting Versus Seal Delta P.

ORIGINAL PAGE IS
OF POOR QUALITY

Since a second set of hardware was available, it was instrumented and static tested. The results were very similar.

Because of the delicacy of the secondary seal and the special assembly technique required, the hardware was returned to the vendor for disassembly and inspection. In addition, the static test fixture was also sent to the vendor to allow rapid checking of any hardware modifications. The seal, when received by the vendor, was retested for correlation of leakage. The leakage measured 92 scfm at 300 psid, compared to 74 scfm at 280 psid prior to shipping. The seal was inspected, and it was found that the carbon face was significantly out of flat, both circumferentially and radially. The face was lapped flat and the leakage was then 45 scfm at 300 psid.

Since this leakage was still too high, the secondary seal assembly was disassembled and inspected. It was found that two axial coil springs were crushed between the carbon segments and the retainer, and that two segments were broken. The damage apparently occurred at assembly. Since rough machined carbon segments were available, replacement segments were manufactured.

Retesting with new secondary seal segments resulted in nearly the same leakage. A 0.002 inch radial taper was ground on the secondary seal seat to account for the clockwise deflection of the insert. This also had very little effect on the leakage. Acceptable leakage of 10 scfm at 300 psid was finally achieved after an axial taper was ground on the bore of the secondary seal and the primary seal face above the seal dam was undercut 0.001 inch to account for suspected counterclockwise rotation of the seal race under pressure loading.

4.0 DYNAMIC TESTING

Prior to dynamic testing. the forward rig housing was reworked to provide thermal insulation to minimize the flow required to maintain the high temperatures required. In earlier testing it was discovered that when the seal functioned properly there was so little flow that convective and radiative cooling of the housing exceeded the heat supplied by the hot pressurization airflow, The rework consisted of manufacturing the insulation can shown in Figure 25.

The testing was to be performed in two parts, first performance mapping and then endurance running. The test plan is shown in Table 1. The test assembly is shown in Figure 25. After the rig was assembled a static leak check was run. The leakage was very small up to 300 psid. Since a 0-300 scfm flow meter was used, there was no indicated leakage.

Upon rig disassembly to install the insulation in the can, a fair amount of debris was found that apparently came from the air supply. Since air entering the heater is filtered, the debris must have come from the heater. Purchasing a high temperature filter would have delayed testing, so one was fabricated from fine mesh Inconel screen.

Prior to the start of the performance testing, the large compressor used for supply air failed during another test program. A delay of several months was encountered.

After the compressor repair, the seal was again static tested, with results similar to earlier static testing. When the rig was started and run at low speed and moderate pressure as a system check, the drive motor tripped off and the speed decreased to zero. The pressure to the system was cut off (manually) as quickly as possible so that the axial load on the seal would be removed.

The seal was removed from the rig and inspected. A fine white powder was found lightly coating about 40% of the surfaces within the test cavity, a small amount of which was found on the seal. This powder was insulation from the can at the forward end of the rig. The design intent was that the insulation would be trapped within the can except for small bleed holes that would allow pressure equalization within the cavity. There was also a rectangular opening (approximately 1 × 2 inches) that was capped with shim stock and tacked with a nichrome welder. Because the pressure dropped so quickly in the test cavity, the pressure drop in the insulation can lagged that within the test cavity; thus, insulation was blown into the test cavity.

The rig was cleaned, the insulation can was cut open, and the insulation removed. If the dead air space in the insulation cavity proved to be an inadequate insulator, the problem would be resolved at that time with other insulation. To ensure that the problem did not recur, the pulley on the drive motor was replaced by one of smaller diameter and the control system changed so that if the motor did drop off line, a valve supplying air to the rig would be shut off, and simultaneously, one venting the rig would be opened.

ORIGINAL PAGE IS
OF POOR QUALITY

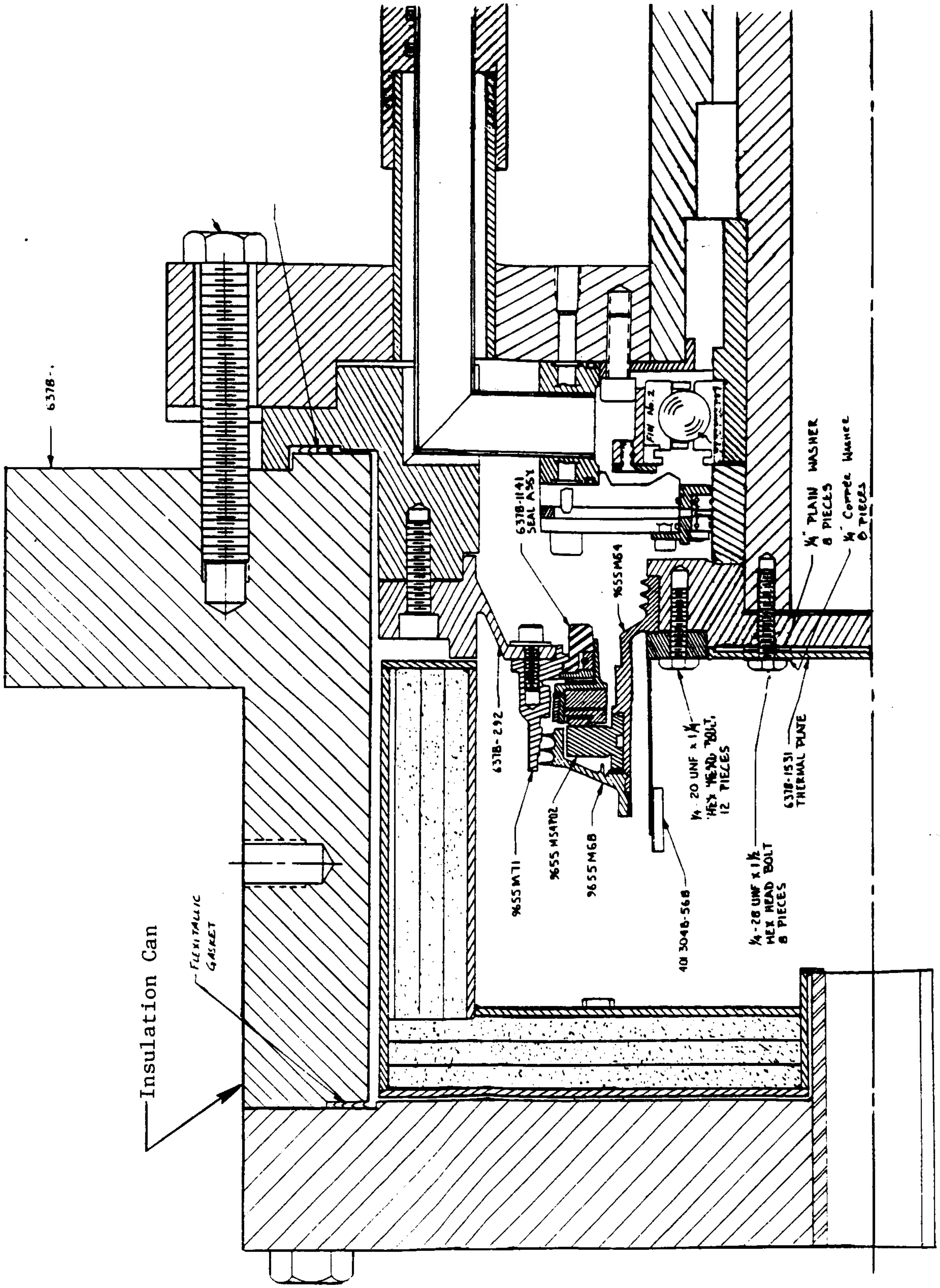

Figure 25. Dynamic Test Setup.

Table 1. Gas-to-Gas-Seal Test Plan.

Performance Mapping

Seal ΔP: 10 to 290 , 35 psi increments
Air Temp: RT to 950 , 290°F increments
Pitchline Velocity: 200 and 400 ft/sec

N, rpm	Temperature, ° F	ΔP, psi								
4900	RT 370 660 950	10	45	80	115	150	185	220	225	290
9800	RT 370 660 950									

Endurance

Cycle A			
N, rpm	Δ, psi	Temperature, ° F	Time, %
1181	9	260	10
7935	202	940	10
7480	125	820	80

Cycle B			
N, rpm	Δ, psi	Temperature, ° F	Time, %
6000	23	600	10
10500	290	950	10
9300	270	950	80

At first it was thought that the test hardware was not damaged. However, closer inspection revealed that wear had occurred on both the seal and the race faces. This may well have been a result of the motor shutdown. When the shutdown occurred, the seal was heavily loaded in the direction of the race (since there was no race/seal relative circumferential speed to generate bearing lift forces which separate the seal and race) and the seal and race could come into contact. Figures 26 and 27 show the "before" and "after" dynamic running seal face measurements. Figure 28 shows the race "after" run measurements. Since the nominal spiral groove depth is only 0.0007 inches, some of the more shallow grooves give a visual indication that surface wear had occurred.

The dam was initially 0.001-0.002 inch high, as shown in Figure 26. After the motor failure, Figure 27 shows that the situation has been reversed, with the dam being approximately 0.001 inch low.

After reassembling the hardware, a static leak test was run. The results are shown in Figure 29. The leakage had approximately doubled. Even though leakage was significantly higher than desired, it was decided to continue mapping to determine leakage characteristics with respect to increased air supply temperature and race rotational speed.

The data shown in Figure 30 were obtained during the mapping. At the high speed point (9800), there was a significant audible rig resonance. It was decided to avoid high speed running throughout the balance of the mapping. The decision not to investigate the source of resonance was based on the severe funding limitations at this point in the program, which were largely due to unanticipated hardware rework which absorbed funding and caused further costs due to increased labor rates.

During this testing, if a test point was held, the leakage would oscillate slowly between some reading and approximately 50% of that reading. This indicates that there is likely to be some heating/cooling of the components that cause the sections to roll with respect to each other. One possible sequence of events is shown in Figure 31.

Because of the instability of the seal, further mapping of the hardware was judged to be not prudent.

At this time in the program, funding was nearly exhausted. In fact, GE had already provided internal funding to make an effort to complete the program. Although backup hardware was available, the backup race would have required rework. It was agreed with the sponsor that the appropriate action at this time would be to write the final report and store the hardware.

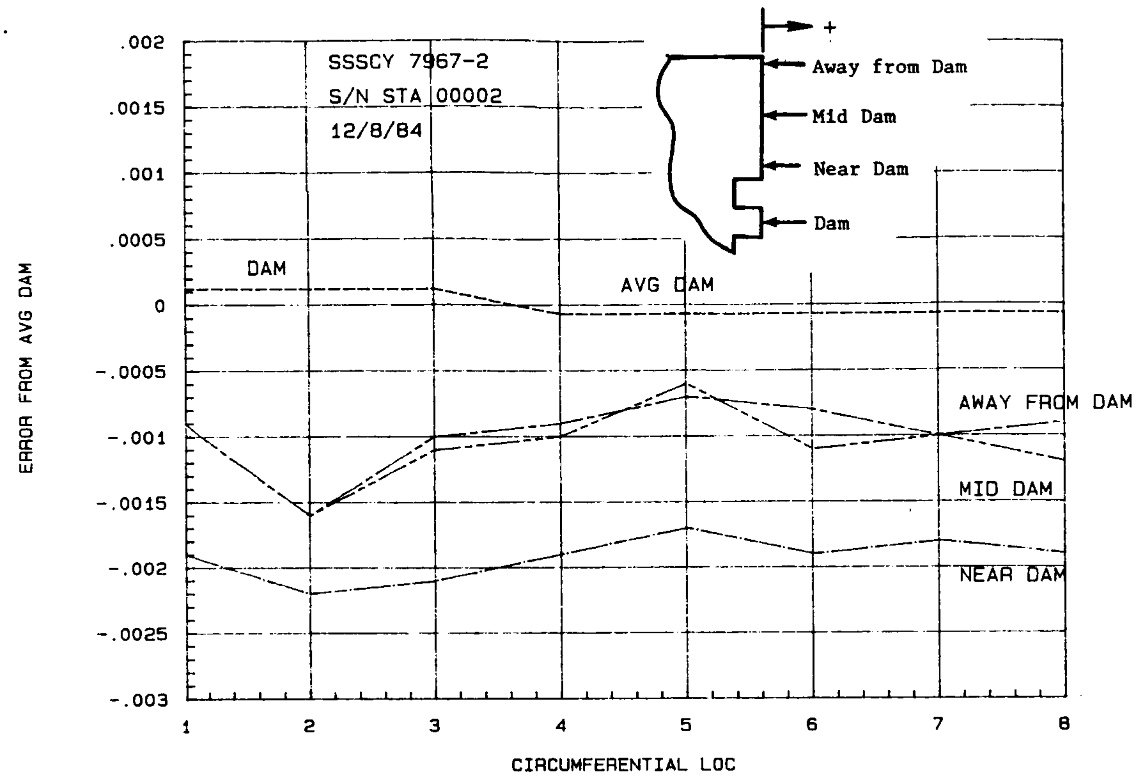

Figure 26. Pretest Carbon Dimensions.

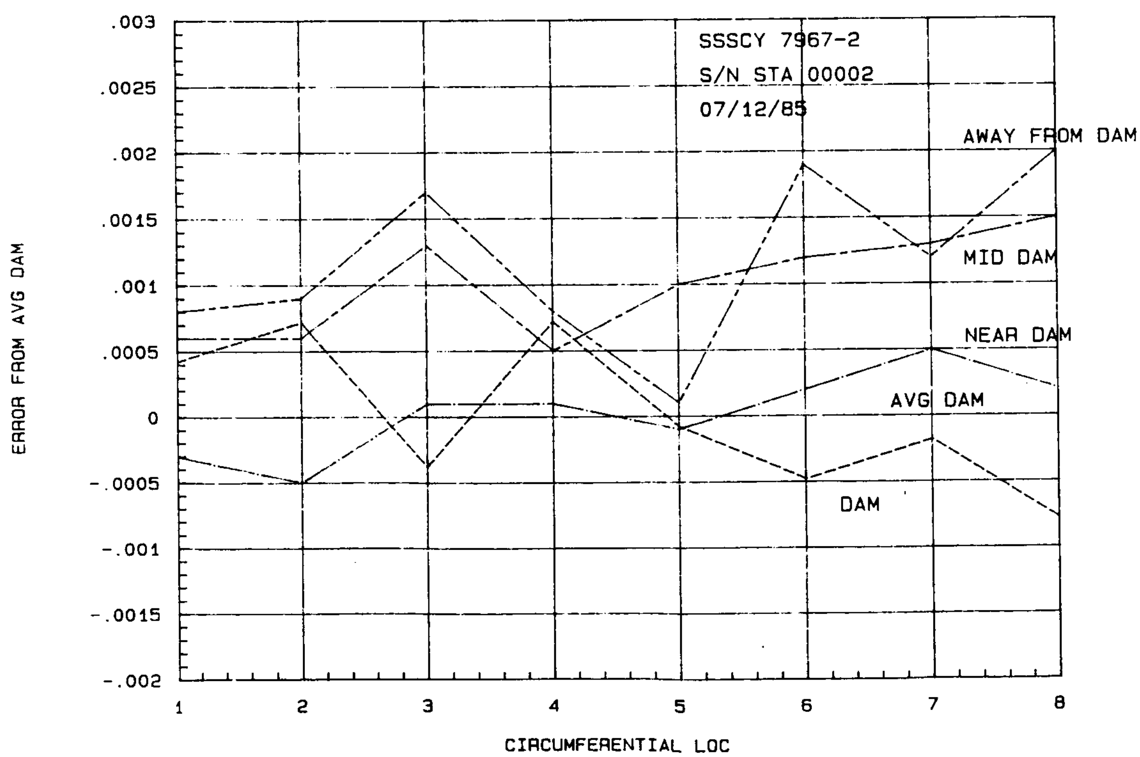

Figure 27. Carbon Dimensions After 2.6 Hours Run Time.

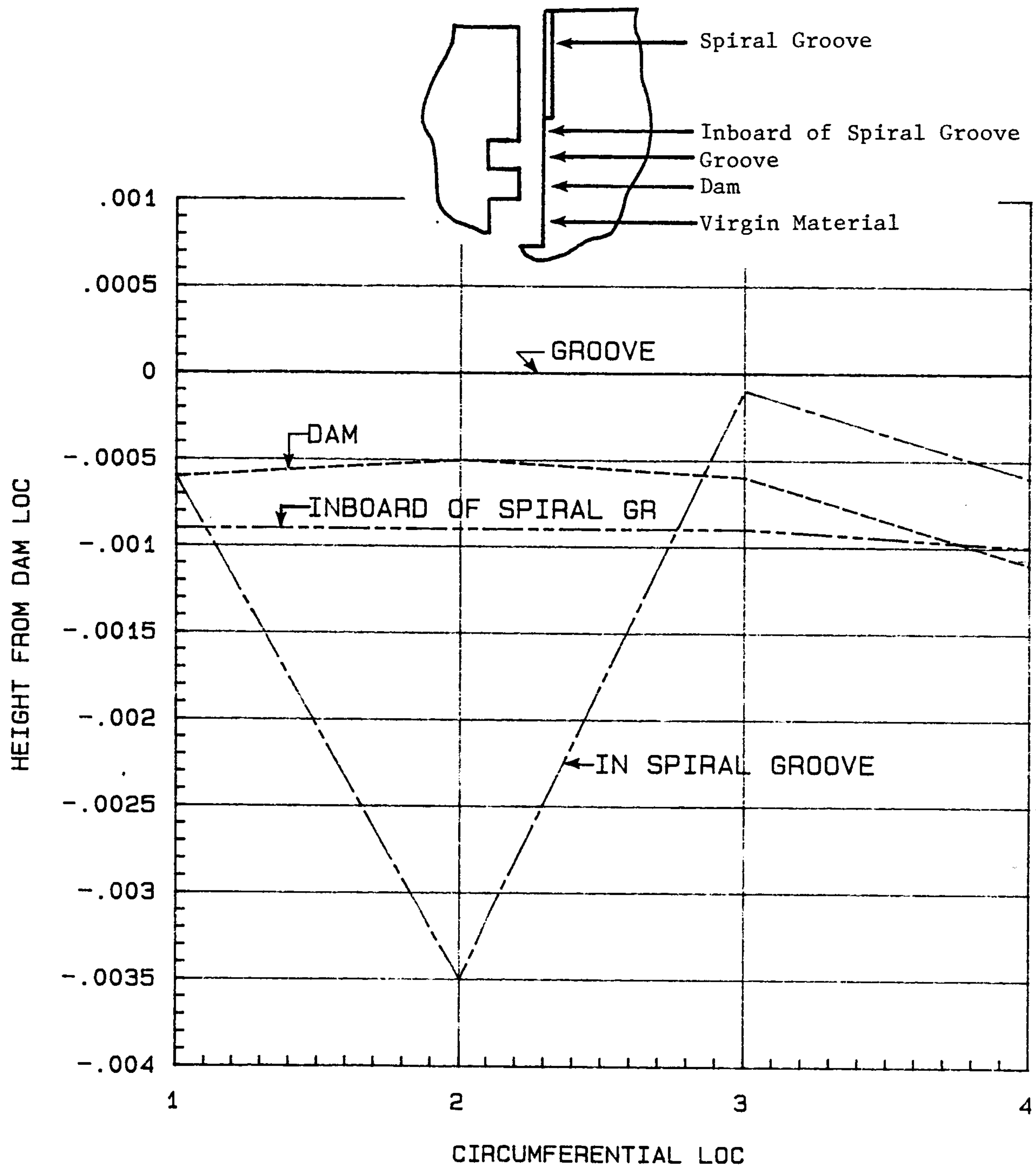

Figure 28. Seal Race Surface Dimensions After 2.6 Hours Run Time.

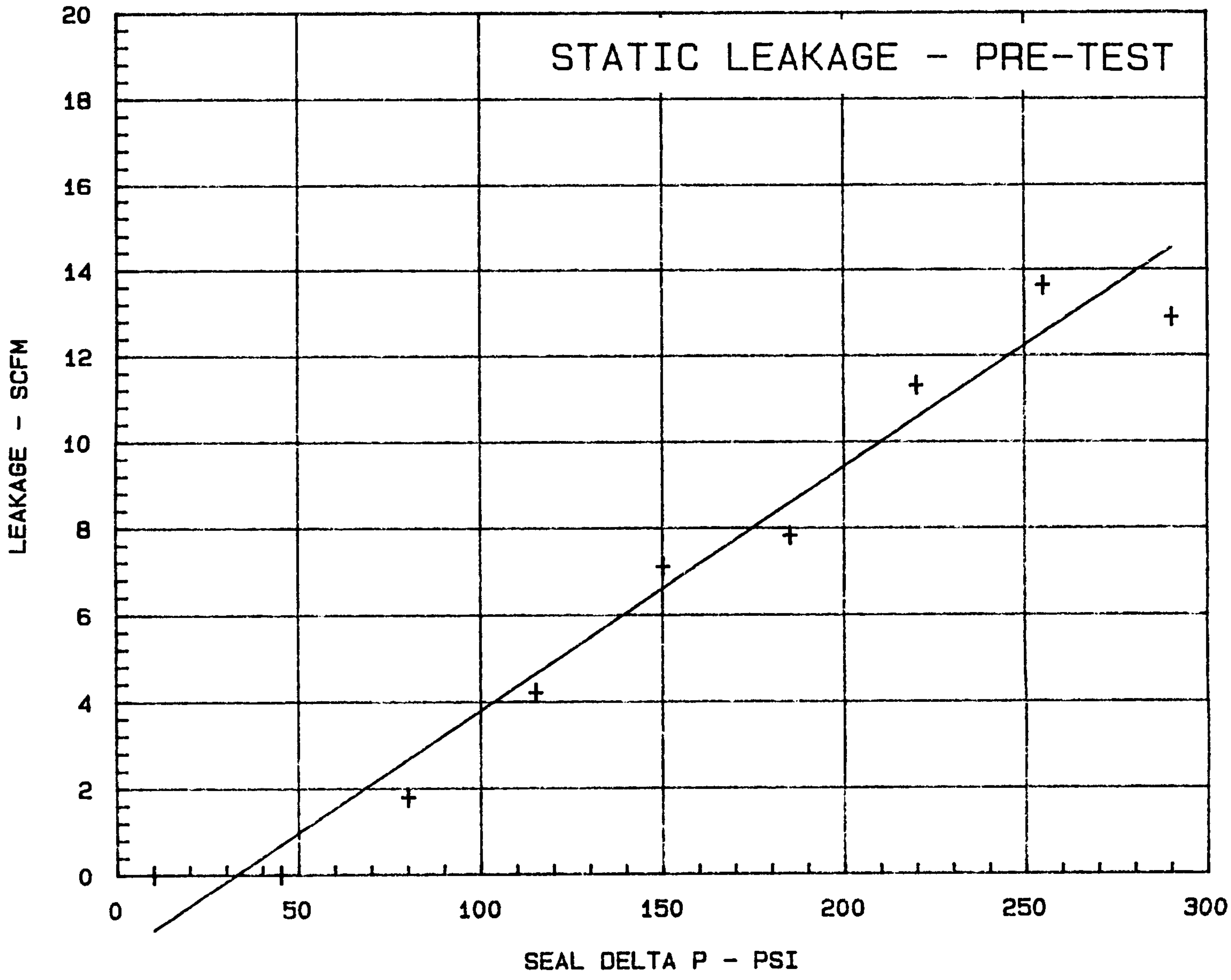

Figure 29. Static Leakage - Pretest.

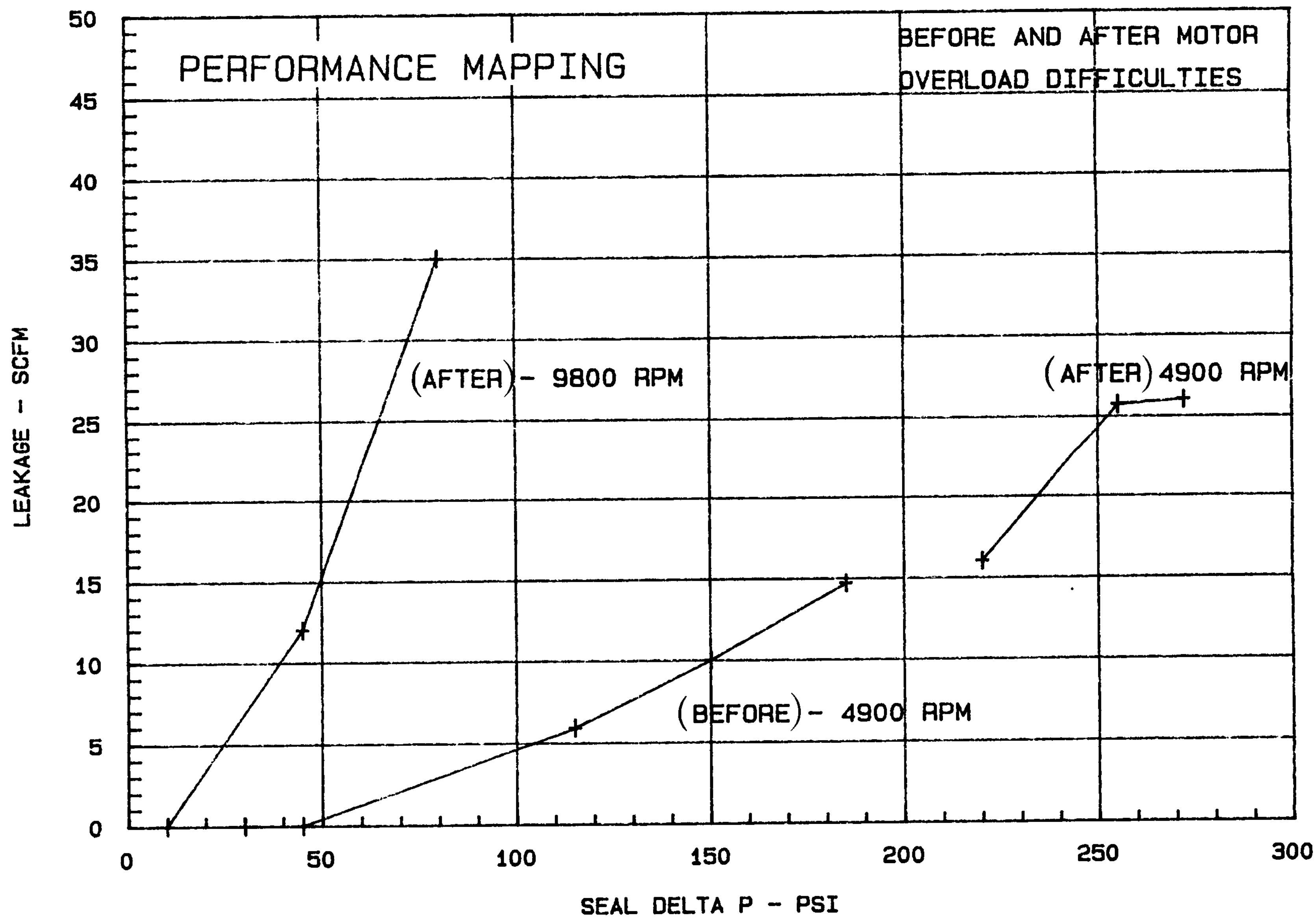

Figure 30. Performance Mapping Before and After Motor Overload.

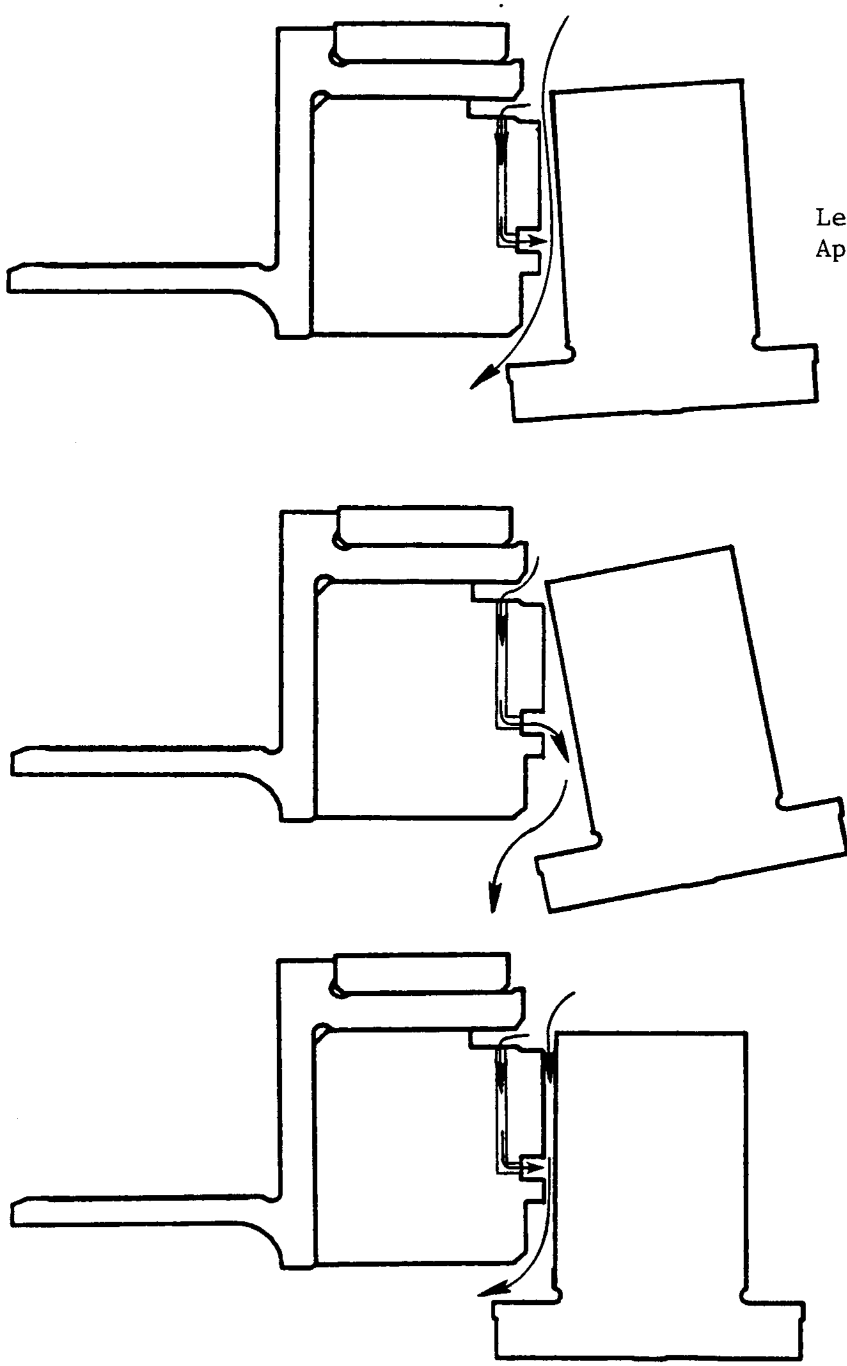

<u>Condition 1</u>
Leakage Cools Faces - OD's Approach One Another

<u>Condition 2</u>
Faces Touch or Nearly Touch - Significant Heating of Surfaces Causes Sections to Rotate to Relieve Touching

<u>Condition 3</u>
Faces Approach Vertical Lower Leakage. Heat Source Gone, Cooling Returns to Condition 1.

Figure 31. Leakage Mechanism.

DISTRIBUTION

	Copies
Department of the Navy Naval Air Systems Command AIR-330 Washington, DC 20360	1
U.S. Navy Marine Engineering Laboratory Friction and Wear Division Annapolis, MD 21490 Attn: R.B. Snapp	1
Department of the Navy Office of Naval Research Arlington, VA 22217 Attn: 411/Lt. R. Miller	1
U.S. Army Research and Technology Laboratory Fort Eustis, VA 23604 Attn: J. White, Chief Propulsion Division	1
AMMRC Watertown, MA 02172 Attn: Dr. R. Singler	1
Commander U.S. Research and Development Command P.O. Box 209 St. Louis, MO 63166 Attn: SVDL-SR/J. Means	1
Avco Corporation Lycoming Division 550 S. Main Street Stratford, CT 06497 Attn: M. O'Brien	1
Mr. Jesse Davis Microtron Corp. 8 Sagamore Hill Drive P.O. Box 588 Port Washington, NY 11050	1

Department of Mechanical Engineering
Technicon-Israel Institute of Technology
Haifa
ISRAEL
Attn: Dr. Izhak Etsion 1

The Boeing Aircraft Company
P.O. Box 3707
Seattle, WA 98124
Attn: W.S. Lambert 1
W.G. Nelson 1

The Boeing Vertol Company
Boeing Center
P.O. Box 16858
Philadelphia, PA 19142
Attn: A.J. Lemanski, MS P-32-09 1

Borg Warner Corporation
Roy C. Ingersoll Research Center
Wolf and Algonquin Roads
Des Plaines, IL 60018 1

Gould, Inc.
17000 St. Clair Avenue
Cleveland, OH 44110
Attn: T. Fazekas 1

Cooper Bessemer
Mt. Vernon, OH 43050
Attn: K. Smith 1

Crane Packing Co.
6400 W. Oakton Street
Morton Grove, IL 60053
Attn: J. Sedy 1

Defense Ceramics Information Center
Battelle Columbus Laboratories
Room 11-9021
505 King Avenue
Columbus, OH 43201 1

Dresser Industries
Dresser Clark Division
P.O. Box 560
Olean, NY 14780
Attn: J.W. Kirkpatrick 1
E. Tanzberger 1

Durametallic Corporation
Kalamazoo, MI 49001
Attn: H. Hummer 1

Franklin Institute Laboratories
20th and Parkway
Philadelphia, PA 19103
Attn: R. Colsher 1

Garrett Corporation
AiResearch Manufacturing Division
9851-9951 Sepulveda Blvd.
Los Angeles, CA 90009
Attn: A. Silver 1

General Electric Company
Advanced Engineering Technologies Department
Cincinnati, OH 45215
Attn: N. Pope 1

Gould Information Center
540 E. 150th Street
Cleveland, OH 44108 1

Koppers Co., Inc.
Metal Products Division
P.O. Box 626
Baltimore, MD 21203
Attn: E. Taschenburg 1

Mechanical Technology, Inc.
968 Albany Shaker Road
Latham, NY 12110
Attn: W. Shapiro 1

Midwest Research Institute
425 Volker Boulevard
Kansas City, MO 64110
Attn: V. Hopkins 1

Garrett Turbine Engine Co.
P.O. Box 5217
Phoenix, AZ 85010
Attn: Mr. Lowell Hollars 1

North American Rockwell Corporation
Rocketdyne Division
6633 Canoga Avenue, AC 51
Canoga Park, CA 91304
Attn: R.E. Burcham 1

Sealol, Inc.
P.O. Box 2158
Providence, RI 02905
Attn: Mr. H.F. Greiner 1

Sikorsky Aircraft
N. Main Street
Stratford, CT 06497
Attn: Carl Keller 1
T. Hayden 1

SKF Industries, Inc.
1100 First Avenue
King of Prussia, PA 19406
Attn: L.B. Sibley 1

Southwest Research Institute
P.O. Drawer 28510
San Antonio, TX 78228
Attn: P.M. Ku 1

St. Marys Carbon Company
1939 State Road
St. Marys, PA 15857
Attn: J.E. Lanzel 1

Stackpole Carbon Co.
St. Marys, PA 15857
Attn: Dr. E.I. Shobert 1

Stein Seal Company
20th Street and Indiana Avenue
Philadelphia, PA 19131
Attn: E. Goldring 1

Teledyne CAE
1330 Laskey Road
Toledo, OH 43612
Attn: Mr. James Gasser 1

Ultra Carbon Corporation
1300 N. Madison Avenue
Bay City, MI 48706
Attn: Del Hughes 1

Union Carbide
Carbon Products Division
P.O. Box 6116
Cleveland, OH 44101
Attn: E. Ferrier 1

Wickes Engineered Materials
1621 Holland
Saginaw, MI
Attn: P. Dahlenberg 1

The University of Tennessee
Dept. of Mechanical and Aerospace Engineering
Knoxville, TN 37916
Attn: Professor W.K Stair 1

Naval Air Propulsion Center
P.O. Box 7176
Trenton, NJ 08628
Attn: Mr. Ray Valori 1

Pratt & Whitney Aircraft Group
Government Products Division
E-40, Box 2691
West Palm Beach, FL 33402
Attn: Mr. Al Peduzzi 1

Solar Turbine, Inc.
San Diego, CA 92112
Attn: T. Batakis 1

NASA Scientific and Technical Information Facility
Attn: Acquisition Branch
PO Box 8757
Baltimore Washington International Airport
MD 21240 25

NASA Lewis Research Center
Attn: Report Control, MS 60-1, Room 225
21000 Brookpark Road
Cleveland, Ohio 44135 2

NASA Lewis Research Center
Attn: Library, MS 60-3
21000 Brookpark Road
Cleveland, Ohio 44135 2

NASA Lewis Research Center
Structures Division
Attn: L.D. Nichols, MS 49-6
21000 Brookpark Road
Cleveland, Ohio 44135 1

NASA Lewis Research Center
Structural Dynamics Branch
Attn: L.J. Kiraly, MS 23-3
21000 Brookpark Road
Cleveland, Ohio 44135 1

NASA Lewis Research Center
Attn: E. DiRusso, MS 23-3
21000 Brookpark Road
Cleveland, Ohio 44135 3